Islam Marzouk, BSc

Numerical studies on 2D thermal finite element analysis

MASTER'S THESIS

to achieve the university degree of

Master of Science

submitted to

Graz University of Technology

Supervisor

Ass.Prof. Dipl.-Ing. Dr.techn. Franz Tschuchnigg

Institute of Soil Mechanics, Foundation Engineering and Computational Geotechnics

Graz University of Technology

Graz, September 2019

Eidesstattliche Erklärung

Ich erkläre an Eides statt, dass ich die vorliegende Arbeit selbstständig verfasst, andere als die angegebenen Quellen/Hilfsmittel nicht benutzt, und die den benutzten Quellen wörtlich und inhaltlich entnommenen Stellen als solche kenntlich gemacht habe. Das in TUGRAZonline hochgeladene Textdokument ist mit der vorliegenden Arbeit identisch.

……. ……
Datum Unterschrift

AFFIDAVIT

I declare that I have authored this thesis independently, that I have not used other than the declared sources/resources, and that I have explicitly marked all material which has been quoted either literally or by content from the used sources. The text document uploaded to TUGRAZonline is identical to the present master's thesis.

……. …….
Date Signature

Acknowledgements

I would like first to express my gratitude to Ass.Prof. Dipl.-Ing. Dr.techn. Franz Tschuchnigg for suggesting this interesting topic. Also, for his guidance and support throughout the duration of working on the thesis.

Moreover, I would like to thank my friends back at home and the ones I knew here during my stay in Graz. They made my stay in Graz full of unforgettable memories.

In addition, I would like to thank my parents and sisters for their continuous support and encouragement.

Last but not least, I would like to thank Abdalla, Mahmoud, Noreen and Zahid for helping me while writing the thesis and for their proof-reading.

Abstract

Considering thermal effects in soil lead to the introduction of a new variable, the temperature. Thermal behaviour interacts with hydraulic and mechanical behaviour (i.e. thermal hydraulic mechanical coupling (THM)). The coupling between these phenomena is complicated and the degree of coupling between one behaviour to another varies (Gens 2010). It is the aim of the research to investigate the application of the thermal analysis in the 2D finite element software PLAXIS. To do this, the thesis focuses on the factors influencing the transfer of temperature in the soil. These factors include the presence of groundwater, thermal parameters of the soil (i.e. thermal conductivity and heat capacity), climate conditions and time.

It was necessary to conduct a literature review to understand the heat transfer mechanisms in soil. Moreover, it was essential to determine soil thermal parameters and typical values for different types of soils. In addition, the influence of temperature on water and soil behaviour was studied. The numerical analysis includes preliminary studies, groundwater flow study, modelling of thermal energy storage (TES) and a case study. Firstly, preliminary studies were carried out, in which the influence of the time steps on the accuracy of the results and on the number of the calculation steps was investigated. Secondly, harmonic and linear temperature functions were studied. After that, a sensitivity analysis for the thermal parameters of soil was carried out. In addition to this, a groundwater flow study was conducted to show the influence of groundwater flow on the temperature distribution. Furthermore, three thermal energy storages (TES) geometries were investigated and the effect of thermal insulation, water situation inside the storage was studied. Finally, a case study which includes modelling of a large-scale test was performed and the results obtained from this analysis were compared to real measurements.

Kurzfassung

Die Berücksichtigung thermischer Effekte im Boden führt zur Einführung einer neuen Variablen, der Temperatur. Das thermische Verhalten steht in Wechselwirkung mit dem hydraulischen und mechanischen Verhalten (thermisch-hydraulischen mechanischen Kupplung (THM)). Die Kopplungseffekte zwischen diesen Phänomenen sind kompliziert und der Grad der Kopplung zwischen einem Verhalten und einem anderen variiert (Gens 2010). Ziel der Forschung ist es, die Anwendung der Thermoanalyse in der 2D-Finite-Elemente-Software PLAXIS zu untersuchen. Zu diesem Zweck konzentriert sich die Arbeit auf die Faktoren, die die Übertragung der Temperatur im Boden beeinflussen. Zu diesen Faktoren gehören das Vorhandensein von Grundwasser, thermische Parameter des Bodens (d.h. Wärmeleitfähigkeit und Wärmekapazität), Klimabedingungen und Zeit.

Es war notwendig, eine Literaturrecherche durchzuführen, um die Wärmeübertragungsmechanismen im Boden zu verstehen. Darüber hinaus war es unerlässlich, bodenthermische Parameter und typische Werte für verschiedene Bodenarten zu bestimmen. Außerdem wurde der Einfluss der Temperatur auf das Wasser- und Bodenverhalten untersucht. Die numerische Analyse umfasst Vorstudien, Grundwasserströmungsstudien, Modellierung von Wärmespeicher und eine Fallstudie. Zunächst wurden Voruntersuchungen durchgeführt, in denen der Einfluss der Zeitschritte auf die Genauigkeit der Ergebnisse und auf die Anzahl der Berechnungsschritte untersucht wurde. Zweitens wurden harmonische und lineare Temperaturfunktionen untersucht. Anschließend wurde eine Sensitivitätsanalyse für die thermischen Parameter des Bodens durchgeführt. Darüber hinaus wurde eine Grundwasserströmungsstudie durchgeführt, um den Einfluss des Grundwasserstroms auf die Temperaturverteilung aufzuzeigen. Anschließend wurden drei mögliche Geometrien von Wärmespeicher modelliert und die Wirkung der Wärmedämmung und die der Wassersituation im Speicher untersucht. Schließlich wurde eine Fallstudie, (Modellierung eines großen Labortests), durchgeführt und die Ergebnisse aus dieser Studie wurde mit den realen Messungen verglichen.

Contents

List of Figures

List of tables

List of symbols and abbreviations

Small letters

c_s specific heat capacity

e void ratio

w_U unfrozen water content

h_{ref} reference height

q_{cond} heat flux generated by conduction

q_{lconv} heat flux generated by liquid convection

q_{vconv} heat flux generated by vapour convection

c_l specific heat capacity of soil water

$\bar{v}_l$ vector of water velocity

c_v specific heat capacity of soil vapour

$\bar{v}_v$ vector of vapour velocity

c_s specific heat capacity of solid (in section 2.2.2)

c_w specific heat capacity of water

c_a specific heat capacity of air

k permeability

Capital letters

THM thermo-hydro mechanical

TH thermo-hydraulic

T temperature

T_{ref} reference temperature

S degree of saturation

S_r degree of saturation

T_o reference temperature

C volumetric heat capacity of soil

OCR overconsolidation ratio

Q heat flux

EPS expanded polystyrene

Greek letters

η porosity

ρ_s density of the solid material

λ_s thermal conductivity of solid material

λ_i thermal conductivity of ice

λ_w thermal conductivity of water

λ_v thermal conductivity of vapour

α thermal expansion coefficient

∇ gradient operator

ρ_l density of soil water

λ_i thermal conductivities of solid, water and air components of soil (in section 2.2.1)

χ_i corresponding volume fractions

χ_s volume fraction of solid

χ_w volume fraction of water

χ_a volume fraction of air

μ viscosity

Introduction

Unlike conventional geotechnical engineering applications, temperature plays a significant role in several applications such as disposal of nuclear waste, energy piles, geothermal energy and ground freezing. In these applications, thermal, hydraulic and mechanical effects interact with each other leading to thermal hydraulic mechanical coupling (THM).

In the first chapter, theoretical background regarding several aspects of temperature is provided. The dominant heat transfer mechanisms in soils are stated. Moreover, the soil thermal parameters, as well as some thermal properties of soils, are defined. Finally, the temperature effects on water and soil behaviour are discussed. Moving to the second chapter, the application of thermal analysis in PLAXIS is illustrated. This is done by discussing the thermal boundary conditions, thermal functions, material thermal parameters required and calculation types.

The third chapter includes several preliminary studies carried out to investigate the effect of time steps on the accuracy of the results and on the number of calculation steps. In addition, two different types of temperature functions were compared and the influence of their amplitude on the temperature distribution was identified. Finally, a sensitivity analysis concerning the thermal parameters of soil was performed.

The fourth chapter deals with the interaction between groundwater and heat flow. The difference between applying cluster and boundary thermal conditions is stated. Moreover, different soil behaviours, as well as different combinations of thermal and hydraulic boundary conditions, were studied.

Thermal energy storage (TES) is discussed in chapter 5. Firstly, a theoretical background is provided. Afterwards, the attempts to model three possible variants for the storage are illustrated. Different setups were created to model the water inside the storage and a comparison between these setups is shown. Finally, the influence of the thermal insulation at the top of the storage on the temperature distribution is studied.

In the final chapter, a case study is presented. It includes the description of a large-scale test, where the temperature distribution in the soil is of interest. In addition, the approach used to model the test and a comparison between the real measurements and the results obtained are provided.

1 Literature review

1.1 Heat transfer mechanisms

There are several phenomena which induce transport of heat in a porous medium. These phenomena include (Farouki 1981):

- Heat conduction
- Heat convection
- Radiation
- Evaporation-condensation process

All possible mechanisms employ that the flow of heat is from warm to cool regions. The contribution of possible mechanisms to heat transfer is affected by soil composition, structure and temperature levels (Farouki 1981).

Figure 1 shows the domain of influence of different heat transfer mechanisms. The predominant heat transfer mechanism is conduction, while convection plays a role in high permeable soils such as gravel (Haigh 2012).

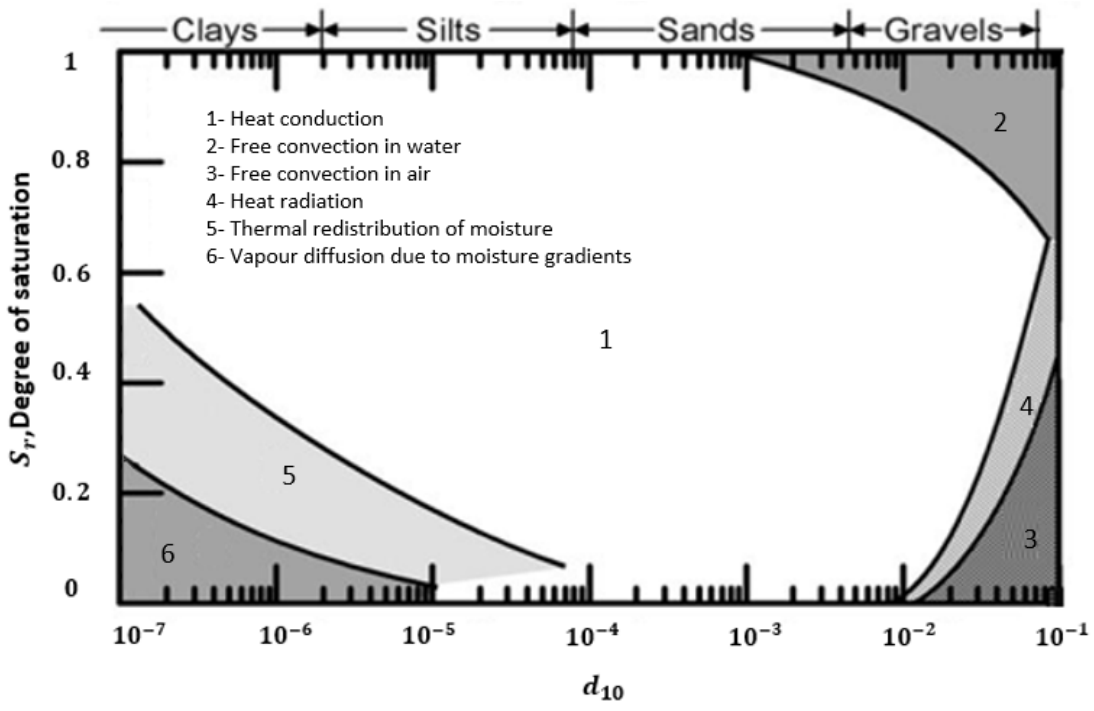

Figure 1 Heat transfer mechanisms domain of influence (Johansen 1977)

1.1.1 Heat conduction

Heat conduction is defined as the transfer of heat from one region of the medium to another region in the same medium. This transfer of heat occurs without visible motion in the medium (Rees 2000).

Heat conduction occurs in soil solids, water and pore air. The mechanism that conduction follows in air or water vapour is by collision between molecules. This collision leads to the increase of their kinetic energy as heat transfers from warm to cool regions. Regarding heat conduction in water, the energy is transferred by breaking and forming hydrogen bonds. Heat conduction in air is usually neglected (Farouki 1981).

The transfer of heat by conduction depends on the dry density of the soil and the degree of saturation. Increasing the dry density of soil and saturation leads to increase of the amount of heat transferred by conduction (Farouki 1981). The heat flux generated by conduction can be presented as follows (Rees 2000):

$$q_{cond} = -\lambda \nabla \mathrm{T}$$

1.1.2 Heat convection

There are two types of convection:

- Free convection
- Forced convection

Free convection

It is defined as a mass transport phenomenon due to temperature gradients. In fluids, it is influenced by changes in density with temperature. The density of a fluid decreases when the temperature increases. As a result of the density decrease, an upward displacement occurs (Farouki 1981).

The degree of saturation plays a significant role in free convection. Free convection starts at a lower temperature gradient in a porous material compared to dry material. In addition, free convection can occur in a material with a smaller grain size when it is saturated (Farouki 1981).

Forced convection

It results from forcing the currents of air or water by pressure differences to move through pores of the soil. The convection effects due to forced convection are not pronounced in sandy soils. However, in very coarse sands they may lead to an increase in the thermal conductivity (Farouki 1981).

The heat flux generated by liquid and vapour convection can be presented as follows (Rees 2000):

$$q_{lconv} = c_l \rho_l \bar{v}_l (T - T_o)$$

$$q_{vconv} = c_v \rho_l \bar{v}_v (T - T_o)$$

1.1.3 Radiation

It takes place across air spaces by heat energy propagated as electromagnetic waves. The most important factor is the temperature of the radiating body. The flow of heat is proportional to the fourth power of the absolute temperature. The radiation usually makes a neglected contribution to heat transfer in soils. In sand, radiation contributes less than 1% of the overall heat transfer at normal temperature. Figure 1 shows when radiation can play a role in heat transfer. Radiation influences the heat transfer in dry gravel size material (Farouki 1981).

1.1.4 Evaporation-condensation process

In case of unsaturated soils, increasing temperature leads to evaporation of water. Figure 1 (region 5) shows when the heat transfer due to the evaporation-condensation process has an effect (Farouki 1981). The magnitude of this effect depends on the quantity of the transferred vapour. When dry conditions prevail, it can have significant effects (Rees 2000).

1.2 Soil thermal parameters

The most important thermal parameters of soil are thermal conductivity and specific heat capacity. The amount of energy required to change the temperature of soil is determined by the specific heat capacity. As a result, the specific heat capacity influences the time required to reach steady-state conditions. While the thermal conductivity influences the heat flow and temperature field in the soil at equilibrium (Haigh 2012).

1.2.1 Thermal conductivity

The thermal conductivity of soil is influenced by its dry density and degree of saturation. Increasing either the dry density or degree of saturation lead to an increase in the thermal conductivity. Other factors influencing the thermal conductivity are mineral composition, time and texture (Hamdhan and Clarke 2010).

There are several models available for calculating the thermal conductivity of the granular materials. These models cannot be used to predict the thermal conductivity accurately for all soil types or for different values of moisture content. Nevertheless, the geometric mean equation is generally used to calculate the thermal conductivity as it has been found to be suitable by several researchers. The geometric mean approach is described below (Thomas and Rees 2009):

The thermal conductivity of soil can be determined from the following equation:

$$\lambda = \prod_{i=1}^{3} \lambda_i{}^{\chi_i}$$

It is described as the product of thermal conductivities of different constituents of soil (i.e. solid, water and air) to the power of volume fractions. The volume fractions for solid, water and air can be obtained from the following equations (Thomas and Rees 2009):

$\chi_s = 1 - \eta$

$\chi_w = \eta S_r$

$\chi_a = \eta(1 - S_r)$

The previous equations show that the thermal conductivity of soil depends on the degree of saturation (Thomas and Rees 2009).

1.2.2 Heat capacity

The amount of energy stored in a material is defined by the heat capacity. Moreover, the heat capacity of materials is necessary when non-steady solutions are of interest. The heat capacity can be calculated by adding the product of density, heat capacity and volume fraction of different constituents of soil (i.e. solid, water and air) as defined in the following equation (Thomas and Rees 2009):

$C = \chi_s \rho_s c_s + \chi_w \rho_w c_w + \chi_a \rho_a c_a$

Other soil thermal parameters include thermal diffusivity. It is defined as the ratio between thermal conductivity and volumetric heat capacity (heat capacity multiplied by density). It defines the quantity of thermal energy that soil can store during the process of heat transfer (Shein & Mady 2016).

1.2.3 Thermal properties of materials

In this section, some typical thermal properties of different materials are shown. In Table 1, thermal parameters of quartz, water and air are presented (Farouki 1981). While in Table 2, thermal parameters of some types of soils are shown as mentioned in (Hamdhan and Clarke 2010). Moreover, the thermal conductivity of some types of rocks are presented in Table 3 (Côté and Konrad 2005). Finally, thermal parameters of some materials used in the numerical analysis in (Gawecka et al. 2017) are shown in table 4.

Table 1 Thermal properties of some materials (Farouki 1981)

Material	Density (kg/m^3)	Specific heat capacity (J/kg K)	Thermal conductivity (W/m K)
Quartz	2650	733	8.4
Water	1000	4168.8	0.6
Air	1.2	1004.8	0.026

Table 2 Thermal properties of some types of soils (Hamdhan and Clarke 2010)

Soil type	Water content (%)	Specific heat capacity (J/ kg K)	Thermal conductivity (W/m K)
China CLAY (saturated)	46.2	2362	1.52
China CLAY (dry)	0	800	0.25
Sandy CLAY	26.5	1696	1.61
Soft grey fine sandy CLAY	41.4	2200	3.03
Stiff dark grey sandy gravelly CLAY	9.6	1125	3.28
Course SAND (dry)	0	800	0.25
Course SAND (saturated)	20.2	1483	3.72
Fine SAND (dry)	0	800	0.15
Fine SAND (saturated)	24.6	1632	2.75
Medium Sand (dry)	0	800	0.27
Medium SAND (saturated)	20.2	1483	3.34

Table 3 Value of thermal conductivities for some rock types (Côté and Konrad 2005)

Rock type	Density (kg/m^3)	Thermal conductivity(W/m°C)
Anorthosite	2730	1.8
Basalt	2900	1.7
Diabase	2980	2.3
Dolostone	2900	3.8
Gabbro	2920	2.2
Gneiss	2750	2.6
Granite	2750	2.5
Limestone	2700	2.5
Marble	2800	3.2
Quartzite	2650	5.0
Sandstone	2800	3.0
Schist	2650	1.5
Shale	2650	2.0
Syenite	2800	2.0
Trap rock	2900	2.0

Table 4 Thermal properties of some materials used in the numerical analysis in (Gawecka et al. 2017)

Material	Specific weight (kN/m^3)	Volumetric heat capacity (kJ/m^3K)	Thermal conductivity (W/mK)
Concrete	24	1920	2.33
Made Ground	18	1900	1.4
Terrace Gravel	20	1900	1.4
London Clay	20	1820	1.79
Lambeth Group Clay	20	1760	2.2
Lambeth Group Sand	20	1760	2.2
Thanet Sand	20	1760	2.4

1.3 Temperature effects on water and soil behaviour

1.3.1 Effects on water

Various properties of water such as unit weight and viscosity influence the permeability. When temperature increases viscosity decreases rapidly. As a result of the decrease of viscosity, permeability increases. The relation between permeability and viscosity is as follows:

$$k\ \alpha\ \frac{\gamma_w}{\mu}$$

From the previous relation, it is obvious that the permeability is inversely proportional to viscosity. Table 5 shows that increasing the temperature of water leads to decreasing of its viscosity (Farouki 1981).

Table 5 Effect of temperature on viscosity of water (Farouki 1981)

Temperature (°C)	Dynamic viscosity (g/cm s) $*10^{-2}$
-10	-
-5	-
0	1.7921
4	-
5	1.5188
10	1.3077
15	1.1404
20	1.005
25	0.8937
30	0.8007
35	0.7225
40	0.656
45	0.5988
50	0.5494

1.3.2 Effect on soil behaviour

Several laboratory experiments illustrating the influence of temperature on the behaviour of soil are available in the literature. The effects of temperature are classified by the loading paths as distinguished in (Laloui 2001):

1. Thermal (thermal behaviour)
2. Isothermal-mechanical (mechanical behaviour)

The 1st loading path shows the effects of varying the temperature applied to the soil while keeping the stress constant. In addition to this, the 2nd loading path shows the effects of applying mechanical loading and keeping the temperature constant meanwhile.

Thermal

Saturated soil can be considered as a two-phase material, the first phase is solid and the other is fluid. When soil is subjected to heat, all its components dilate. In case of normally consolidated clay, it contracts when subjected to heat and a large portion of this deformation is irreversible after cooling (Laloui 2001). These results can be illustrated by the experiment done by (Campanella and Mitchell 1968).

A specimen of saturated drained illite was subjected to a temperature increase from 66°F to 140°F (19℃ to 60℃) and then the temperature was decreased to 66°F. During the test, the specimen was maintained under constant effective stress of 2 kg/cm^2 (200 kPa). The incremental temperature changes are denoted by points as shown in Figure 2 (Campanella and Mitchell 1968).

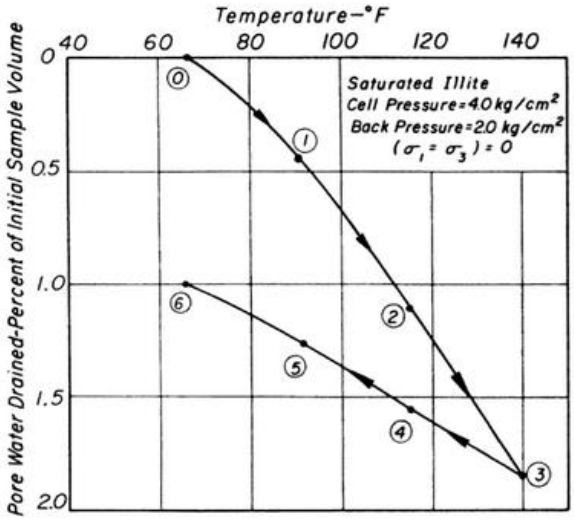

Figure 2 Effects of temperature variation on saturated illite (Campanella and Mitchell 1968)

During heating, the illite sample settles and the volume change can be considered as non-linear. While during cooling, the illite sample shows a linear volume increase. After the end of the heating-cooling cycle, the sample developed irreversible strains due to the thermal loading. Although there was no change in effective stresses, in other words, the soil is densifying (i.e. overconsolidated behaviour) (Laloui 2001).

The magnitude of deformation due to temperature heating-cooling cycle depends on several factors. These factors include plasticity, soil type and overconsolidation ratio (OCR). This can be anticipated from Figure 3. Dilation increases with the increase of OCR. Moreover, the change of the behaviour from contraction to dilation depends on the type of soil (Cekerevac and Laloui 2004).

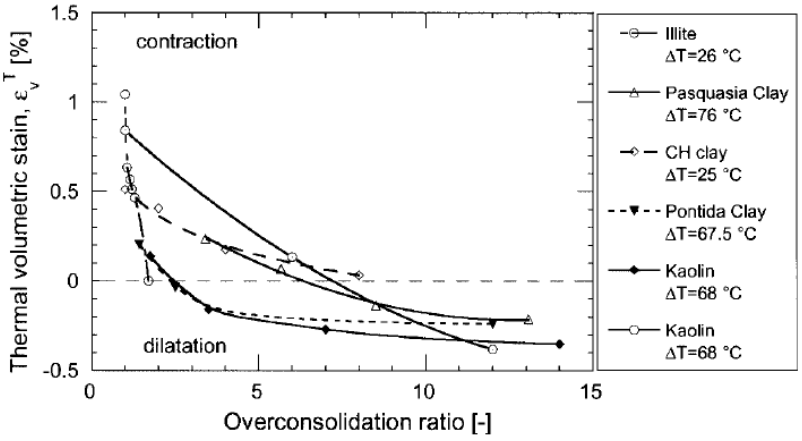

Figure 3 Influence of overconsolidation ratio on the thermal volumetric strain of clays (Cekerevac and Laloui 2004)

Another representation of the effect of OCR on the mechanical behaviour of soil is the experiment done by (Baldi et al. 1991). In this experiment, saturated Boom clay was subjected to a heating-cooling cycle between 20℃ to 95℃. The results are shown in Figure 4. The sample with OCR=6 (overconsolidated sample) dilates when heated and contracts when the temperature decreases. At the end of the cycle, the thermally induced strains are mostly reversible. On the other hand, the sample with OCR=1 (normally consolidated sample) behaves differently. Upon heating, the sample shows contractive behaviour. After cooling, the sample contracts again but with much smaller volumetric strain compared to the heating phase. At the end of the cycle, irreversible strains with large magnitude are developed. Moving to the sample with OCR=2 (lightly overconsolidated sample), it shows similar behaviour to the normally consolidated sample but with developing less irreversible volumetric strains (Gens 2010).

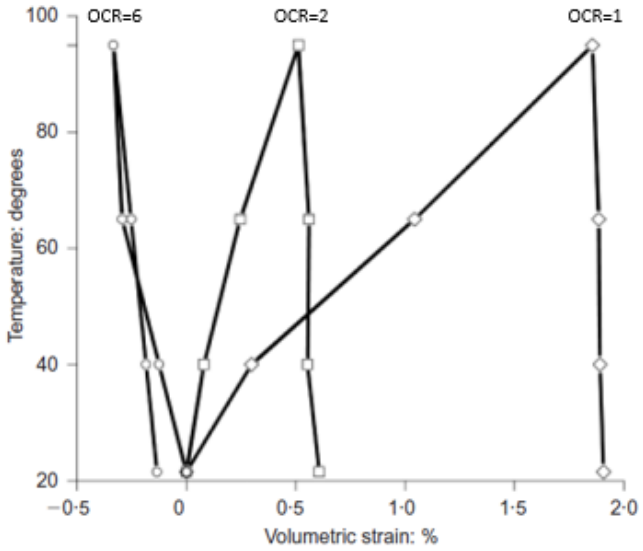

Figure 4 Thermal behaviour of boom clay with different OCRs (Baldi et al. 1991)

Isothermal-mechanical

In this section, the temperature effects on the mechanical behaviour of soil are illustrated by distinguishing between 3 different stress conditions:

1. Isotropic stress conditions
2. Deviatoric stress conditions
3. Undrained behaviour

1. Isotropic stress conditions:

The influence of temperature on consolidation was studied by (Campanella and Mitchell 1968). They performed a triaxial consolidation test on three illite samples. The test was performed at a different temperature for each sample. The temperatures were 76.5°F (25℃), 100°F (38℃) and 124.5°F (52℃). They were consolidated at effective stress of 2 kg/cm^2 (200 kPa). The results are shown in Figure 5 (Campanella and Mitchell 1968).

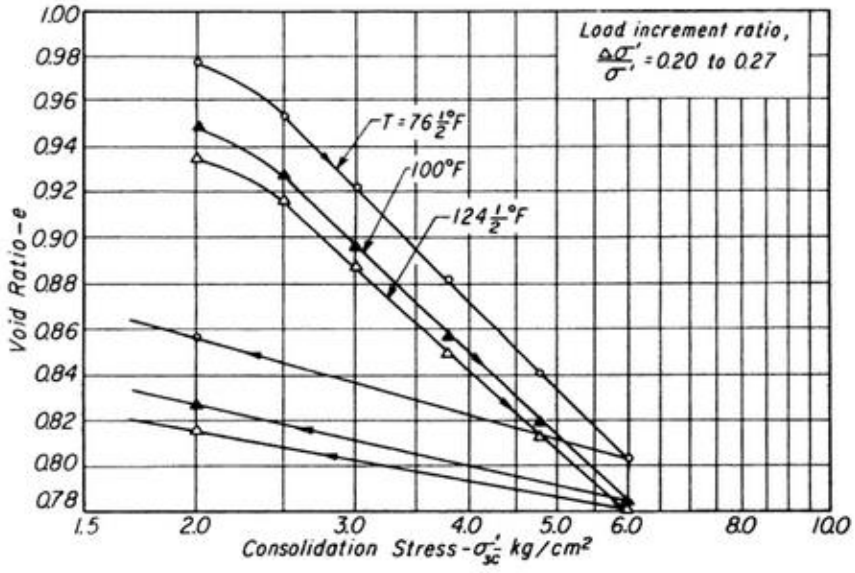

Figure 5 Isotropic consolidation of illite sample at three different temperatures (Campanella and Mitchell 1968)

The results show that the higher the temperature, the lower the void ratio. The three samples had the same void ratio prior to applying the stress, therefore, the reason for the lower void ratios is the temperature. Moreover, the compressibility of illite is not influenced by temperature because all the consolidation curves are parallel. The test concludes that the predominant effect of temperature on consolidation is on void ratios. Increasing the temperature lead to a decrease in void ratio at given initial consolidation stress (Campanella and Mitchell 1968).

Figure 6 shows the influence of temperature on preconsolidation pressure. Several results from the literature are shown in (Cekerevac and Laloui 2004). These results showed that the preconsolidation pressure decreases non-linearly with the increase of temperature. The preconsolidation pressure defines the elastic limit which separates elastic pre-yield from plastic post-yield behaviour in isotropic conditions (Cekerevac and Laloui 2004).

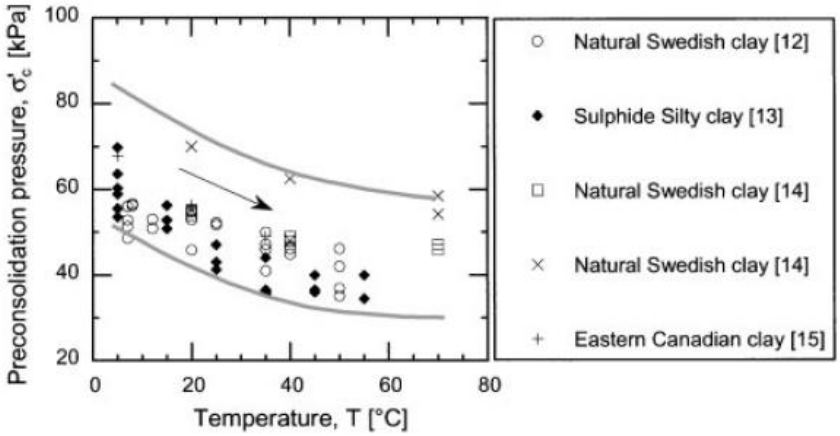

Figure 6 Influence of temperature on preconsolidation pressure (Cekerevac and Laloui 2004)

2.Deviatoric stress conditions:

There is a contradiction in the literature regarding the temperature effects on strength. Some researchers concluded that the increase in temperature decreases strength, while others conclude that heating causes a slight increase in strength (Laloui 2001).

Figure 7 shows the effect of temperature on the friction angle, it can be anticipated that the temperature dependency is not pronounced. The friction angle is mostly independent on the temperature (Cekerevac and Laloui 2004).

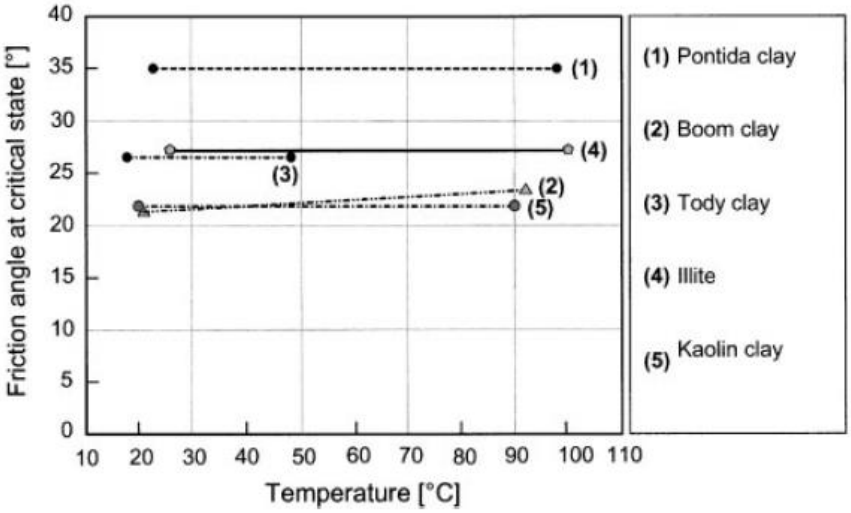

Figure 7 Effect of temperature on friction angle at critical state (Cekerevac and Laloui 2004)

3.Undrained behaviour:

The effect of temperature on the pore water pressures is shown in Figure 8. Newfield clay was subjected to temperature cycling in a triaxial cell. The sample had a water content of 19%. The temperature variation was between 14℃ and 35℃. The effective consolidation pressures were 20, 40 and 60 psi (138, 276 and 414 kPa). The results shown in Figure 8 are for the 40 psi. Porewater pressures increased for the four temperature cycles (Plum and Esrig 1969).

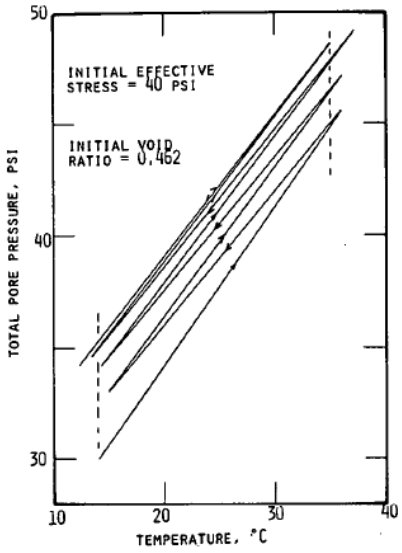

Figure 8 Porewater pressures resulting from undrained temperature cycling of Newfield clay (Plum and Esrig 1969)

2 Thermal analysis in PLAXIS

PLAXIS 2D is a two-dimensional finite element software used to perform stability, deformation and flow analysis for different types of geotechnical problems. This chapter aims to provide the reader with an overview of the thermal features which are implemented in PLAXIS.

PLAXIS thermal features include thermo-hydro-mechanical (THM) coupling for unsaturated soils, fully coupled formulation, availability of temperature for user-defined soil models (UDSM), the effect of temperature on the permeability, anisotropic thermal expansion, vapour flux and thermal boundary conditions such as convective boundary conditions (PLAXIS 2015).

In addition, PLAXIS provides a possibility to carry out analysis for ground freezing and freeze pipes. However, the main limitation of THM implementation in PLAXIS is that temperature does not have an effect on the retention curve and on the mechanical properties (PLAXIS 2015).

For a more comprehensive structure, this chapter is divided into four main topics:

1. Thermal conditions
2. Thermal functions
3. Material thermal properties
4. Calculation types

These topics illustrate the boundary conditions and the material parameters required when thermal calculations are performed.

2.1 Thermal conditions

Thermal boundary conditions are applied to the model to define the transfer of temperature within this model. These thermal boundary conditions need to be defined when thermal calculations are carried out. Thermal conditions can be applied on clusters or on lines (PLAXIS 2018).

2.1.1 Cluster related thermal conditions

Temperature and energy conditions can be defined for clusters. In the case of energy conditions, the cluster can be producing or absorbing energy. In this case, a heat flux, Q, should be defined. While in case of temperature conditions, a prescribed temperature (T_{ref}) should be defined (PLAXIS 2018). Figure 9 shows a cluster (marked in red) where thermal conditions can be applied to.

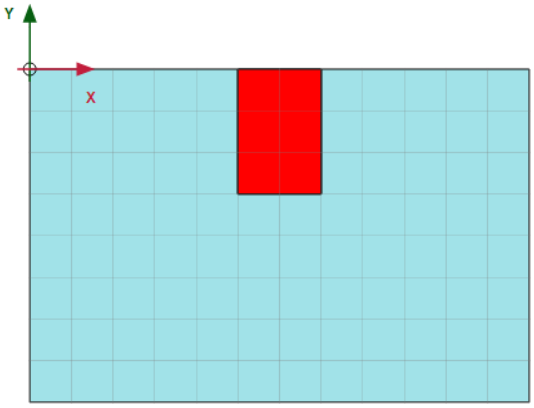

Figure 9 Possibility to apply thermal conditions to clusters

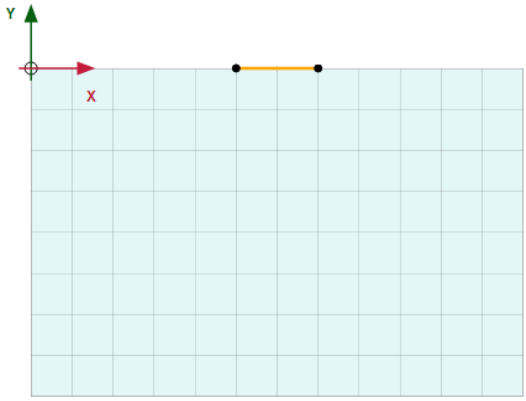

Figure 10 Line thermal boundary condition

2.1.2 Line base thermal flow boundary conditions

Several thermal boundary conditions can be applied to lines. A closed boundary condition prevents heat flux from occurring across it. A temperature boundary condition prescribes a temperature distribution along the boundary. In addition, energy boundary conditions can be applied to lines as well. Inflow and outflow boundary conditions prescribe heat flux into or out of the model respectively. Inflow boundary condition may be used as a heater, whereas, outflow boundary condition may be used as a cooler. The convection boundary condition is a convective boundary where a medium with a certain temperature is defined. This medium transfers its temperature onto that boundary (PLAXIS 2018). An example of a line thermal boundary condition is shown in Figure 10.

2.2 Thermal functions

The change of thermal conditions with time is described by thermal functions. Thermal functions can be applied to thermal flow boundary conditions, clusters and to climate conditions. Three thermal functions are described in this section.

2.2.1 Harmonic

The harmonic function allows the temperature to change harmonically with time. Example of a harmonic function is shown in Figure 11.

2.2.2 Linear

The linear function allows the temperature to decrease or increase linearly with time. Example of a linear function is shown in Figure 12.

2.2.3 Table

The signal from table function allows the definition of a function by inserting time and temperature manually. It can be used to describe a temperature function where linear increase and decrease occur in the same time cycle. Example of a signal form table function is shown in Figure 13.

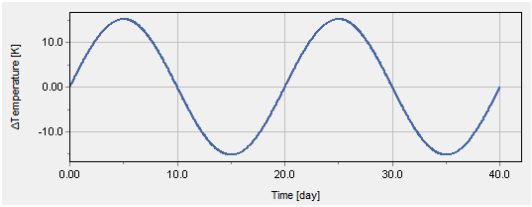

Figure 11 Harmonic function

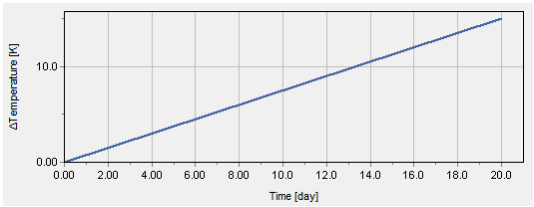

Figure 12 Linear function

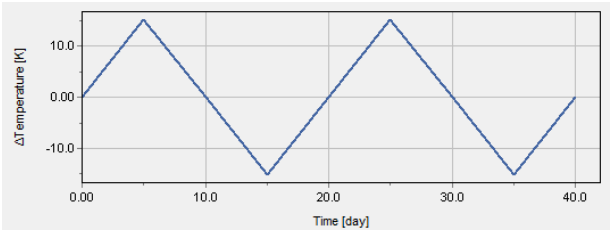

Figure 13 Signal from table function

2.3 Material thermal properties

Thermal parameters are required when temperature effects are considered in the analysis. Thermal parameters include:

- Specific heat capacity
- Thermal conductivity
- Density
- Thermal expansion coefficients
- Unfrozen water content

Specific heat capacity

Heat capacity was defined in the previous chapter. The amount of heat that can be stored in a solid material is obtained by multiplying the density with the specific heat capacity. The heat storage of the soil is composed of the heat storages of the different constitutes of soil (i.e. soil particles and fluid). In PLAXIS the unit of specific heat capacity is (kJ/t/K) (PLAXIS 2018).

The following situations are considered in PLAXIS:

- Non-porous material: $(\rho c)_{soil} = \rho_s c_s$
- Dry material: $(\rho c)_{soil} = (1 - n)\rho_s c_s$

Thermal conductivity

Thermal conductivity was defined in the previous chapter. The total thermal conductivity of soil is composed of thermal conductivities of the different constitutes of soil (i.e. soil particles and pore fluid). In PLAXIS the unit of thermal conductivity is (kW/m/K) (PLAXIS 2018).

The following situations are considered in PLAXIS:

- Non-porous material: $\lambda_{soil} = \lambda_s$
- Dry material: $\lambda_{soil} = (1 - n)\lambda_s$
- Phase transition (e.g. frozen soil) $\lambda_{soil} = (1 - n)\lambda_s + nS[(1 - w_U)\lambda_i + w_U\lambda_w] + n(1 - S)\lambda_v$
- Other cases: $\lambda_{soil} = (1 - n)\lambda_s + nS\lambda_w + n(1 - S)\lambda_v$

Density

The density of soil material describes the density of soil particles. In PLAXIS the unit of soil density is t/m^3. The density contributes to the total heat capacity (PLAXIS 2018).

Thermal expansion coefficients

The thermal expansion is the strain per unit of temperature. It describes how much the material expands when the temperature increases. There are three expansion coefficients for the three directions (x, y and z). If the thermal expansion coefficients are equal in the three directions, hence the thermal expansion is isotropic. PLAXIS can deal with anisotropic thermal expansions as well. In PLAXIS the unit of thermal expansion is (1/K) (PLAXIS 2018).

Unfrozen water content

When dealing with frozen soil situations such as ground freezing and permafrost soils, the unfrozen water content can be defined. When the soil is frozen, part of the water inside the soil is in solid-state and another part may be in liquid state. To describe this phenomenon, the unfrozen water content defines the remaining portion of water in liquid state as a function of temperature (PLAXIS 2018).

2.4 Calculation types

This part defines the possibilities of thermal calculations presented in PLAXIS. In PLAXIS, it is possible to perform:

- Thermal calculations
- Coupled analysis (thermo-hydraulic (TH) coupling)
- Flow analysis (climate conditions)

2.4.1 Thermal calculations

The thermal calculations include the following types (PLAXIS 2018):

- Steady-state thermal flow
- Transient thermal flow
- Using temperatures from the previous phase
- Earth gradient

Steady-state thermal flow

Steady-state thermal flow depends on the thermal flow boundary conditions. The temperature distribution across the model is obtained by a steady-state thermal flow finite elements calculation (PLAXIS 2018).

Transient thermal flow

Transient thermal flow depends on the thermal flow boundary conditions. The temperature distribution across the model is obtained by a transient thermal flow finite element calculation (PLAXIS 2018).

The difference between steady-state and transient thermal flow is in time. In transient thermal flow, the heat transfer changes with time until a steady-state is reached. In case of transient thermal flow, time-dependent functions can be assigned to thermal boundary conditions.

Using temperatures from the previous phase

Using temperatures from the previous phase connects the current phase to the previous one. The temperature distribution in the current phase starts with a value equals to the previous phase (PLAXIS 2018).

Earth gradient

Earth gradient depends on the thermal flow parameters defined for the model. The thermal flow parameters include the following:

- Reference temperature (prescribed temperature defined in Kelvin (K))
- Reference height (prescribed height defined in Meter (m))
- Earth gradient (prescribed gradient defined in Kelvins per Meter (K/m))

Earth gradient is not a finite element calculation (PLAXIS 2018). There are three scenarios when the reference height is assigned:

- h_{ref} = ground level
- h_{ref} < ground level
- h_{ref} > ground level

h_{ref} = ground level

When the reference height is the same as the ground level, the temperature distribution in the model is calculated in terms of multiplying the earth gradient by the depth of the model. Figure 14 is used to illustrate the procedure. The model in Figure 14 is 20 m deep, the reference temperature is 280 K and the earth gradient has a value of 0.025 K/m.

The temperature on top of the model is 280 K, while the temperature at the bottom of the model equals to $280 + (0.025 * 20) = 280 + 0.5 = 280.5$ K

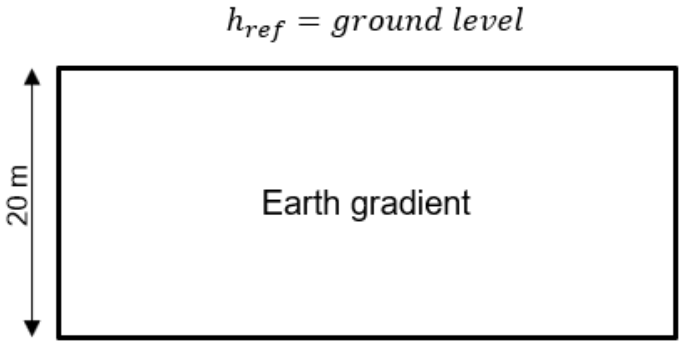

Figure 14 h_{ref} = ground level

h_{ref} < ground level

When the reference height is lower than the ground level, the temperature distribution in the height between the ground level and the reference height is calculated by a steady-state thermal flow. Below the reference height, the temperature distribution is calculated by the earth gradient.

Figure 15 is used to illustrate the procedure; the reference height is 5 m lower than the ground level. In this 5 m, the temperature distribution is calculated in terms of steady-state thermal flow, while below the reference height the temperature distribution is calculated in terms of earth gradient.

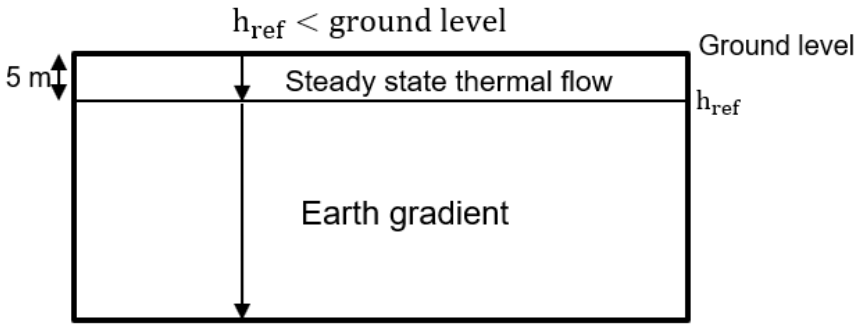

Figure 15 h_{ref}< ground level

h_{ref} > ground level

When the reference height is higher than the ground level, the temperature distribution between the reference height and the ground level is calculated by earth gradient. Figure 16 is used to illustrate the procedure. The model has a depth of 20 m, the reference height is set to 10 m above the ground level, the reference temperature is 280 K and the earth gradient is 0.025 K/m. The temperature at the ground level equals to $280 + (0.025 * 10) = 280.25$ K. While the temperature at the bottom of the model equals to $280.25 + (0.025 * 20) = 280.75$ K.

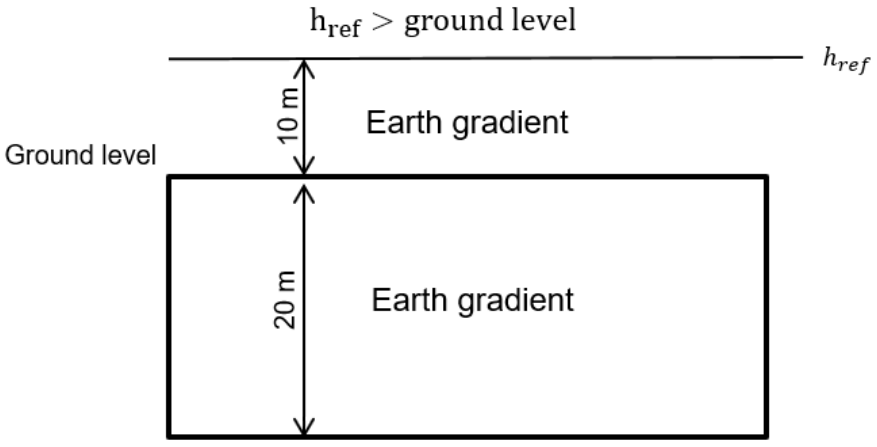

Figure 16 h_{ref} > ground level

2.4.2 Coupled analysis

Groundwater flow plays an important role in the transfer of the temperature in the ground, therefore there are coupling effects between thermal and hydraulic behaviour (TH coupling). PLAXIS is capable of performing semi-coupled TH-M analysis as well as fully-coupled transient THM calculations. The former can be used to analyse the effects of temperature on stress and displacements (i.e. time in not considered). The latter can be used for time-dependent problems when the effects of temperature on stress, deformation and groundwater flow are of interest (i.e. time is considered). The possible combinations for thermal calculations are shown in Table 6 (PLAXIS 2018).

Table 6 Possible combinations for thermal calculations (PLAXIS 2018)

Calculation type	Pore pressure calculation type	Thermal calculation type
Flow only	Phreatic	Earth gradient Steady-state thermal flow Transient thermal flow
Flow only	Steady-state groundwater flow	Earth gradient Steady-state thermal flow
Plastic	Phreatic	Earth gradient Use temperatures from the previous phase Steady-state thermal flow
Plastic	Use pressures from the previous phase	Earth gradient Use temperatures from the previous phase Steady-state thermal flow
Plastic	Steady-state groundwater flow	Earth gradient Use temperatures from the previous phase Steady-state thermal flow
Fully coupled flow-deformation	Transient groundwater flow	Use temperatures from the previous phase

Climate conditions

Climate conditions are applied on the ground surface. For the climate conditions, the following is defined (PLAXIS 2018):

- Air temperature (temperature of the air)
- Surface transfer (heat transfer coefficient)
- Time dependency (if the air temperature is not constant, temperature functions can be defined)

3 Preliminary studies

In this chapter, three preliminary studies are presented:

1. 1D heat flow
2. Temperature functions study
3. Sensitivity analysis

The first study is a simple 1D heat flow model investigated in PLAXIS and the results are compared to the analytical solution presented in (Willemsen 2011). Moreover, this model is used to carry out a study showing the importance of choosing adequate values of time steps and their influence on the accuracy of the results. Finally, a comparison between PLAXIS and CODE_BRIGHT was performed.

The second study is a temperature functions study. Temperature functions were discussed in chapter 3 (section 3.2). The study shows the effect of the amplitude on the final results and the difference between harmonic and linear functions.

The third study is a sensitivity analysis for the soil thermal parameters. Thermal conductivity and heat capacity were varied and the influence of this variation on the final result was investigated.

3.1 1D heat flow

3.1.1 Analytical solution and model

The temperature evolution in a homogeneous non-porous column of material is described as follows (Willemsen 2011):

$$T(y,t) = U(y,t) + V(y)$$

The previous equation consists of two components, transient component $U(y,t)$ and a steady-state component $V(y)$. These two components are described as follows (Willemsen 2011):

$$V(y) = T_0 - \frac{Q}{\lambda} y$$

$$U(y,t) = \frac{8Q}{\lambda\pi^2} \sum_{i=0}^{\infty} \frac{(-1)^i}{(2i+1)^2} \sin\left(\left(i+\frac{1}{2}\right)\pi y\right) e^{-\frac{\pi^2 \lambda t (1+i)^2}{C_s \rho_s}}$$

Adding the previous two equations results in the temperature evolution (Willemsen 2011):

$$T(y,t) = \frac{8Q}{\lambda\pi^2} \sum_{i=0}^{\infty} \frac{(-1)^i}{(2i+1)^2} \sin\left(\left(i+\frac{1}{2}\right)\pi y\right) e^{-\frac{\pi^2 \lambda t (1+i)^2}{C_s \rho_s}} - \frac{Q}{\lambda} y + T_0$$

The geometry for the column used for this study is shown in Figure 17. The column has a length of 0.1 m and a height of 1 m. The parameters used for this study is shown in Table 7.

At the beginning of the analysis (t=0), the column has a uniform temperature T_0. A heat flux Q is applied at the top of the column and the temperature at the bottom is fixed by a thermal boundary condition with a value equal to T_0.

Table 7 Parameters used for the 1D study (Willemsen 2011)

Drainage type	Non-porous
E	$200 \times 10^3\ kN/m^3$
ν	0.3
T_0	273.15 K
Q	-773.15(W/m^2)
λ	14.6 ($W\ /m\ K$)
C_S	460 ($J\ /kg\ K$)
ρ_s	7800 (kg/m^3)
$\alpha_x, \alpha_y, \alpha_z$	$0.01\ \times 10^{-3}\ 1/K$

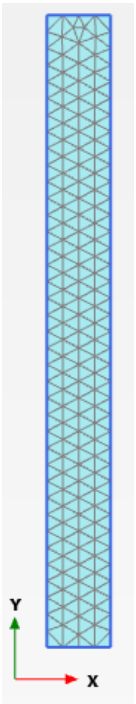

Figure 17 Geometry of the column

3.1.2 Time steps study

For this study, a time interval of 500,000 seconds was chosen. Moreover, 4 different time steps were chosen to compare their influence on the final results. The results are shown in Figure 18.

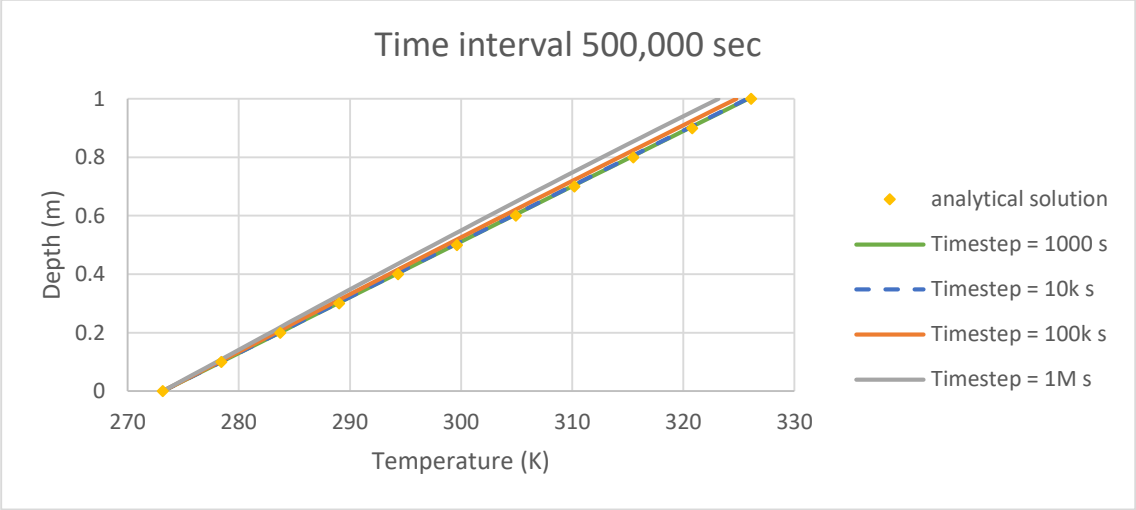

Figure 18 The influence of Time steps on the final result

Setting the time step to 1000 and 10,000 seconds lead to results matching the results obtained from the analytical solution. While increasing the value of time step to 100,000 and 1,000,000 seconds deviated from the analytical solution.

In addition to this study, another investigation was carried out to check the influence of maximum time steps on the number of calculation steps. For this study, four time steps were chosen 4000, 40k, 400k, and 4M seconds. For each time step, the maximum time steps were varied. The results for the 4000 seconds time step are shown in Figure 19. The results for the other time steps are shown in the appendix (A.1).

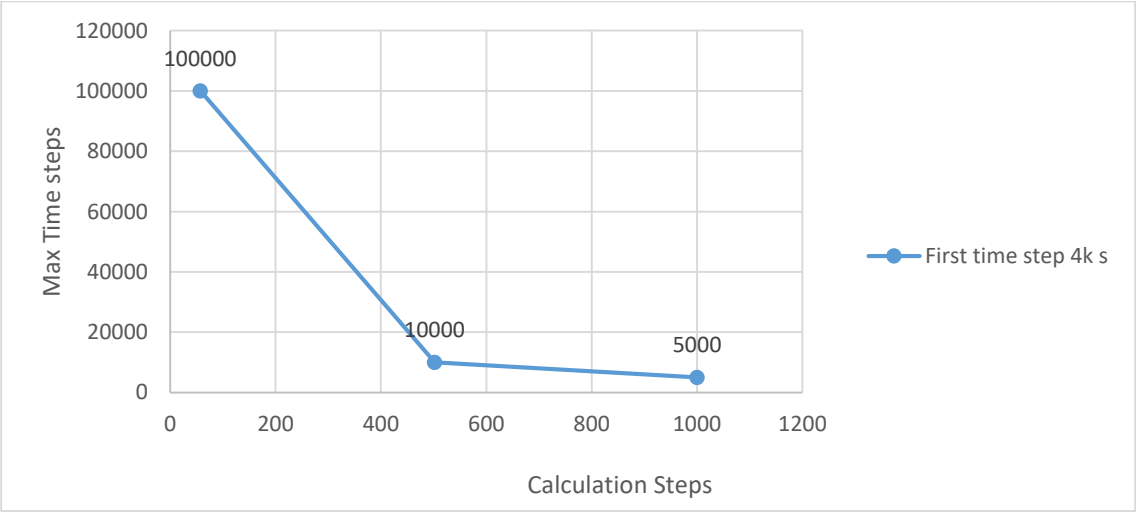

Figure 19 influence of maximum time steps on the number of calculation steps (4000 s)

Three values for maximum time steps were chosen, 5000, 10000 and 100000 seconds. Increasing the maximum time steps lead to a dramatic decrease in the number of calculation steps.

3.1.3 Comparison with CODE_BRIGHT

CODE_BRIGHT is a tool used to handle coupled problems in the geological medium. The code is able to couple mechanical, hydraulic and thermal problems in geological medium (Codebright 2018).

The same column investigated in the previous section is used for the comparison. The geometry of the model in CODE_BRIGHT is shown in Figure 20. The same parameters used in PLAXIS were used for the analysis done by CODE_BRIGHT. The results obtained from CODE_BRIGHT are shown in Figure 21 (the temperature in CODE_BRIGHT is in Celsius and was converted to Kelvin for comparison with PLAXIS). The results obtained from PLAXIS and CODE_BRIGHT perfectly fit.

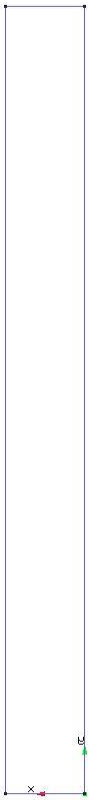

Figure 20 Geometry of the model in CODE_BRIGHT

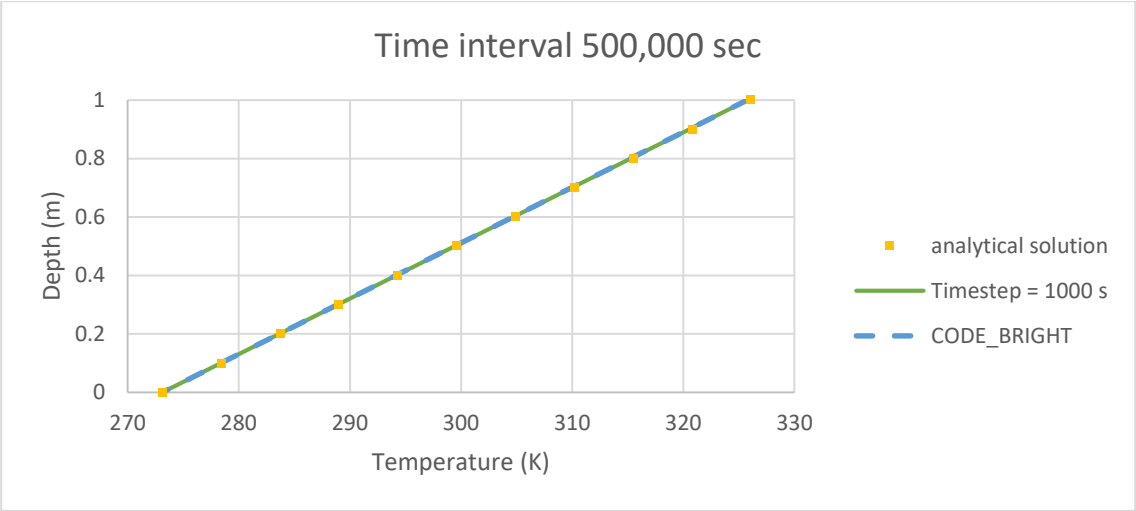

Figure 21 Comparison between analytical solution, PLAXIS and CODE_BRIGHT

3.2 Temperature functions study

The model used for this study is available in PLAXIS tutorial manual (lesson 15) (PLAXIS 2018). The model is shown in Figure 22, the soil parameters used for this study are described in PLAXIS tutorial manual (lesson 15) and shown in Table 7. Two temperature functions were studied:

- Harmonic temperature function
- Linear temperature function (defined as signal from table function)

The temperature is applied as a climate condition. The temperature function is assigned to this climate condition. The period of the cycle of the two functions was 40 days. Six cycles were studied (after 40, 80, 120, 160, 200 and 240 days), the amplitude variation was as follows:

- 5
- 10
- 15
- 20

The amplitude of 5 means that the temperature increases 5 K and decreases 5 K within the same cycle. Figures 23 and 24 show the linear and harmonic temperature functions respectively. A vertical cross-section exactly in the middle of the model was chosen to plot the temperature distribution along the depth of the model.

Table 8 soil parameters

Parameter	Value
Material model	Mohr-Coulomb
Soil unit weight above phreatic level γ_{unsat}	20 kN/m^3
Soil unit weight below phreatic level γ_{sat}	20 kN/m^3
Young's modulus	40,000 kN/m^2
Poisson's ration ν	0.2
Friction angle ϕ	32°
Cohesion c	2 kN/m^2
Permeability (x& y directions) (k_x & k_y)	0.2877 m/day

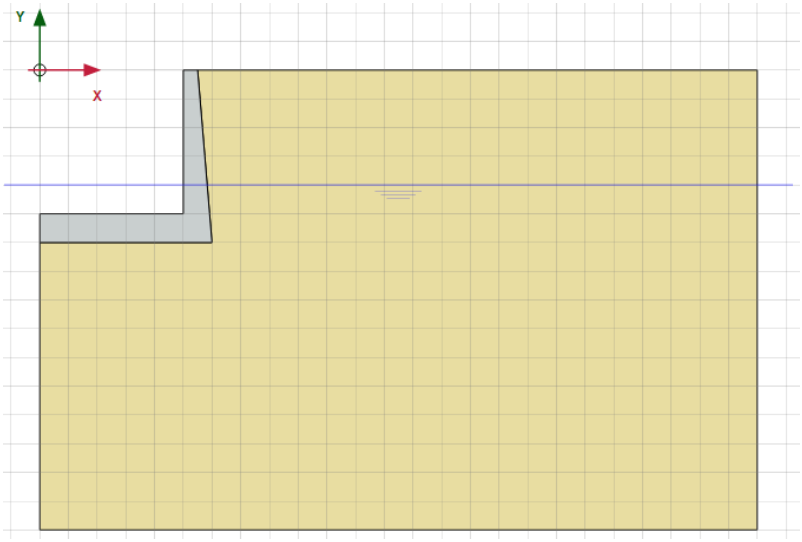

Figure 22 Model used for temperature functions study

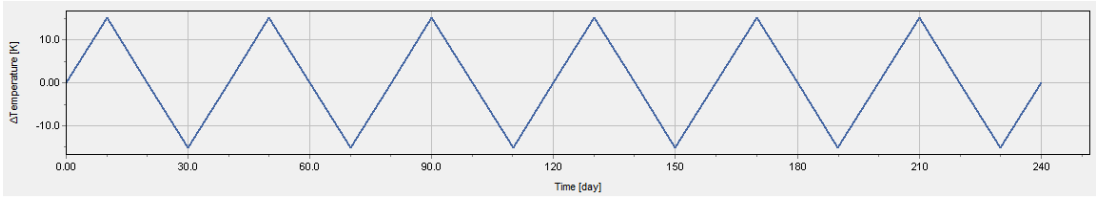

Figure 23 Linear function (amplitude 15)

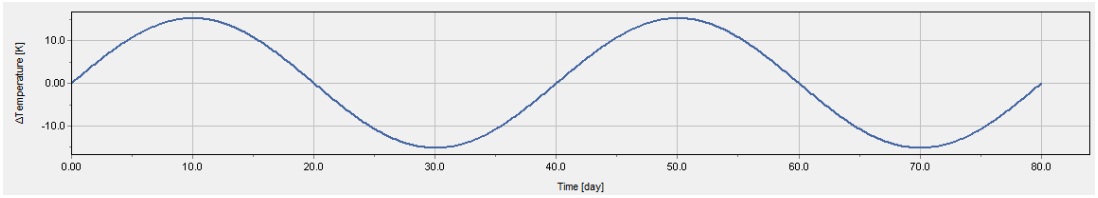

Figure 24 Harmonic function (amplitude 15)

The temperature distribution for the harmonic function for different amplitudes is shown in Figures 25, 26, 27 and 28. Harmonic function with low amplitude (5 & 10) lead to illogical results. For example, there is no explanation for the different temperature distribution after the 6th cycle (240 days) in Figure 25 and after the 4th cycle (160 days) in Figure 26. However, increasing the amplitude (15 & 20) lead to logical results. The same behaviour was observed for the linear function. The results for the linear function is shown in the appendix (A.2).

Finally, a comparison between the two temperature functions was carried out. Figure 29 shows the comparison after the 1st cycle (the comparison after the other cycles is shown in the appendix (A.2)). The soil seems to store more temperature in case of harmonic function.

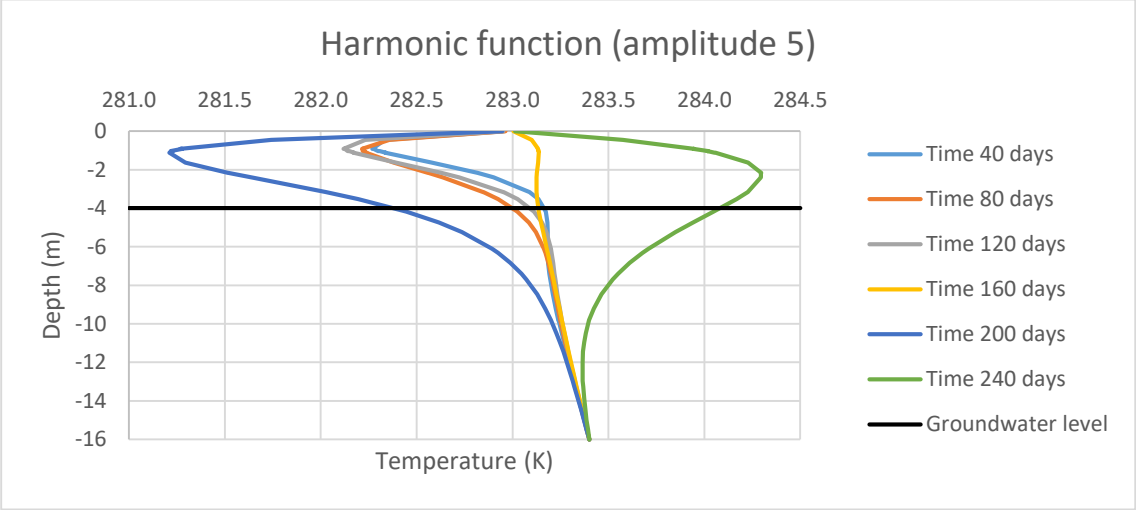

Figure 25 Temperature distribution after 6 cycles for harmonic function (amplitude 5)

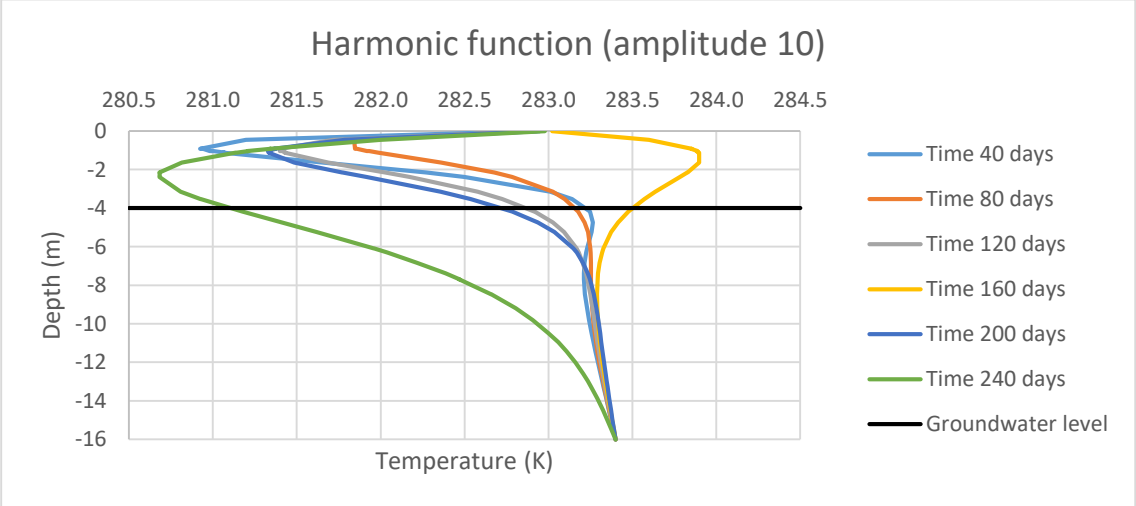

Figure 26 Temperature distribution after 6 cycles for harmonic function (amplitude 10)

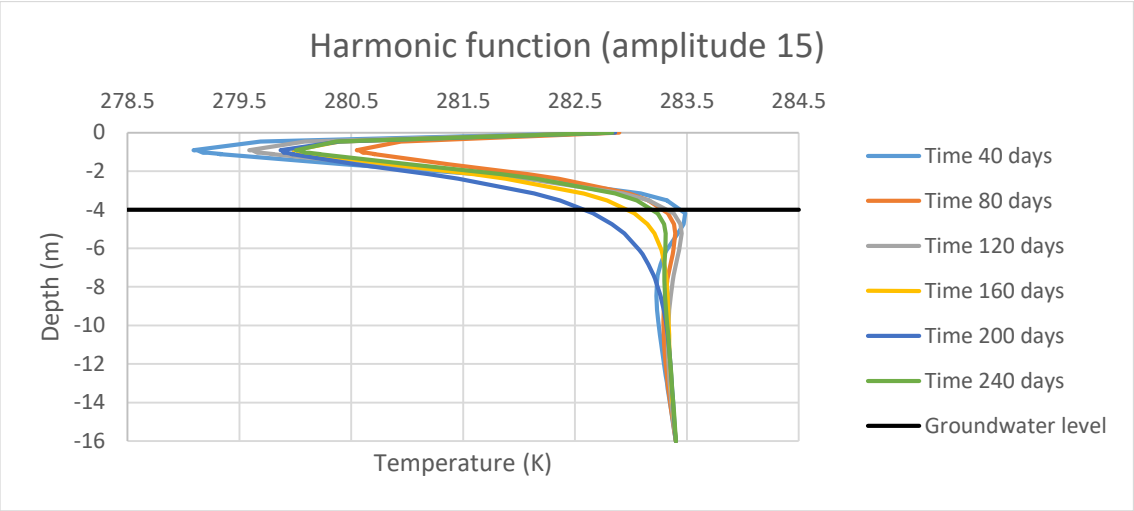

Figure 27 Temperature distribution after 6 cycles for harmonic function (amplitude 15)

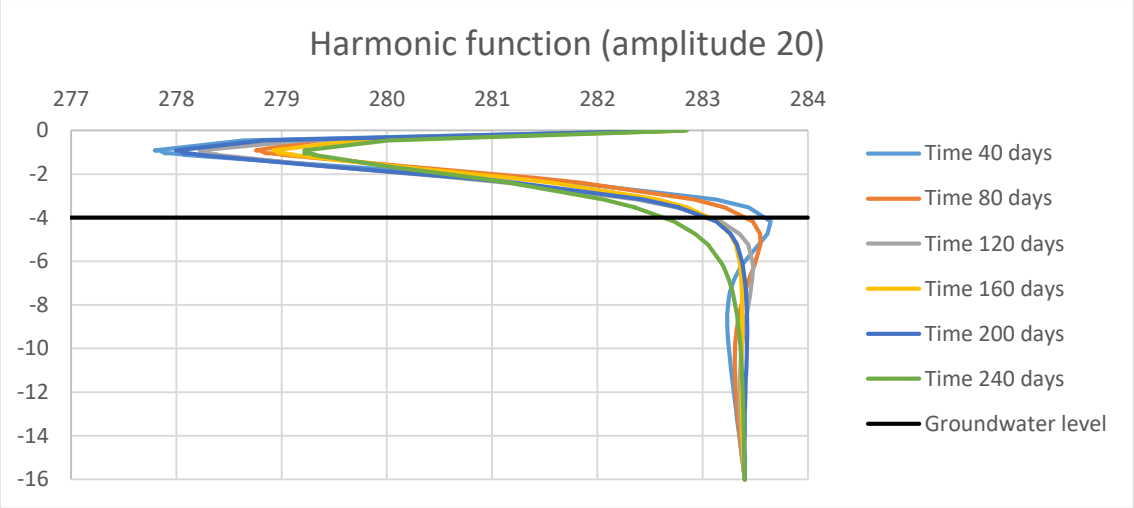

Figure 28 Temperature distribution after 6 cycles for harmonic function (amplitude 20)

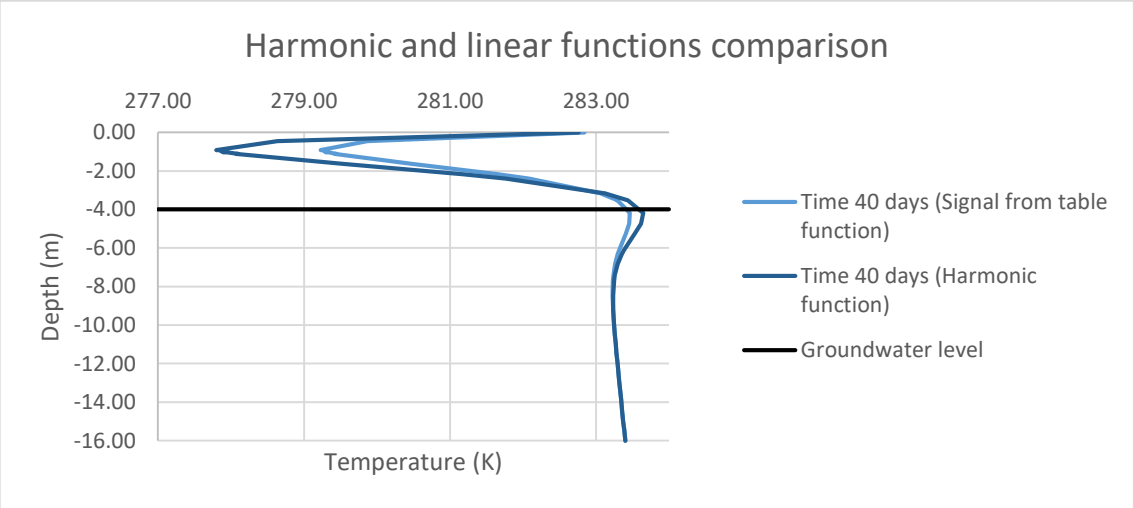

Figure 29 Harmonic and linear functions comparison after 40 days (1st cycle)

3.3 Sensitivity analysis

The model used for the thermal parameters sensitivity analysis is shown in Figure 30. It is a simplified version of the model used in the previous study. The temperature was applied as a climate condition and linear function (defined as signal from table function) with an amplitude of 15 was defined (Figure 31). The soil parameters are shown in Table 7.

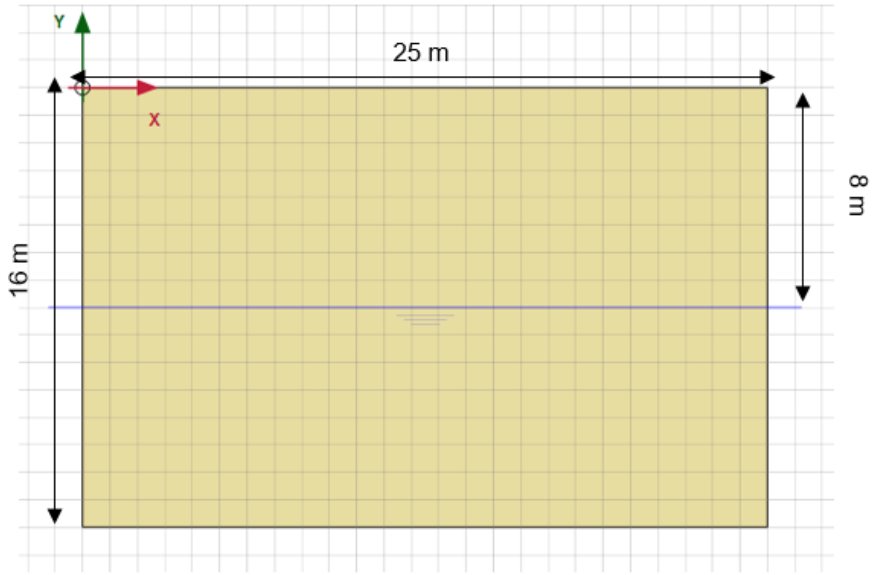

Figure 30 Sensitivity analysis model

The values used for the thermal conductivity are shown in Table 9, while the values used for the heat capacity are shown in Table 10. Regarding the thermal conductivity, a value of 4 W/m K was used as a first setup. Afterwards, this value was multiplied and divided by 10 to obtain high and low values respectively. The same procedure was done for the heat capacity.

Table 9 Thermal conductivity sensitivity analysis

Setup	Thermal conductivity (W/m K)
First setup	4
High value	40
Low value	0.4

Table 10 Heat capacity sensitivity analysis

Setup	Heat capacity (kJ/t K)
First setup	860
High value	8600
Low value	86

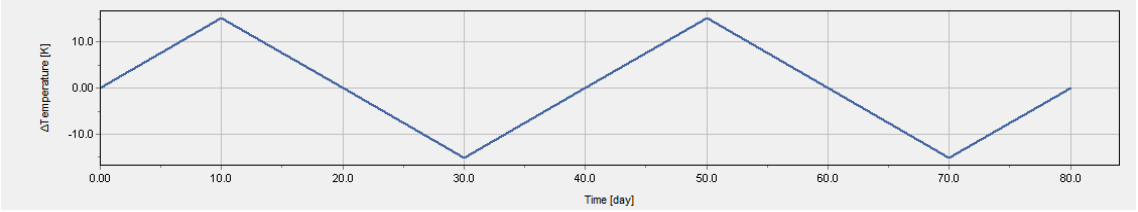

Figure 31 Temperature function used for the sensitivity analysis

The cross-section used for plotting the temperature distribution is located in the middle of the model as shown in Figure 32. The temperature is plotted after the first 10 days (1st temperature increment) and 30 days (1st temperature decrement).

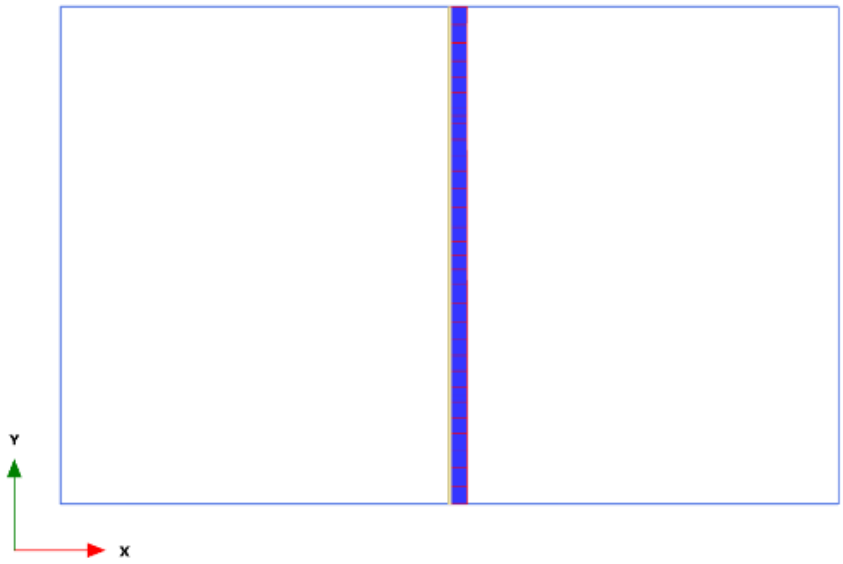

Figure 32 Cross-section used for plotting the temperature

3.3.1 Thermal conductivity

The temperature distribution after 10 days is shown in Figure 33. Figure 33 shows that the higher the thermal conductivity, the more temperature is transferred to the soil. The reason for this is that increasing the thermal conductivity increases the rate by which the heat is transferred. The temperature distribution after 30 days is shown in the appendix (A.3)

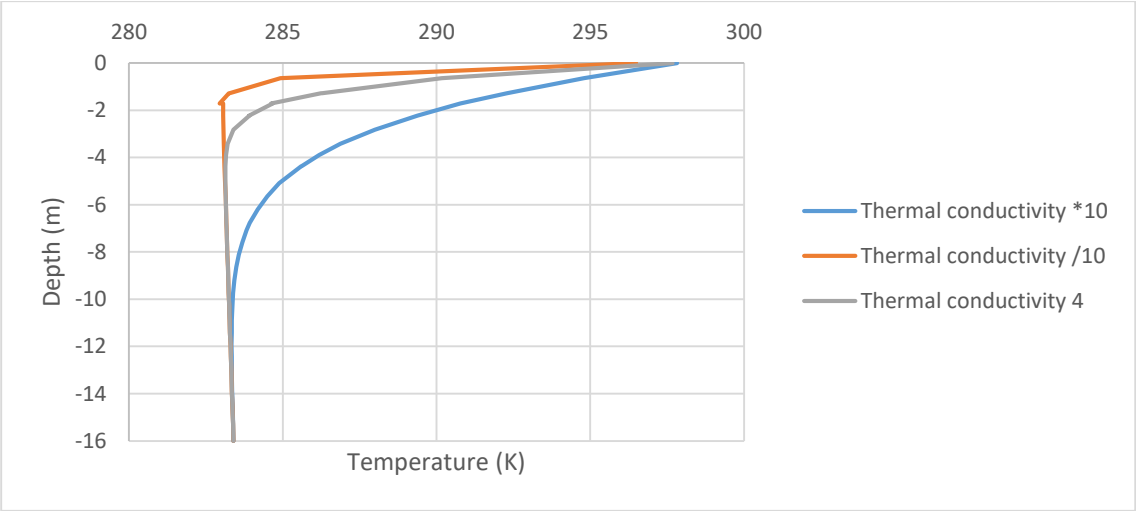

Figure 33 Thermal conductivity sensitivity analysis after 10 days

3.3.2 Heat capacity

The temperature distribution after 10 days is shown in Figure 34. Figure 33 shows that the higher the heat capacity, the less temperature is transferred to the soil. The reason for this is that increasing the heat capacity increases the energy required to change the temperature of the soil. In other words, the lower the heat capacity, the easier the change of the temperature of the soil. The temperature distribution after 30 days is shown in the appendix (A.3)

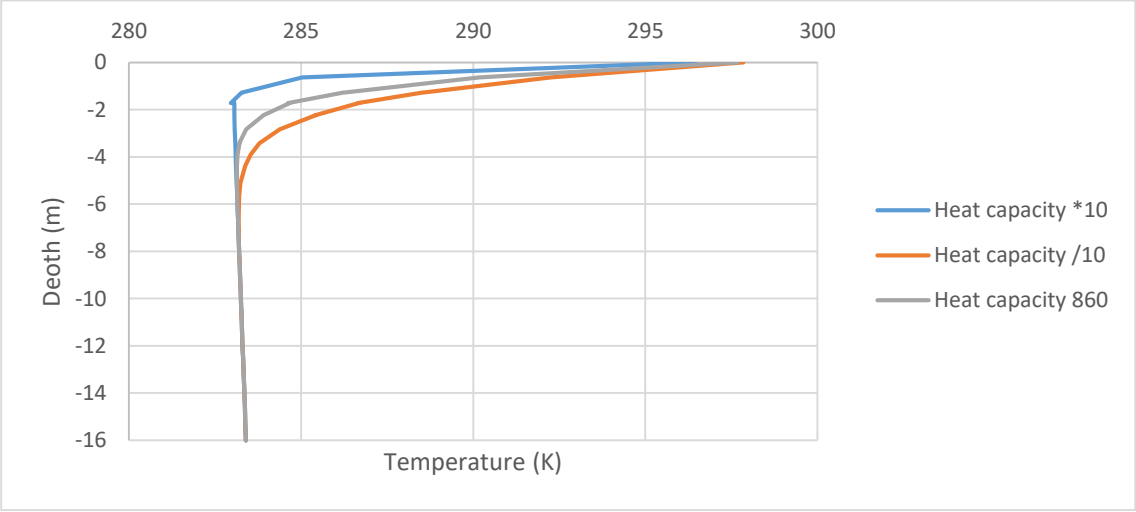

Figure 34 Heat capacity sensitivity analysis after 10 days

4 Groundwater flow study

The concept behind this study is to investigate the effect of groundwater flow on the temperature distribution. In order to achieve this, it was necessary to define a groundwater flow in the model. It was done by modelling two water levels with head difference. The model is shown in Figure 35. Moreover, a rectangular cluster was defined to act as a source of temperature. The soil parameters are shown in Table 8.

This chapter includes three sections, the first section illustrates the first trial to apply temperature by assigning cluster thermal conditions to the rectangular cluster. The second section describes the second approach used for applying temperature by defining thermal boundary conditions on the clusters' sides. Finally, a new model was created with horizontal groundwater flow. This model does not feature groundwater flow, however, it represents a possible groundwater table scenario.

The analysis is based on applying an initial uniform temperature of 290 K (16.85 ℃) through the model. Afterwards, the heating phase starts by applying a temperature of 320 K (46.85 ℃) to the rectangular cluster (Figure 36). Then, time analysis was performed to check the temperature distribution with the groundwater flow. For this reason, it was necessary to keep the temperature inside the cluster constant throughout the time analysis.

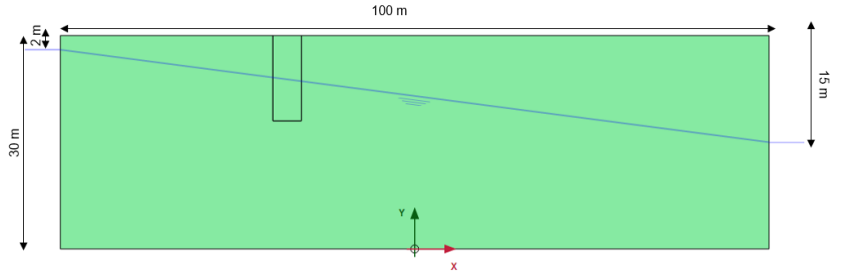

Figure 35 Groundwater flow study model

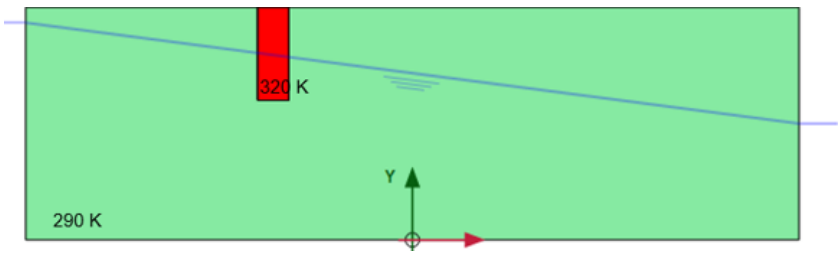

Figure 36 Temperature inside the cluster and across the model

4.1 Cluster thermal condition

The first approach was to apply a cluster thermal condition to the rectangular cluster. However, this approach did not achieve the requirement to keep the temperature constant inside the cluster throughout the time analysis.

In order to investigate time effects, fully coupled flow-deformation analysis should be used for calculation type. When using this calculation type, it is only possible to use temperatures from the previous calculation phase, which in turn means that the cluster thermal boundary condition will not be active in the time analysis. As a consequence, the temperature inside the cluster dissipates as time passes. The temperature distribution across the model after 1000 days is shown in Figure 37. Other time intervals are shown in the appendix (B.1)

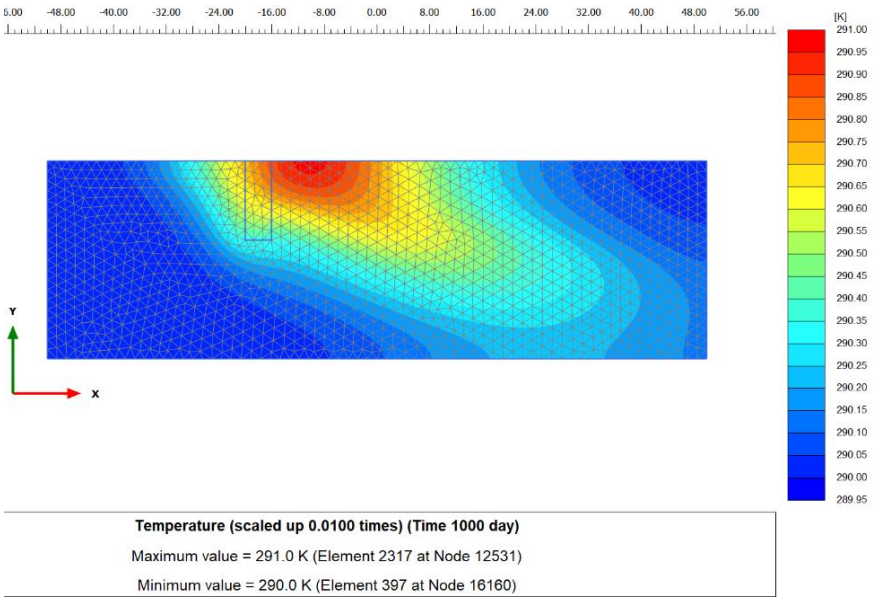

Figure 37 Temperature distribution after 1000 days for cluster thermal boundary condition

The cluster was modelled as a dry cluster, which means that no groundwater flow was allowed inside the cluster. The groundwater flow is shown in Figure 38.

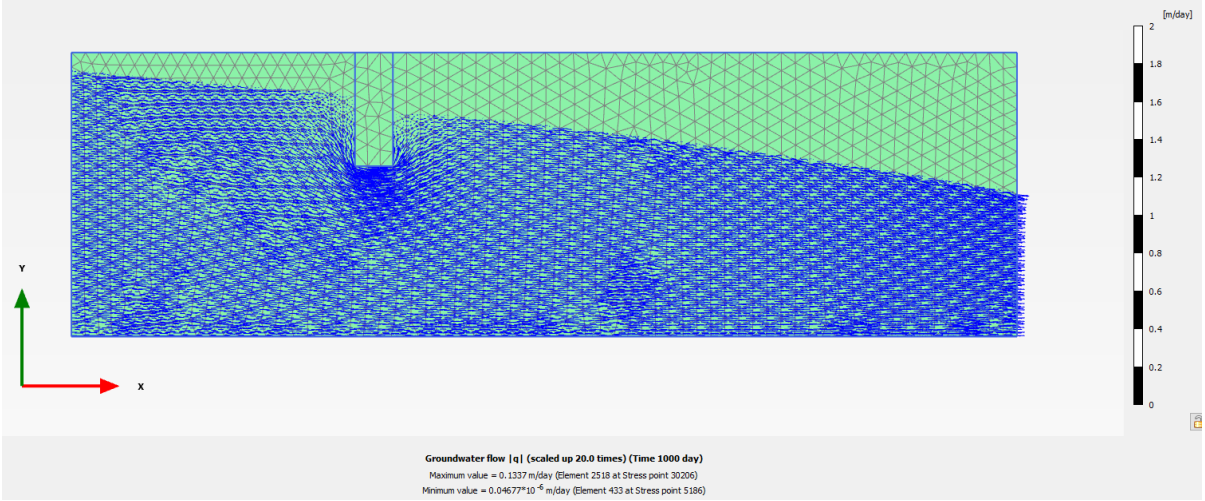

Figure 38 Groundwater flow after 1000 days

4.2 Thermal boundary conditions

As mentioned before, it was required to keep the temperature within the rectangular cluster constant throughout the time analysis. The first approach could not fulfil this requirement which leads to the necessity to perform another trial.

In this approach, thermal boundary conditions were defined along the sides of the rectangular cluster as seen in Figure 39. The three thermal boundary conditions had a temperature of 320 K.

The three red nodes on the thermal boundary conditions are used to check the instant application of the temperature. The temperature in the lower node with respect to time is shown in Figure 40. The results of the other nodes are shown in the appendix (B.2).

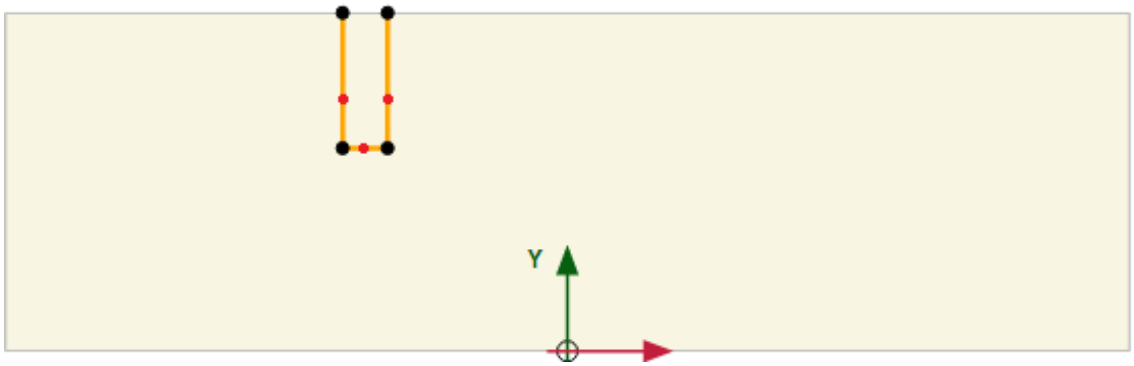

Figure 39 Thermal boundary conditions applied on the sides of the rectangular cluster

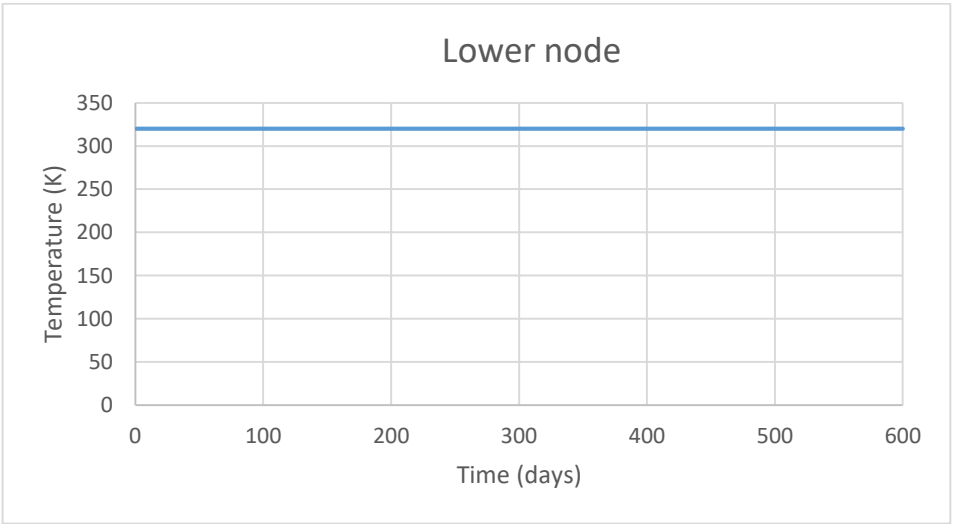

Figure 40 Temperature in the lower node

4.2.1 Comparison between different soil behaviour

Three different behaviours for the soil inside the rectangular cluster were compared:

1. Dry cluster
2. Non-porous cluster
3. Drained behaviour

4 cross-sections were chosen for the comparison. The cross-sections are shown in Figure 41. Cross-section 1 is located on the left side of the rectangular cluster, while cross-section 3 is located on the right side of the cluster. Cross-section 2 is located exactly in the middle of the cluster, while cross-section 4 is located at the right boundary of the model. Three time intervals were chosen for the comparison, after 100, 600 and 1500 days. The temperature distribution at the four cross-sections after 600 days is shown in Figures (42-45). The other results are shown in the appendix (B.2).

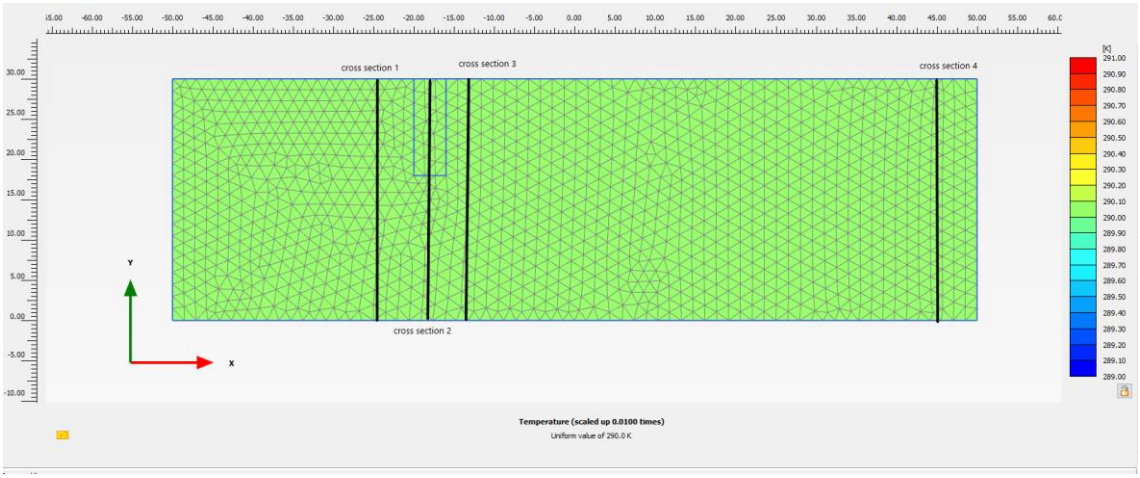

Figure 41 location of the cross-sections (groundwater flow study)

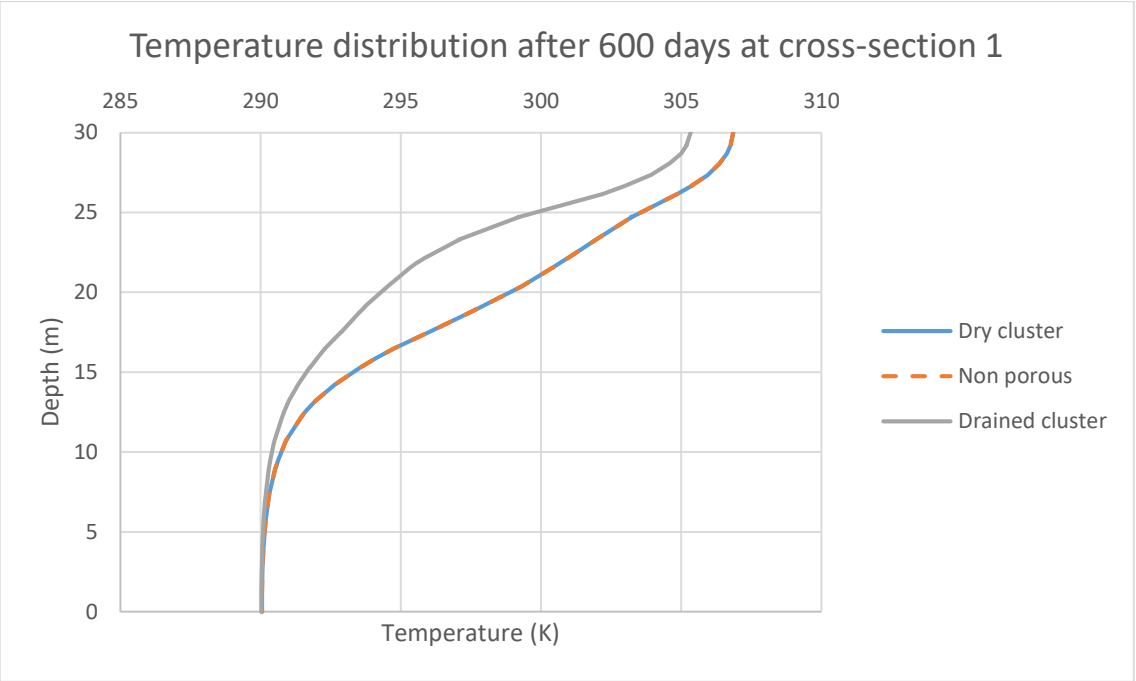

Figure 42 Temperature distribution at cross-section 1 after 600 days

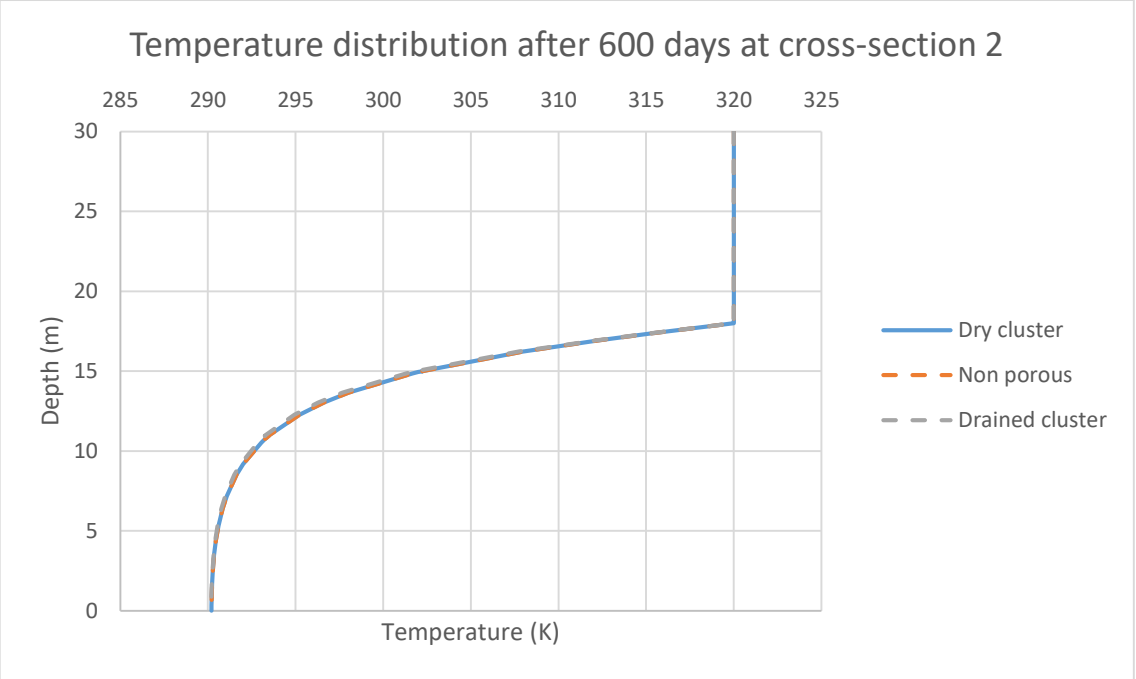

Figure 43 Temperature distribution at cross-section 2 after 600 days

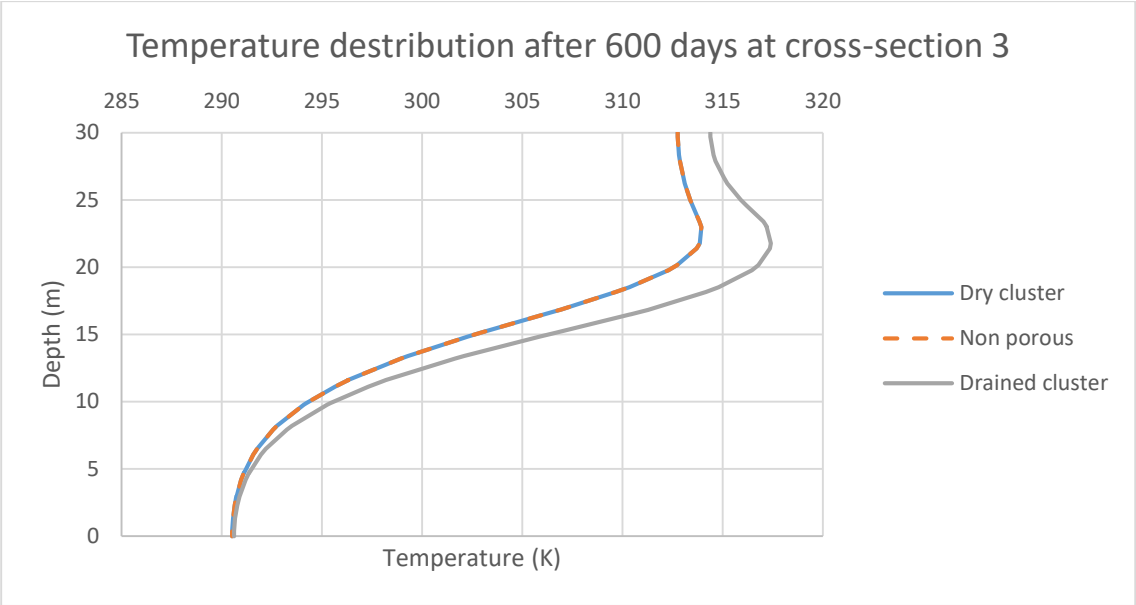

Figure 44 Temperature distribution at cross-section 3 after 600 days

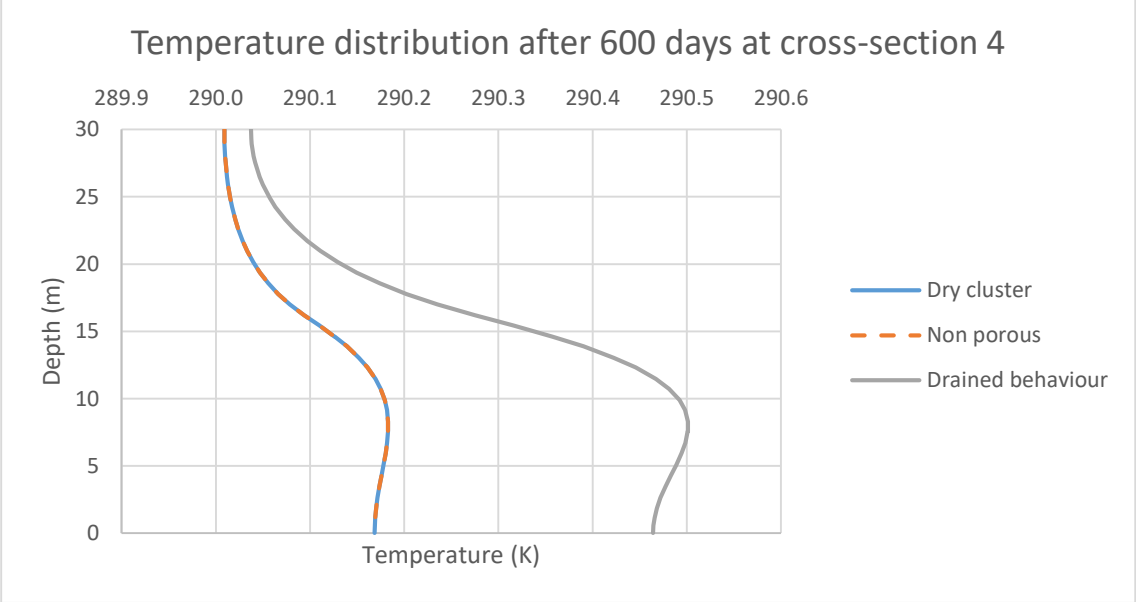

Figure 45 Temperature distribution at cross-section 4 after 600 days

The results show that the dry and non-porous clusters are identical. The drained behaviour showed slightly different temperature distribution compared to the dry and non-porous clusters.

The groundwater flow for the three behaviour types as well as the temperature distribution through the model after 600 days is shown in Figures (46-51). The results for the other time intervals are shown in the appendix (B.2)

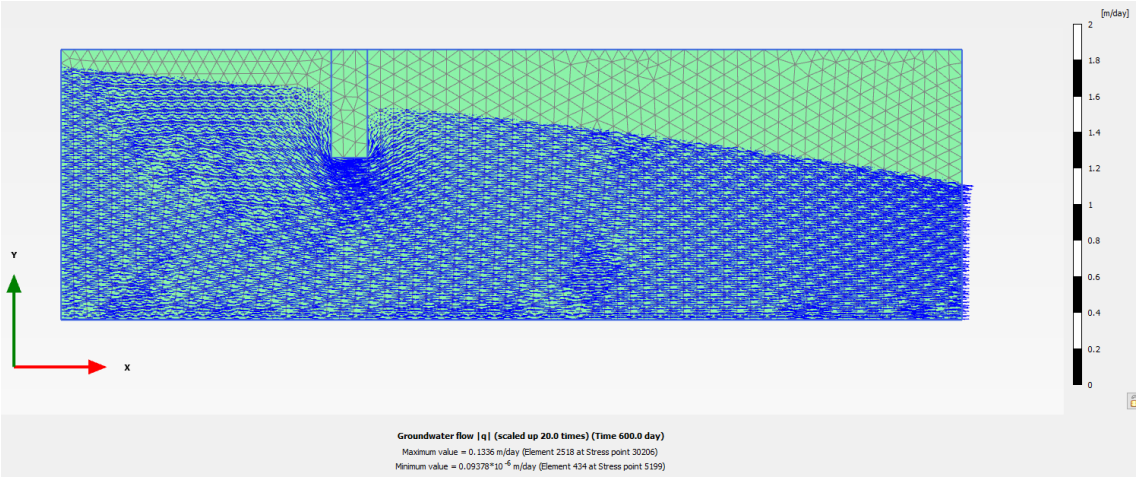

Figure 46 Groundwater flow for the dry cluster

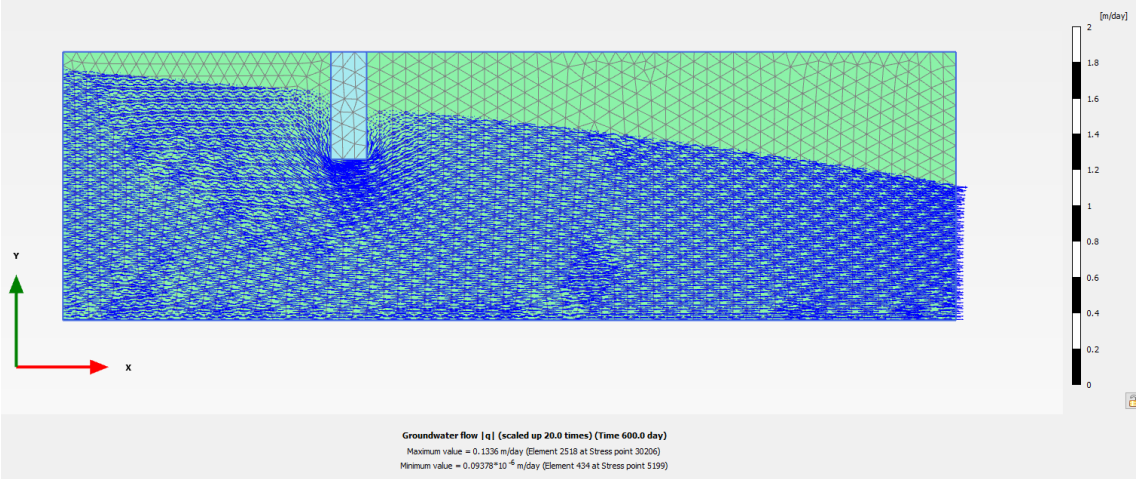

Figure 47 Groundwater flow for the non-porous cluster

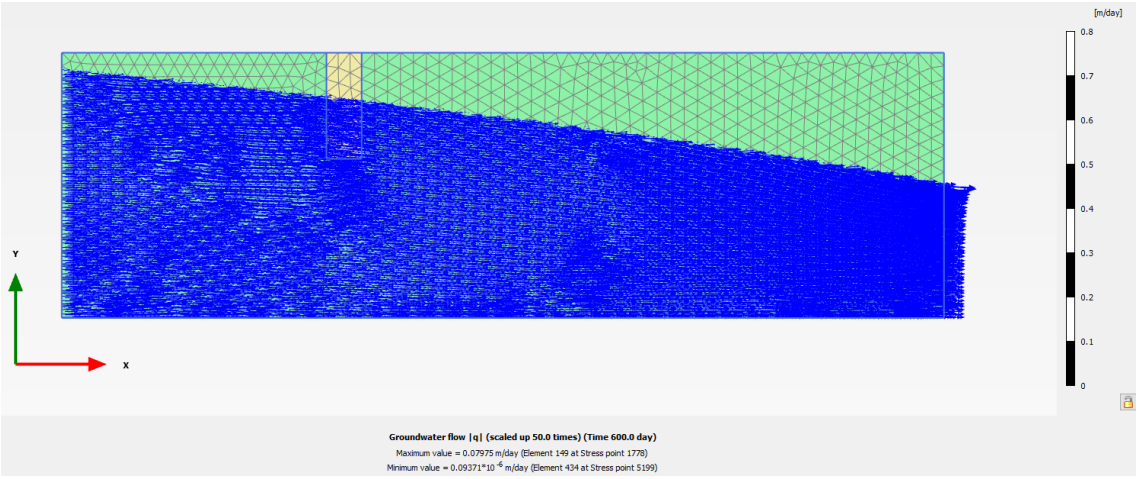

Figure 48 Groundwater flow for the drained cluster

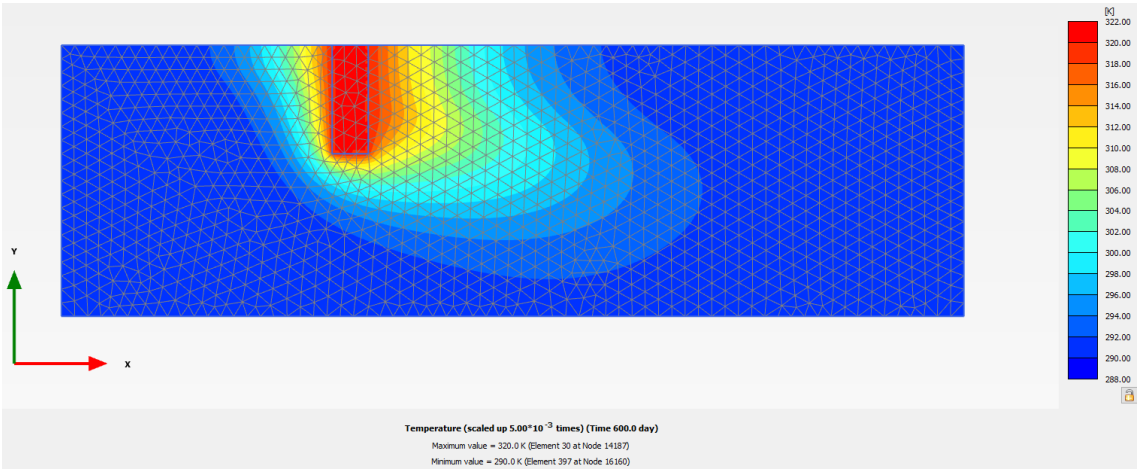

Figure 49 Temperature distribution after 600 days (dry cluster)

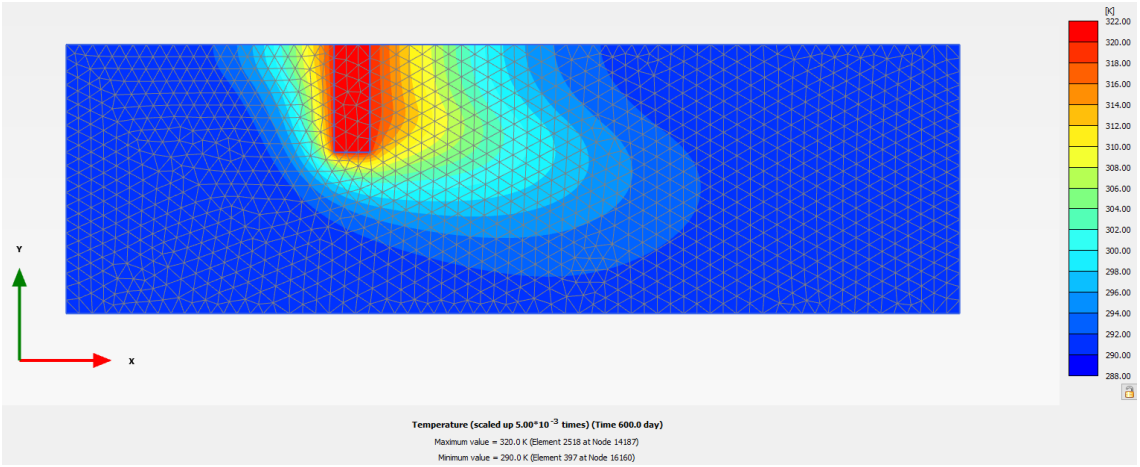

Figure 50 Temperature distribution after 600 days (non-porous cluster)

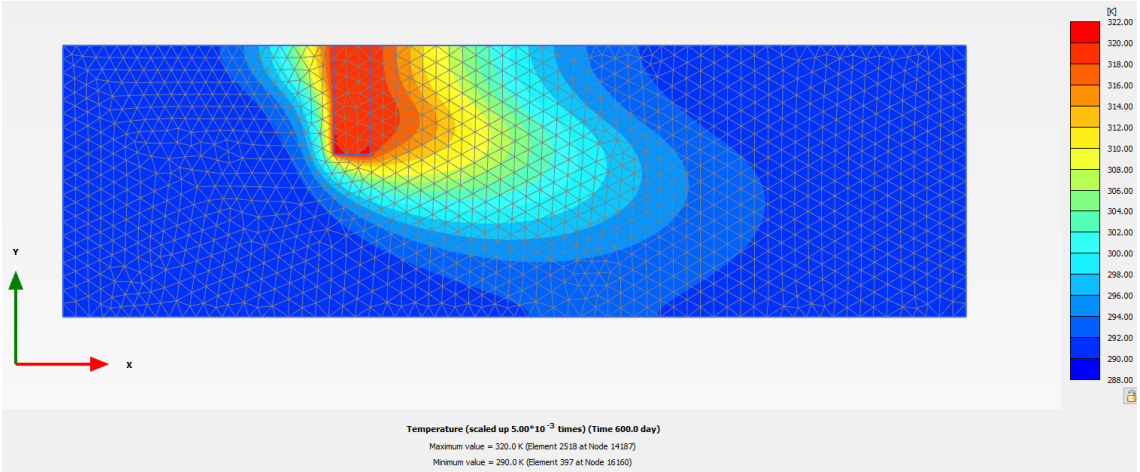

Figure 51 Temperature distribution after 600 days (drained cluster)

4.2.2 Boundary conditions

In the previous studies, temperature thermal boundary conditions were applied along the sides of the rectangular cluster. Regarding the groundwater flow boundary conditions, the lower groundwater flow boundary condition (at the lower boundary of the model) was closed.

4.2.3 Comparison between boundary conditions

The aim of this comparison is to investigate the effect of closed temperature boundary conditions. This was done by closing the four groundwater flow boundary conditions (at the four boundaries of the model). Afterwards, two closed temperature boundary conditions were applied along the right and lower boundaries of the model (Figure 52).

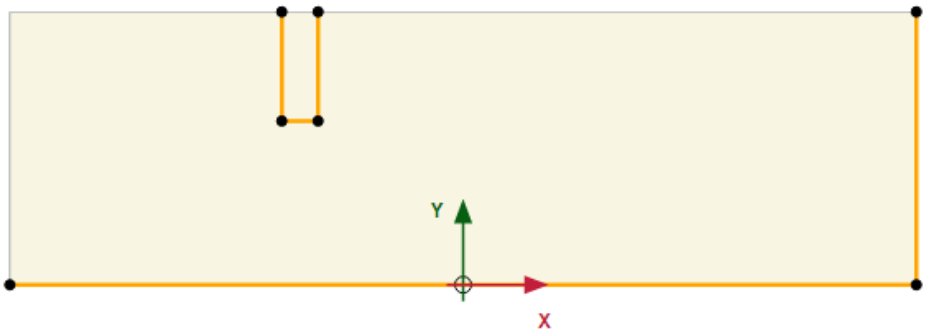

Figure 52 Closed temperature boundary conditions

The comparison is carried out between the following two scenarios:

1. Scenario 1: The four groundwater flow boundary conditions are closed (no closed temperature boundary conditions are applied)
2. Scenario 2: The four groundwater flow boundary conditions are closed and two closed temperature boundary conditions are applied at the right and lower boundaries of the model as shown in Figure 52.

The location of the two cross-sections is shown in Figure 53. Two time intervals were chosen for the comparison, after 10,000 and 50,000 days.

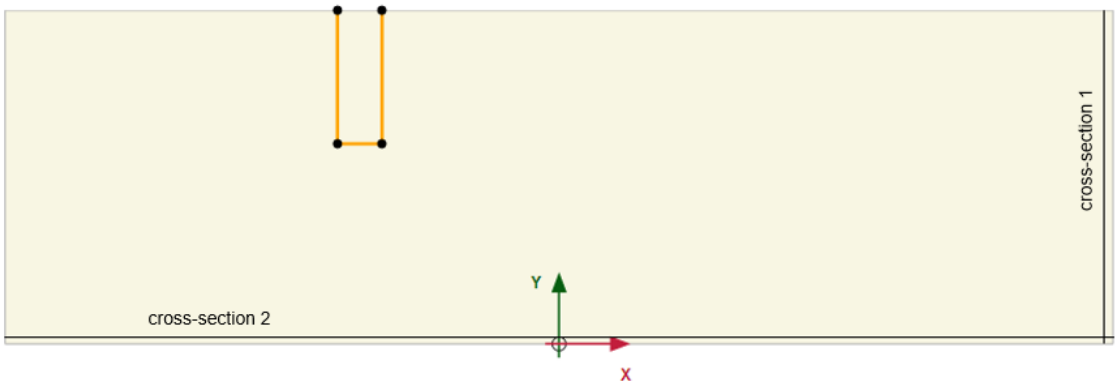

Figure 53 Location of the two cross-sections

The temperature distribution after 50,000 days at cross-sections 1 and 2 is shown in Figures 54 and 55 respectively. The results after 10,000 days are shown in the appendix (B.2)

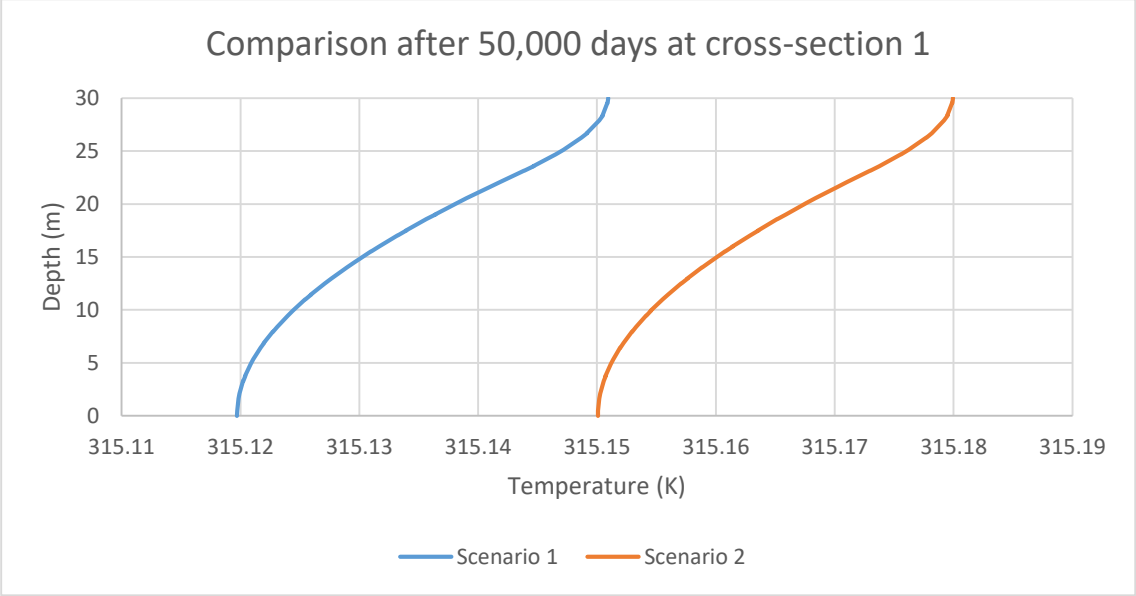

Figure 54 Temperature distribution at cross-section 1

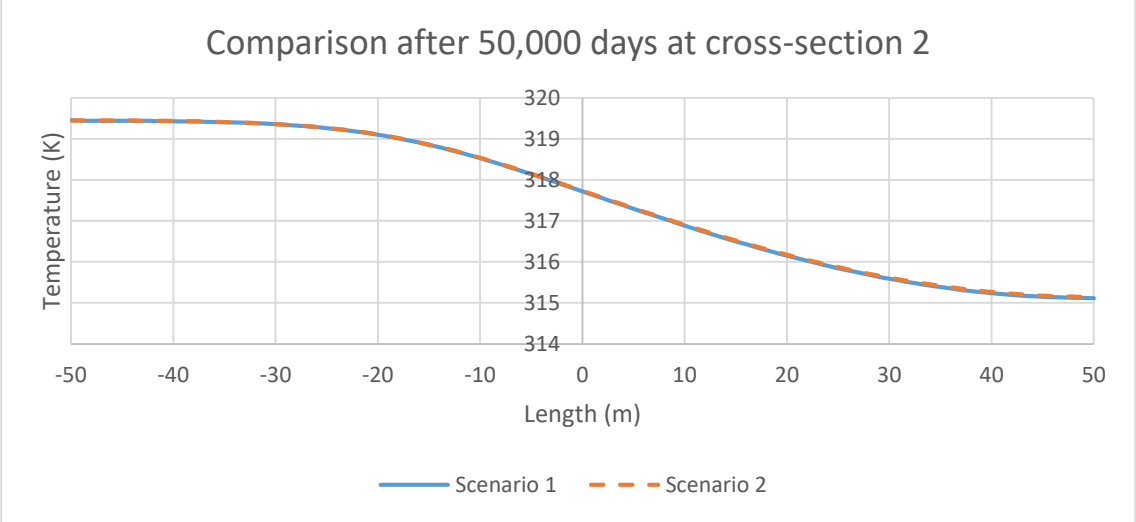

Figure 55 Temperature distribution at cross-section 2

The results show that the scenario with closed temperature boundary conditions (scenario 2) has slightly more temperature than the other scenario (scenario 1). The temperature distribution for scenario 2 after 50,000 days is shown in Figure 56. The temperature distribution for scenario 1 is shown in the appendix (B.2).

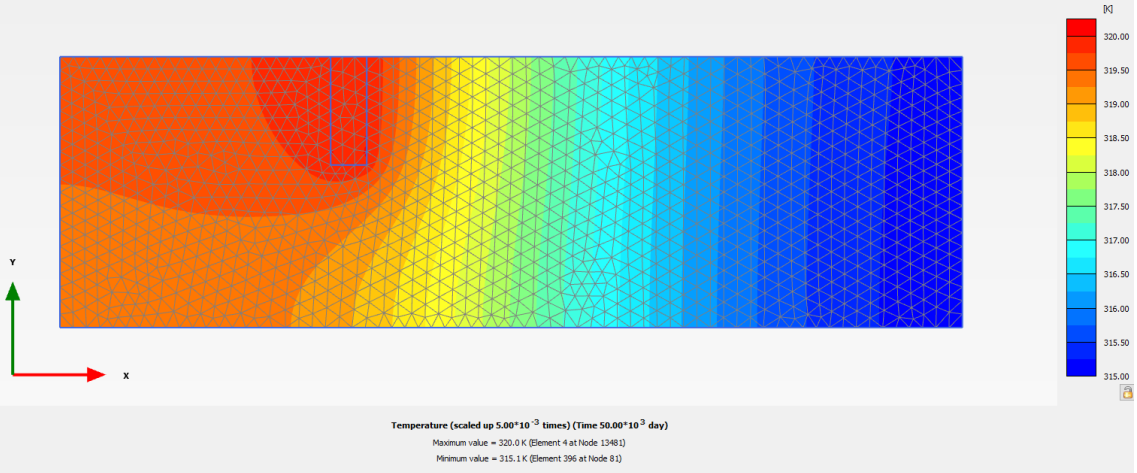

Figure 56 Scenario 2 after 50,000 days

4.3 Horizontal groundwater table

In this analysis, the same geometry and soil parameters as the previous model are used. The groundwater level in this model is horizontal (Figure 57). In this study, the model has a uniform temperature of 283.15 K (10℃), while the rectangular cluster has a temperature of 363.15 K (90℃). The analysis was done by two approaches:

1. Cluster thermal conditions in the rectangular cluster
2. Thermal boundary conditions along the sides of the rectangular cluster

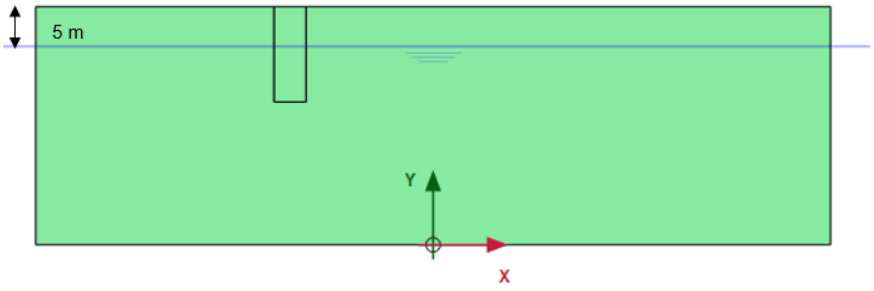

Figure 57 Geometry of the horizontal groundwater table model

For the two approaches, the rectangular cluster was dry. The temperature distribution for the two approaches after 1000 days is shown in Figures (58-59). As mentioned before, the cluster thermal conditions do not keep the temperature constant inside the cluster, unlike the thermal boundary conditions. This can be seen in Figure 58, where the temperature varies within the rectangular cluster.

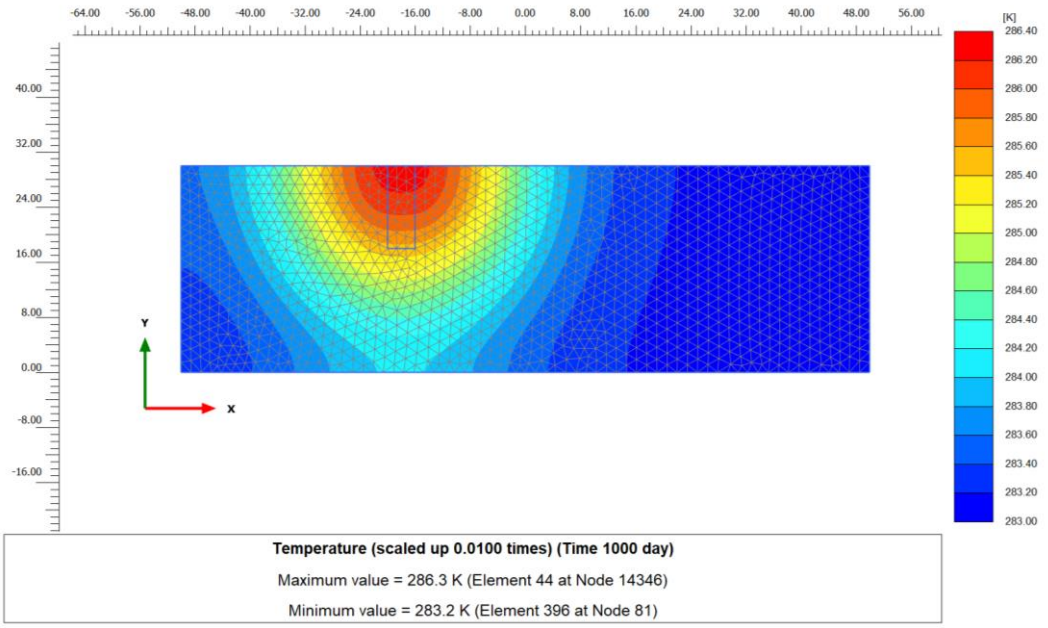

Figure 58 Temperature distribution after 1000 days (1st approach)

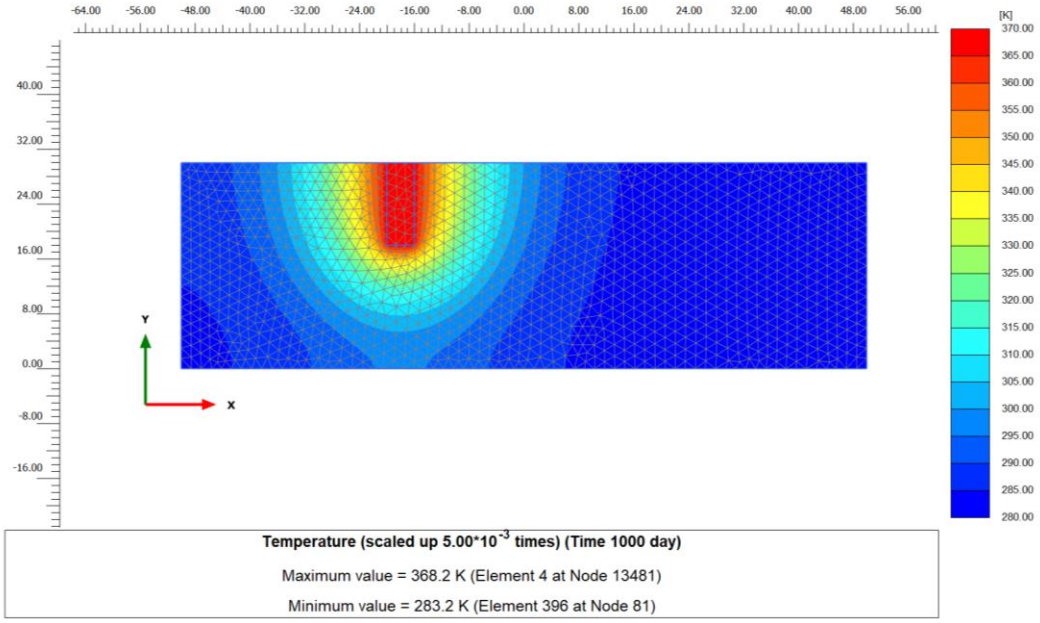

Figure 59 Temperature distribution after 1000 days (2nd approach)

5 Thermal energy storage (TES)

This chapter deals with one of the applications where considering temperature effects is necessary. The first part of the chapter provides the reader with an overview on TES. The second part illustrates TES models proposed by (Khan 2019). Afterwards, the procedure by which these models were modelled in PLAXIS is described.

5.1 Theoretical background

Recently, noticeable improvements in the field of renewable energy have made new energy resources, competitive to conventional energy in terms of reliability and efficiency. Solar energy is considered as a clean, emission-free and affordable energy resource. Despite these advantages, there are some limitations. The misalignment between energy supply and demand is considered as one of the biggest limitations of solar energy technology. As a result, the concepts of energy storage became an essential method to overcome this limitation (Xu 2014).

The thermal energy storage (TES) was first investigated back in the 1970s during the energy shortage crisis. Storing the energy means that the solar energy will not only meet the demands of heating and domestic water supply but can also offer a heat source throughout the year regardless of the weather variations or seasonal constraints (Xu 2014).

There are two possibilities for storing solar energy, either short-term (diurnal) or long-term (seasonal). The decision to choose whether diurnal or seasonal storage depends on the demand and availability. The idea behind the seasonal thermal energy storage (STES) technique, is using solar thermal collectors which harvest the available solar radiation in summer. Afterwards, the harvested energy is stored in large tanks or in the ground in order to be used in winter. STES systems are considered an efficient way of heating applications in the building sector (Shah 2018).

STES is strongly influenced by several parameters such as (Dahash 2018) (Ochs 2009):

- Geometry (e.g. cylindrical or conical)
- Type (e.g. as tank or pit)
- Operating temperature
- Ground conditions (e.g. groundwater table)
- Storage medium (e.g. water or gravel-water)
- Used materials

There are main four storage concepts (Ochs 2009):

- Tank TES with/without liners (Figure 60)
- Pit thermal energy storage (PTES) (Figure 60)
- Borehole thermal energy storage (BTES)
- Aquifer thermal energy storage (ATES)

BTES and ATES are cost-effective compared to the tank or pit TES. However, they provide much lower volumetric thermal capacity. In addition, they are not feasible for all locations as they require special geological conditions, unlike tank or pit TES which can be built at nearly every location (Ochs 2009).

It is important to consider external losses when designing STES. When designing pits, it should be designed in a way to have a minimum value of area to volume ratio (A/V ratio) and height to diameter ration (h/d ratio) in range of 1. However, due to boundary conditions such as groundwater, rock layers and architectural restrictions, the h/d ratio usually has a lower value than 1. Table 11 shows the parameters of several large-scale PTES (Ochs 2015).

Table 11 Parameters of several PTES (Ochs 2015)

Project	Mannheim	Wolfsburg	Marstal I	Marstal II	Droninglund
Volume (m^3)	30000	10000	10000	75000	62000
Slope	1/1.3	½	½	½	½
Height (m)	15	8	6.5	16	14.5
Surface area (m^2)	75 × 50	51 × 51	65 × 42	113 × 88	92 × 92
A/V (1/m)	0.31	0.52	0.56	0.27	0.29
h/d	0.35	0.23	0.16	0.23	0.23

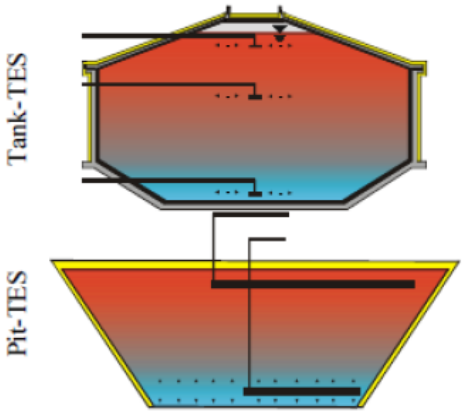

Figure 60 Tank and pit TES (Ochs 2009)

5.2 TES models

In the master's thesis done by (Khan 2019), several models were proposed to construct the storages. In this thesis, only three models are discussed, specifically variant 1, variant 2 and variant 3.

5.2.1 Variant 1

The proposed model is shown in Figure 61. The storage has a height of 12 m and a slope of 2:3. The groundwater table is 3 m below the ground level. The temperature in the soil and groundwater is nearly 10℃. The upper soil layer consists mainly of gravel and sand with a permeability of 10^{-5} m/day. The lower soil layer consists of low permeable silty clay sand with a permeability of 10^{-9} m/day.

Regarding the storage, a watertight layer is installed along the sides of the storage, in order to seal the storage. Moreover, floating insulation is applied on top of the storage for thermal insulation. The temperature of the water inside the storage is kept at nearly 90℃.

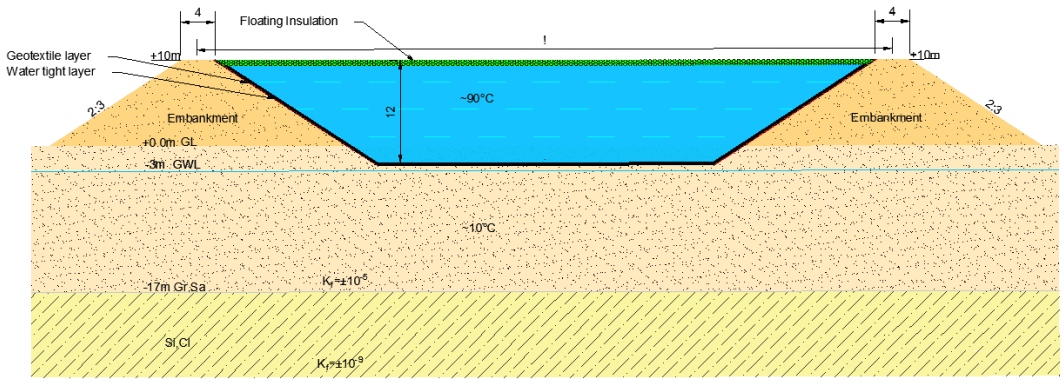

Figure 61 Variant 1 (thermal insulation only on top) (Khan 2019)

5.2.2 Variant 2

The proposed model is shown in Figure 62. The storage has a height of 26 m and a slope of 2:3. The groundwater table is 3 m below the ground level. The temperature in the soil and groundwater is nearly 10℃. The upper soil layer consists mainly of gravel and sand with a permeability of 10^{-5} m/day. The lower soil layer consists of low permeable silty clay sand with a permeability of 10^{-9} m/day.

The watertight layer and the floating insulation are present as in variant 1. In this variant, the storage is constructed below the groundwater table. Therefore, groundwater lowering is necessary. As a result, two cut-off walls are installed. The cut-off walls are made of bentonite cement slurry. The pump located near the walls is used to pump out water in case of the rising of the groundwater.

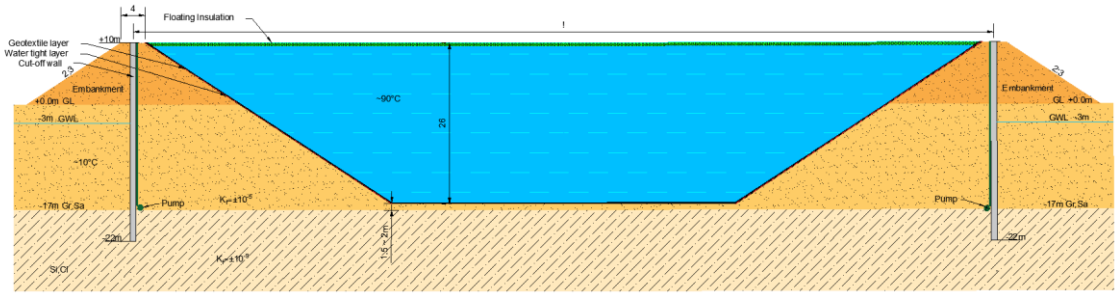

Figure 62 Variant 2 (thermal insulation only on top) (Khan 2019)

5.2.3 Variant 3

The proposed model is shown in Figure 63. This variant is exactly the same as the previous one except for the addition of thermal insulation layer along the sides of the storage.

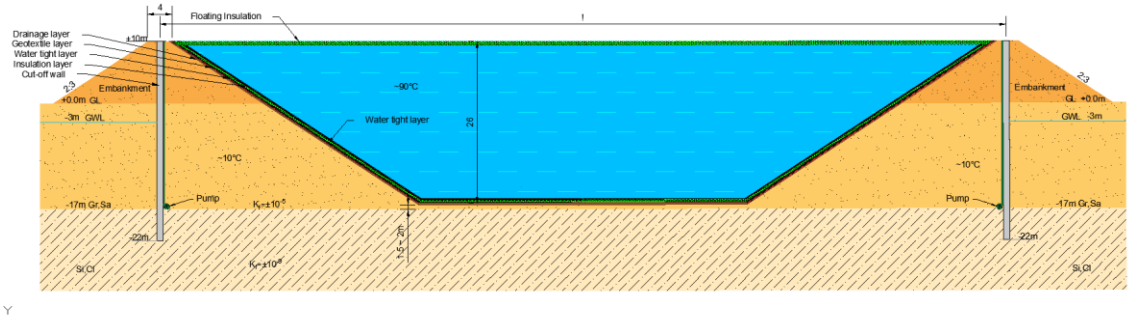

Figure 63 Variant 3 (thermal insulation on top & sides) (Khan 2019)

5.2.4 Other variants

Two more variants were added to study the influence of the thermal insulation. Variant 4 has thermal insulation along the sides of the storage (no thermal insulation on top). While variant 5 does not have any thermal insulation. Table 12 provides a comparison between the three variants.

Table 12 Comparison between the three variants

Variant	1	2	3	4	5
Top thermal insulation	Present	Present	Present	-	-
Water sealing along sides of the storage	Present	Present	Present	Present	Present
Thermal insulation along sides of the storage	-	-	Present	Present	-

5.3 Modelling of variant 1

As seen from the previous section, the storage is filled with water which is heated up to 90℃. However, in PLAXIS it is not possible to run models with clusters not containing soil. Therefore, it was necessary to try other approaches in order to model the behaviour inside the storage. The following was carried out:

- Using thermal boundary condition instead of the storage
- Modelling water as soil

The geometry of the model is shown in Figure 64. The storage has a length of 100 m. Before proceeding with the two approaches mentioned before, it was necessary to carry out preliminary studies first to check the water situation inside the storage.

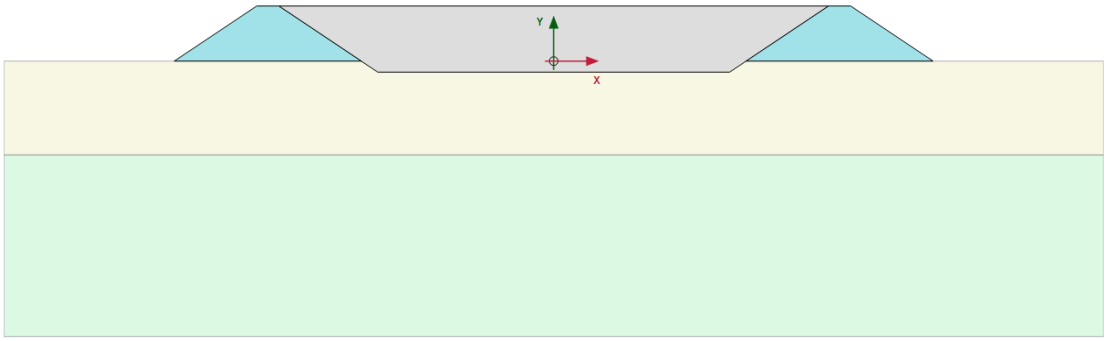

Figure 64 Variant 1 in PLAXIS

5.3.1 Preliminary studies

In these studies, modelling water as a soil layer was investigated. The parameters of "water soil" are shown in Table 13. The same 1D column defined in section (4.1) was used for these studies. The investigation was carried out by checking several aspects such as:

- The difference between applying temperature and convective thermal boundary conditions
- The influence of adding groundwater table to the water modelled as soil

Table 13 Parameters of water as soil

Material model	Linear elastic
Soil unit weight above phreatic level γ_{unsat}	10 kN/m^3
Soil unit weight below phreatic level γ_{sat}	10 kN/m^3
Poisson's ration ν	0.499
Heat capacity	4181 $kJ/t/K$
Thermal conductivity	0.6 $W/m/K$
Soil density	1 t/m^3
Thermal expansion (x,y & z) components $(\alpha_x, \alpha_y \,\&\alpha_z)$	0.21×10^{-3} $1/K$

In the first comparison, a temperature thermal boundary condition of 363.15 K (90℃) was applied on top of the column. Two different setups were checked after 60 days:

1. Defining water level on top of the column
2. No water level is defined

The results of this comparison are shown in Figure 65. The results show that the presence of water level on top of the column leads to a slight increase in the temperature distribution along the column compared to the situation where there is no water level defined.

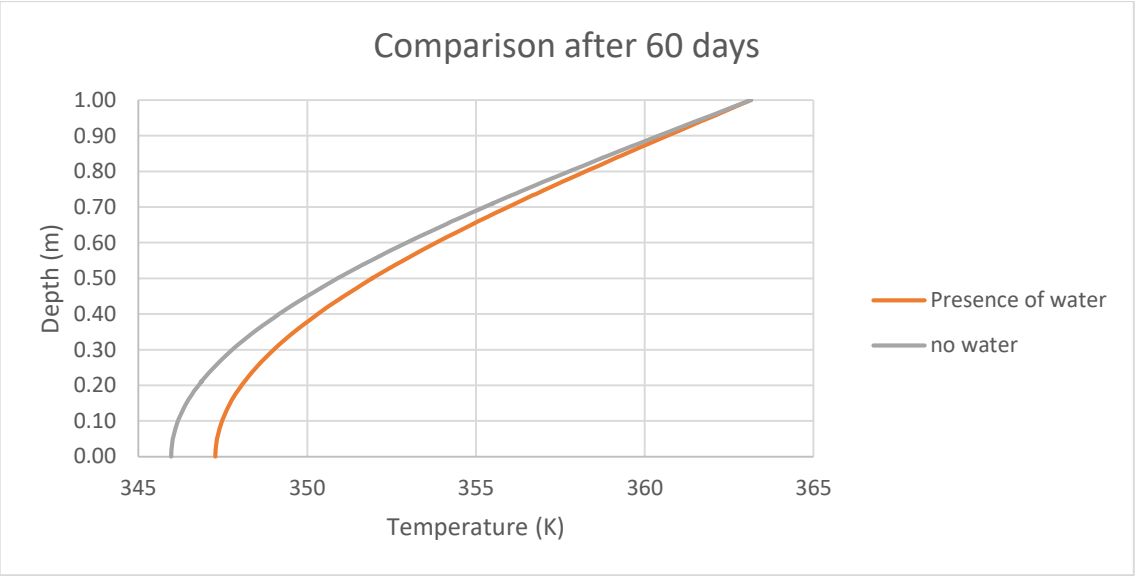

Figure 65 Comparison between presence and absence of water

In the second comparison, a convective thermal boundary condition was applied on top of the column. Four different setups were checked after 60 days:

1. Defining water level on top of the column
2. No water level is defined

The results of this comparison are shown in Figure 66. As noticed from the previous result, the setup with no water level defined resulted in a temperature distribution slightly less than the other setup where water level was defined on top of the column.

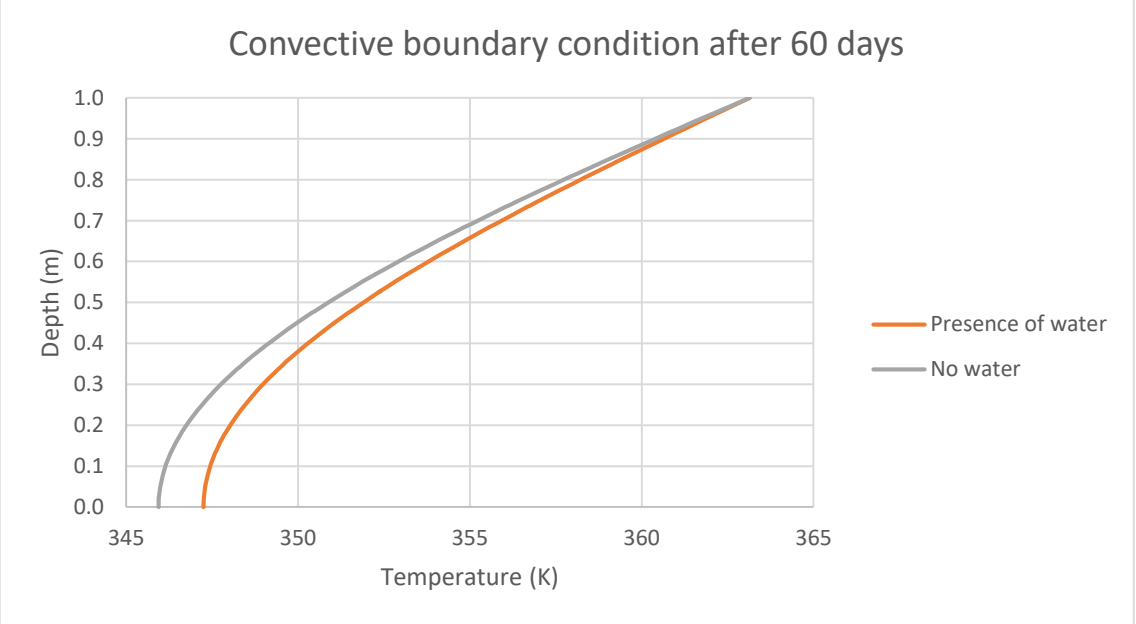

Figure 66 Comparison between presence and absence of water (convective boundary condition)

In the third comparison, the temperature and convective thermal boundary conditions were compared. There was no water level defined on top of the column in this comparison. The result is shown in Figure 67. The temperature boundary condition has a slightly higher temperature than the convective boundary condition. This was expected as the convective boundary condition does not transfer the total amount of its temperature to the adjacent medium, unlike the temperature boundary condition, which transfers the full amount of its temperature.

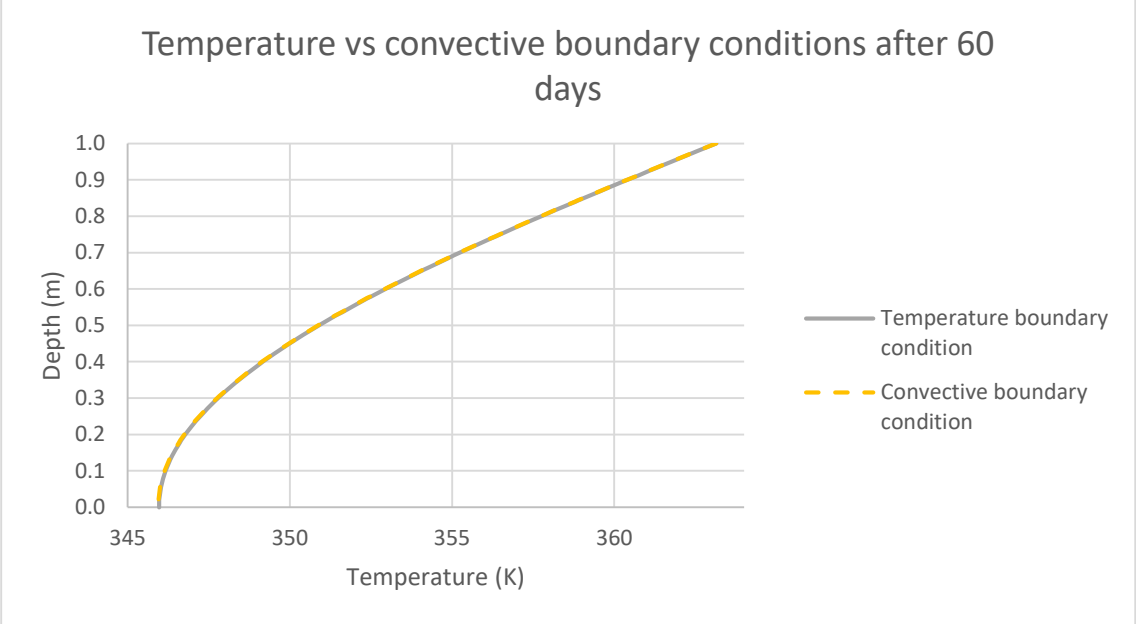

Figure 67 Comparison between temperature and convective boundary conditions (no defined water level)

In the final comparison, the temperature and the convective boundary conditions were again compared but this time, with a defined water level on top of the column. As noticed from the previous comparison, the convective boundary condition results in a slightly lower temperature compared to the temperature boundary condition.

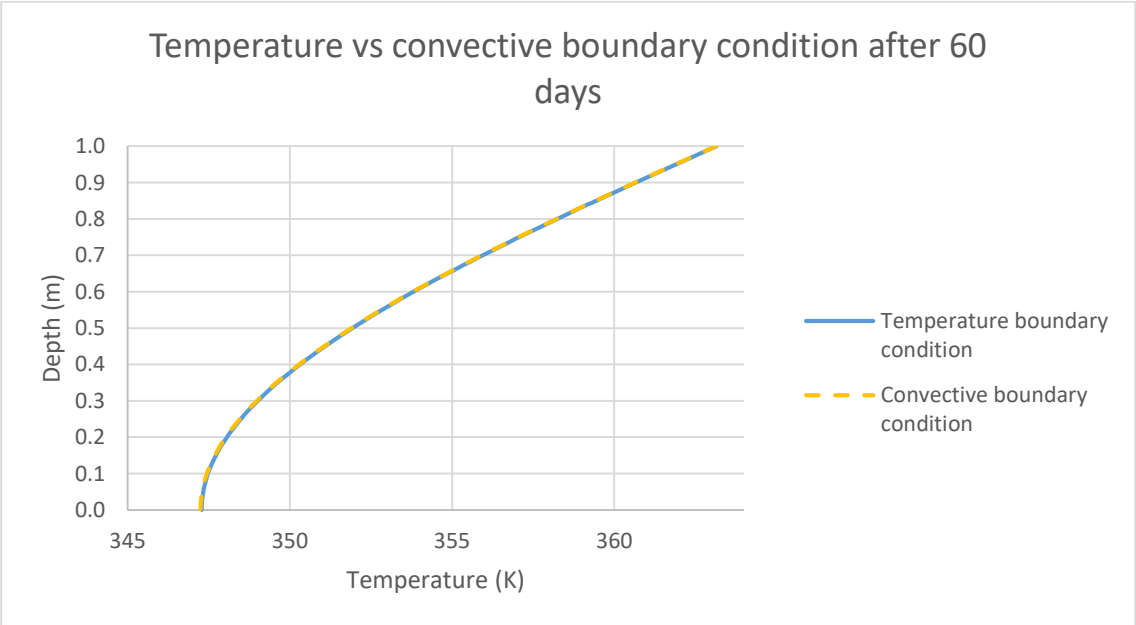

Figure 68 Comparison between temperature and convective boundary conditions

The preliminary studies showed that:

- The presence of groundwater increases the temperature
- The temperature boundary condition results in slightly higher temperature compared to the convective boundary condition

5.3.2 Thermal boundary conditions instead of the storage

The first approach to model variant 1 was by applying convective boundary condition along the sides of the storage. The convective boundary condition has a temperature of 363.15 K (90℃) and it substitutes the water inside the storage. Therefore, the storage cluster is modelled as an empty cluster with thermal boundary conditions along its sides. Figure 69 shows the geometry of the model in PLAXIS. Figure 70 shows the location of the convective boundary condition. The parameters of the soil used are shown in Table 14.

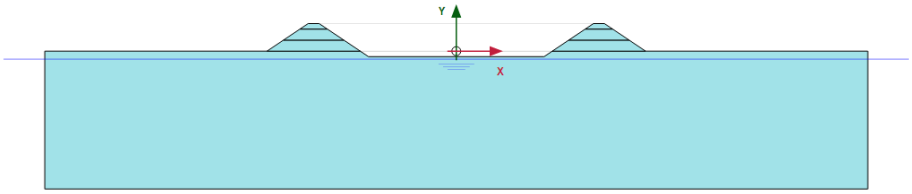

Figure 69 Variant 1 (one soil layer)

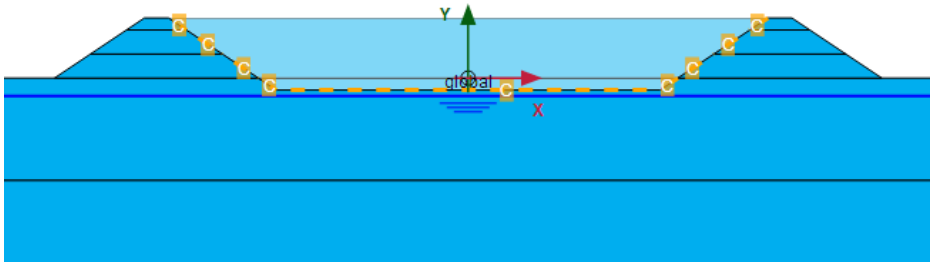

Figure 70 variant 1 convective boundary condition

Table 14 Variant 1 soil parameters

Material model	Mohr-Coulomb
Young's modulus	$25 \times 10^3\ kN/m^2$
Poisson's ration ν	0.2
Cohesion	$10\ kN/m^2$
Poisson's ration ν	0.499
Friction angle	35°
Heat capacity	$860\ kJ/t/K$
Thermal conductivity	$4\ W/m/K$
Soil density	$2.6\ t/m^3$
Thermal expansion (x,y & z) components $(\alpha_x, \alpha_y\ \&\alpha_z)$	$0.5 \times 10^{-6}\ 1/K$

In the first calculation phase, the model has a uniform temperature of 283.15 K (10°C) (Figure 71). In the following calculation phase, the convective boundary conditions are activated. The temperature distribution after 1000 days is shown in Figure 72 and for other time intervals, the results are shown in the appendix (C.1).

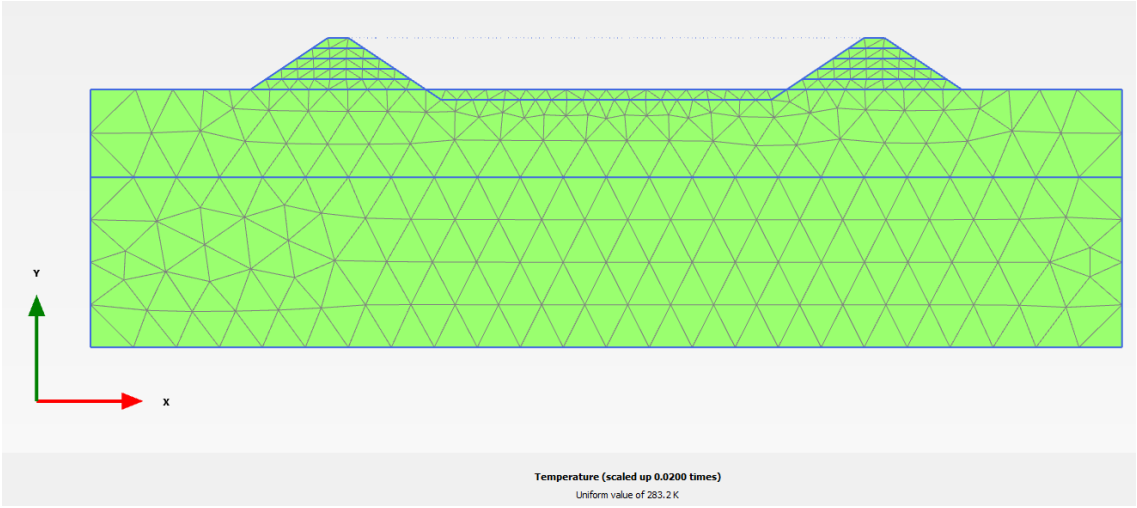

Figure 71 Variant 1 uniform temperature

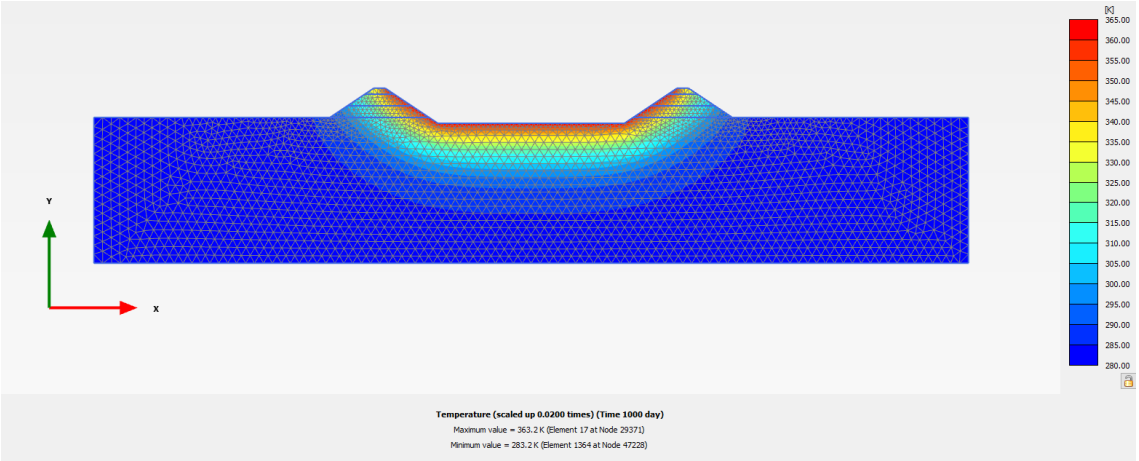

Figure 72 Temperature distribution after 1000 days (Variant 1 convective boundary condition)

5.3.3 Modelling water as soil

In this approach, the "water soil" (parameters are shown in Table 12) is defined for the storage cluster (Figure 73). In addition, a water level is defined on top of the storage (Figure 74). The first trials to run the model lead to failure in calculation steps as the soil body collapsed. As a result, the material model of soil was changed to linear elastic. Moreover, the young's modulus of water was increased to 25000 kN/m^2. The temperature applied in the storage by means of a cluster thermal condition with a temperature of 363.15 K (90℃). The results from this trial after 100, 1000 and 5000 days are shown in Figures (75-77).

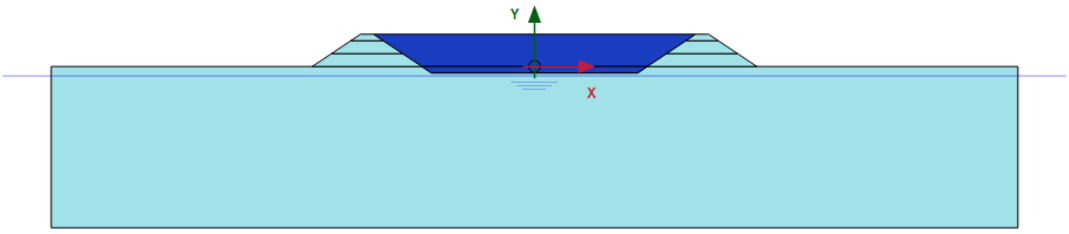

Figure 73 Water as soil

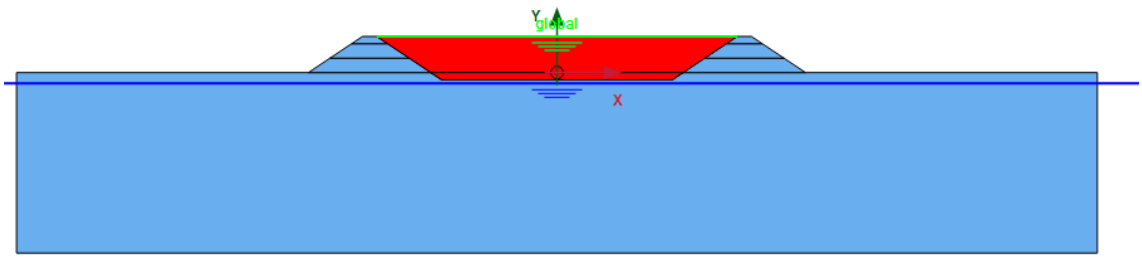

Figure 74 Water level on top of the storage cluster

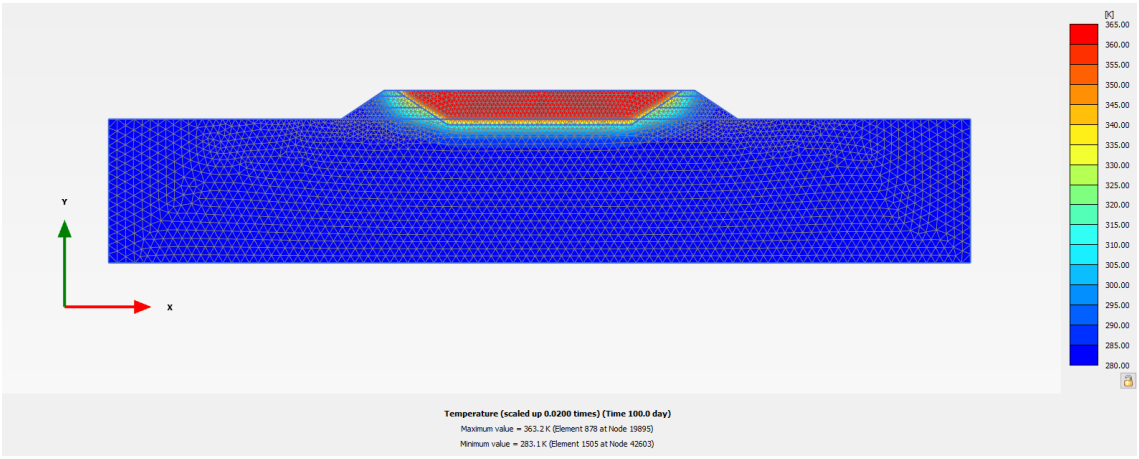

Figure 75 Temperature distribution after 100 days (linear elastic)

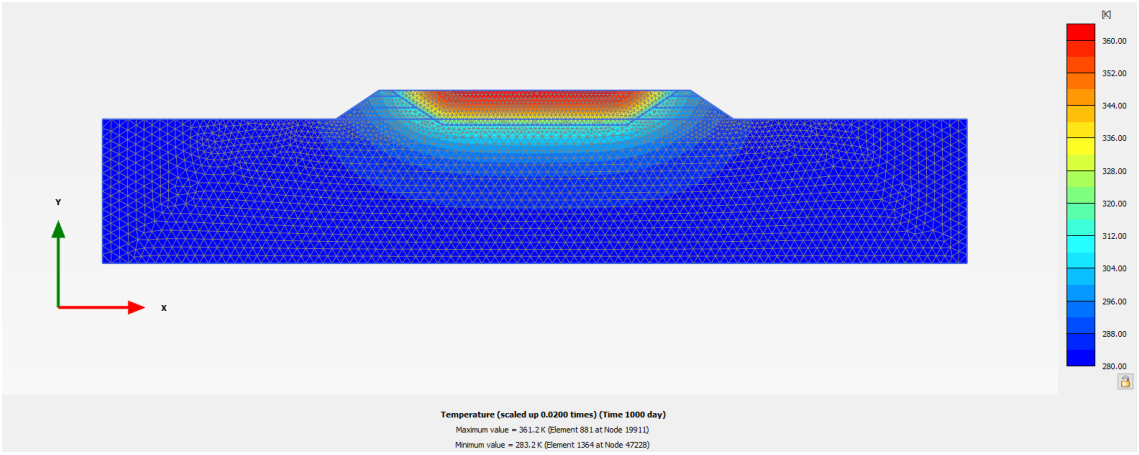

Figure 76 Temperature distribution after 1000 days (linear elastic)

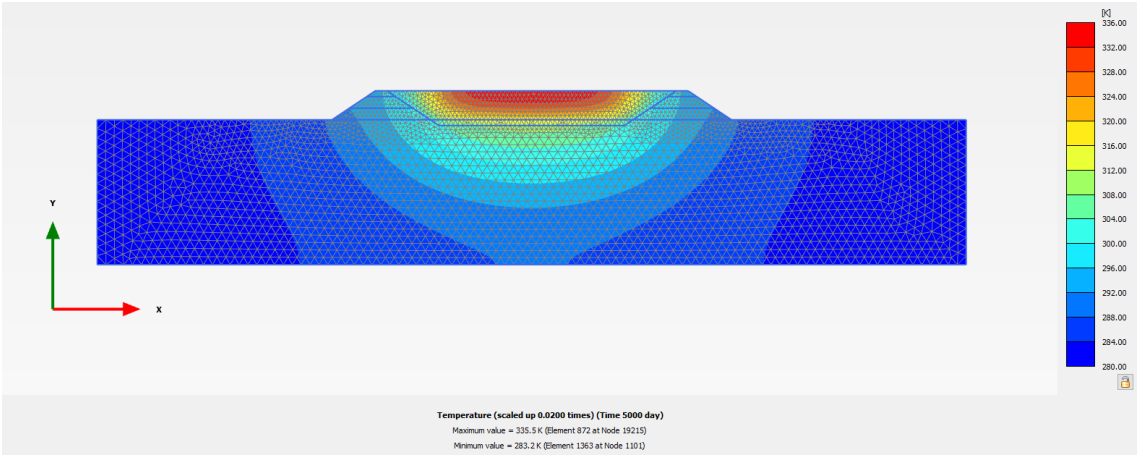

Figure 77 Temperature distribution after 5000 days (linear elastic)

In the following trials, the material model of the soil was switched back to Mohr-Coulomb with increasing the value of cohesion to 30 kN/m^2. The temperature distribution after 1000 days is shown in Figure 78. Comparison between linear elastic and Mohr-Coulomb material models cross-section 2 (Figure 84) after 1000 days is shown in Figure 79.

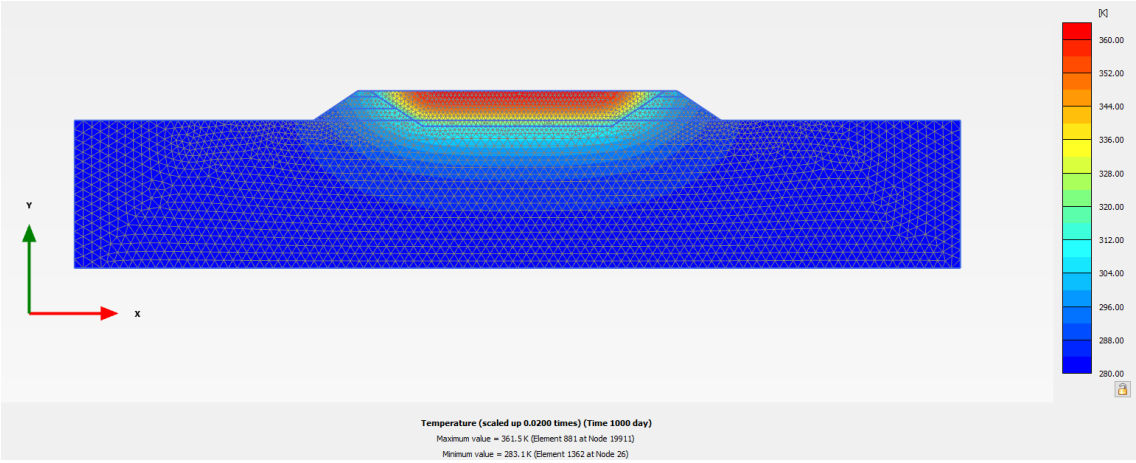

Figure 78 Temperature distribution after 1000 days (Mohr-Coulomb)

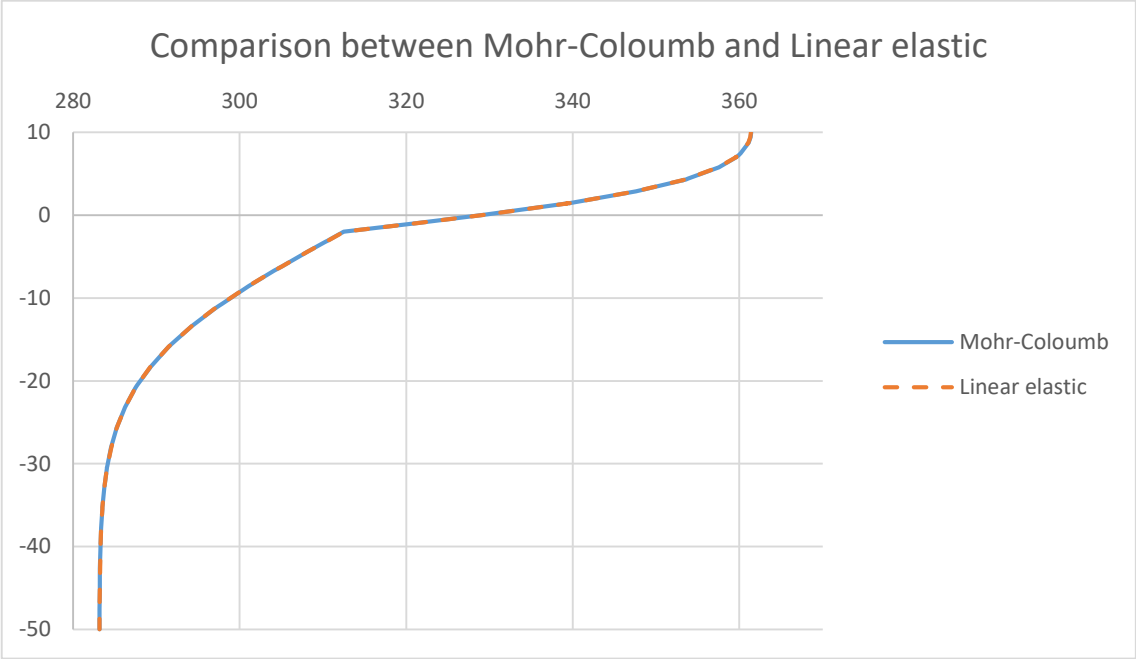

Figure 79 Comparison between Mohr-Coulomb and Linear elastic material behaviours

Figure 79 shows that the temperature distribution is nearly the same regardless the material model.

Several boundary conditions setups were compared to investigate their influence on the temperature distribution:

1. Setup 1: temperature boundary condition on top and convective boundary conditions along the sides of the storage (Figure 80)
2. Setup 2: temperature boundary conditions along the sides (Figure 81)
3. Setup 3: convective boundary conditions along the sides (Figure 82)
4. Setup 4: only temperature boundary condition on top (Figure 83)

All the thermal boundary conditions had a temperature of 363.15 K (90℃). Two cross-sections were used for comparing the four setups (Figure 84).

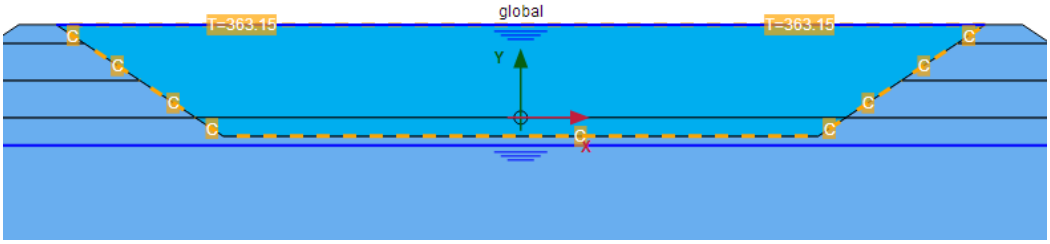

Figure 80 Boundary conditions (setup 1)

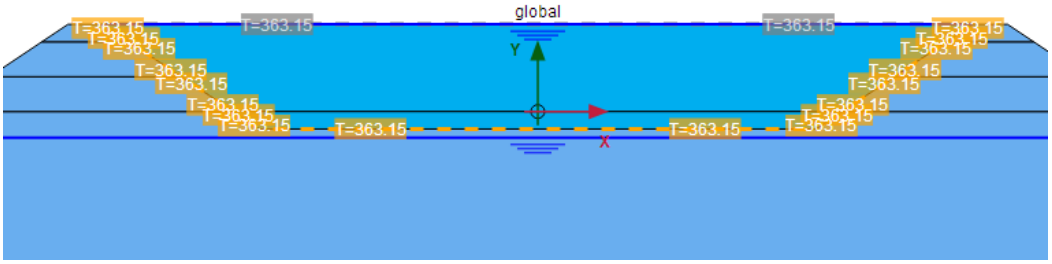

Figure 81 Boundary conditions (setup 2)

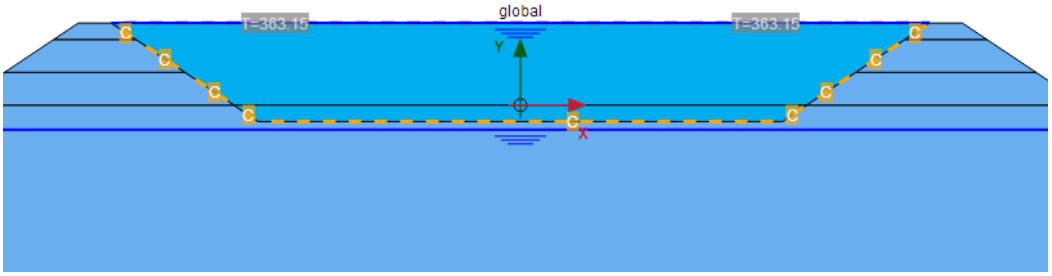

Figure 82 Boundary conditions (setup 3)

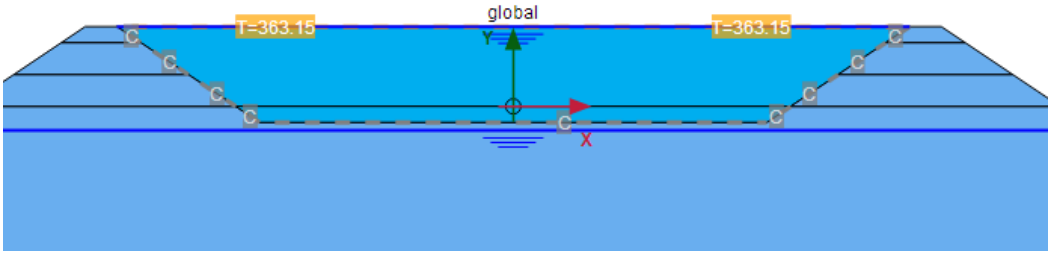

Figure 83 Boundary conditions (setup 4)

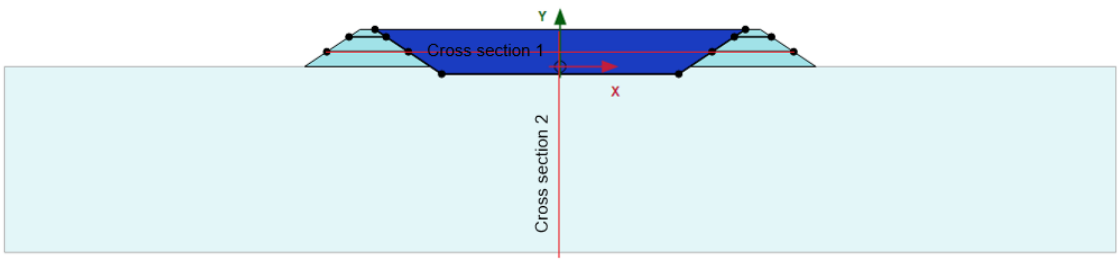

Figure 84 Location of the two cross-sections

The temperature distribution at the two cross-sections is shown in Figures (85 & 86). The differences between setups 1,2 and 3 are small to be noticed. Setup 4 resulted in lower temperature distribution compared to the other setups.

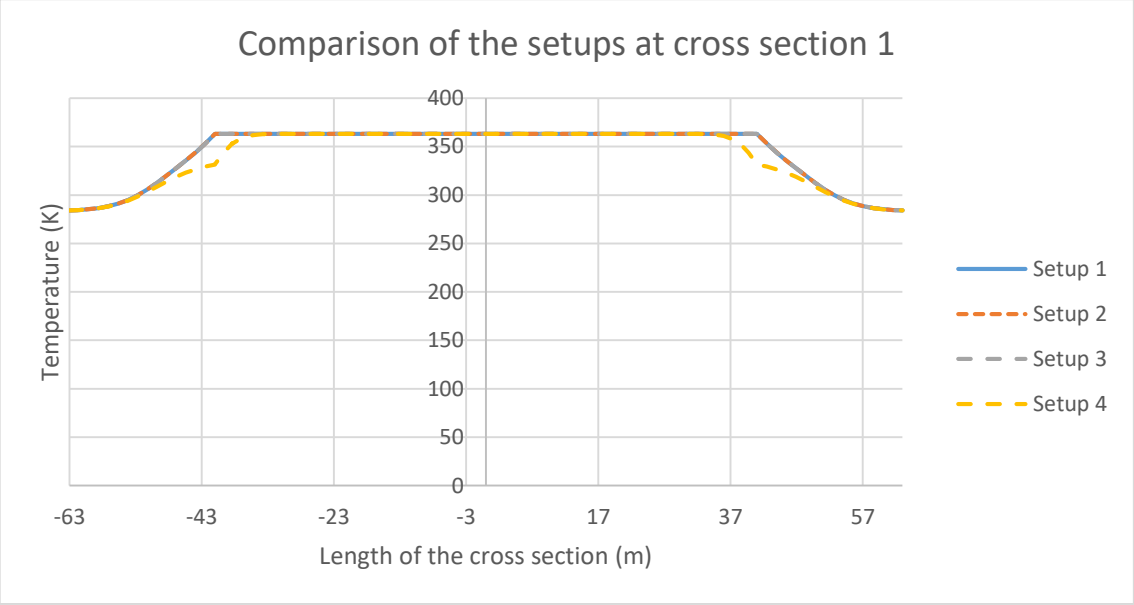

Figure 85 Temperature distribution at cross-section 1

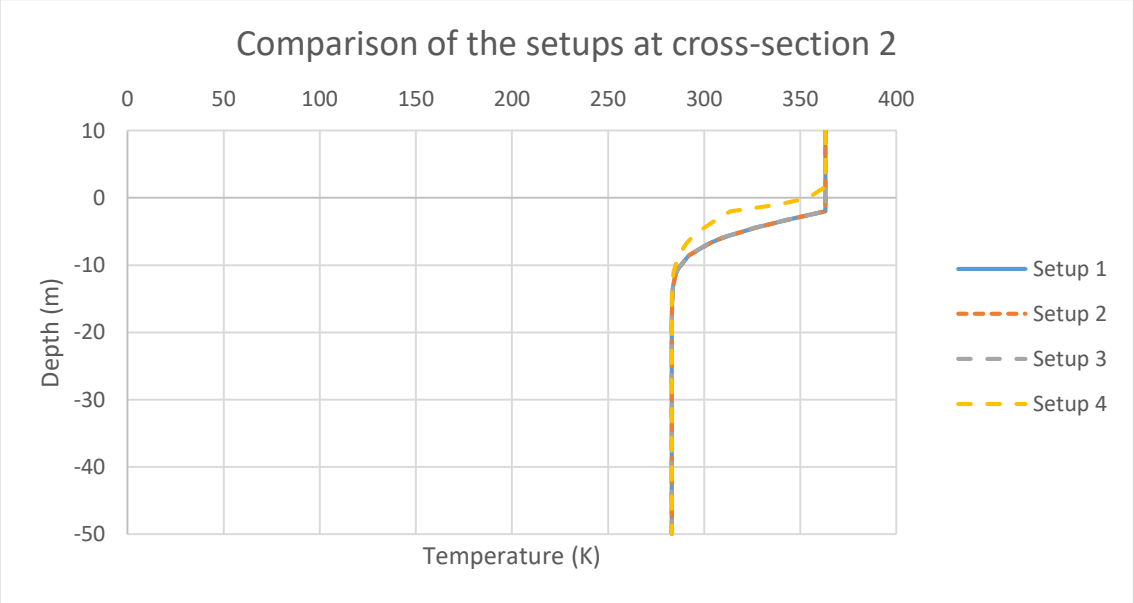

Figure 86 Temperature distribution at cross-section 2

5.4 Modelling of variants 2 and 3

The model used for variants 2 and 3 is shown in Figure 87. For these variants, due to the collapse of soil during calculation phases, the cohesion was increased to 75 kN/m^2, which does not influence the obtained temperature field (i.e. aim of the studies).

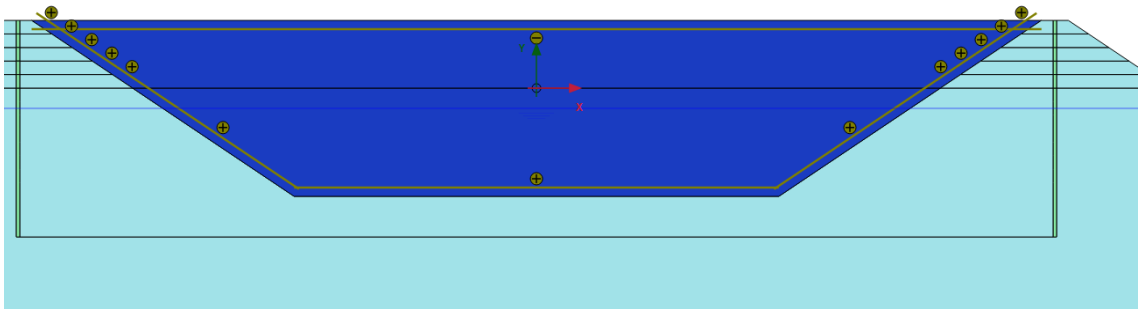

Figure 87 Geometry of variants 2 and 3

The difference between the two variants is in the role of the interfaces on the sides of the storage. In variant 2, the interfaces along the sides are only used to seal the storage (preventing the water flow out of the storage). While in variant 3, it is used for sealing and for thermal insulation as well. The thermal resistance for the interfaces was set to 3.52 K.m^2/W (thermal resistance of Expanded polystyrene (EPS)).

The temperature distribution after 1000 days for the two variants is shown in Figures (88 & 89). Moreover, a comparison between the two variants was carried out at two cross-sections. The location of the cross-sections is shown in Figure 90.

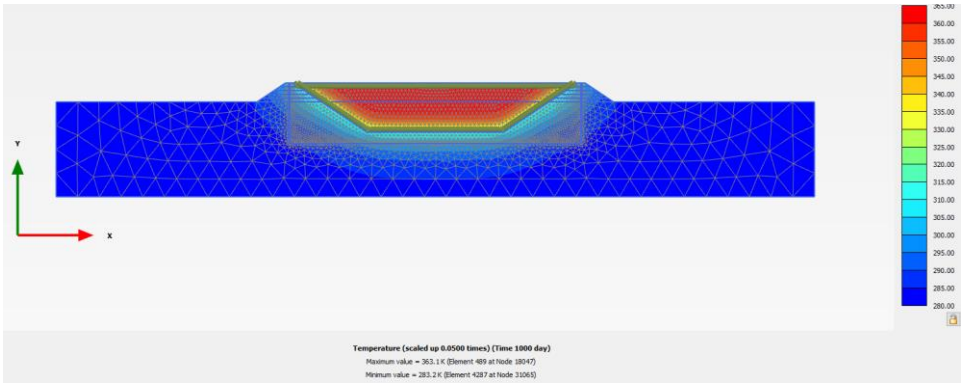

Figure 88 Temperature distribution after 1000 days (variant 2)

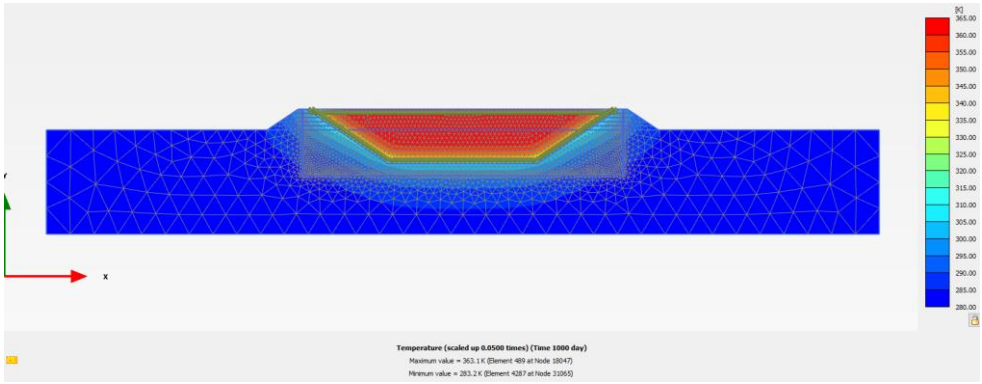

Figure 89 Temperature distribution after 1000 days (variant 3)

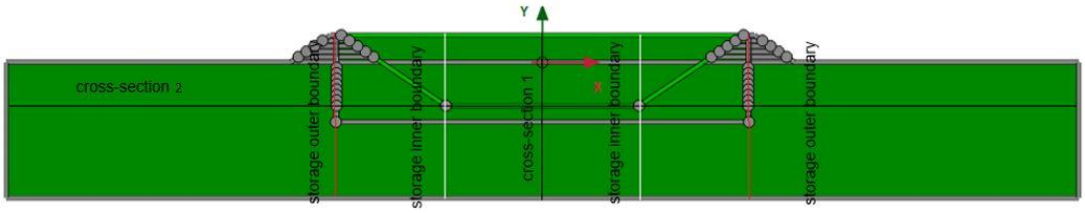

Figure 90 Location of the two cross-sections

The temperature distribution at the two cross-sections is shown in Figure 91 and 92 respectively. Figure 91 shows that below the storage, variant 2 has higher temperature compared to variant 3. This was expected as variant 2 has no thermal insulation along the sides, therefore, the temperature of the storage is transferred to the soil beneath the storage. On the other hand, inside the storage variant 3 has higher temperature. The reason for this is due to the presence of the thermal insulation along the sides which in turn stores the temperature inside the storage compared to variant 2 which has no thermal insulation on sides. The same conclusion applies to Figure 92 where variant 3 has a higher temperature inside the storage (exactly on the lower side of the storage) and variant 2 has higher temperature outside the sides of the storage.

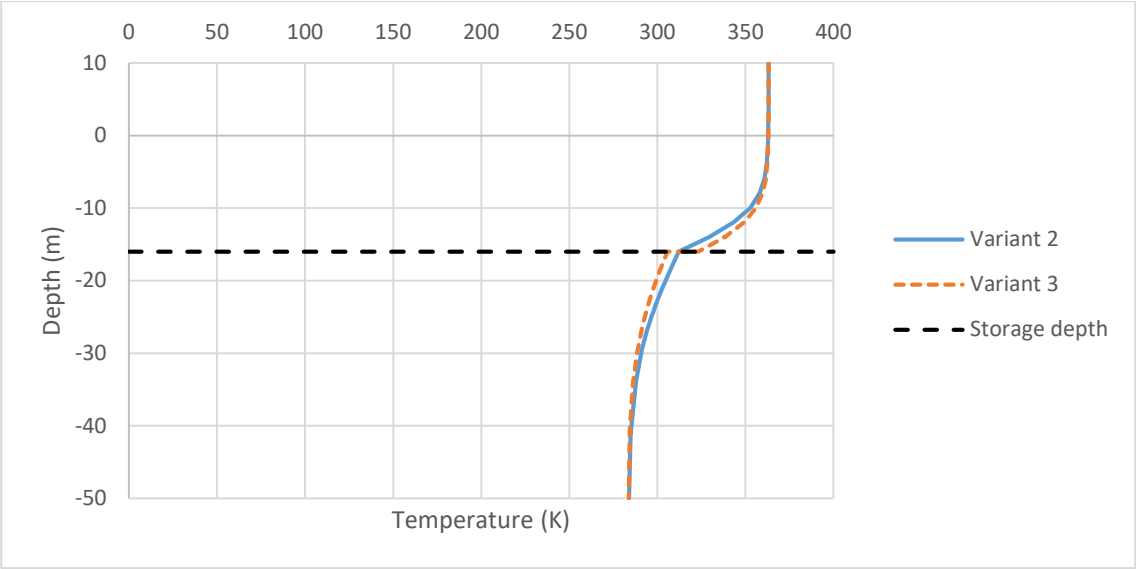

Figure 91 Temperature distribution at cross-section 1

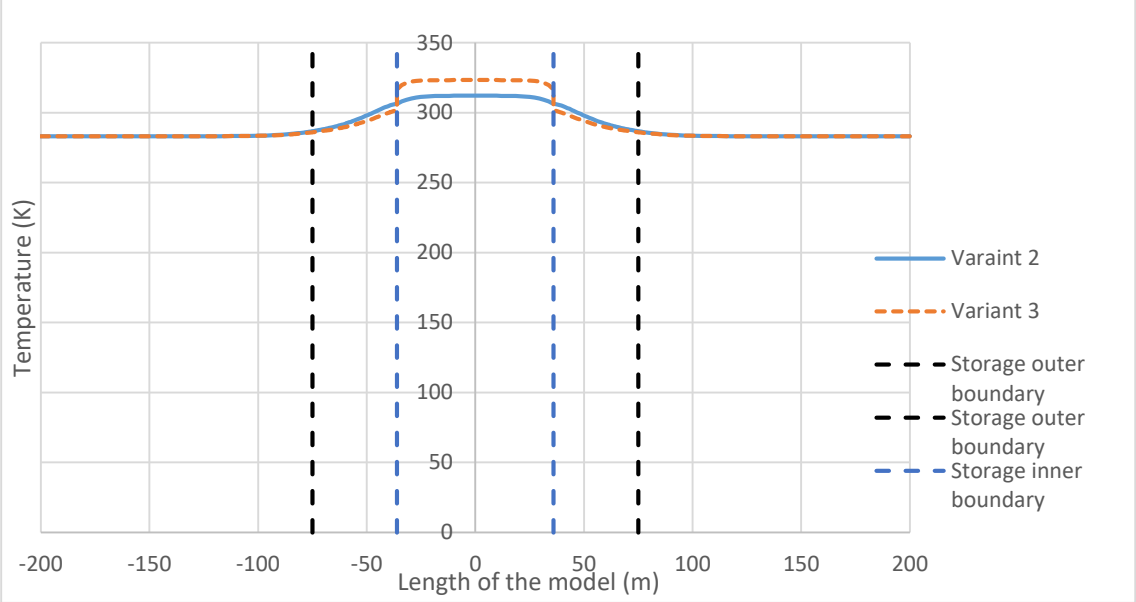

Figure 92 Temperature distribution at cross-section 2

Further analyses regarding the temperature dissipation were performed. Three points inside the storage were chosen to check the temperature evolution with time. The location of the points is shown in Figure 93, point A is located on top of the storage, point B in the middle of the storage and point C lies at the bottom of the storage. The time analysis was done for 10,000 days for variants 2 and 3. The results are shown in Figures 94 and 95.

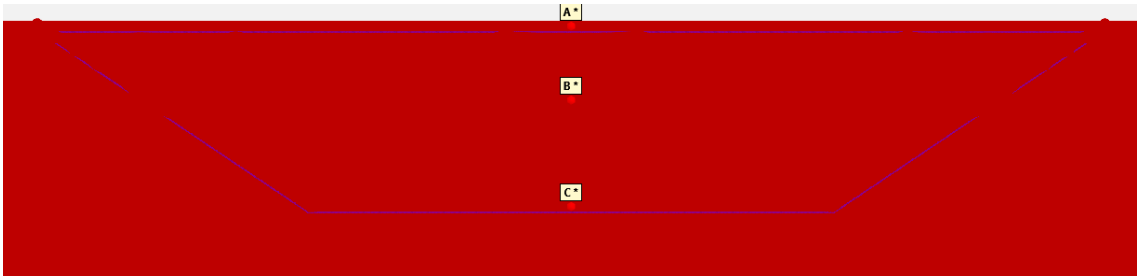

Figure 93 Location of the three points

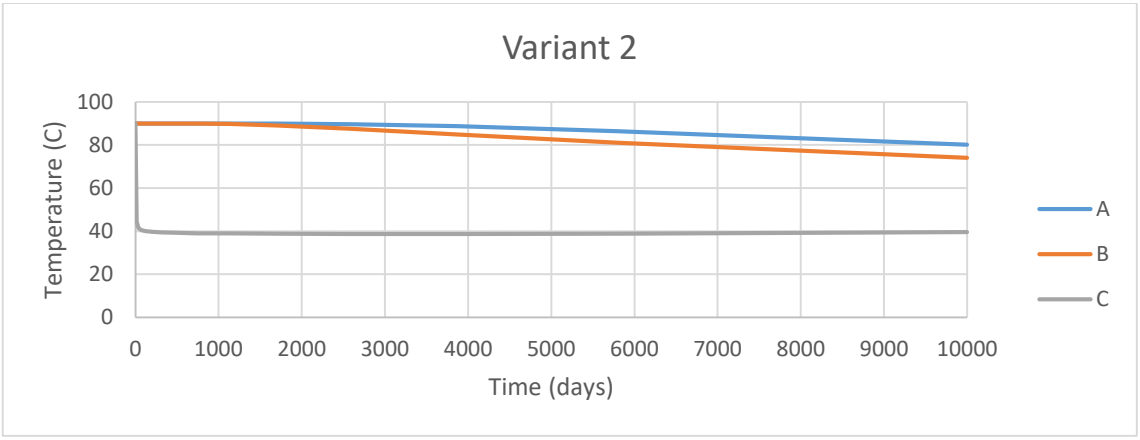

Figure 94 Temperature evolution at the three points (variant 2)

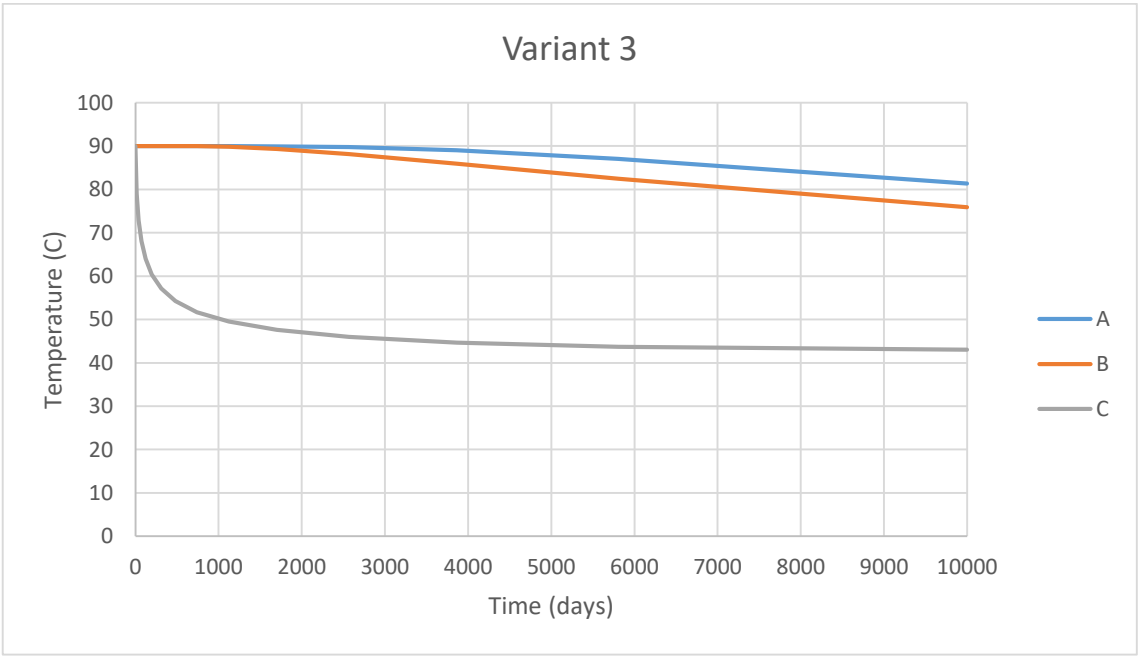

Figure 95 Temperature evolution at the three points (variant 3)

In case of variant 2, points A and B dissipate much less temperature compared to point C which losses about 50℃ after 40 days. Regarding variant 3, point C losses about 20℃ after 40 days.

Comparison between the two variants at point B is shown in Figure 96. The results of the other two points are shown in the appendix (C.2). The comparison shows the influence of the thermal insulation along the sides of the storage. The temperature at the nodes inside the storage is lower in variant 2.

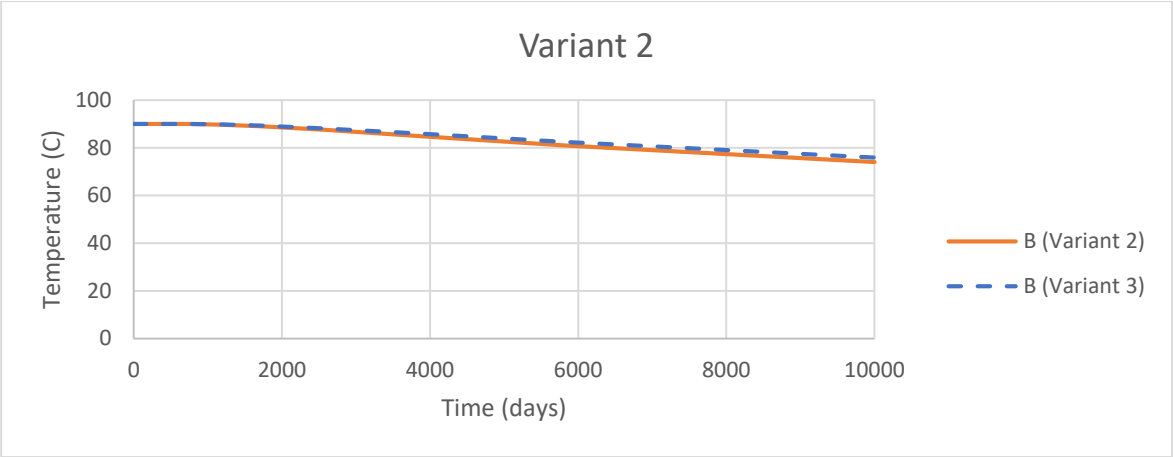

Figure 96 Comparison between Variants 2 & 3 at point B

5.5 Comparison between different scenarios

In this section, three setups for the model are compared. Each setup has four scenarios. The three setups are:

1. Setup 1: Presence of water as soil and water level inside the storage cluster (Figures 97 & 99)
2. Setup 2: Presence of water as soil only inside the storage cluster (without water level) (Figures 98 & 99)
3. Setup 3: Presence of soil and water level inside the storage cluster (Figures 97 & 100)

The four scenarios are as follows:

1. Scenario 1: Variant 2 (thermal insulation only on top of the storage)
2. Scenario 2: Variant 3 (thermal insulation on top and the sides of the storage)
3. Scenario 3: Thermal insulation on sides only (no thermal insulation on top)
4. Scenario 4: No thermal insulation at all

For each setup, the four scenarios are compared. Afterwards, each scenario is compared to different setups. Four time intervals were chosen, 100, 500, 1500 and 4000 days.

Top thermal insulation is discussed in details in section (5.6).

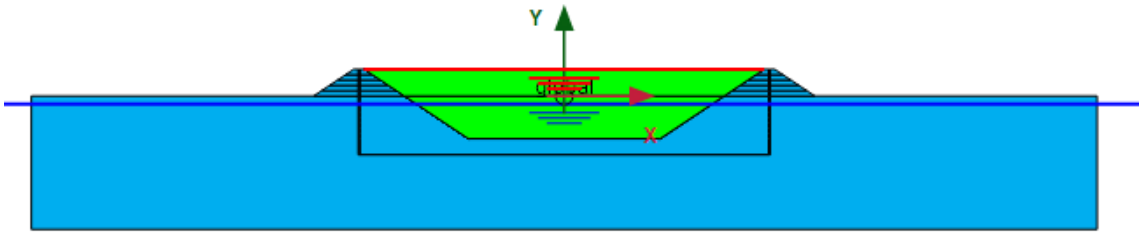

Figure 97 Water level inside the storage (Setups 1 & 3)

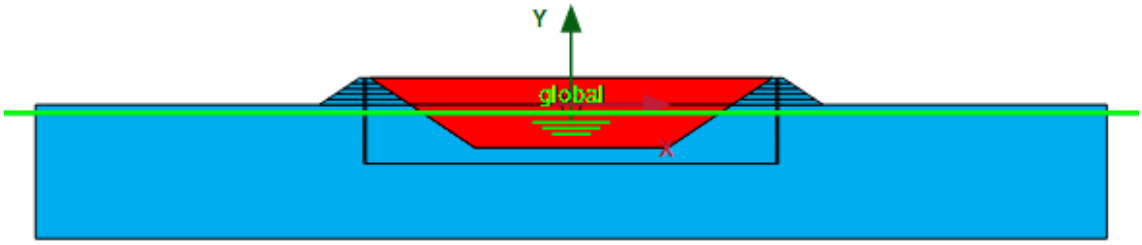

Figure 98 No water level inside the storage (Setup 2)

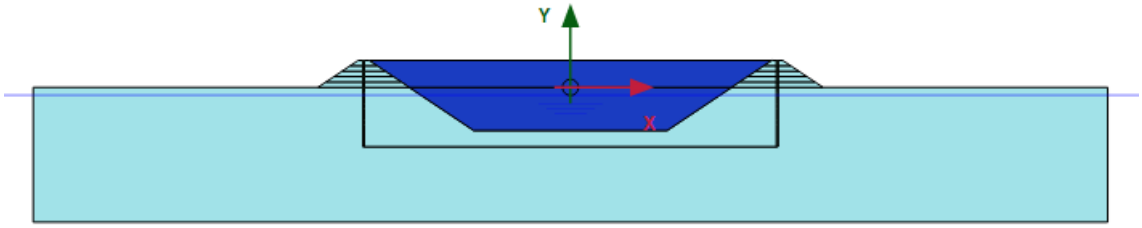

Figure 99 “Water soil” for setups 1 & 2

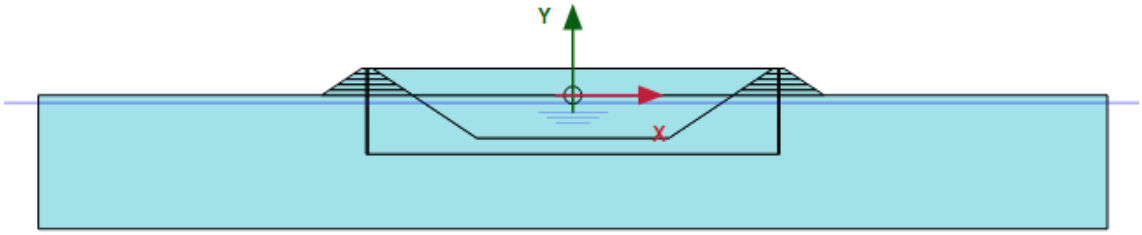

Figure 100 Setup 3

Two cross-sections were chosen for the comparisons. The location of the two cross-sections is shown in Figure 101.

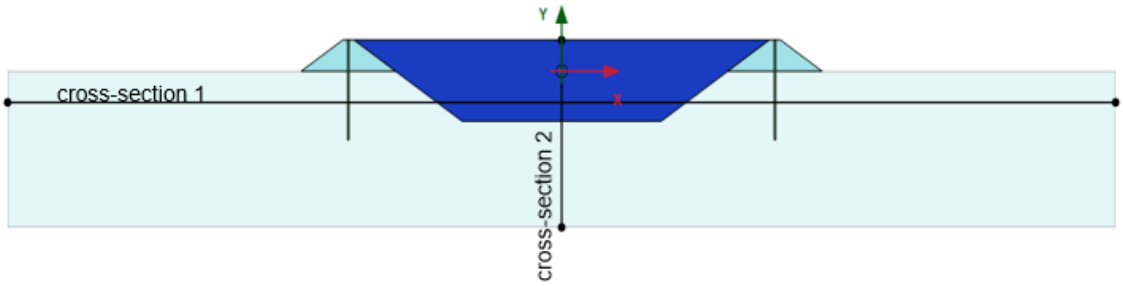

Figure 101 Location of the two cross-sections

5.5.1 Setup 1

Temperature distribution after 1500 days for the four scenarios is shown in Figures (102-105) respectively. The results after 100, 500 and 4000 days are shown in the appendix (C.3)

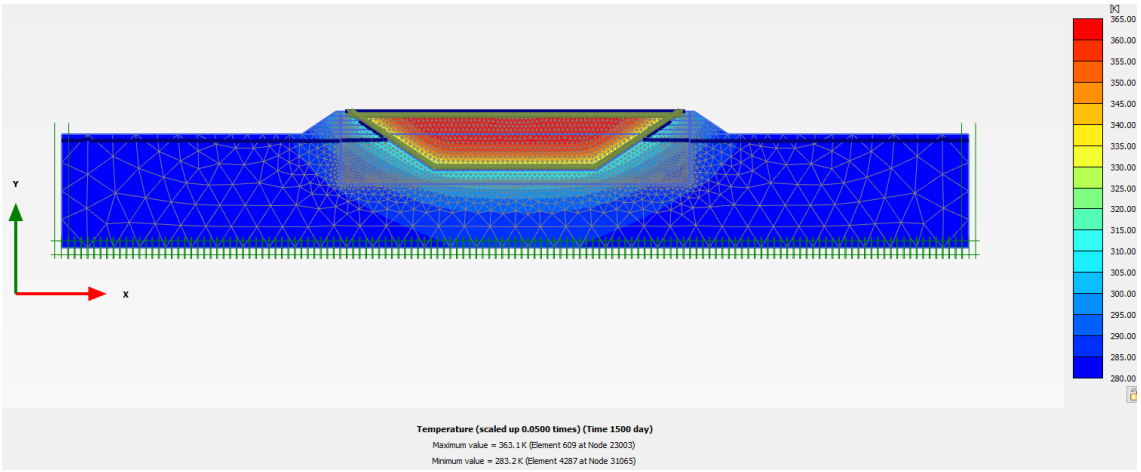

Figure 102 Temperature distribution after 1500 days (Setup 1 scenario 1)

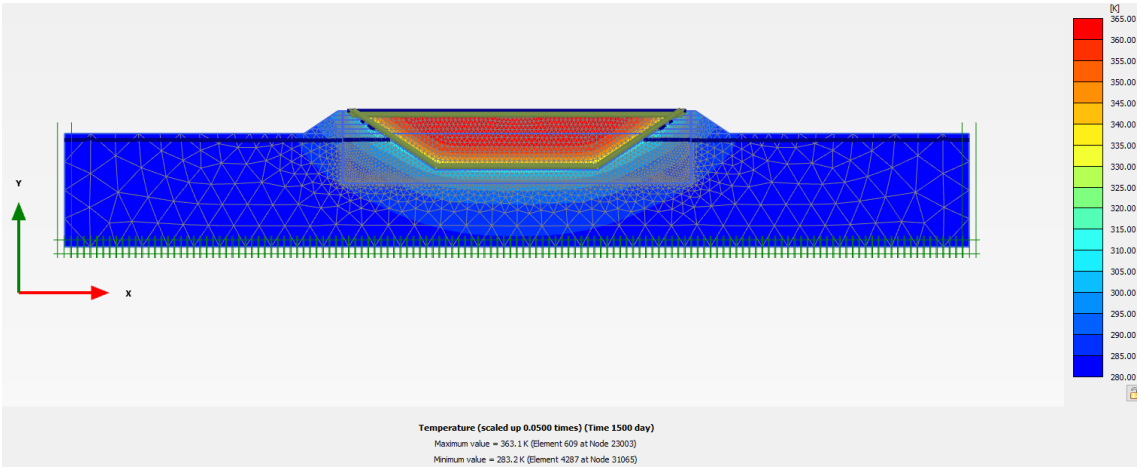

Figure 103 Temperature distribution after 1500 days (Setup 1 scenario 2)

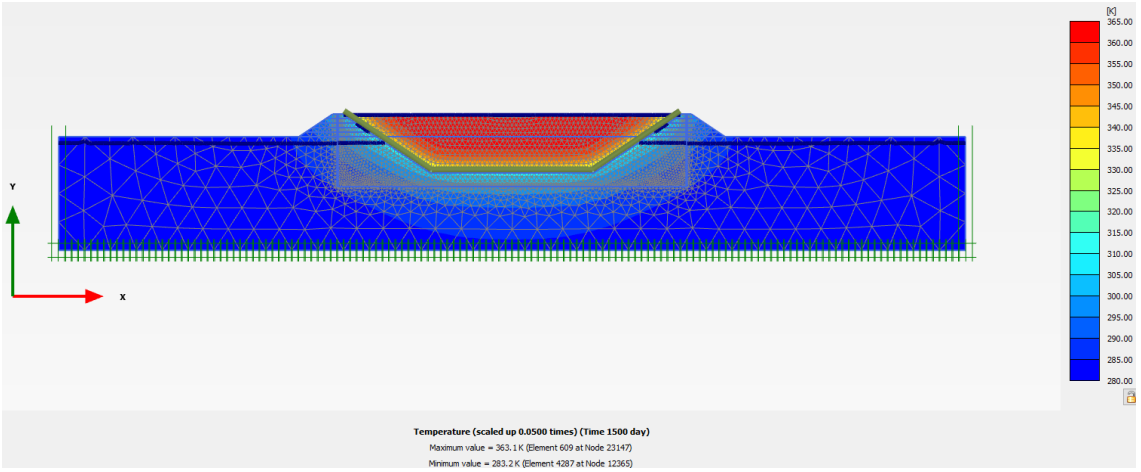

Figure 104 Temperature distribution after 1500 days (Setup 1 scenario 3)

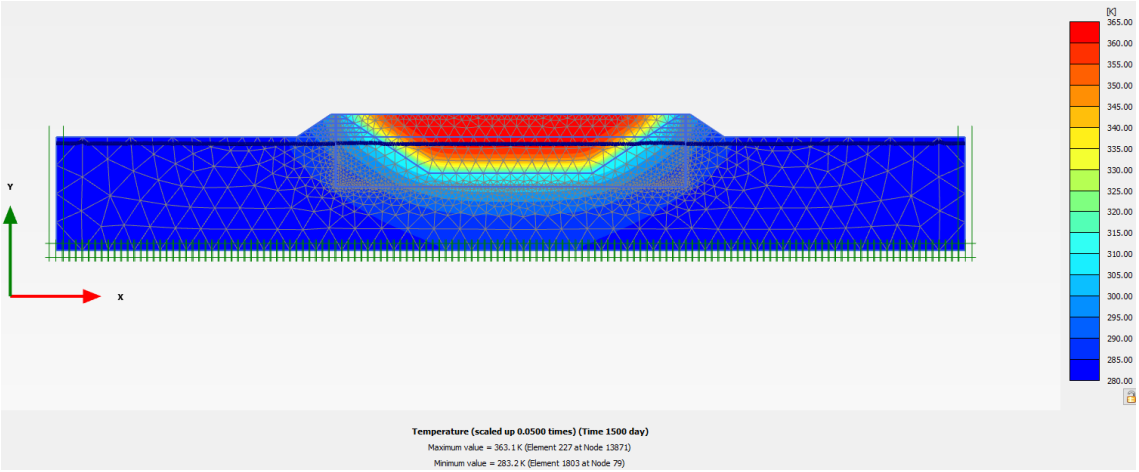

Figure 105 Temperature distribution after 1500 days (Setup 1 scenario 4)

The temperature distribution at the two cross-sections after 4000 days is plotted in Figures (106 & 107). The results of the other time intervals are shown in the appendix (C.3). The temperature plotted in the following comparisons is converted from Kelvin (temperature unit in PLAXIS) to degrees Celsius.

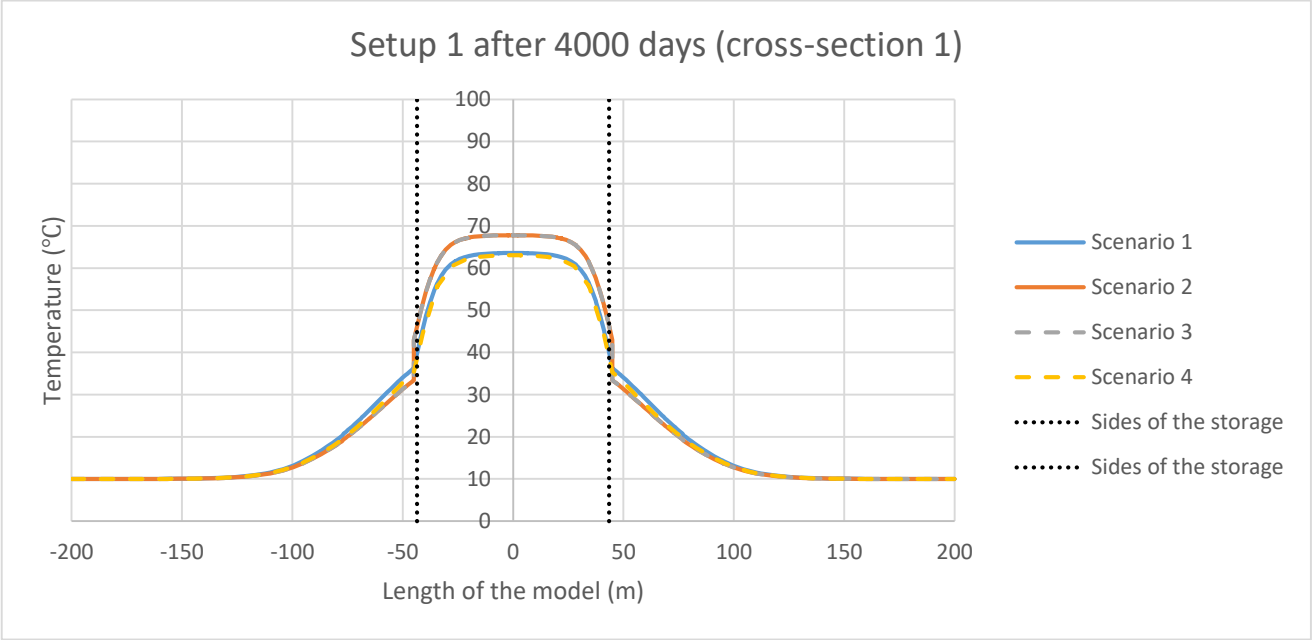

Figure 106 Setup 1 cross-section 1 after 4000 days

Figure 106 shows that inside the storage, scenarios 1 and 4 have a lower temperature compared to scenarios 2 and 3. The reason for this is the presence of thermal insulation along the sides of the storage in scenarios 2 and 3, which allow these scenarios to store more temperature inside the storage compared to scenarios 1 and 4. Top thermal insulation is discussed in section (5.6).

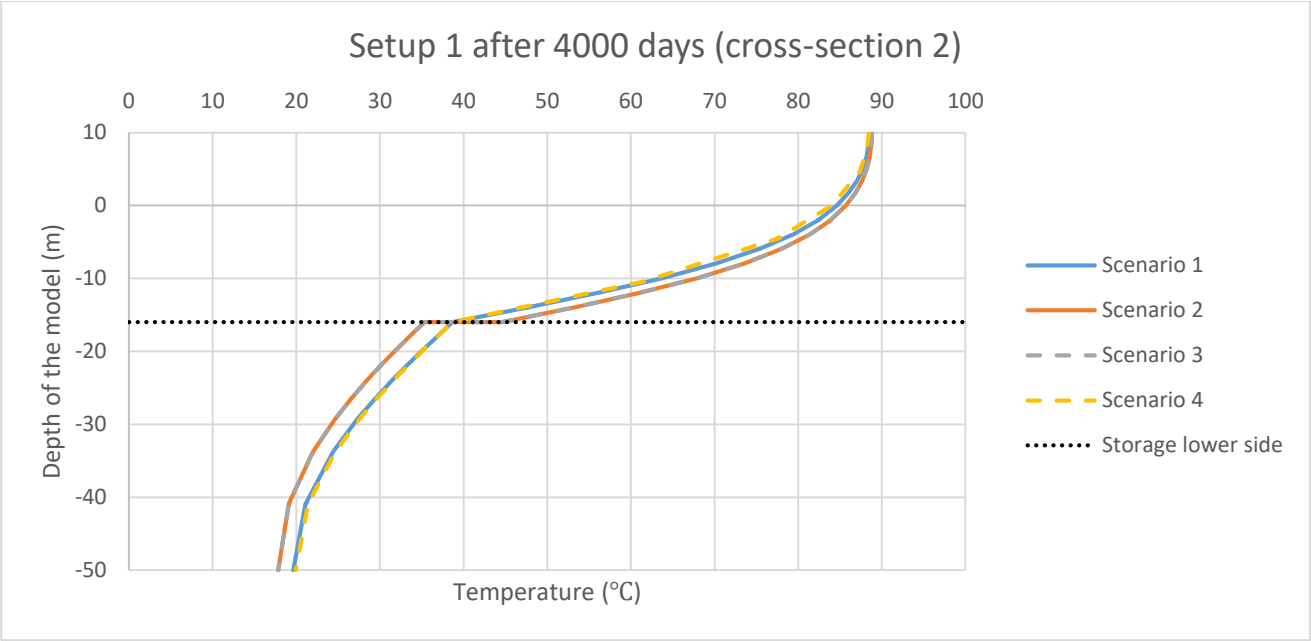

Figure 107 Setup 1 cross-section 2 after 4000 days

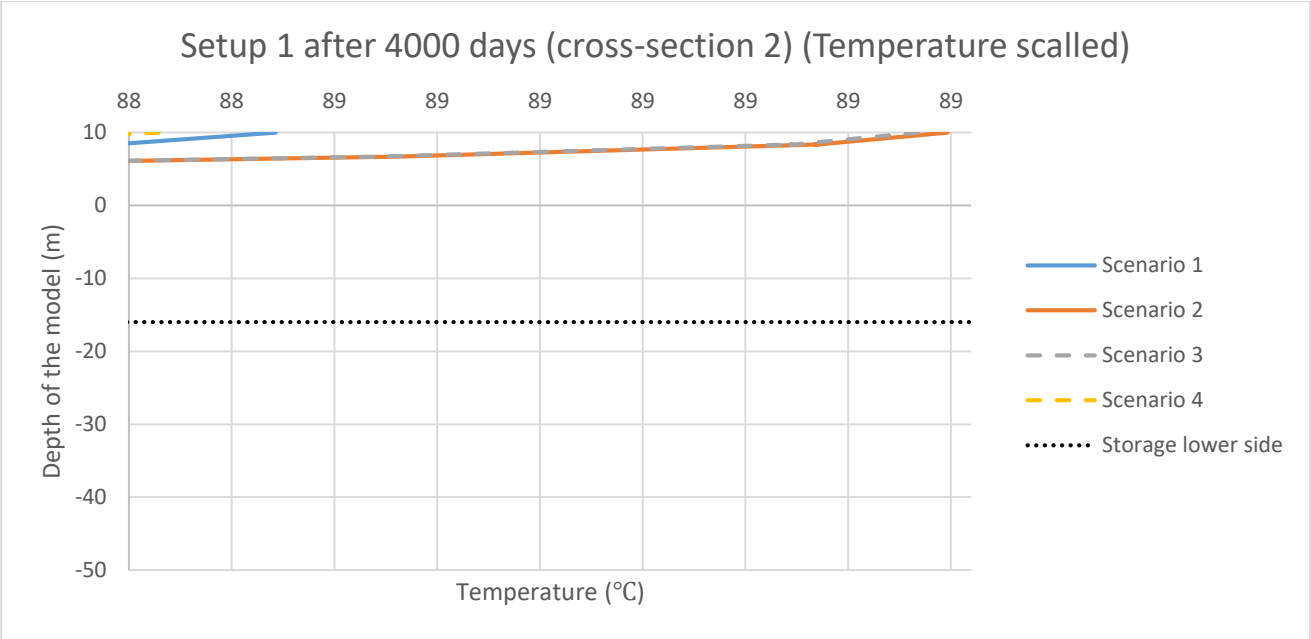

Figure 108 Setup 1 cross-section 2 after 4000 days (Temperature scaled)

Figure 107 shows that scenarios 1 and 4 have a higher temperature compared to scenarios 2 and 3 below the storage and lower temperature inside the storage. As scenarios 1 and 4 do not have thermal insulation along the sides, more temperature is transferred from the storage to the adjacent soil layers below. Moreover, the absence of thermal insulation on along the sides for scenario 1 and 4 lead to the dissipation of the temperature inside the storage faster than scenario 2 and 3.

Figure 108 shows the difference in temperature between the two scenarios after scaling the temperature. The differences are too small to be noticed (0.01 ℃). Top thermal insulation is discussed in section (5.6).

5.5.2 Setup 2

The same approach used to present the results for setup 1, is used for setup 2. The temperature distribution for the scenarios after 1500 days is shown in Figures (109-112). The results for other time intervals are shown in the appendix (C.4).

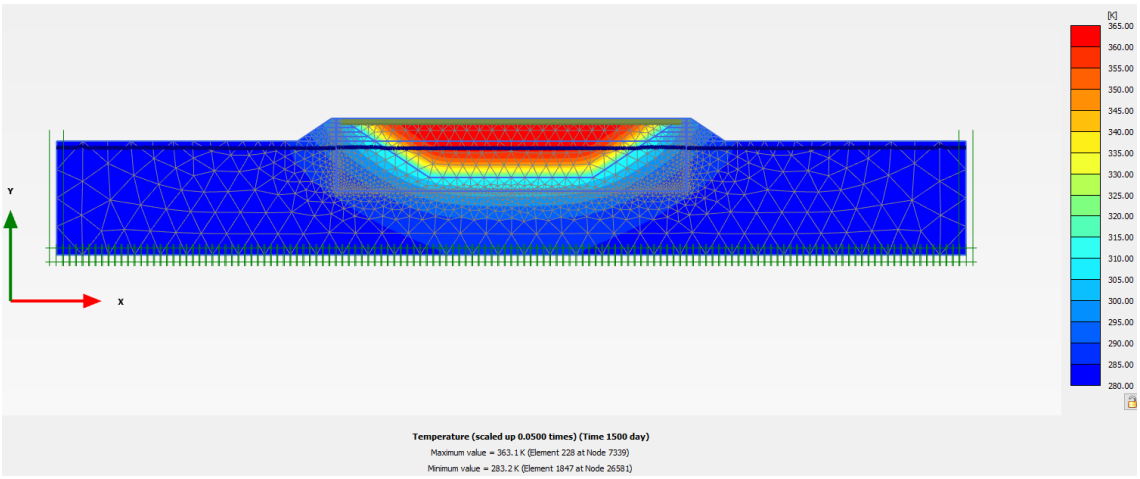

Figure 109 Temperature distribution after 1500 days (Setup 2 scenario 1)

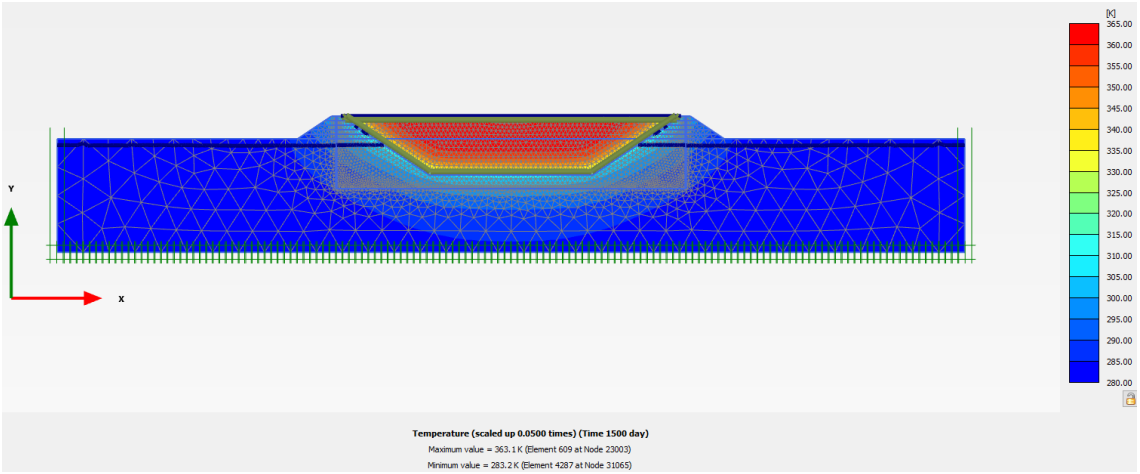

Figure 110 Temperature distribution after 1500 days (Setup 2 scenario 2)

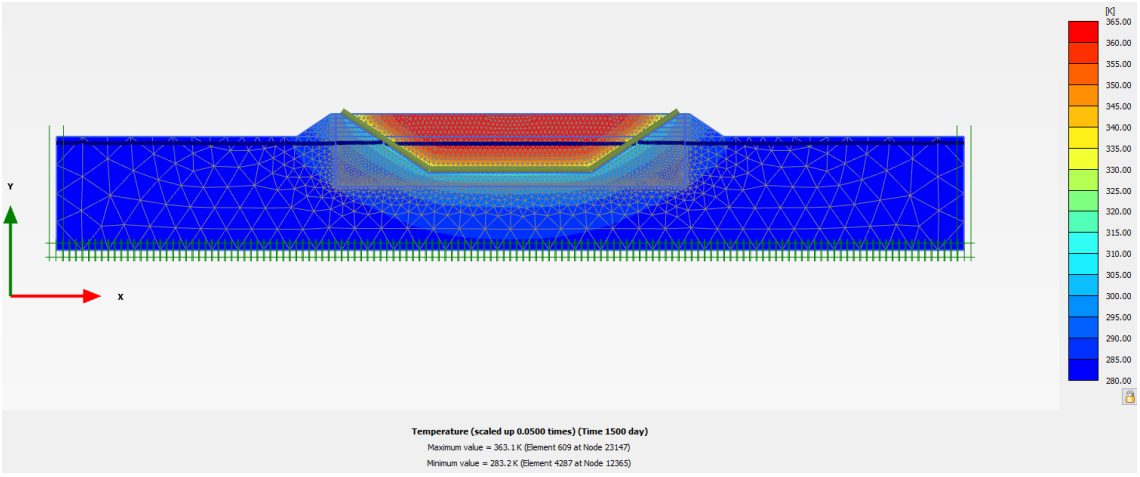

Figure 111 Temperature distribution after 1500 days (Setup 2 scenario 3)

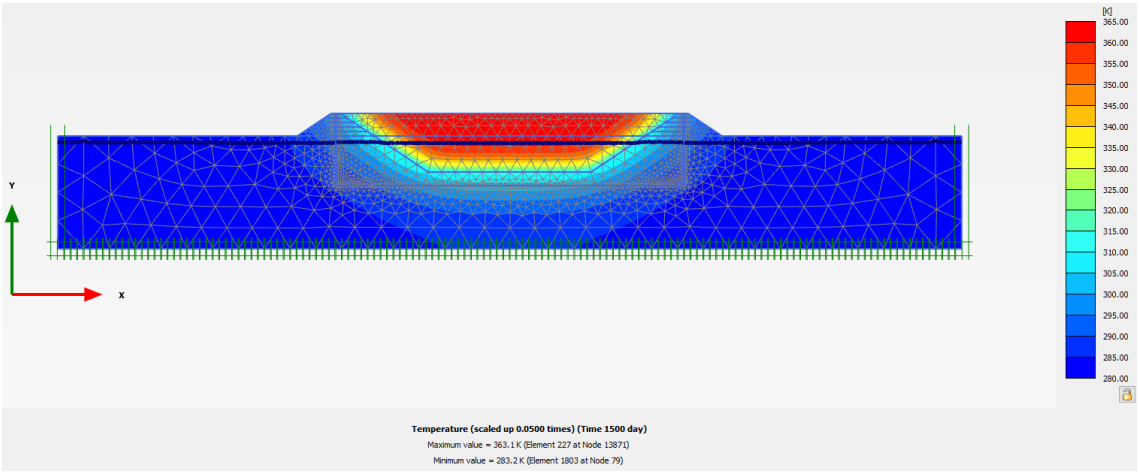

Figure 112 Temperature distribution after 1500 days (Setup 2 scenario 4)

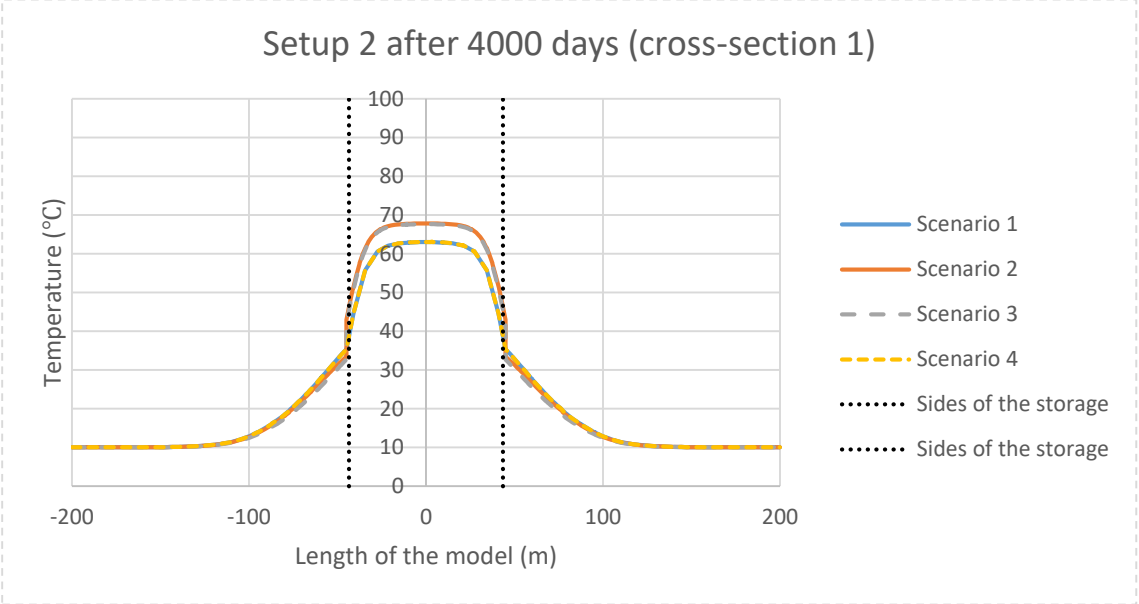

Figure 113 Setup 2 cross-section 1 after 4000 days

The temperature distribution at the two cross-sections after 4000 days is shown in Figures (113 & 114) respectively. The results for the other time intervals are shown in the appendix (C.4). Figure 111 shows the same observations as setup 1. Scenarios 1 and 4 have a lower temperature inside the storage. Moreover, from Figure 114 the influence of the thermal along the sides of the storage is clear. Scenarios 1 and 4 have a higher temperature below the storage and lower temperature inside the storage. Figure 115 shows the influence of the thermal insulation on the top of the storage after scaling the temperature. The differences in this setup between the temperature on the top of the storage for scenarios 2 and 3 is 0.19 ℃. Top thermal insulation is discussed in section (5.6).

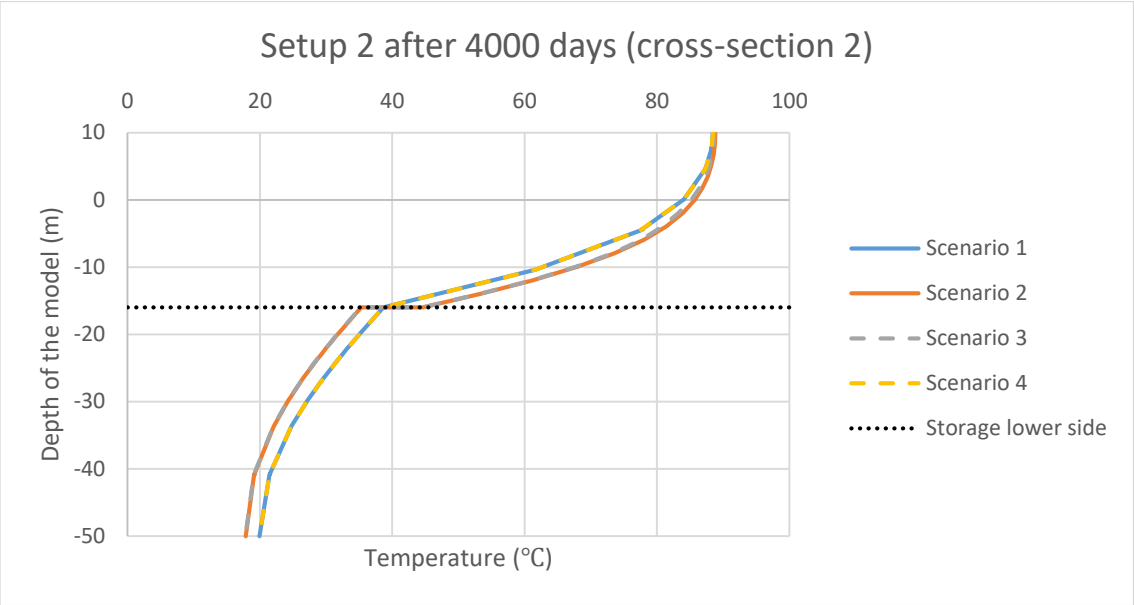

Figure 114 Setup 2 cross-section 2 after 4000 days

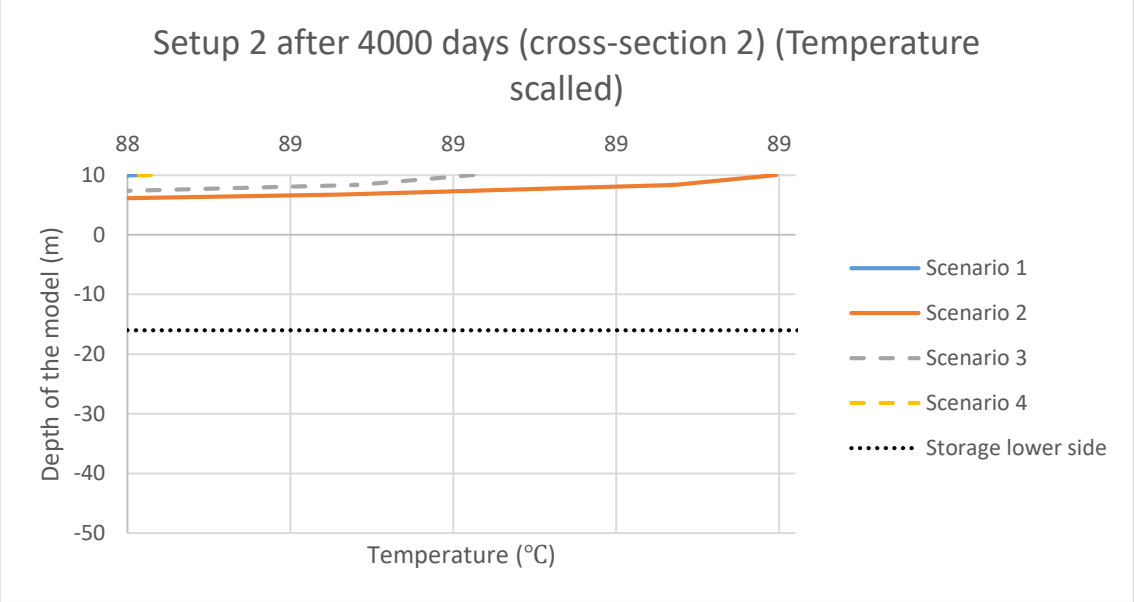

Figure 115 Setup 2 cross-section 2 after 4000 days (Temperature scaled)

5.5.3 Setup 3

The temperature distribution for the scenarios after 1500 days is shown in Figures (116-119). The results for other time intervals are shown in the appendix (C.5).

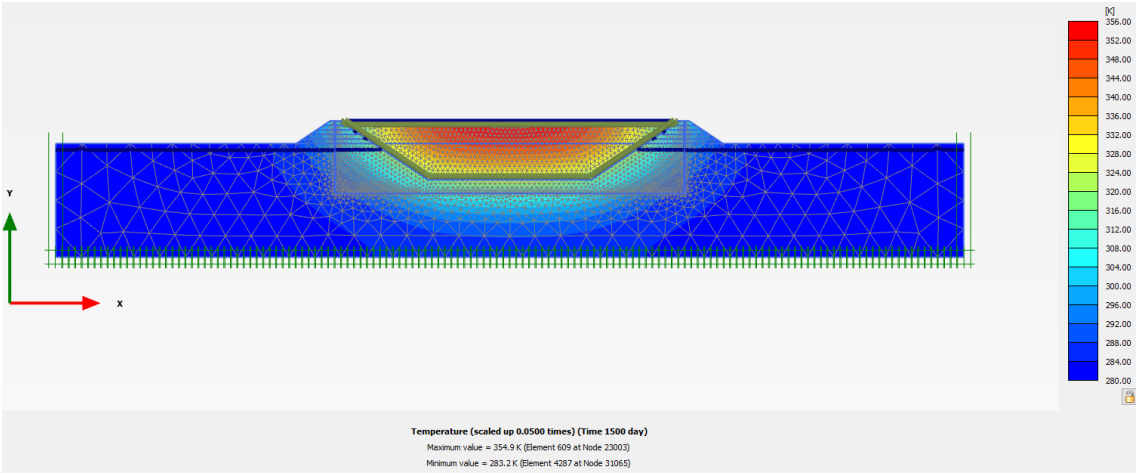

Figure 116 Temperature distribution after 1500 days (Setup 3 scenario 1)

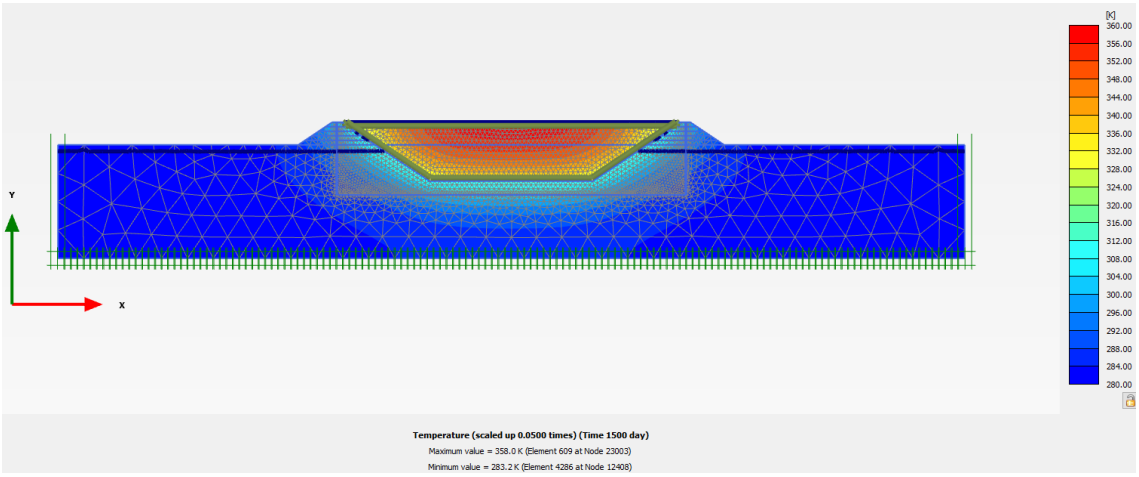

Figure 117 Temperature distribution after 1500 days (Setup 3 scenario 2)

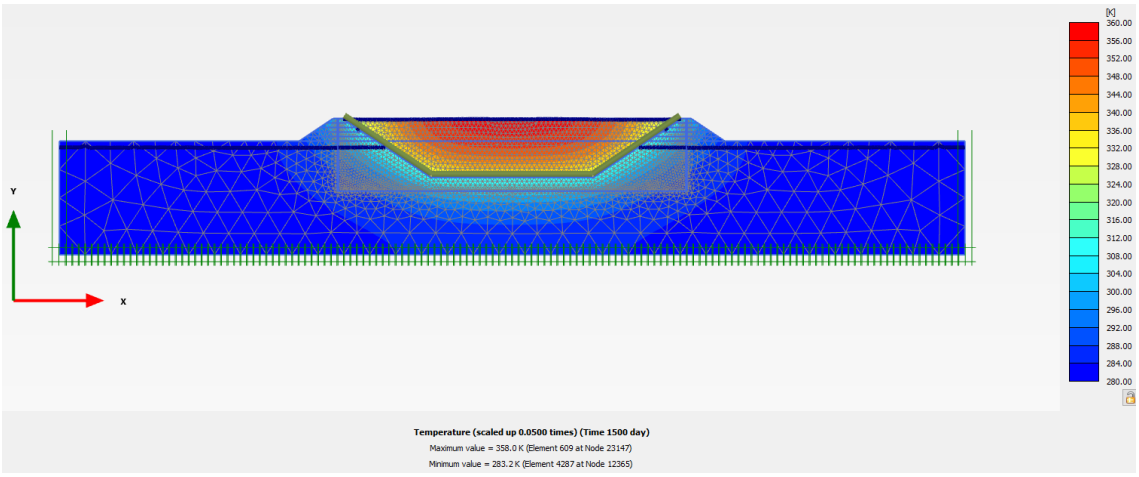

Figure 118 Temperature distribution after 1500 days (Setup 3 scenario 3)

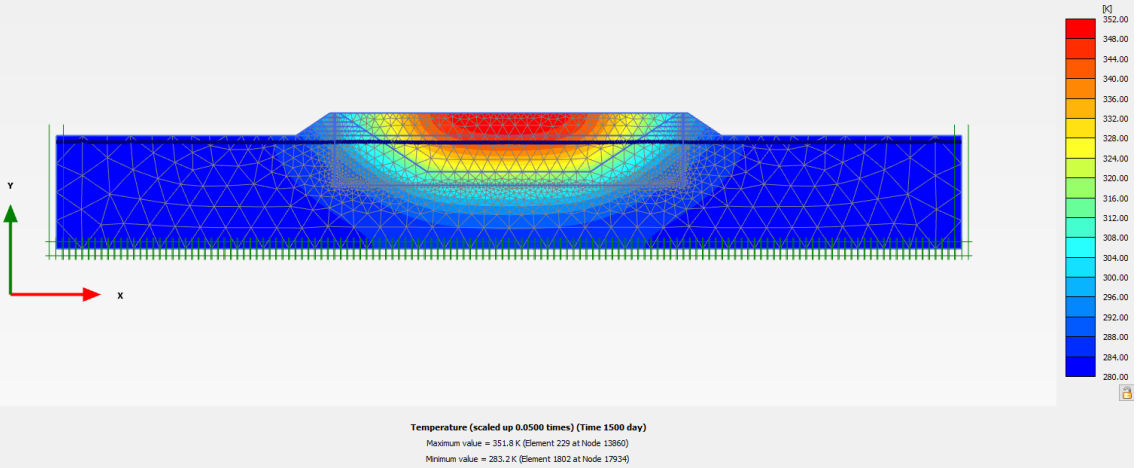

Figure 119 Temperature distribution after 1500 days (Setup 3 scenario 4)

The temperature distribution at the two cross-sections after 4000 days is shown in Figures (120 & 121) respectively. The results for the other time intervals are shown in the appendix (C.5).

The results in Figure 120 show that inside the storage, scenario 4 has the lowest temperature followed by scenario 1. Scenarios 2 and 3 have a similar temperature.

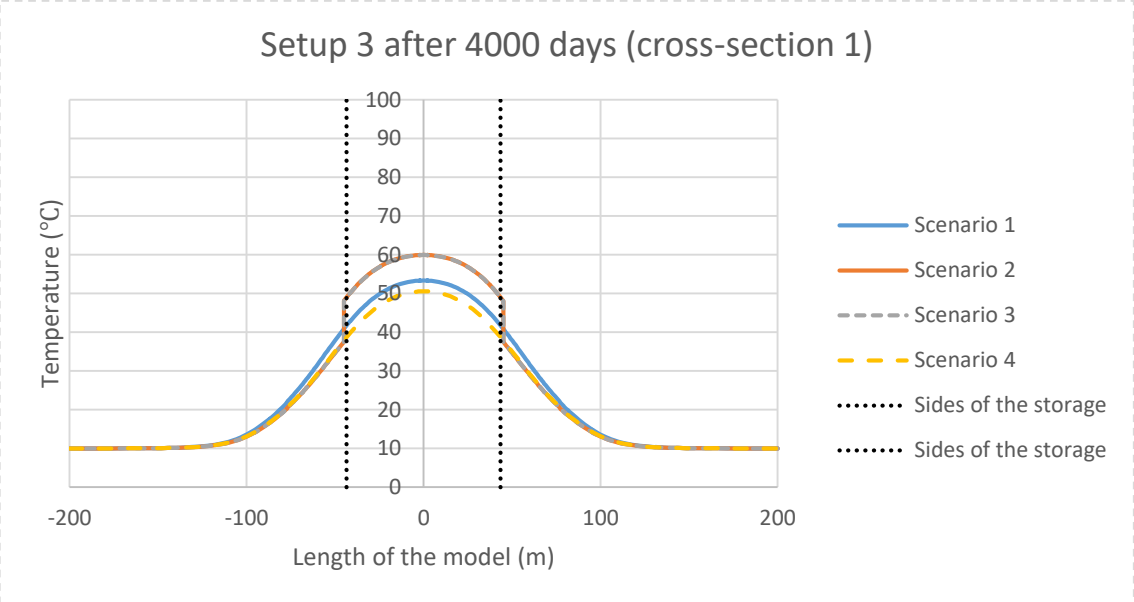

Figure 120 Setup 3 cross-section 1 after 4000 days

As noticed from Figure 120, Figure 121 shows that scenario 4 has the lowest temperature inside the storage followed by scenario 1 and scenarios 2 and 3 are nearly similar in terms of temperature. Figure 122 shows the differences in temperature on top of the storage after scaling the temperature. The difference between scenario 2 and 3 is 0.04℃. Top thermal insulation is discussed in section (5.6).

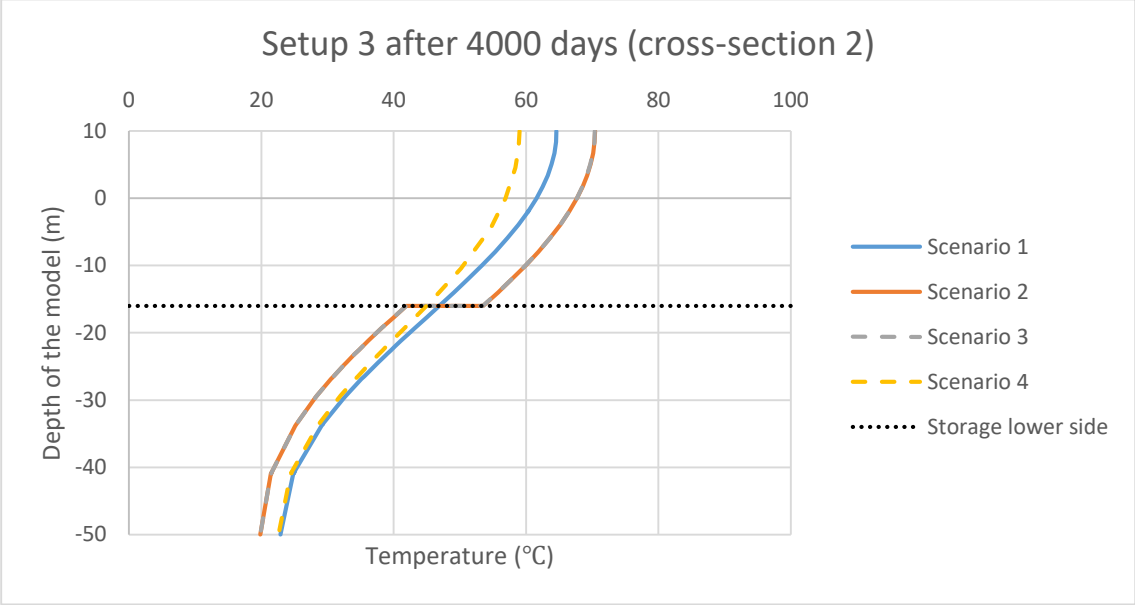

Figure 121 Setup 3 cross-section 2 after 4000 days

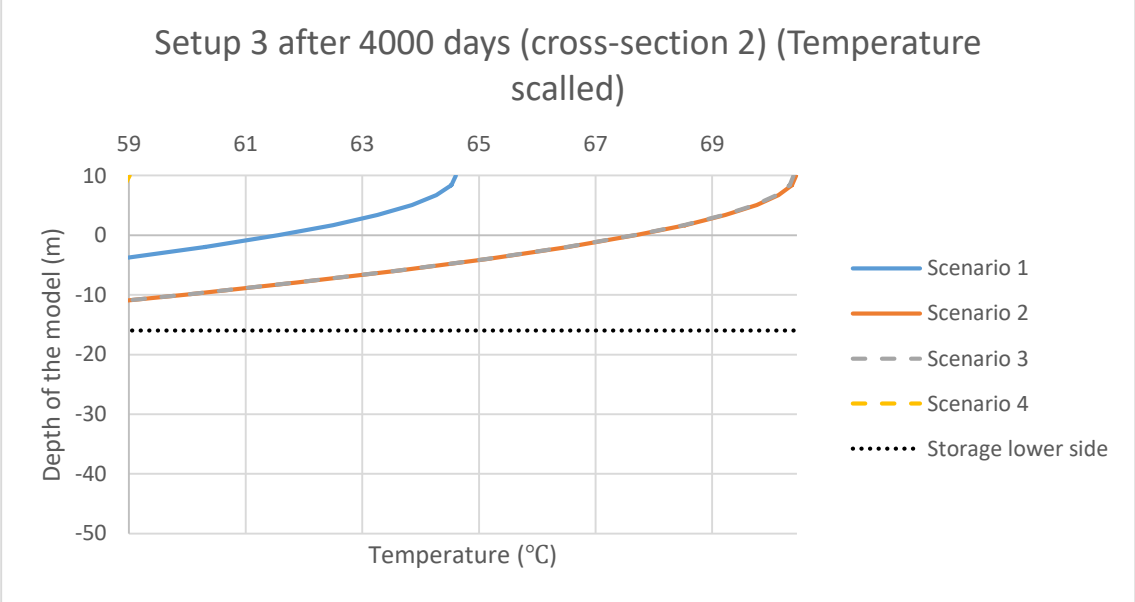

Figure 122 Setup 3 cross-section 2 after 4000 days (Temperature scaled)

5.5.4 Comparison between setups

In this subchapter, a comparison between the three setups for each scenario is performed. Since the observations are similar, the temperature distribution after 1500 days at the two cross-sections for scenario 1 is shown in Figures (123 & 124) respectively. The results for the other scenarios are shown in the appendix (C.6).

From Figure 123 it is clear that setup 3 results in the lowest temperature inside the storage. Setups 1 and 2 are nearly similar. Figure 124 shows that setup 3 has a higher temperature below the storage and lower temperature inside the storage. Moreover, setup 1 has slightly higher temperature compared to setup 2 inside the storage.

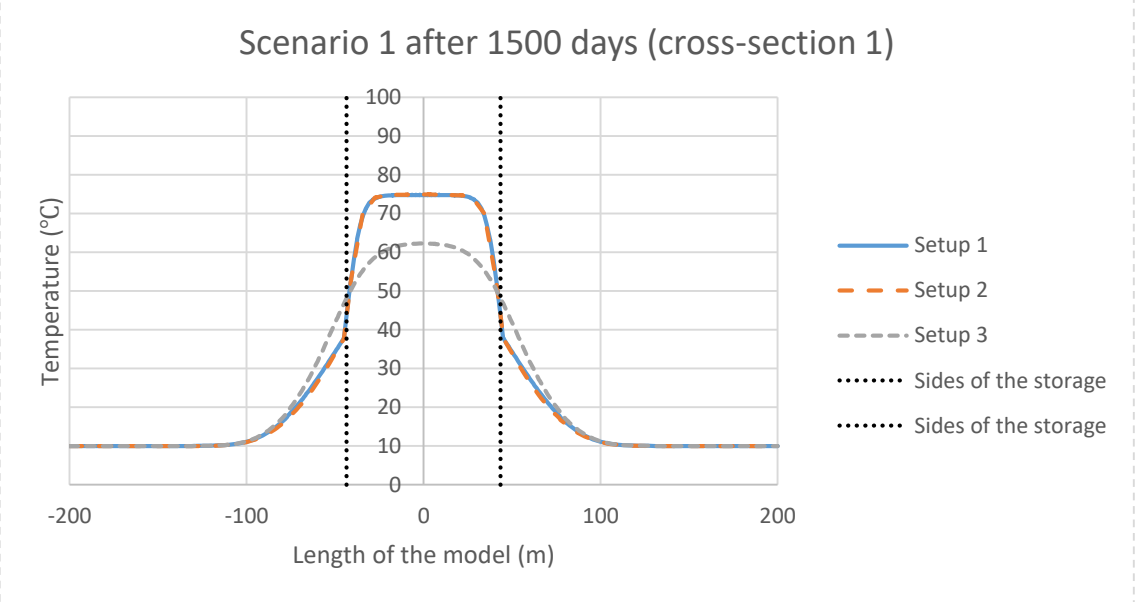

Figure 123 Scenario 1 cross-section 1 after 1500 days

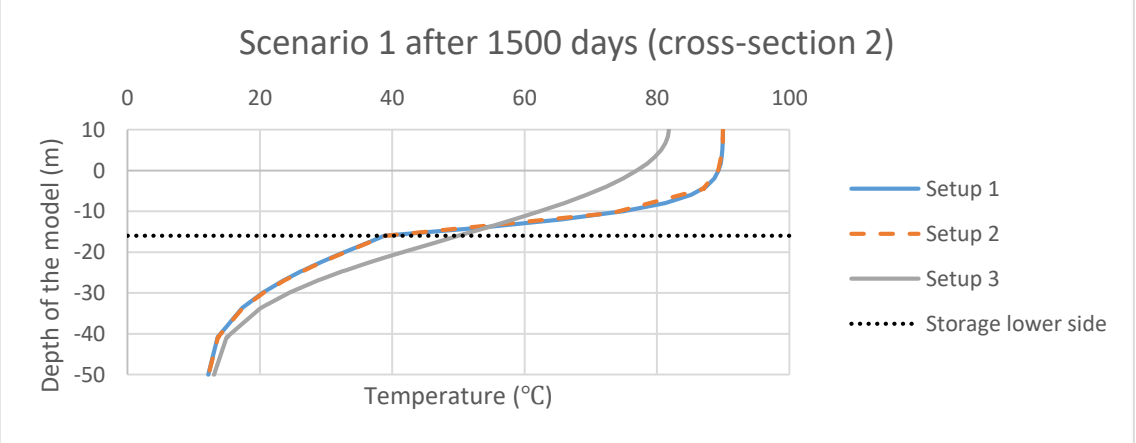

Figure 124 Scenario 1 cross-section 2 after 1500 days

5.6 Thermal insulation on top of the storage

As mentioned in the previous subchapter, the efficiency of using an interface to model the thermal insulation on top of the storage was questionable. As a result, further studies were carried out to check the influence of thermal insulation at the top of the storage on the temperature distribution.

In order to check the influence of the top insulation, climate conditions were applied. The climate conditions will influence the temperature distribution on top of the model. The air temperature has a value of 20°C with an amplitude of 10 and a period of 50 days (Figure 125).

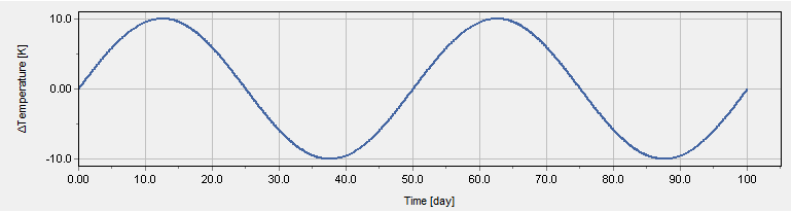

Figure 125 Temperature function

This study focuses on setup 2 described previously. Three scenarios were compared, scenarios 2 and 3 defined in the previous subchapters and a new scenario. Basically, the new scenario is scenario 2 with infinite thermal resistance on top of the storage. Three time intervals were chosen for the study. The time analysis was done after 500, 1500 and 4000 days.

The temperature distribution for the three scenarios after 1500 days is shown in Figures (126-128). The results for other time intervals are shown in the appendix (C.7).

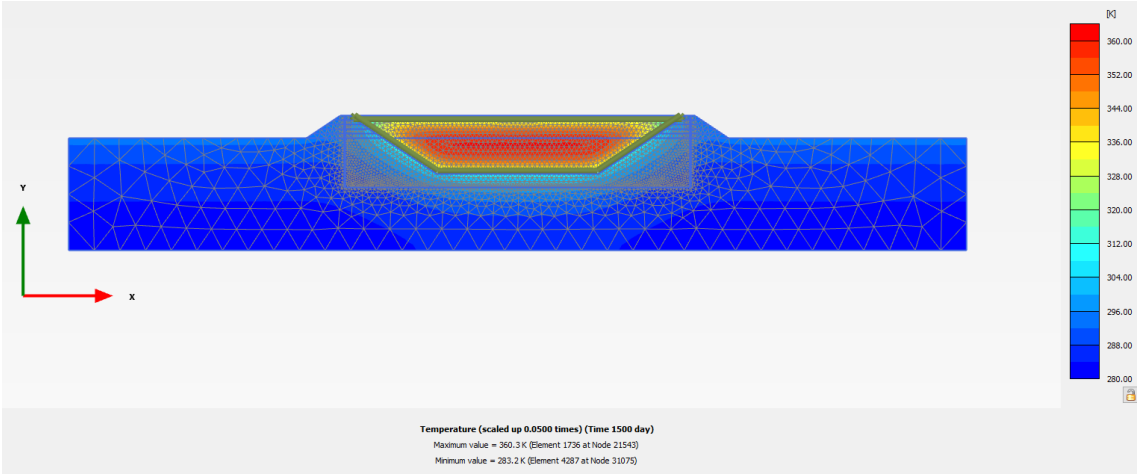

Figure 126 Setup 2 Scenario 2 after 1500 days (Top thermal insulation study)

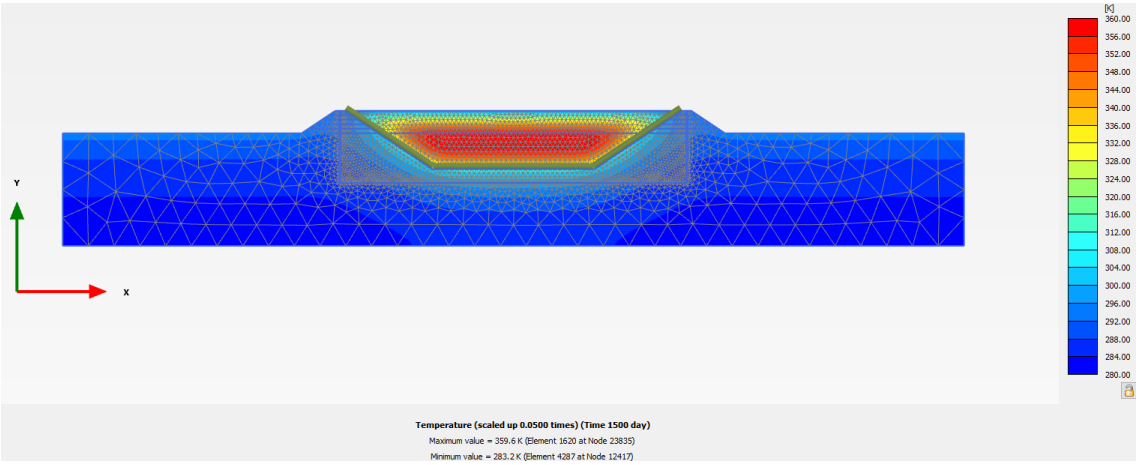

Figure 127 Setup 2 Scenario 3 after 1500 days (Top thermal insulation study)

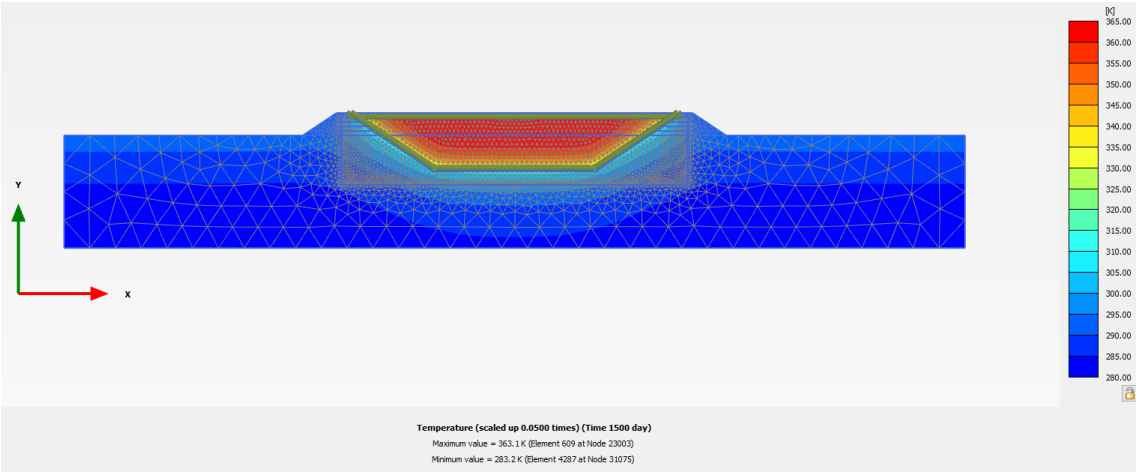

Figure 128 Setup 2 Scenario 2 (infinite top thermal resistance) after 1500 days (Top thermal insulation study)

The comparison is carried out at cross-section 2 (Figure 101). The temperature distribution after 500, 1500 and 4000 is plotted in Figures (129-131) respectively.

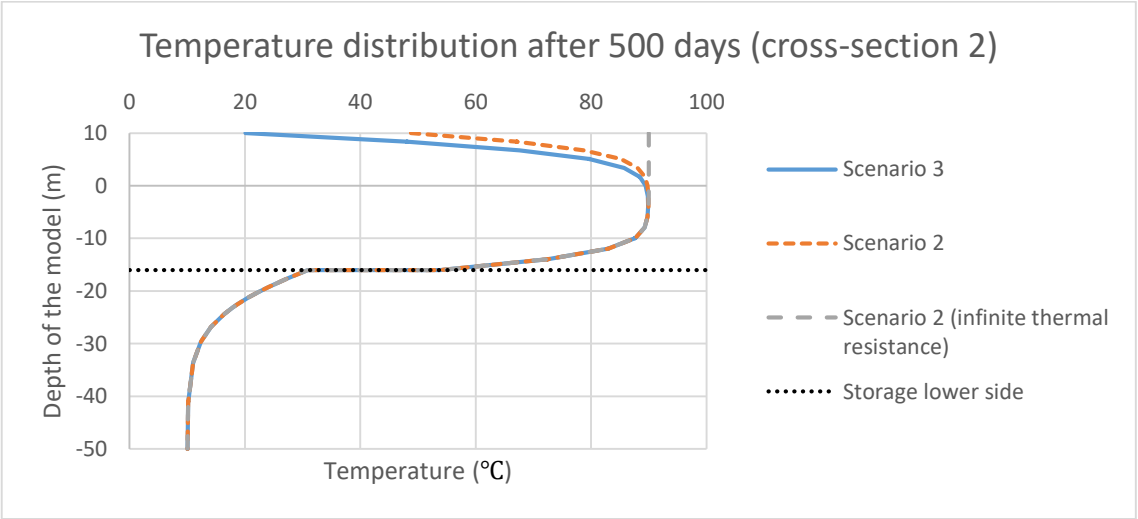

Figure 129 Temperature distribution after 500 days (Top thermal insulation study)

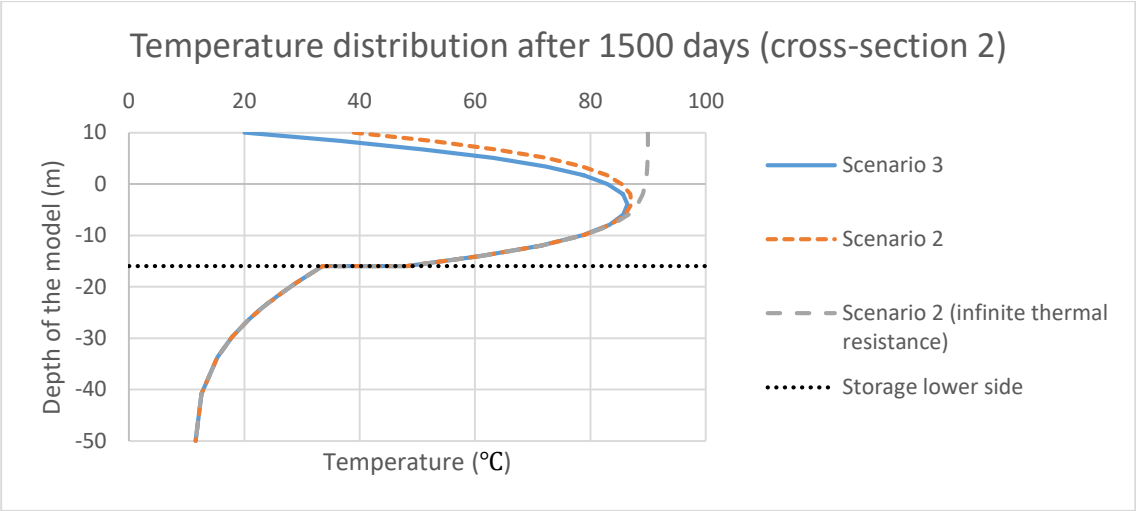

Figure 130 Temperature distribution after 1500 days (Top thermal insulation study)

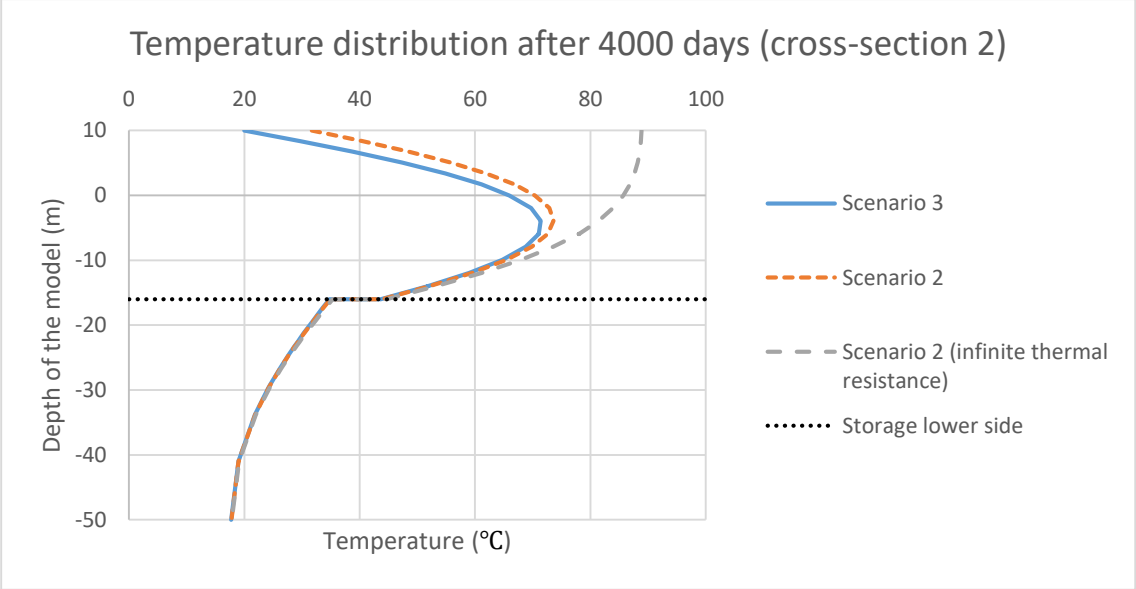

Figure 131 Temperature distribution after 4000 days (Top thermal insulation study)

The results show the impact of the top thermal insulation on the temperature distribution inside the storage. After 500 days the difference in temperature between scenarios 2 and 3 at top of the storage is 28.64 ℃. After 1500 days the difference is 18.92 ℃ and after 4000 days the difference is 18.94 ℃. Moreover, the scenario with infinite thermal resistance on top keeps the temperature inside the tank at 90℃ after 500 days. As time proceeds, the temperature in this scenario starts to dissipate with much smaller rate than the other scenarios.

This study showed that the modelling approach used in the previous studies was not correct as the top thermal insulation was not effective due to the absence of climate conditions.

6 Case study

In this chapter, a large-scale test carried out by the Austrian Federal Railways (ÖBB), Keller Grundbau and the Institute of Soil Mechanics and Foundation Engineering at Graz University of Technology (ÖBB et al. 2018) is illustrated. Several trials to model this test in PLAXIS were performed. The results from these trials as well as comparisons between the measurements and the results are presented.

6.1 Problem description

The construction project of St. Kanzian consists of several tunnels. While tunnelling Untersammelsdorf Tunnel, damage patterns in the transition area between piles and the soil were found. The soil type is Seeton, it is a geological layer consisting of soft and unstable clay minerals. These damage patterns can be attributed to several factors, one of these factors is the temperature distribution which is the reason behind the test (ÖBB et al. 2018).

6.2 Test description

In order to investigate the problem described in the previous subchapter, a large-scale test was performed. The aim of the test is to study the influence of the temperature change of the piles on properties of the Seeton. As a result, the installation of a pile in a soil body was simulated. The soil body of Seeton was artificially produced, while the pile was simulated as a concrete body (ÖBB et al. 2018).

The concrete and Seeton are placed in a 7.5 m^3 dump container shown in Figure 132. The longitudinal cross-section is shown in Figure 133. The sides and the floor of the container are covered by a thermally insulating layer of EPS. The rectangular concrete block has a thickness of 80 cm (ÖBB et al. 2018).

Figure 132 Dump container (ÖBB et al. 2018)

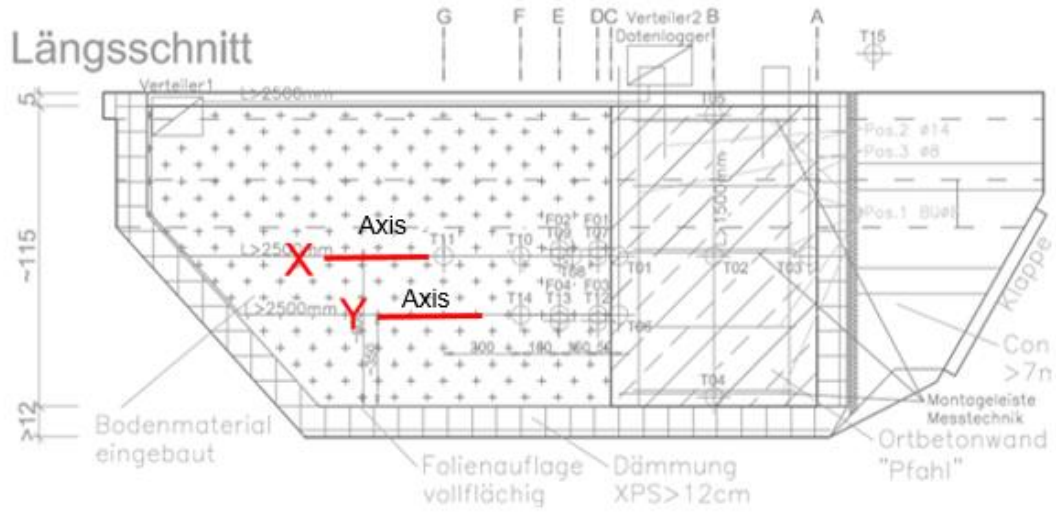

Figure 133 Longitudinal cross-section (ÖBB et al. 2018)

Table 15 Measuring sensors (ÖBB et al. 2018)

T01	Concrete body X-axis (horizontal axis), A-C (vertical axes)
T02	
T03	
T04	Top of the concrete body
T05	Bottom of the concrete body
T06	Concrete body Y-axis (horizontal axis), C (vertical axis)
T07	Soil body X-axis (horizontal axis)
T08	
T09	
T10	
T11	
T12	Soil body Y-axis (horizontal axis)
T13	
T14	
T15	Air temperature

The X and Y axes shown in Figure 133 are the two sensor levels. The X-axis is about 60 cm above the ground, while Y-axis is about 35 cm above the ground. The points (T01-T15) shown in Figure 131 are the sensor points of the thermocouples used to measure the temperature. Table 15 shows the location of the thermocouples (ÖBB et al. 2018).

6.3 Test results

The measured temperatures are not absolute temperatures; they are relative to the temperature at the beginning of the measurements. Moreover, there was a brief interruption of the measuring procedure at test hours of 50 and 105. This interruption was not corrected by correction values (ÖBB et al. 2018).

6.3.1 Air temperature

The air temperature was recorded by sensor T15. The results are shown in Figure 134. In the Figure, the periodic temperature fluctuations of the air temperature are shown. Moreover, some measured values from the Seeton and concrete are presented (dotted lines). It is noticed that daily fluctuations have almost no influence on the recorded temperatures inside the test container. Only two sensors (T02 and T03) inside the concrete body, show small periodically fluctuations. However, these two measuring points are not used for the studying of the transport of temperature between the concrete body and the Seeton. As a result, the daily air temperature fluctuation can be neglected (ÖBB et al. 2018).

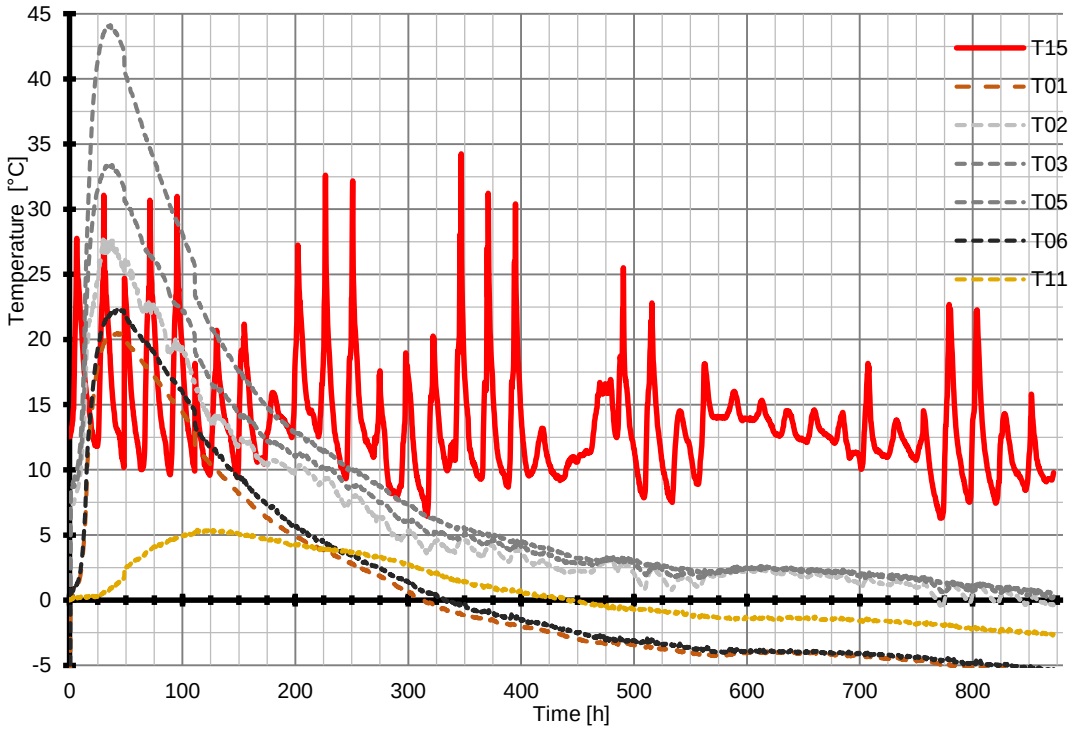

Figure 134 Temperature at T15 (ÖBB et al. 2018)

6.3.2 Temperature distribution in concrete

The temperature distribution in concrete is shown in Figures (135 & 136). The results show that the two sensors T04 and T03 in the connection with the insulation layer have high temperatures. In addition, the two sensors T01 and T06 in the connection with the soil body have almost an identical temperature (ÖBB et al. 2018).

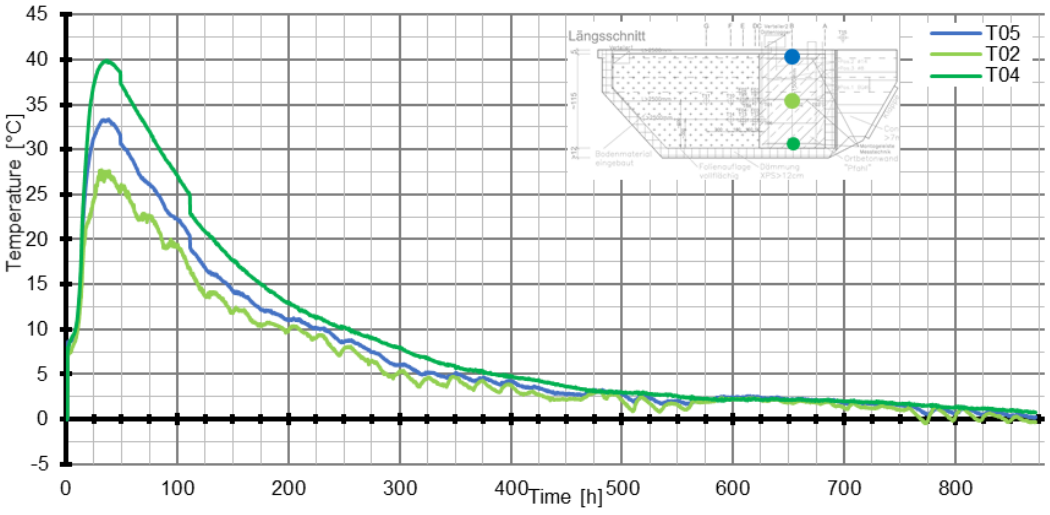

Figure 135 Relative temperature distribution in concrete (vertical B-axis) (ÖBB et al. 2018)

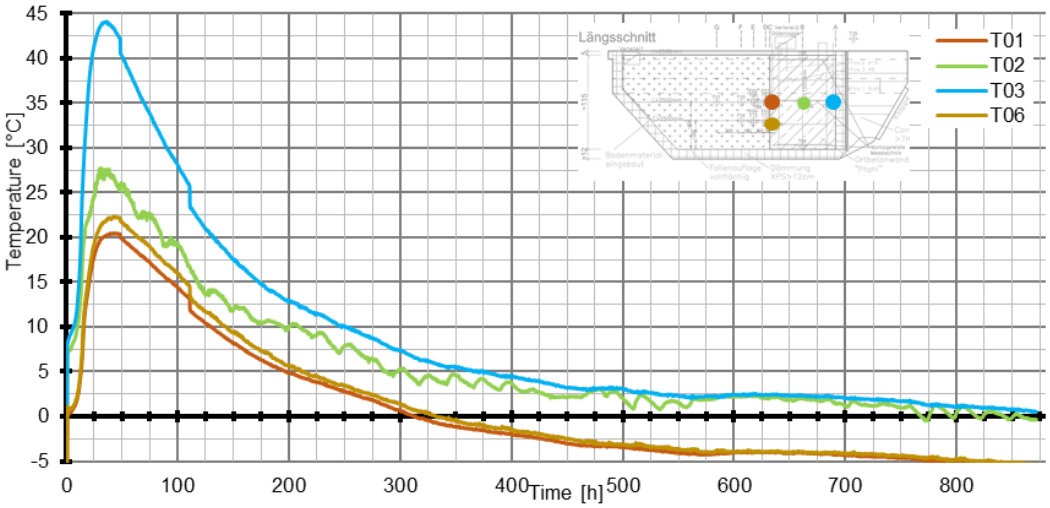

Figure 136 Relative temperature distribution in concrete (horizontal X &Y axes) (ÖBB et al. 2018)

6.3.3 Temperature distribution along Y-axis

The temperature distribution along Y-axis is shown in Figure 137. It can be noticed that the maximum temperature due to the hydration of concrete is about 22.5℃ and was reached after 50 hours. At the same time, the maximum temperature at sensor T12 in the soil body was reached. This behaviour suggests that the thermal conductivity of concrete and soil is the same. T13 and T14 show that increasing the distance from the concrete body lead to a reduction in the temperature, thus less influence from the hydration of the concrete. Another observation is regarding the heat capacity of the soil, T01 and T06 cooled much faster than T12-T14 which shows that the heat capacity of the soil is higher than that of concrete (ÖBB et al. 2018).

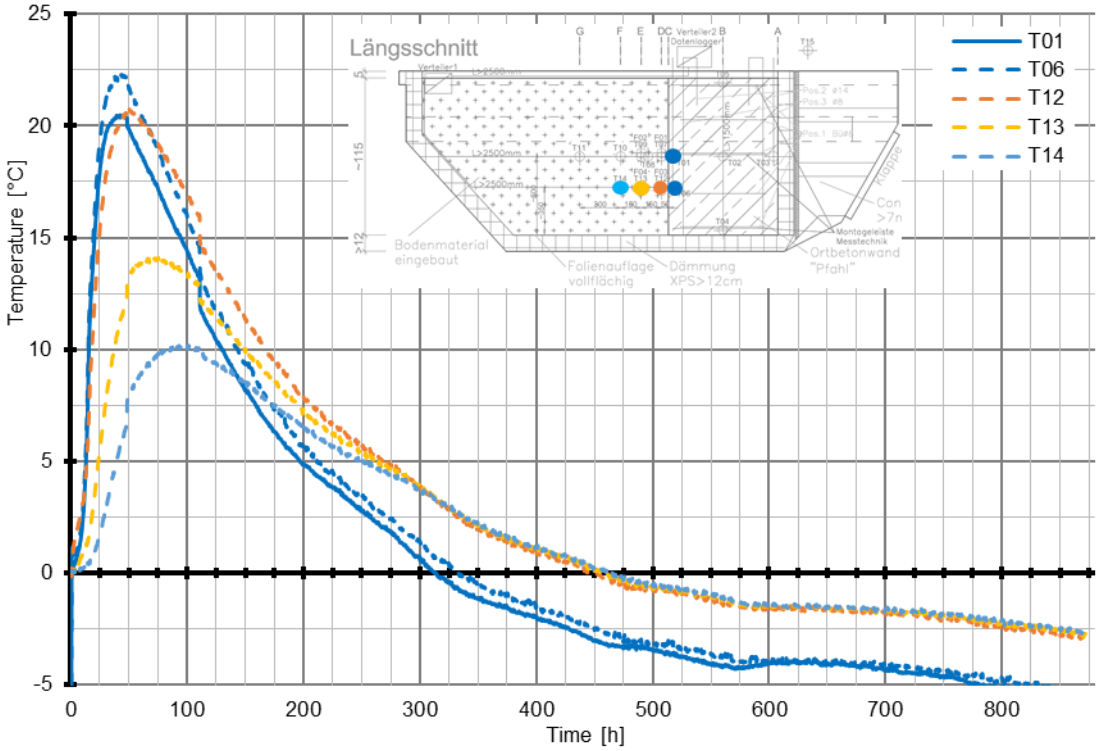

Figure 137 Relative temperature Y-axis (ÖBB et al. 2018)

6.3.4 Temperature distribution along X-axis

The temperature distribution along X-axis is shown in Figure 138. Both Figures (135&136) show the influence of the hydration of concrete on the temperature distribution in the soil. This influence decreases when the distance increases but still has an effect even at long distances (T11). Moreover, the results show that there is a difference in heat capacity between soil and concrete but the thermal conductivity is the same.

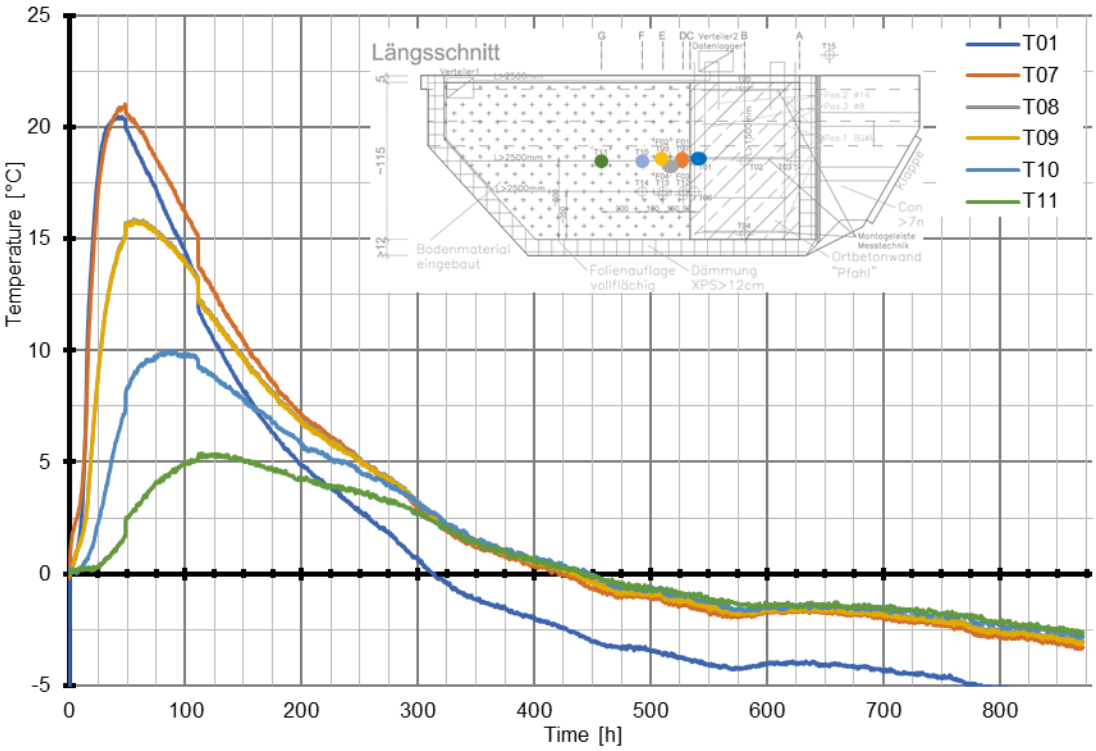

Figure 138 Relative temperature X-axis (ÖBB et al. 2018)

6.4 Test modelling

In order to model the test in PLAXIS, the temperature in the concrete body was used as an input for time-dependent temperature boundary conditions. This was done by creating four different setups varying in geometry and boundary conditions. The parameters used for modelling the Seeton are shown in Table 16.

Table 16 Parameters of Seeton

Parameter	Value
Material model	Mohr-Coulomb
Soil unit weight above phreatic level γ_{unsat}	20 kN/m^3
Soil unit weight below phreatic level γ_{sat}	20 kN/m^3
Young's modulus	10,000 kN/m^2
Poisson's ration ν	0.3
Friction angle ϕ	25°
Cohesion c	5 kN/m^2

6.4.1 Setup 1

The temperature in the first setup is applied by means of two vertical time-dependent temperature boundary conditions as shown in Figure 139. The temperature boundary condition on the right takes the measurements of T03 as an input, while the one on the left takes the measurements of T06 as an input. The light blue soil layer simulates the Setoon, while the concrete body is denoted by the brown layer and the thermal insulation is modelled by the yellow layer. The mesh of setup 1 is shown in the appendix (D.1)

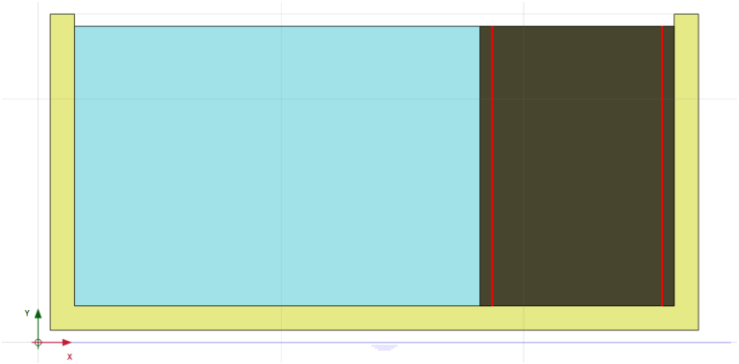

Figure 139 Setup 1

6.4.2 Setup 2

In the second setup, the temperature is applied by means of three vertical time-dependent temperature boundary conditions. Measurements of T03, T02 and T06 are used as inputs for the right, middle and left boundary conditions respectively. The geometry of setup 2 is shown in Figure 140. The mesh of setup 2 is shown in the appendix (D.1)

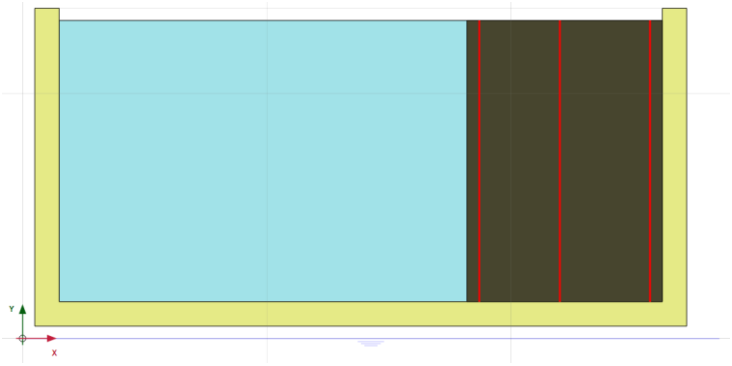

Figure 140 Setup 2

6.4.3 Setup 3

In this setup, only one vertical time-dependent temperature boundary condition is used for applying temperature. This boundary condition uses the measurements of T06 as an input. The concrete body to the right side of the boundary condition was removed. The geometry of setup 3 is shown in Figure 141. The mesh of setup 3 is shown in the appendix (D.1)

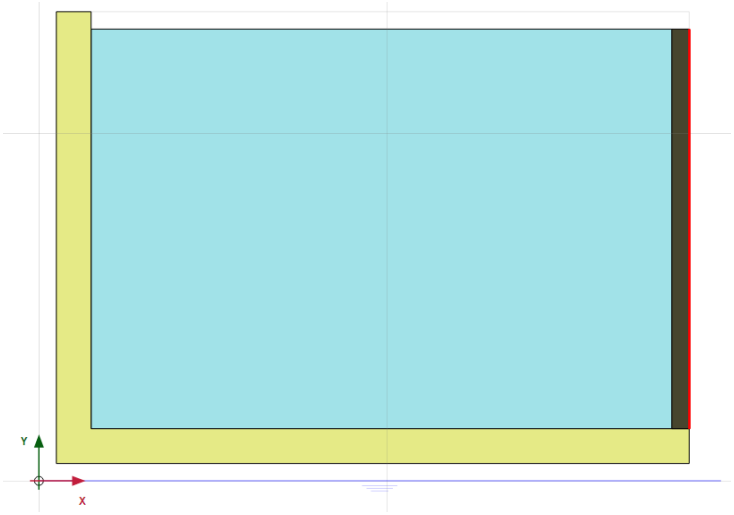

Figure 141 Setup 3

6.4.4 Setup 4

The temperature in setup 4 is applied by means of a vertical time-dependent temperature boundary condition. This boundary condition uses measurements of T06 as an input. In this setup, the boundary condition is applied directly on the transition part between the concrete body and the Seeton. Therefore, concrete is not modelled in this setup. The geometry is shown in Figure 142. The mesh of setup 4 is shown in the appendix (D.1)

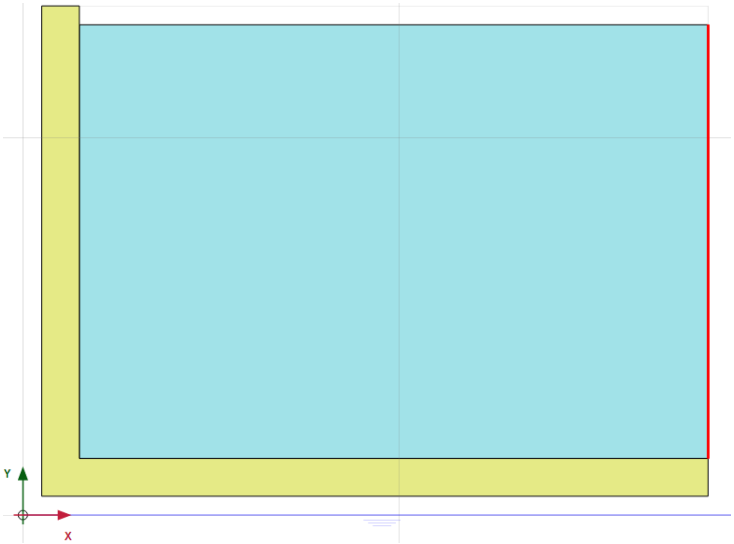

Figure 142 Setup 4

The time interval for the analysis was set to 872 hours as given in the test results. The thermal parameters used for Seeton, concrete and EPS are defined in Table 17. The results are shown for the two axes Y and X. Two variations for the four setups were performed. Once with applying water level on top of the Seeton and for the other variation, no water conditions were present. The results for setup 3 (no water conditions) are shown in Figures (143 & 144). The results for other setups and variations are shown in the appendix (D.1)

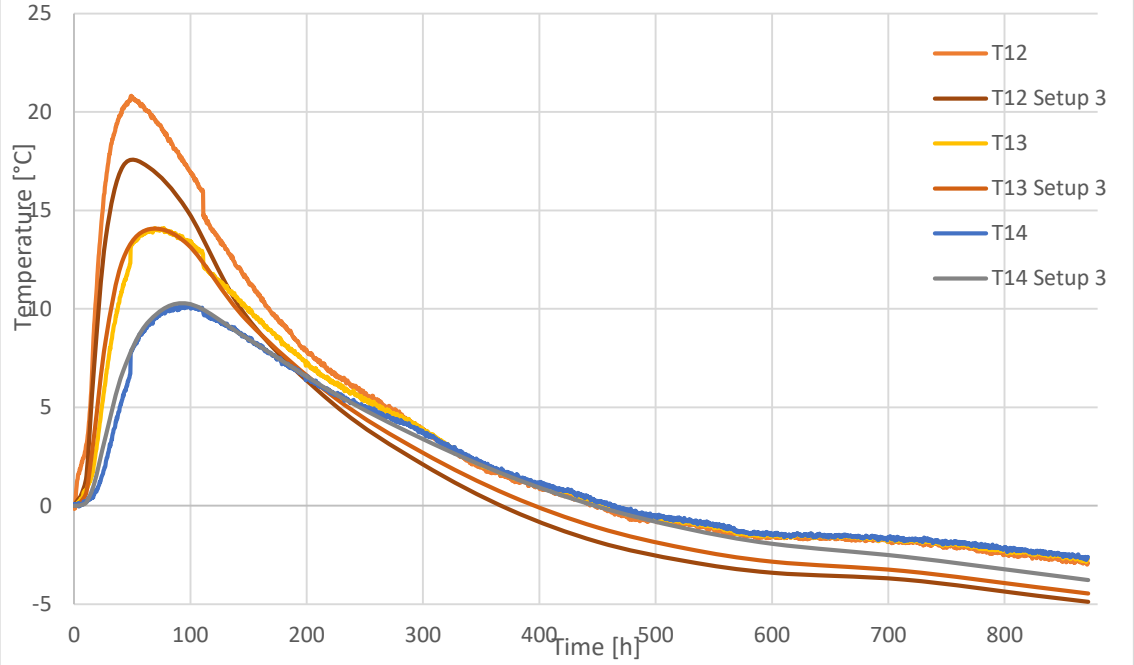

Figure 143 Comparison: measurements and setup 3 at Y-axis

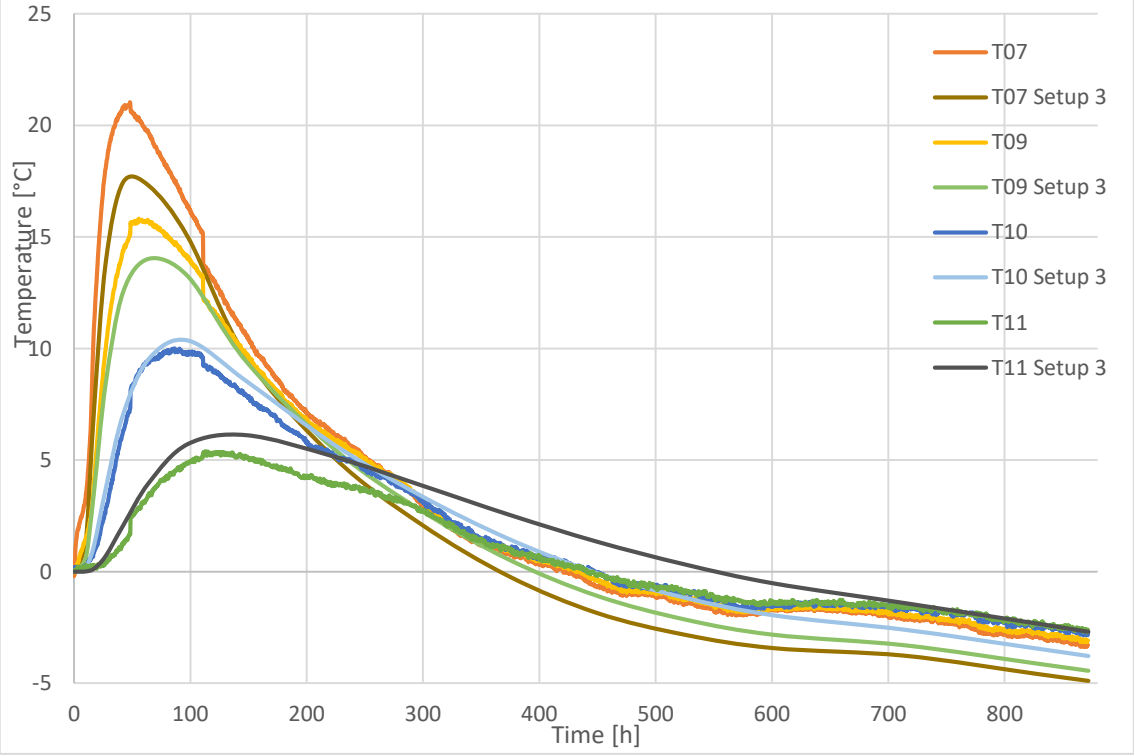

Figure 144 Comparison: measurements and setup 3 at X-axis

Figure 143 shows that there is a good fit to the peak temperature of measurements at T13 and T14. However, at T12 the obtained peak temperature is less than the measured temperature. Moreover, the end temperatures at the three points are less than the measured temperatures. The measurements show that the temperature at the three sensors are nearly equal after 300 hours, unlike the results obtained which show that there is always a difference in temperature between the three points.

Figure 144 shows similar observations, at T07 and T09 the peak temperature is lower than the measures ones. Regarding T10, the obtained peak temperature shows a good fit to the measured peak temperature. At T11, the obtained peak temperature is higher than the measured one.

The three main differences can be summarized as follows:

1. The peak temperature at the points near the concrete (T07 & T12) is lower than the measured temperature
2. The end temperature at all points (except T11) is lower than the measured temperature
3. After approximately 300 hours, the temperature at the measurement points is nearly equal. On the other hand, the temperature obtained is not equal even at the end of the analysis.

Table 17 Thermal parameters for Seeton, concrete and EPS

Seeton		Concrete		EPS	
Heat capacity (kJ/t/K)	Thermal conductivity (W/m/K)	Heat capacity (kJ/t/K)	Thermal conductivity (W/m/K)	Heat capacity (kJ/t/K)	Thermal conductivity (W/m/K)
900	2	800	2	1300	0.0341

6.5 Setup 3

Several variations for setup 3 in terms of thermal conductivity and heat capacity for Seeton and concrete were studied. For all of the variations, water level on top of the Seeton was applied. The thermal parameters for all of the variations are shown in Table 16.

Table 18 Setup 3 variations

	Seeton		Concrete	
Variations	Heat capacity (kJ/t/K)	Thermal conductivity (kJ/t/K)	Heat capacity (kJ/t/K)	Thermal conductivity (kJ/t/K)
1	690	3.8	690	3.8
2	690	3	690	3
3	690	2.18	690	2.18
4	740	3.14	740	3.14
5	960	3.8	900	3.8
6	960	2	900	2
7 (climate conditions)	690	2.18	690	2.18

The results for variation 3 are shown in Figures (145 & 146). Regarding variation 7, the measurement point T15 was used as an input for time-dependent climate conditions. The results for all other variations are shown in the appendix (D.2). The two figures show that the three main differences described in the previous subchapter are still present.

This study shows that with further investigation regarding the input of temperature and thermal parameters, it is most probably possible to better predict the temperature distribution with time in the soil due to changes in the temperature in the concrete.

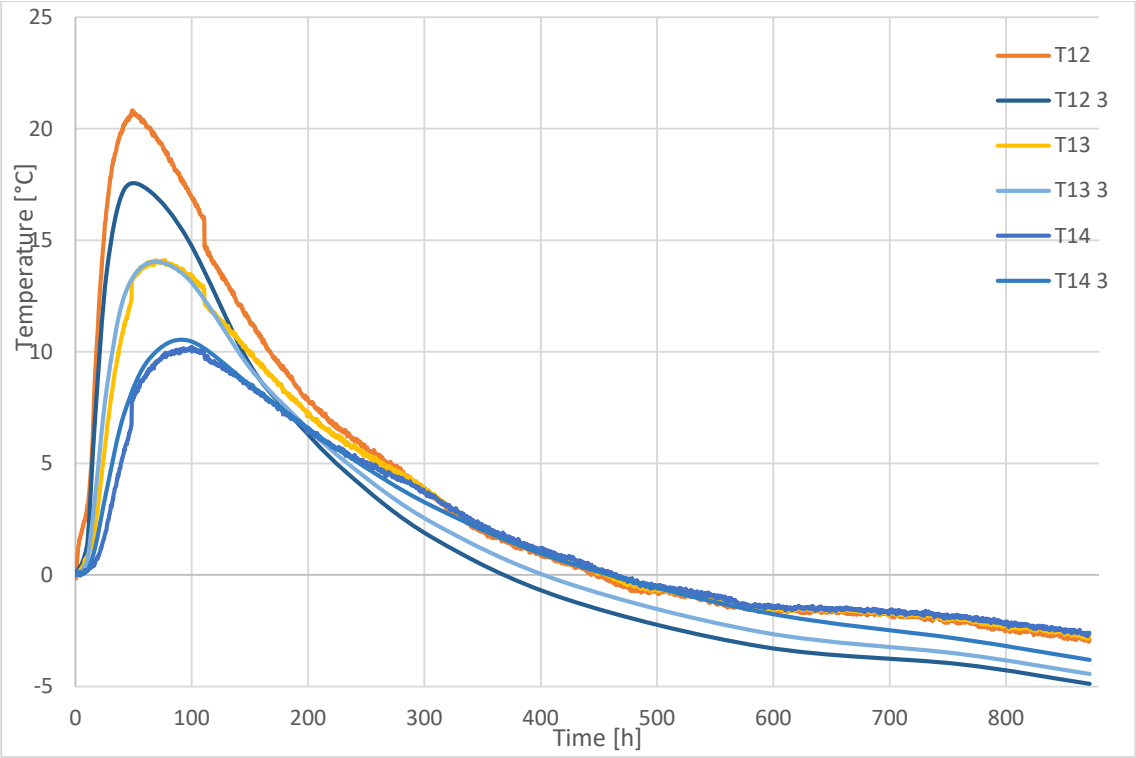

Figure 145 Comparison between real measurements and Setup 3 variation 3 (Y-axis)

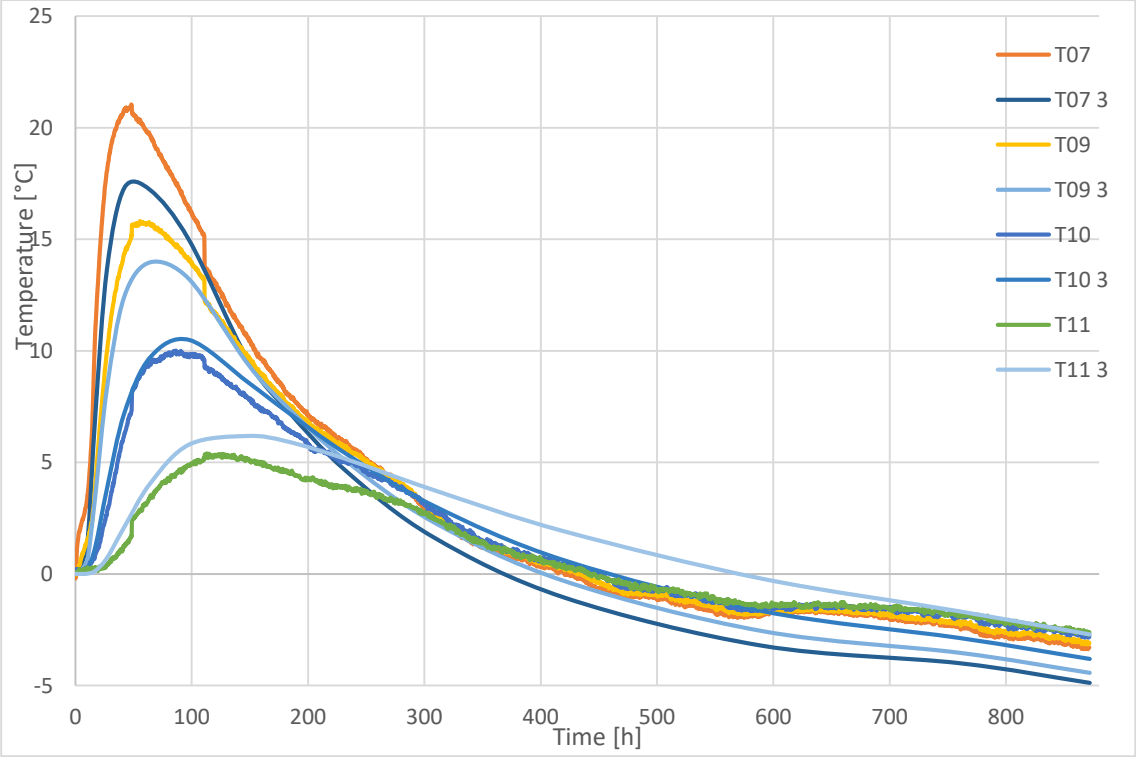

Figure 146 Comparison between real measurements and Setup 3 variation 3 (X-axis)

Conclusion

i. Preliminary studies

Time steps have an influence on the accuracy of the final result. In addition, maximum time steps have a significant effect on the number of calculation steps. Increasing the maximum time steps results in reducing the number of calculation steps dramatically.

The temperature distribution due to climate conditions depends on the amplitude of the function. Temperature functions with low amplitudes resulted in illogical results compared to the ones with higher amplitudes.

The sensitivity analysis shows the influence of varying the value of thermal conductivity and heat capacity on the temperature distribution. Increasing the thermal conductivity increases the rate by which the temperature is transferred. Increasing the heat capacity increases the heat storage of soil (i.e. more energy is required to change the temperature of soil)

ii. Groundwater flow study

This study showed the difference between applying cluster thermal condition and thermal boundary conditions. At the beginning of the time analysis, the cluster thermal condition starts to dissipate its temperature. As time increases, more temperature dissipates. On the other hand, temperature boundary conditions have constant temperature through the time analysis. As a result, in problems where applying constant temperature is of interest using cluster thermal conditions is not recommended.

Dry soil cluster and non-porous behaviour resulted in exactly the same temperature distribution as expected. When closed temperature boundary conditions were applied, it is concluded that the model had slightly higher temperature than the case without closed temperature boundary conditions.

iii. Thermal energy storage (TES)

In Finite element method, it is not possible to run models with empty soil clusters. This limitation made it necessary to try several approaches to simulate the situation in the storage, where only water is present.

Thermal insulation along the sides and top of the storage was modelled by means of interfaces. Applying climate conditions to the model showed that the interface on top of the storage is insulating the temperature, unlike the previous cases. It is concluded that, the first approaches used to model the storage were not correct. The approach used in section (5.6) should be used.

iv. Case Study

The case study showed that it is most probably possible to predict the temperature distribution in soil due to temperature changes in concrete. However, further investigation concerning the temperature input and thermal parameters is required to reach a better fit with the real measurements.

References

Baldi G., Hueckel T., Peano A. & Pellegrini R., Developments in modelling of thermo-hydro-geomechanical behaviour of Boom clay and clay-based buffer materials, Report EUR 13365, Commission of the European Communities, Nuclear science and technology, 1991.

Campanella, R. G., and Mitchell, J. K. Influence of Temperature Variations on Soil Behavior. Jour. Soil Mech. and Found. Div., ASCE, Proc. Paper 5958, Vol. 94, No. SM3, p. 709-734, 1968.

Cekerevac, Cane, and Lyesse Laloui. Experimental Study of Thermal Effects on the Mechanical Behaviour of a Clay. *International Journal for Numerical and Analytical Methods in Geomechanics* 28 (3): 209–28, 2004.

CODE_BRIGHT. CODE_BRIGHT user's guide, 2019.

Côté, Jean, and Jean-Marie Konrad.A Generalized Thermal Conductivity Model for Soils and Construction Materials. *Canadian Geotechnical Journal* 42 (2): 443–58. https://doi.org/10.1139/t04-106, 2005.

Dahash, Abdulrahman & Bianchi Janetti, Michele & Ochs, Fabian. Detailed Axial Symmetrical Model of Large-Scale Underground Thermal Energy Storage, 2018.

Farouki, O. T. Thermal properties of soils, CRREL Monograph 81-1. Hanover, NH: US Army Corps of Engineers, Cold Regions Research and Engineering Laboratory, 1981.

Gawecka, K. A., D. M. G. Taborda, D. M. Potts, W. Cui, L. Zdravković, and M. S. Haji Kasri. "Numerical Modelling of Thermo-Active Piles in London Clay." Proceedings of the Institution of Civil Engineers: Geotechnical Engineering 170 (3): 201-219. doi:10.1680/jgeen.16.00096, 2017.

Gens, A. Soil–Environment Interactions in Geotechnical Engineering. *Géotechnique* 60 (1): 3–74. https://doi.org/10.1680/geot.9.p.109, 2010.

Haigh, Stuart. Thermal conductivity of sands. Géotechnique. 62. 617-625. 10.1680/geot.11.P.043, 2012.

Hamdhan, I. N., & Clarke, B. G. Determination of Thermal Conductivity of Coarse and Fine Sand Soils, 2010.

Johansen, O. 1977. Thermal Conductivity of Soils, 1977.

Khan, Zahid. Thermal Insulation Materials for Geotechnical Applications such as Seasonal Thermal Energy Storages, 2019.

Laloui, Lyesse. Thermo-Mechanical Behaviour of Soils, 2001

ÖBB, Keller Grundbau and Institute of Soil Mechanics and Foundation Engineering at Graz University of Technology. Temperaturausbreitung Pfahlwand Bauvorhaben St.Kanzian, 2018.

Ochs, F, and W Heidemann. Modeling Large-Scale Seasonal Thermal Energy Stores. *Effstock 2009: Thermal Energy Storage for Efficiency and Sustainability*, 2009

Ochs, Fabian. 2015. Large-Scale Thermal Energy Stores in District Heating Systems – Simulation Based Optimization, 2015.

PLAXIS. PLAXIS Reference Manual, 2018

PLAXIS. PLAXIS Tutorial Manual, 2018

PLAXIS. 2015. Thermal and Coupled THM Analysis, 2015

Plum, R. L., and Esrig, M. I. 1969. Some temperature effects on soil compressibility and pore water pressure. In Effects of temperature and heat on engineering behavior of soils. Highway Research Board, Washington, DC. Special Report, No. 103: 231–242, 1969

Rees, S. W., Adjali, M. H., Zhou, Z., Davies, M. & Thomas, H. R. Ground heat transfer effects on the thermal performance of earth-contact structures. Renewable Sustainable Energy Rev.4, No. 2, 213–265, 2000

Shah, Sheikh Khaleduzzaman & Aye, Lu & Rismanchi, Behzad. Seasonal thermal energy storage system for cold climate zones: A review of recent developments. Renewable and Sustainable Energy Reviews. 97. 10.1016/j.rser.2018.08.025, 2018

Shein Evgeny, V & Mady, Ahmed. Soil thermal parameters assessment by direct method and mathematical models. Journal of Soil Science and Environmental Management, 2016.

Thomas, H.R. & Rees, S. W. Measured and simulated heat transfer to foundation soils. Géotechnique. 59. 365-375. 10.1680/geot.2008.59.4.365, 2009

Willemsen, Lucas Abraham. Validation and Verification of Thermo- Hydro-Mechanical (THM) Coupling in Plaxis, 2011

Xu, Jianjian & Z. Wang, R & Li, Y. A review of available technologies for seasonal thermal energy storage. Solar Energy. 103. 10.1016/j.solener.2013.06.006, 2014.

Appendix

A.1 Additional results for the time steps study

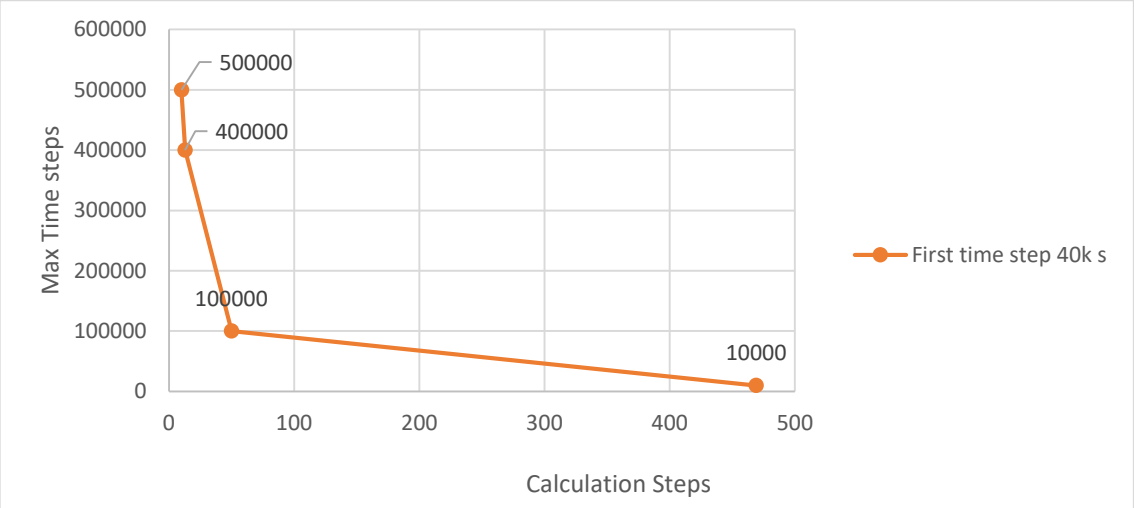

Figure A.1 Influence of maximum time steps on the number of calculation steps (40,000 s)

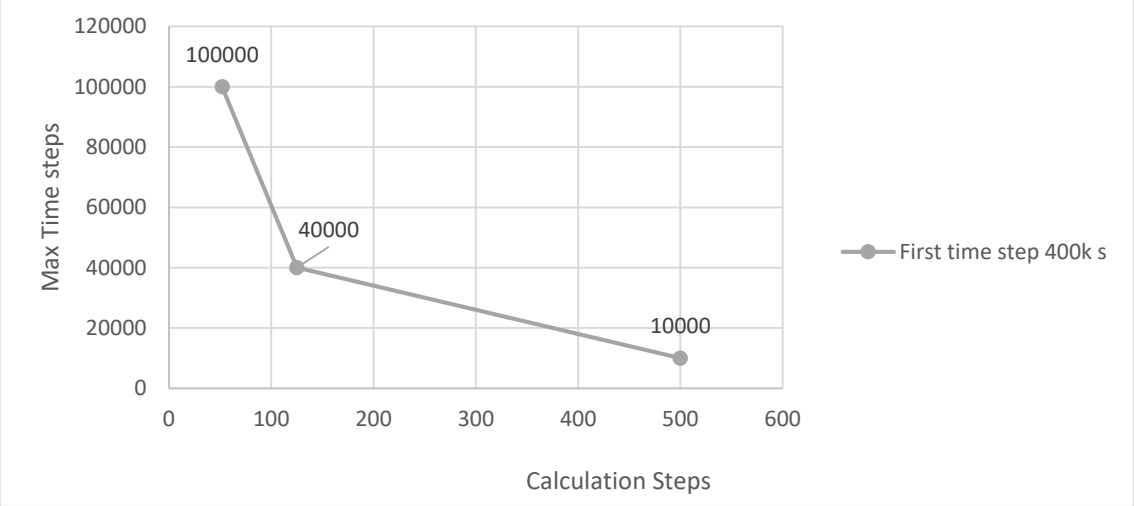

Figure A.2 Influence of maximum time steps on the number of calculation steps (400,000 s)

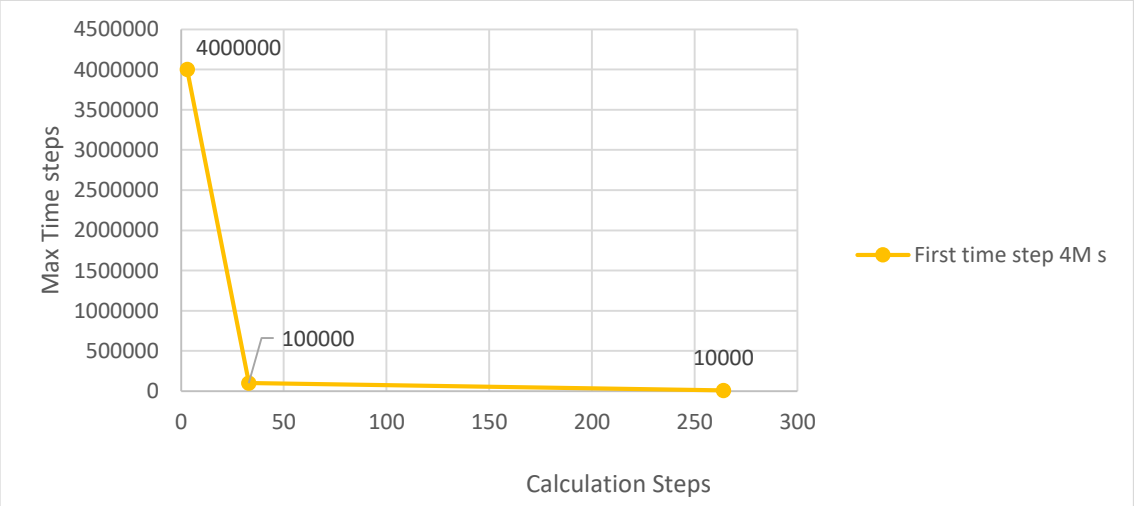

Figure A.3 Influence of maximum time steps on the number of calculation steps (4,000,000 s)

A.2 Additional results for the temperature functions study

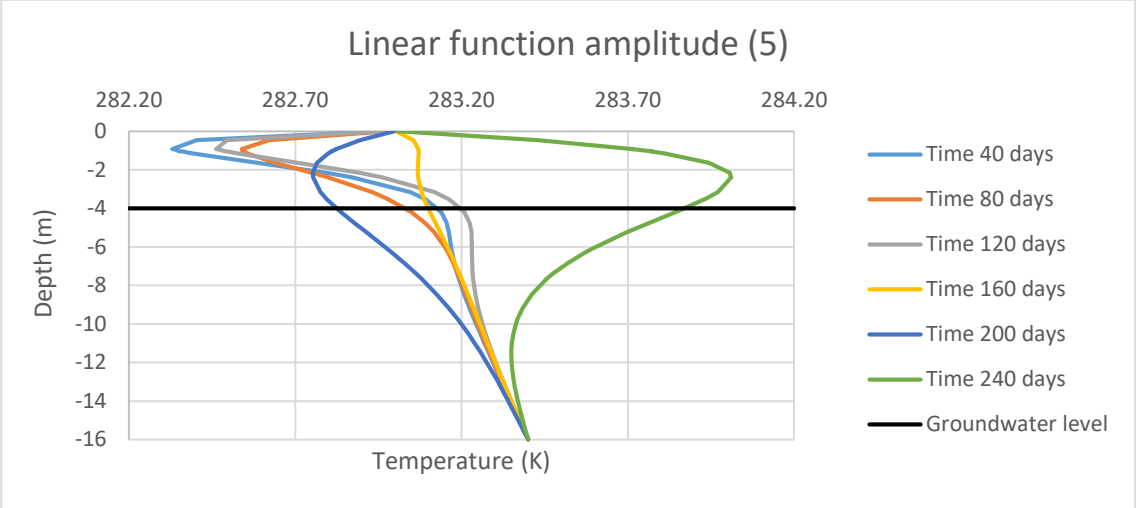

Figure A.4 Temperature distribution after 6 cycles for linear function (amplitude 5)

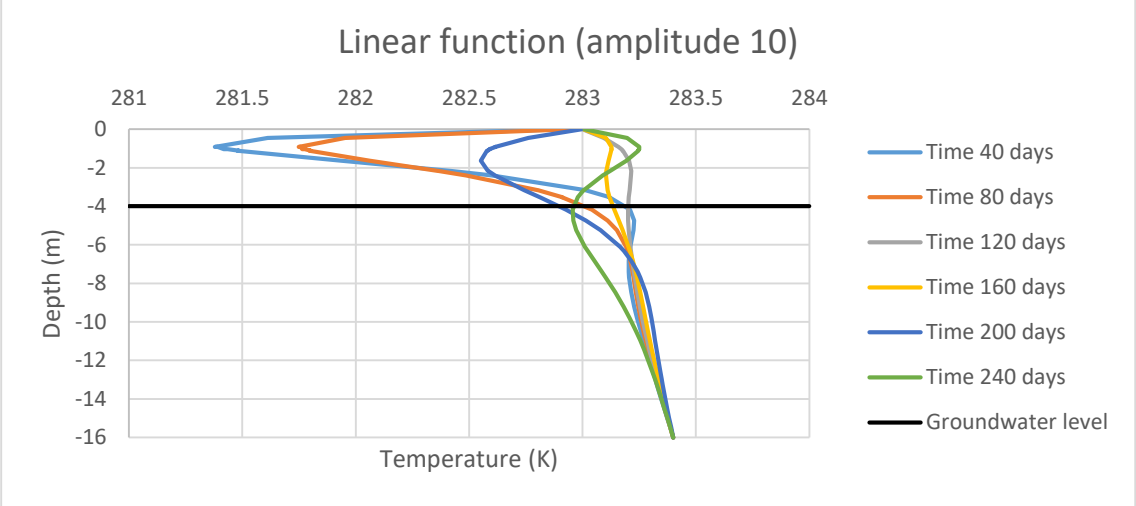

Figure A.5 Temperature distribution after 6 cycles for linear function (amplitude 10)

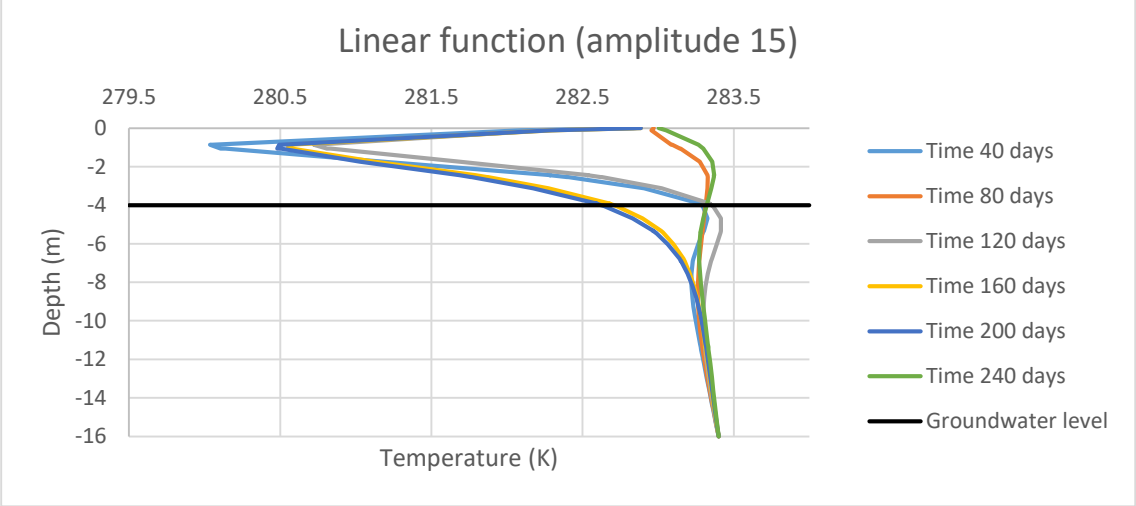

Figure A.6 Temperature distribution after 6 cycles for linear function (amplitude 15)

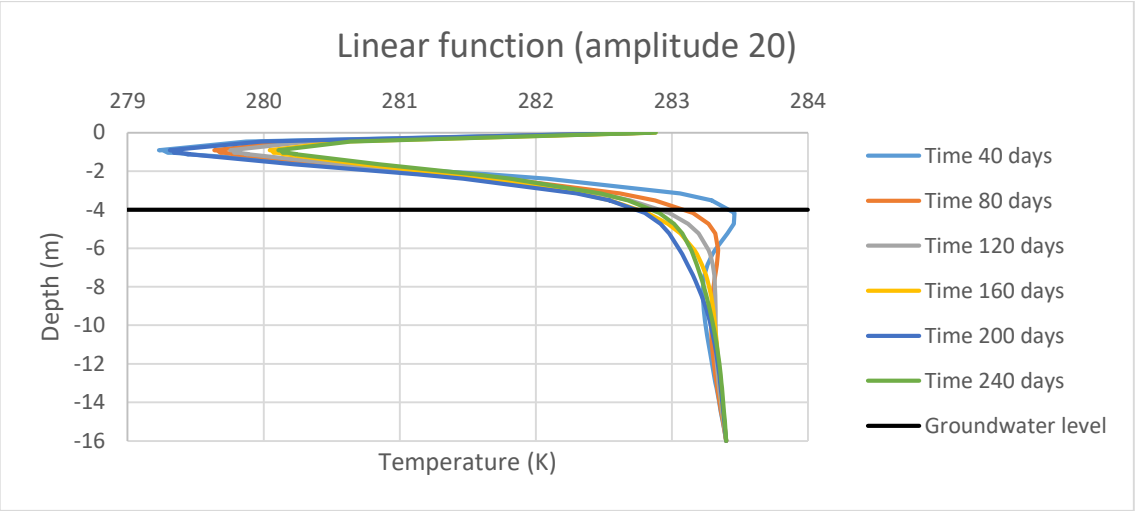

Figure A.7 Temperature distribution after 6 cycles for linear function (amplitude 20)

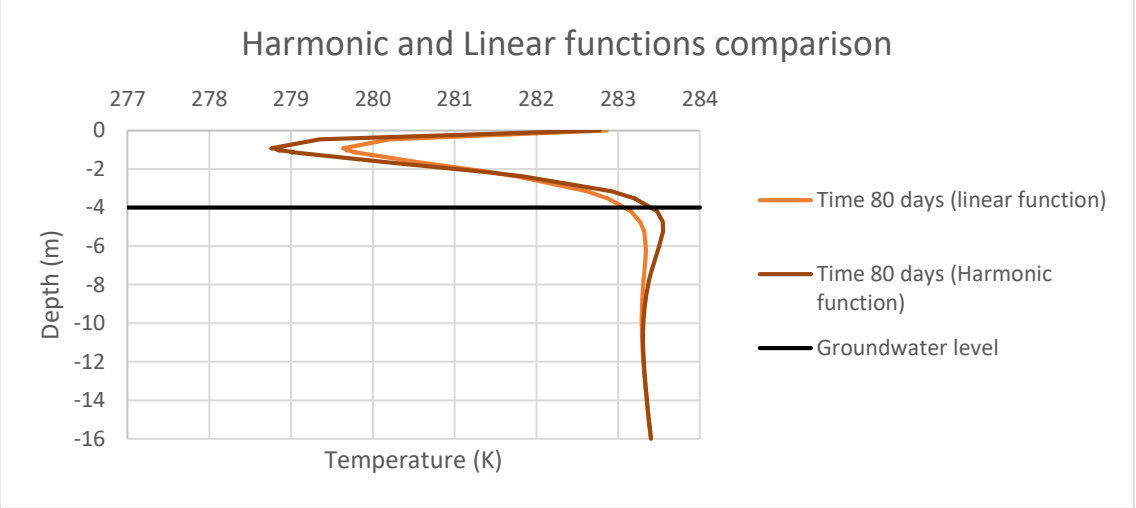

Figure A.8 Harmonic and linear functions comparison after 80 days (2nd cycle)

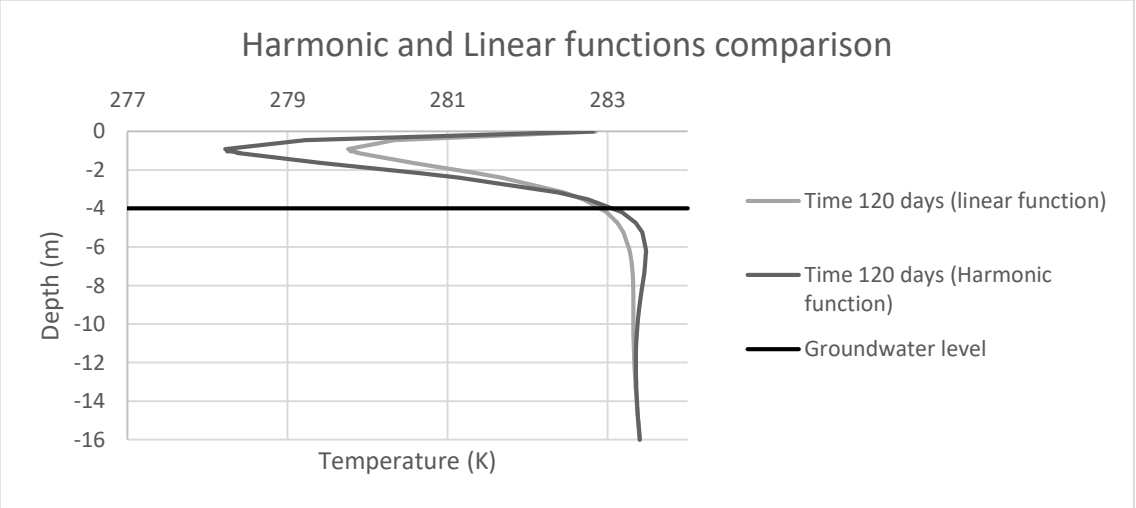

Figure A.9 Harmonic and linear functions comparison after 80 days (3rd cycle)

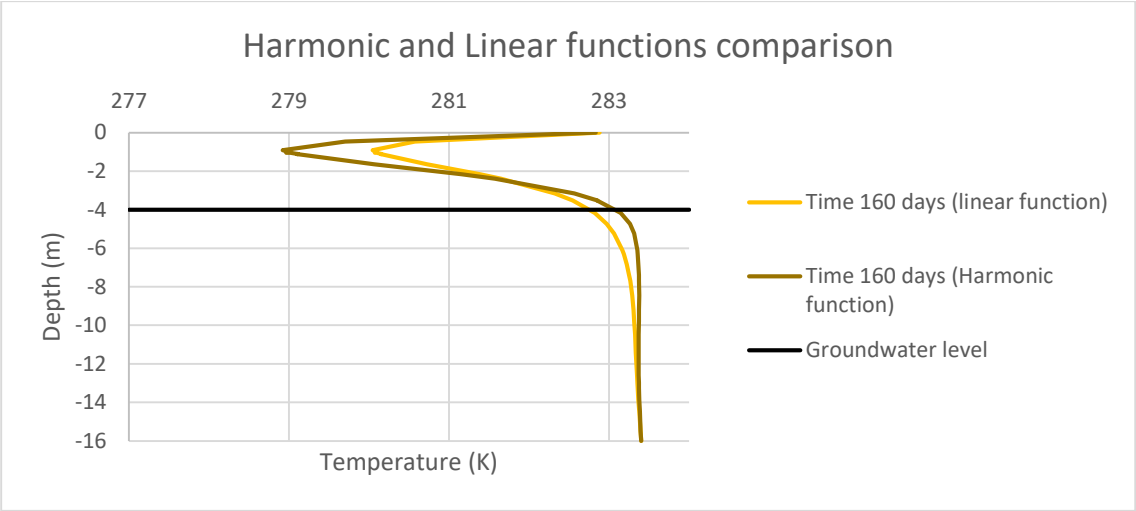

Figure A.10 Harmonic and linear functions comparison after 80 days (4th cycle)

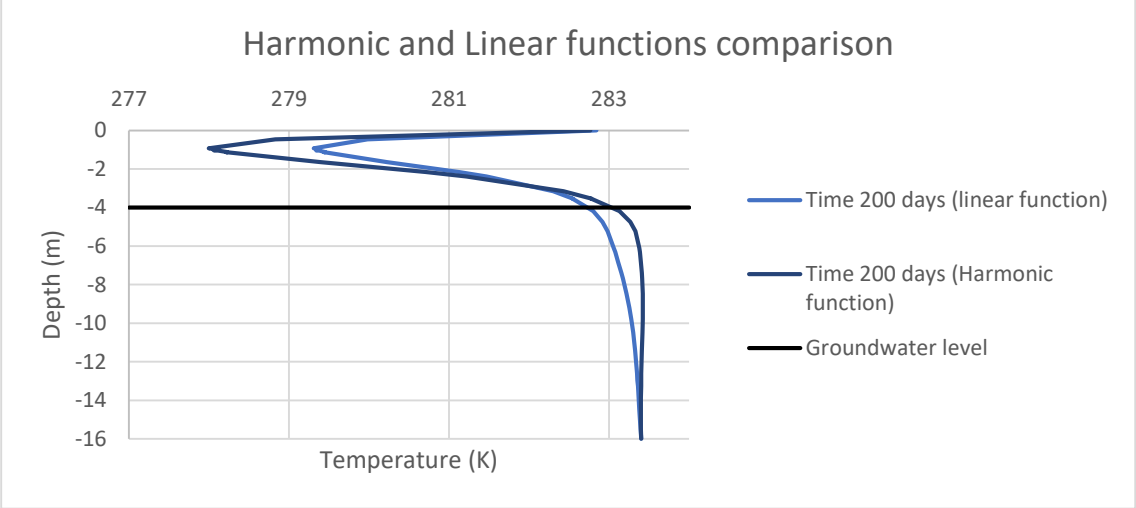

Figure A.11 Harmonic and linear functions comparison after 80 days (5th cycle)

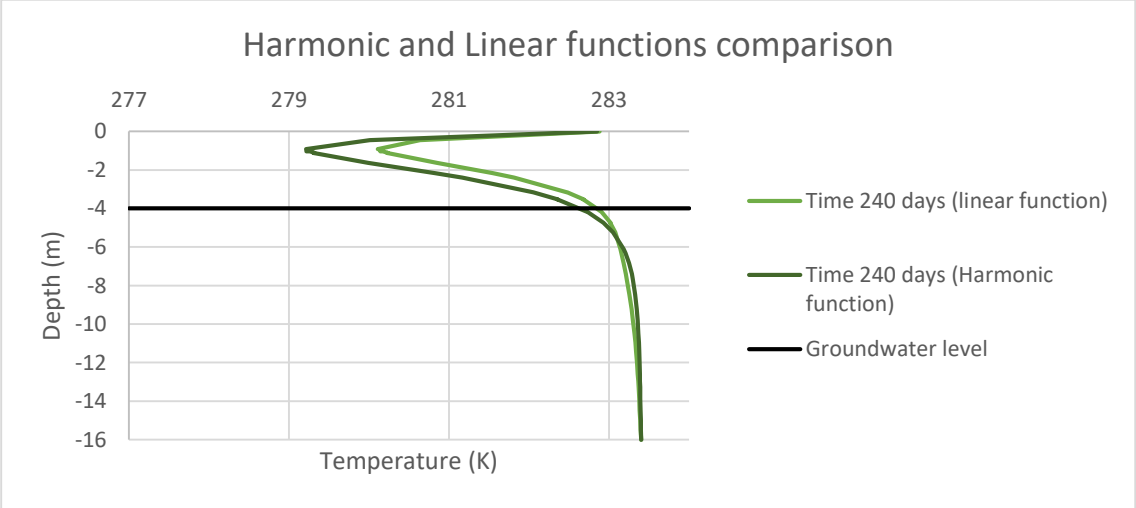

Figure A.12 Harmonic and linear functions comparison after 80 days (6th cycle)

A.3 Additional results for the sensitivity analysis

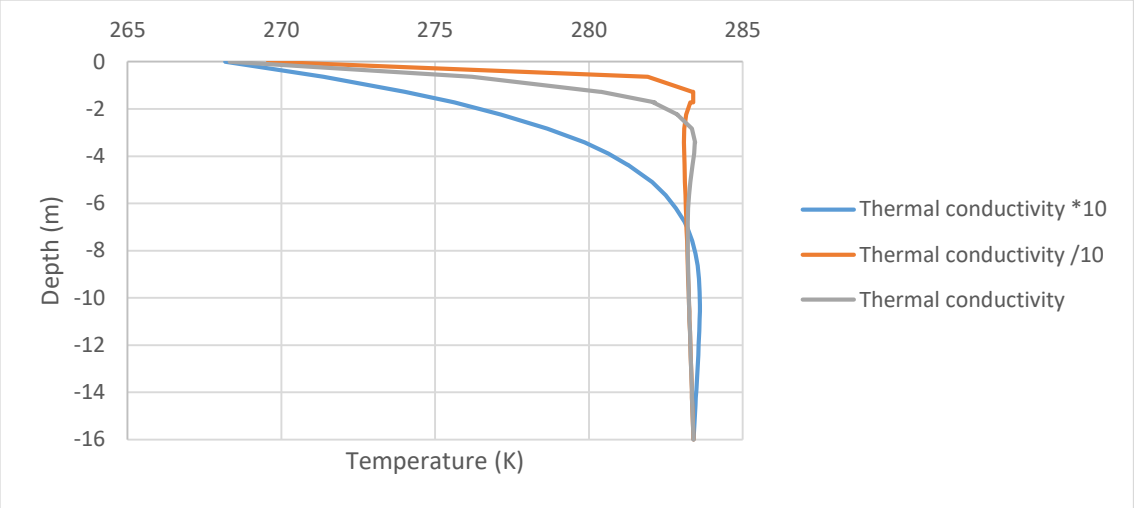

Figure A.13 Thermal conductivity sensitivity analysis after 30 days

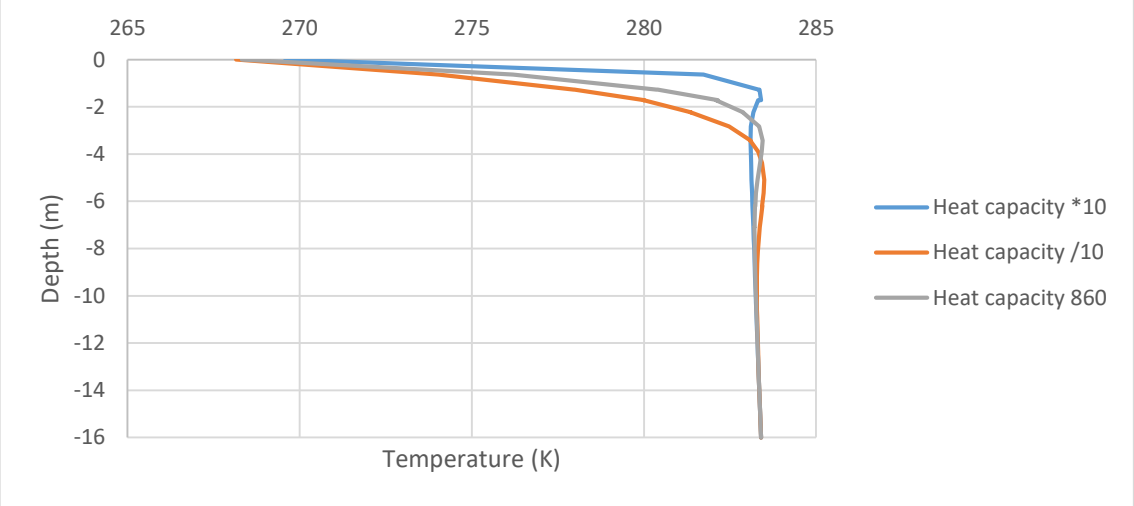

Figure A.14 Heat capacity sensitivity analysis after 30 days

B.1 Additional results for the cluster thermal boundary study

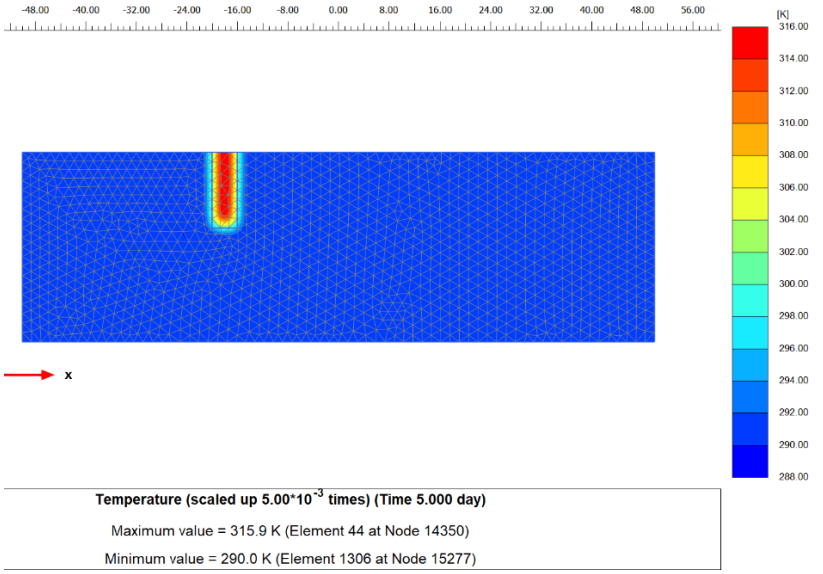

Figure B.1 Temperature distribution after 5 days for cluster thermal boundary condition

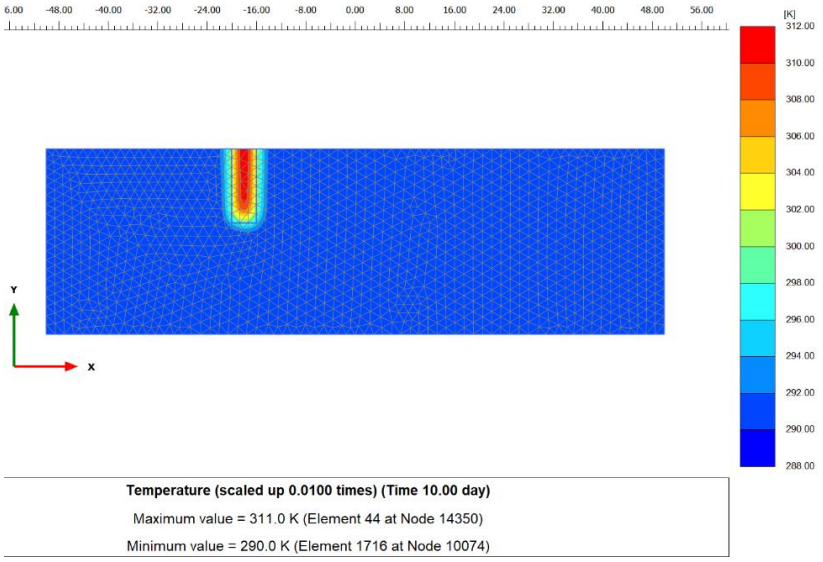

Figure B.2 Temperature distribution after 10 days for cluster thermal boundary condition

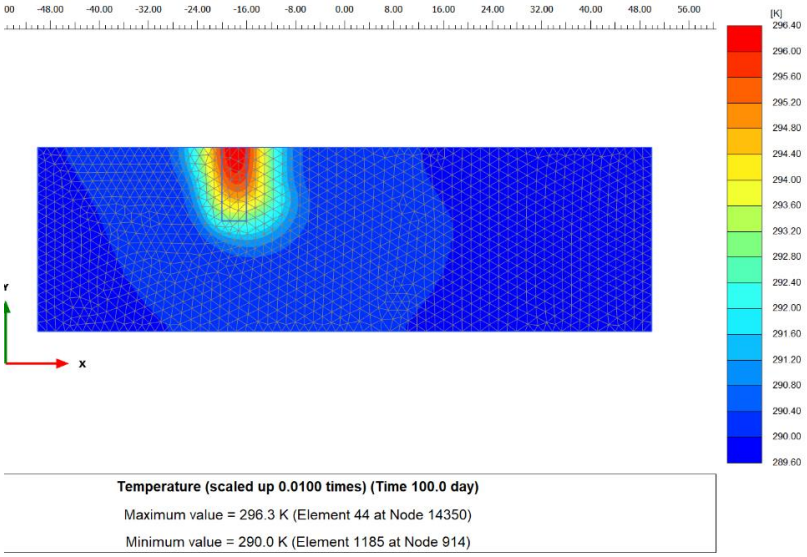

Figure B.3 Temperature distribution after 10 days for cluster thermal boundary condition

B.2 Additional results for thermal boundary conditions study

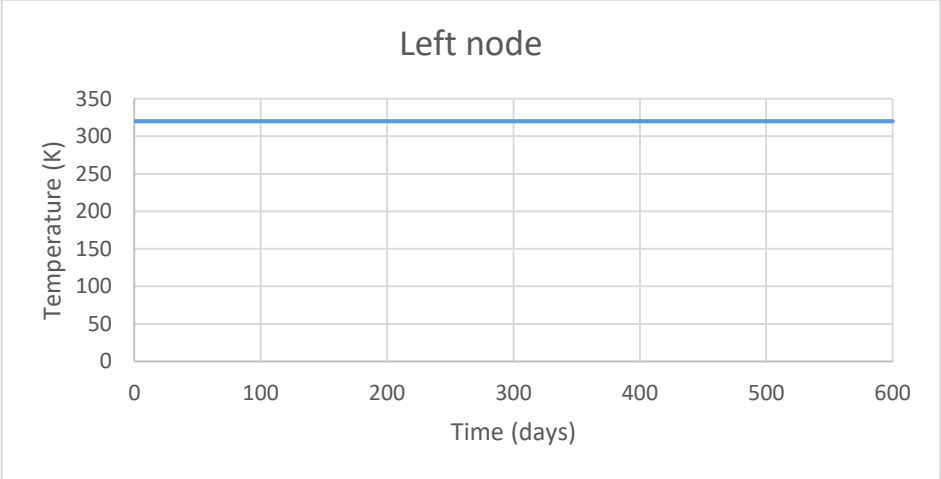

Figure B.4 Temperature in the left node

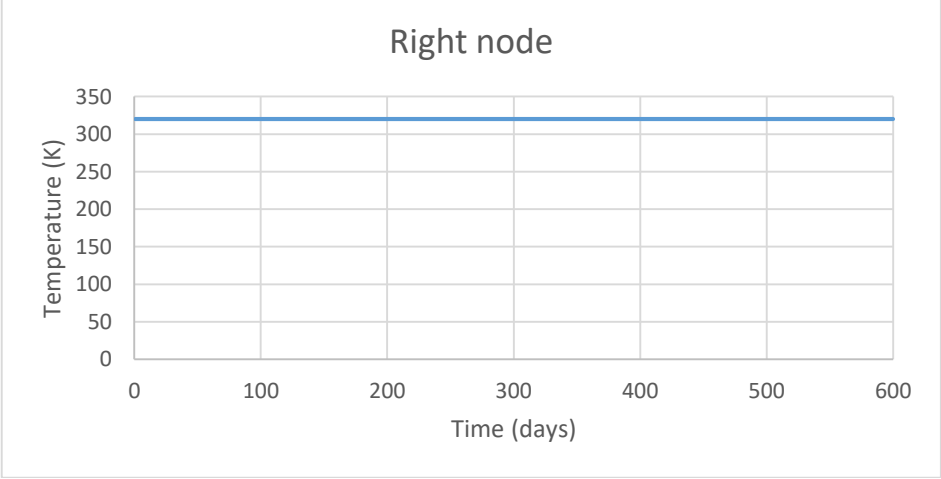

Figure B.5 Temperature in the right node

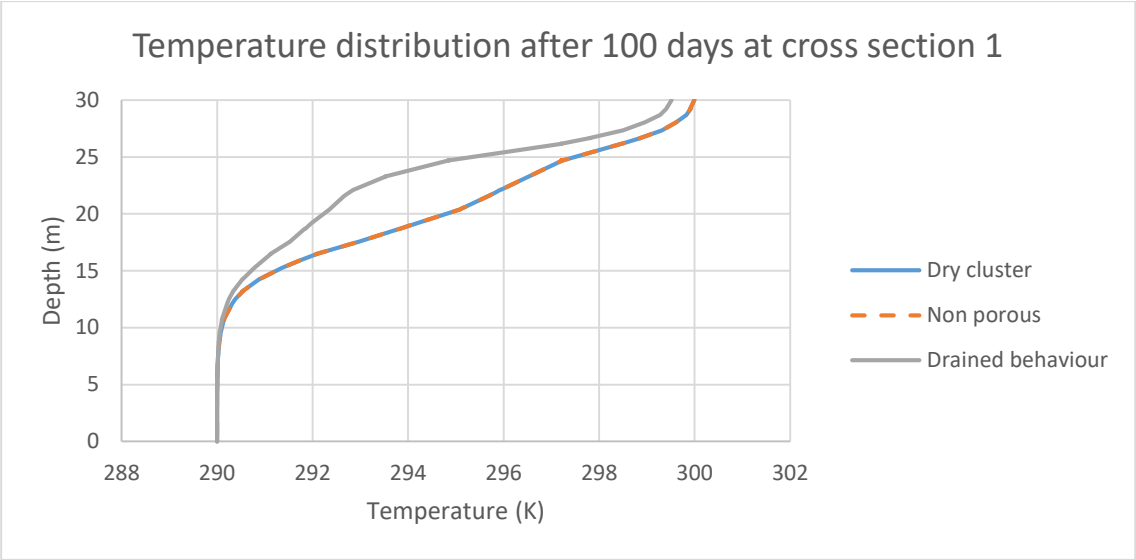

Figure B.6 Temperature distribution at cross-section 1 after 100 days

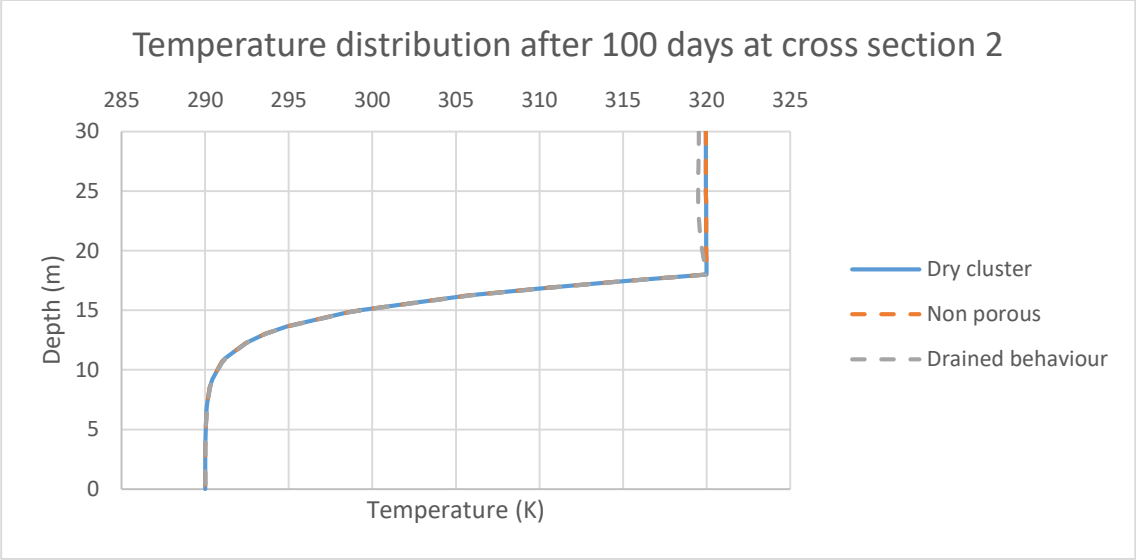

Figure B.7 Temperature distribution at cross-section 2 after 100 days

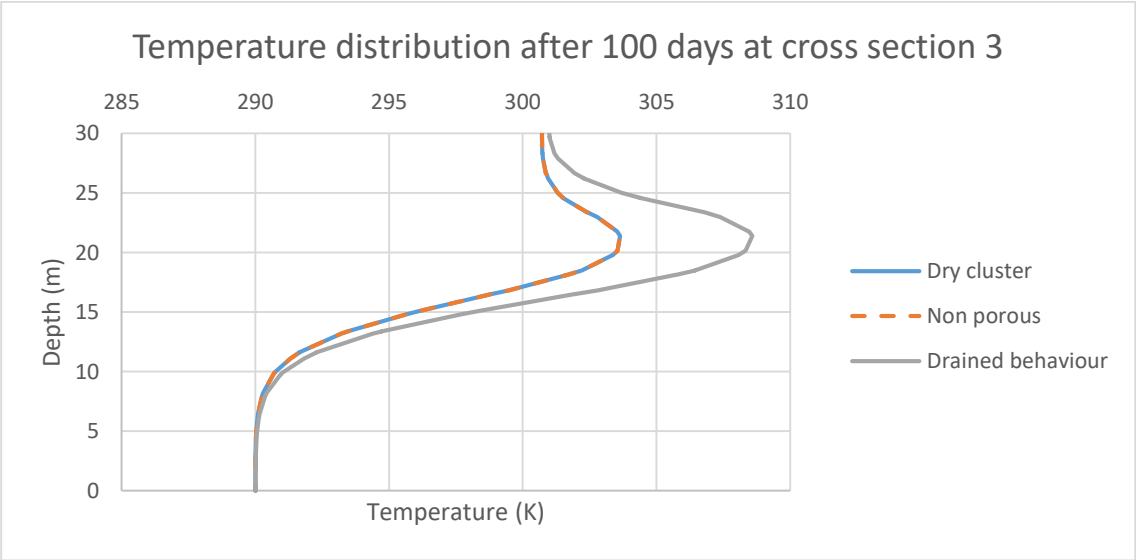

Figure B.8 Temperature distribution at cross-section 3 after 100 days

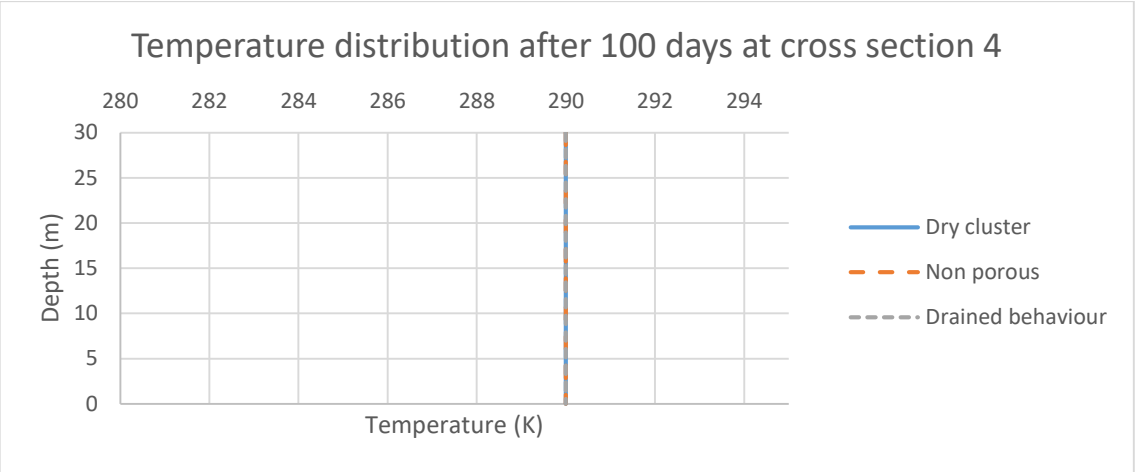

Figure B.9 Temperature distribution at cross-section 4 after 100 days

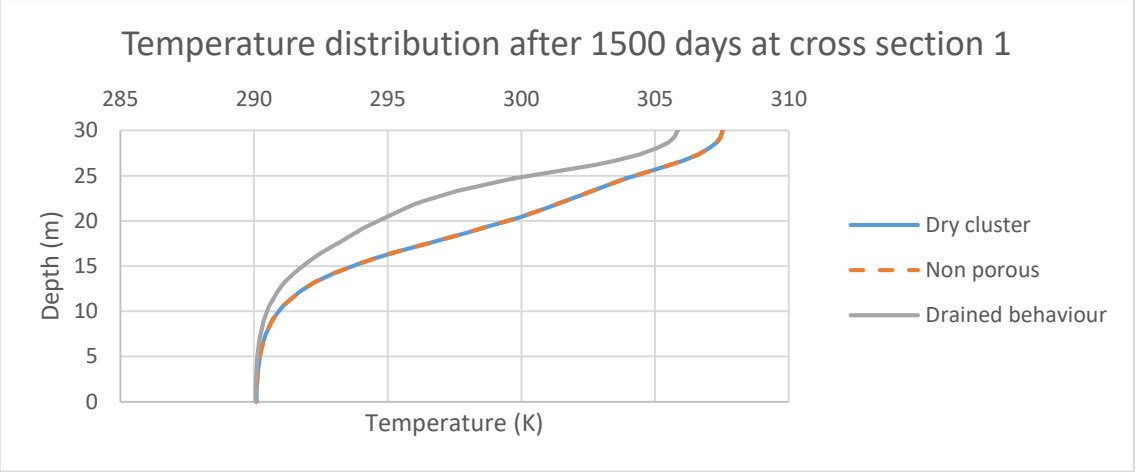

Figure B.10 Temperature distribution at cross-section 1 after 1500 days

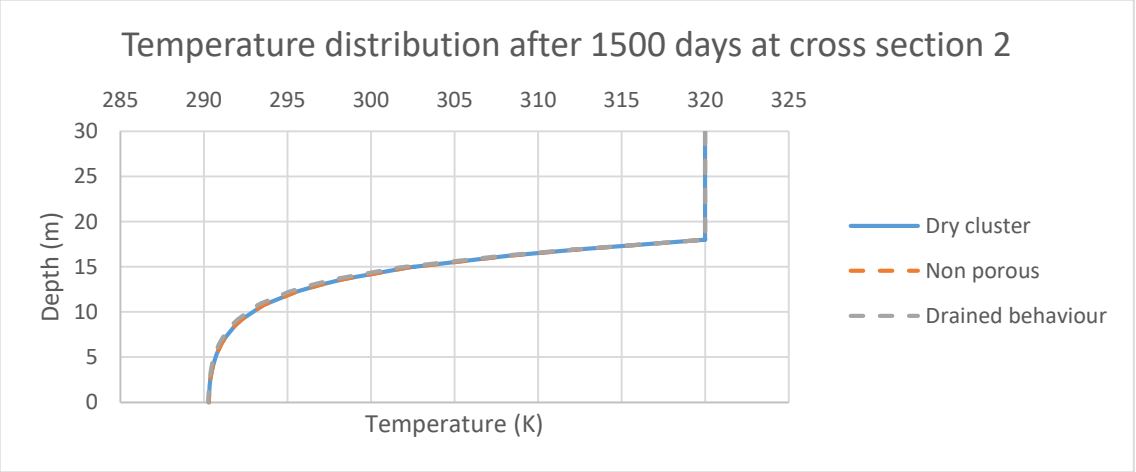

Figure B.11 Temperature distribution at cross-section 2 after 1500 days

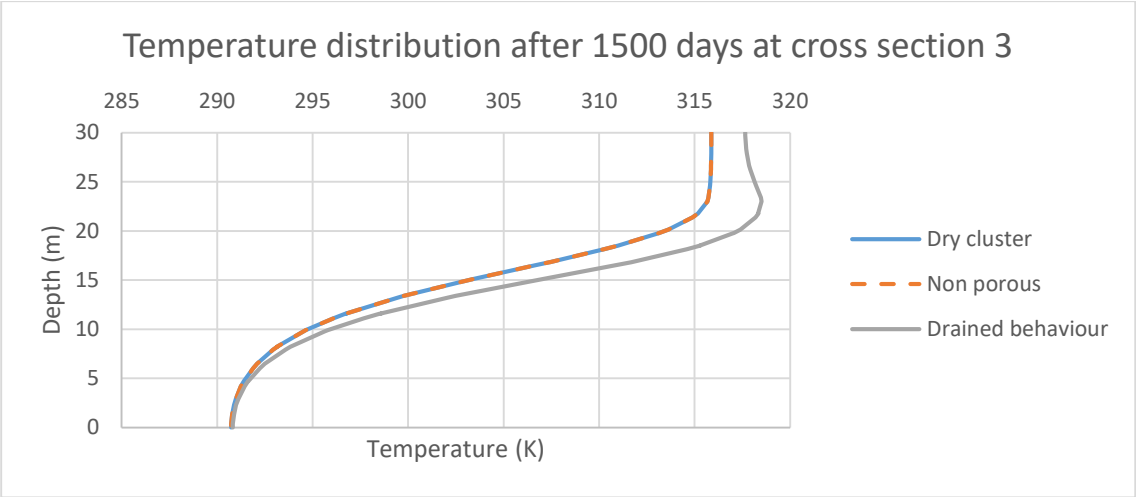

Figure B.12 Temperature distribution at cross-section 3 after 1500 days

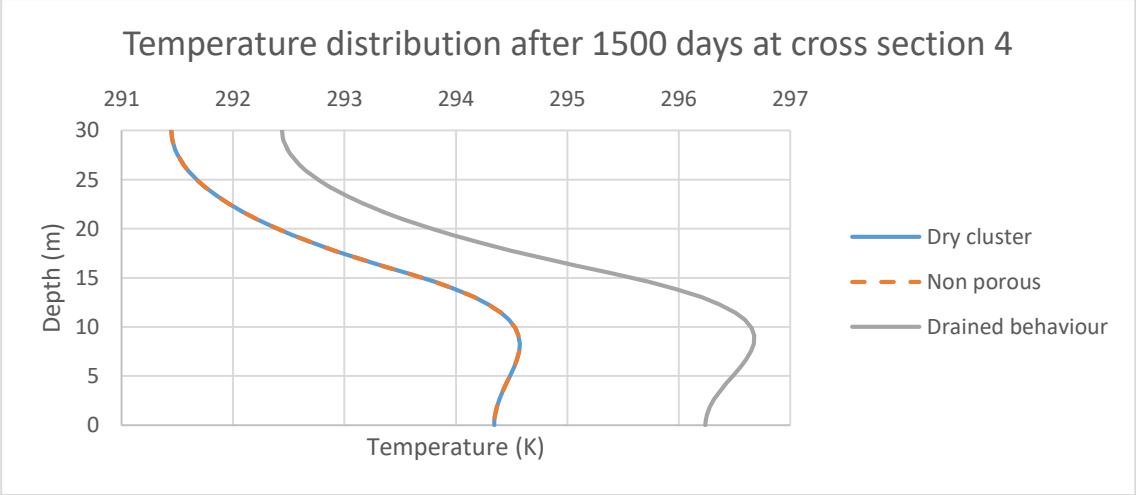

Figure B.13 Temperature distribution at cross-section 4 after 1500 days

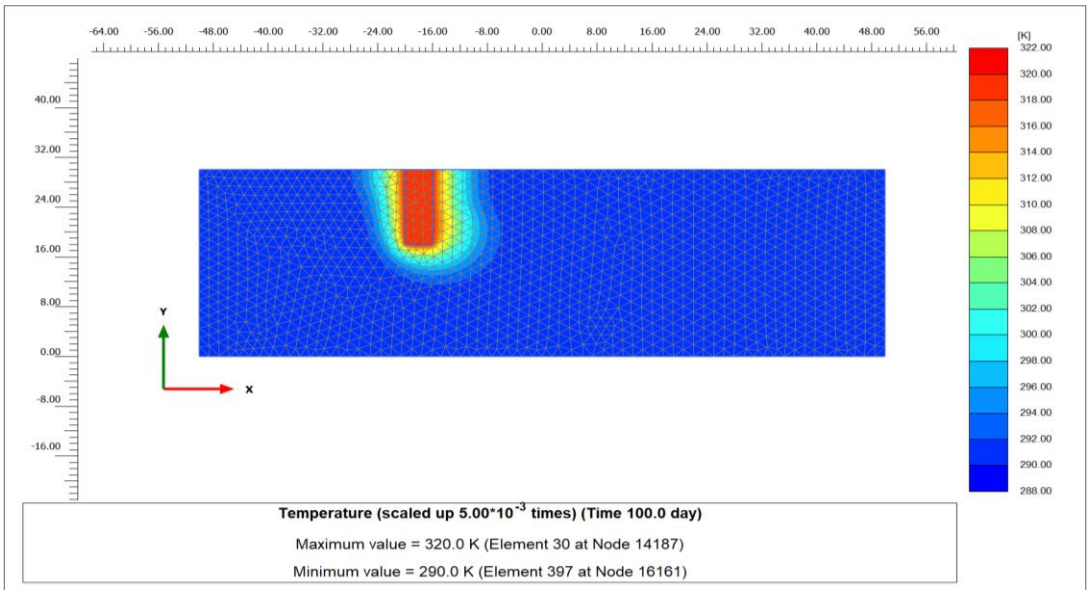

Figure B.14 Temperature distribution after 100 days (dry cluster)

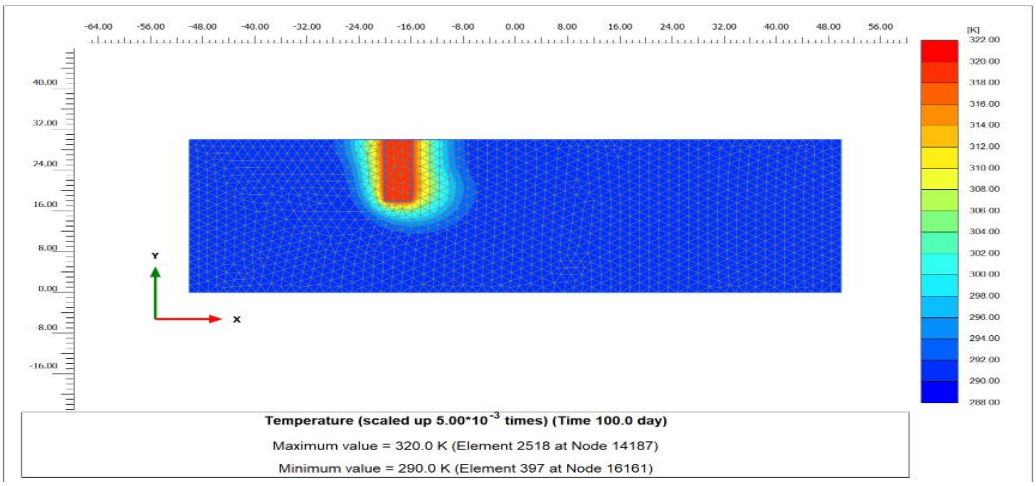

Figure B.15 Temperature distribution after 100 days (non-porous cluster)

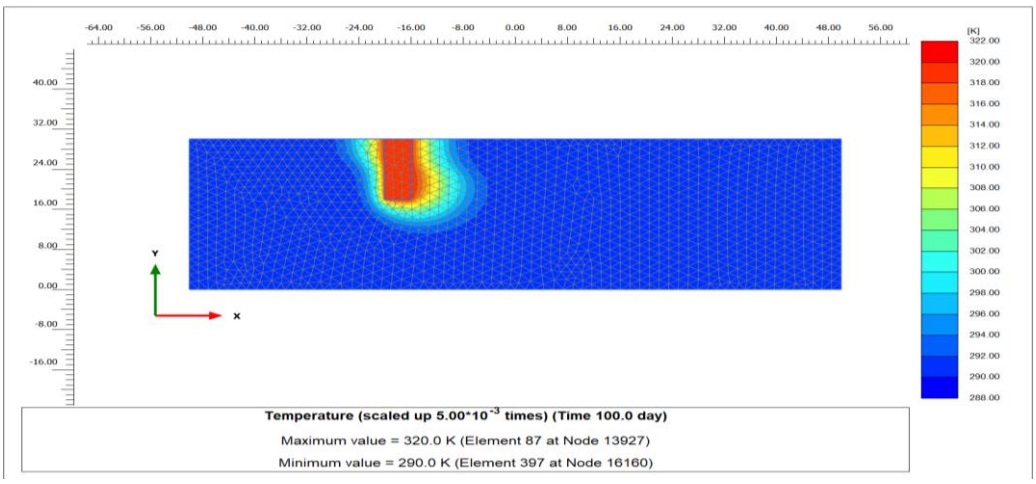

Figure B.16 Temperature distribution after 100 days (drained cluster)

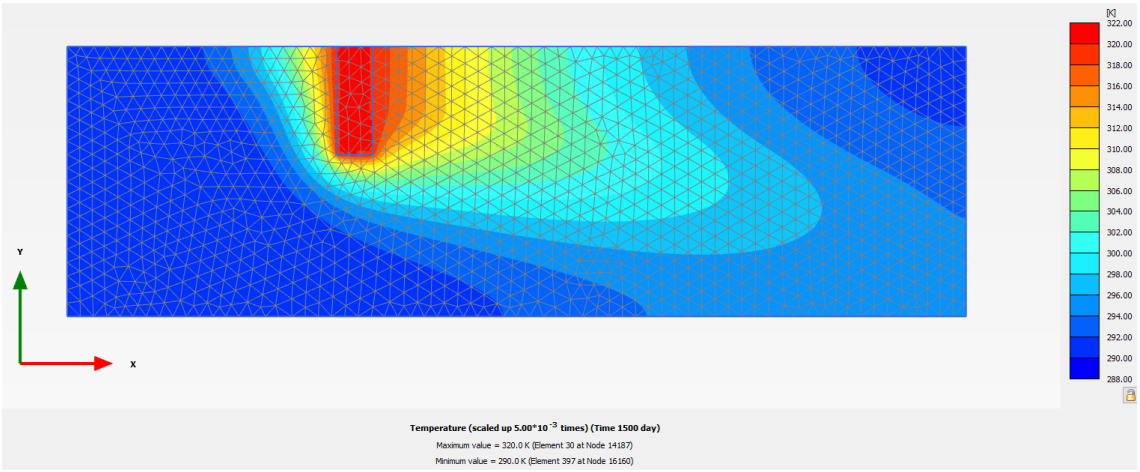

Figure B.17 Temperature distribution after 1500 days (dry cluster)

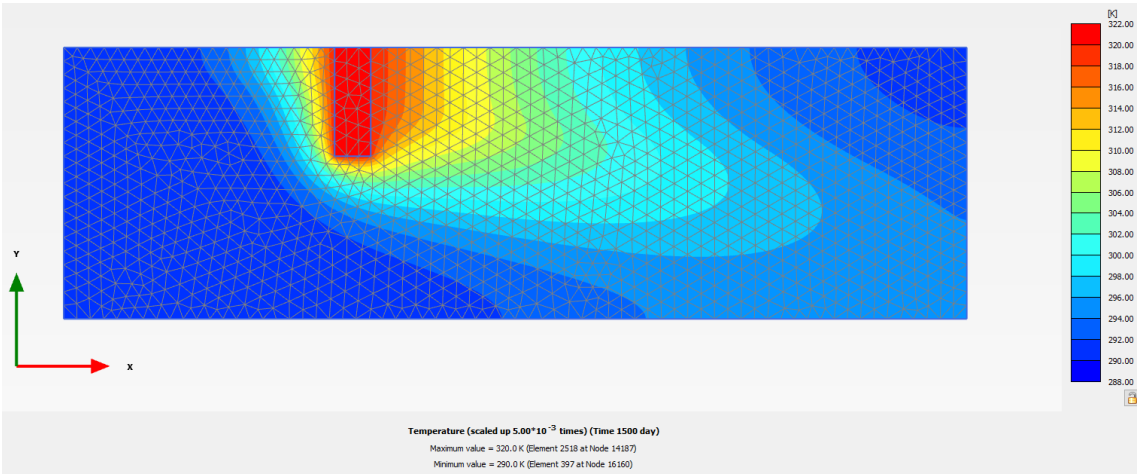

Figure B.18 Temperature distribution after 1500 days (non-porous cluster)

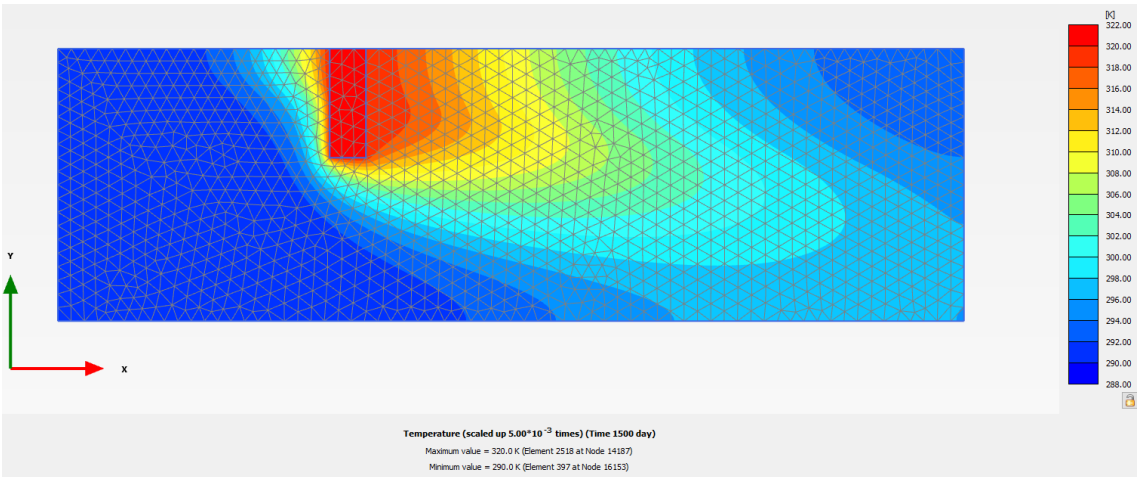

Figure B.19 Temperature distribution after 1500 days (drained cluster)

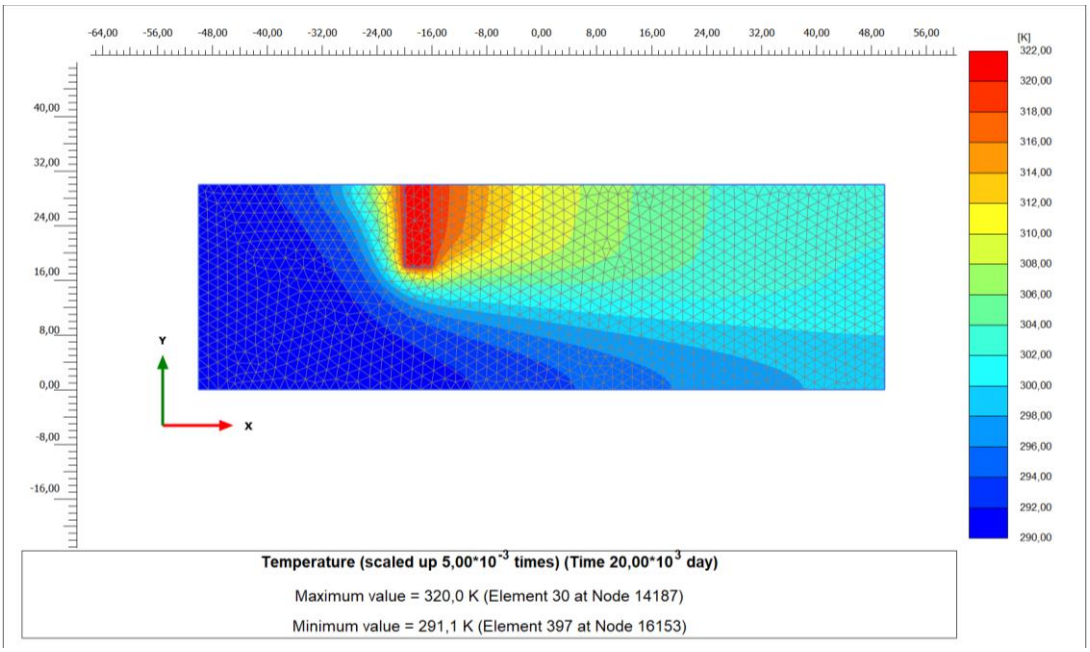

Figure B.20 Temperature distribution after 20,000 days (dry cluster)

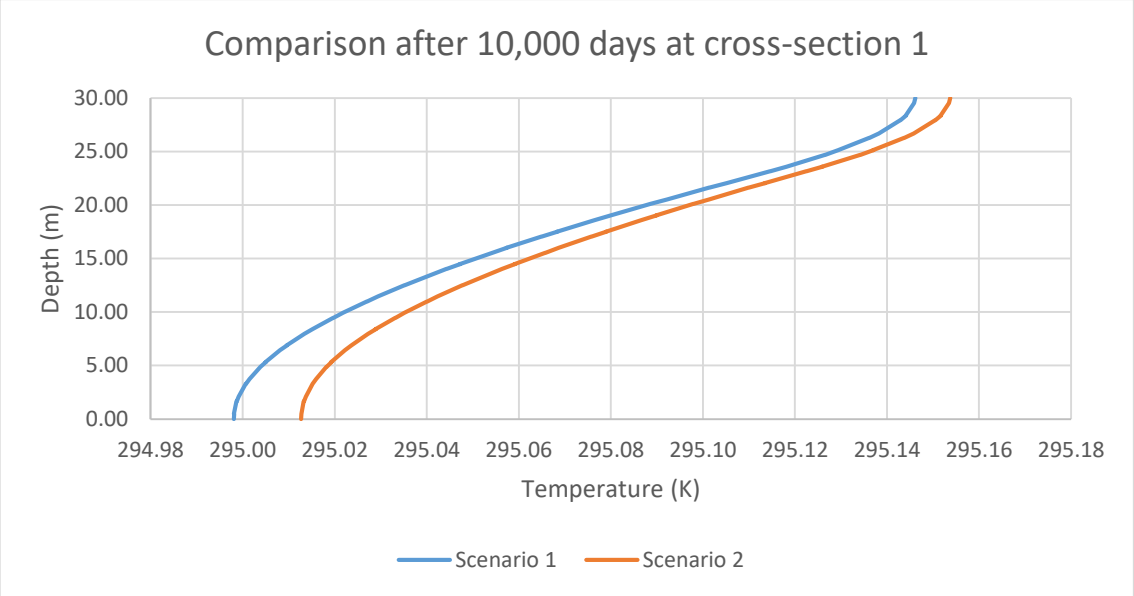

Figure B.21 Comparison between different boundary conditions after 10,000 days (cross-section 1)

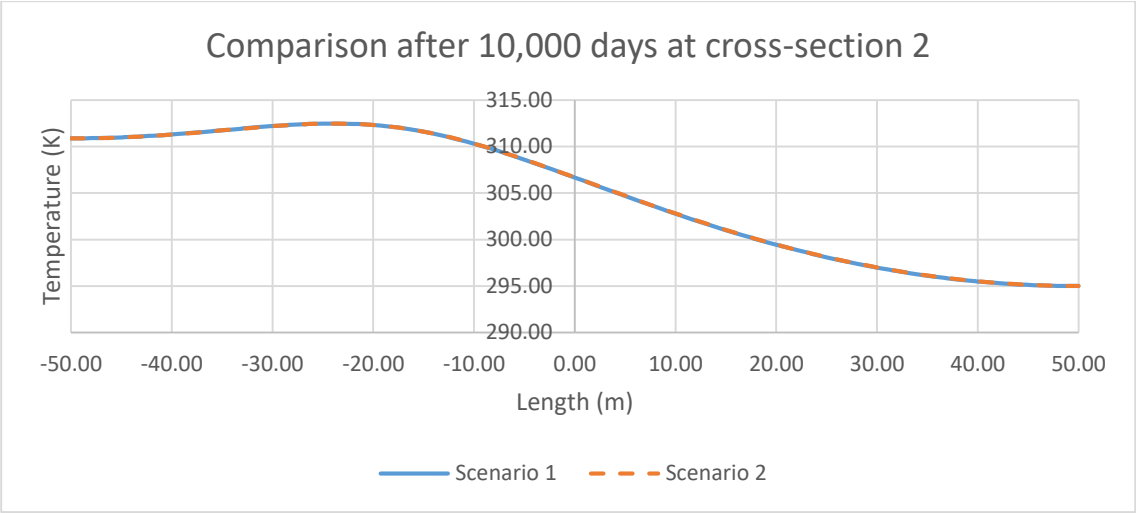

Figure B.22 Comparison between different boundary conditions after 10,000 days (cross-section 2)

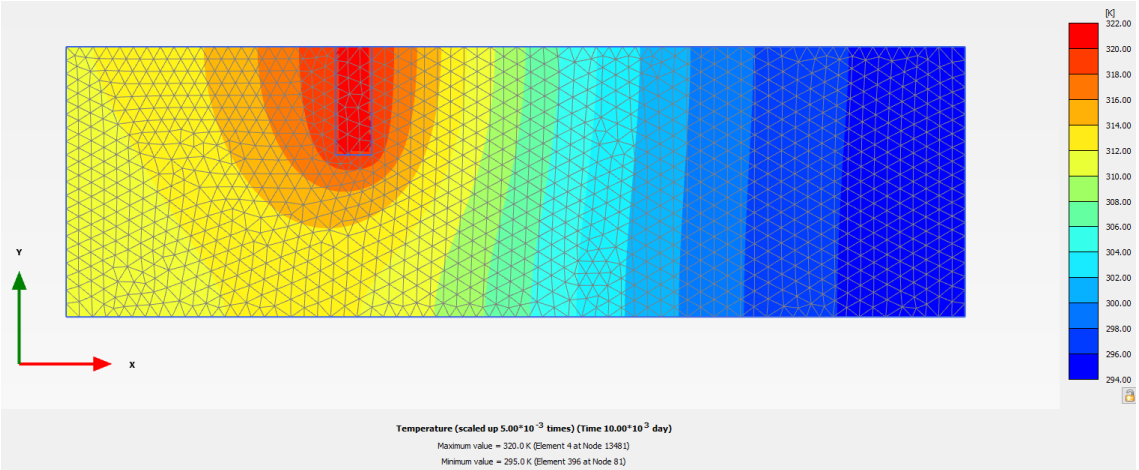

Figure B.23 Temperature distribution after 10,000 (Scenario 1)

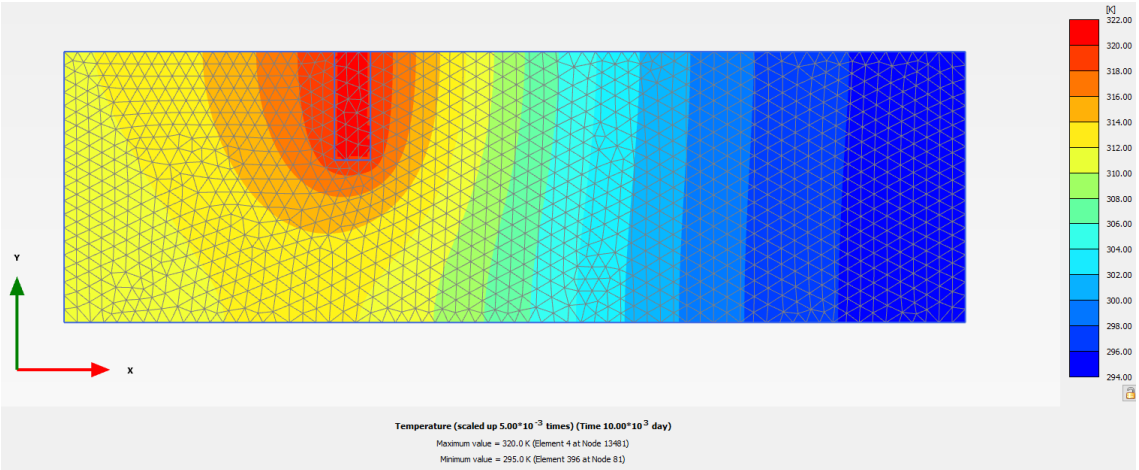

Figure B.24 Temperature distribution after 10,000 (Scenario 2)

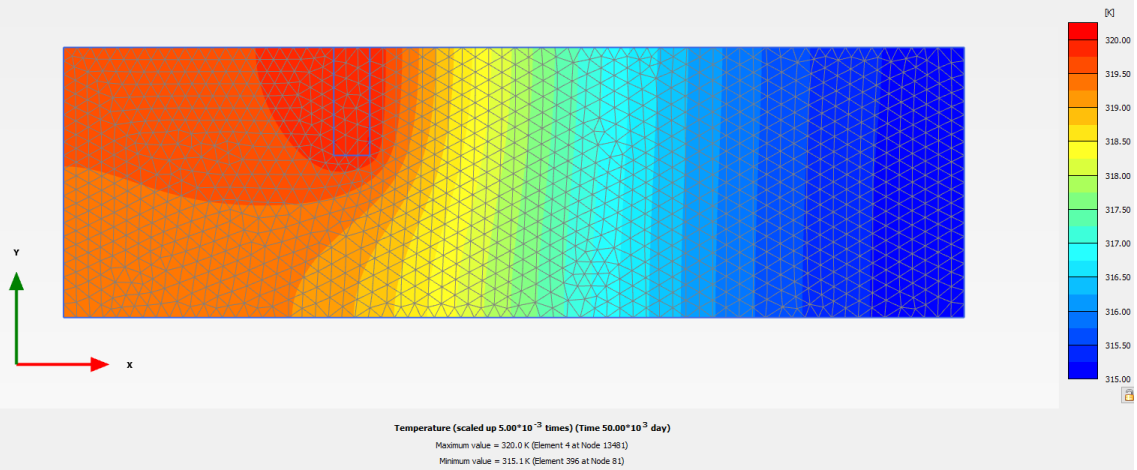

Figure B.25 Temperature distribution after 50,000 (Scenario 1)

C.1 Additional results for modelling of variant 1

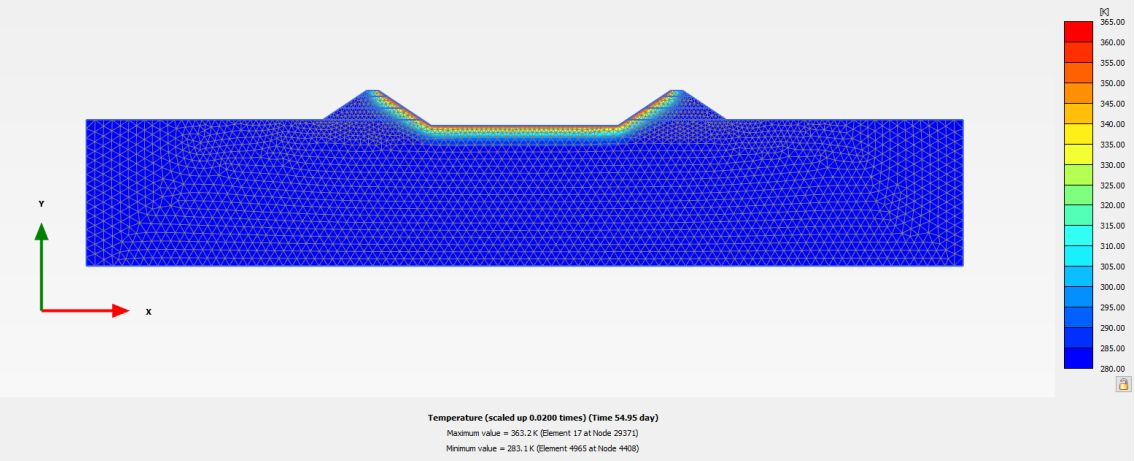

Figure C.1 Temperature distribution after 55 days (Variant 1 convective boundary condition)

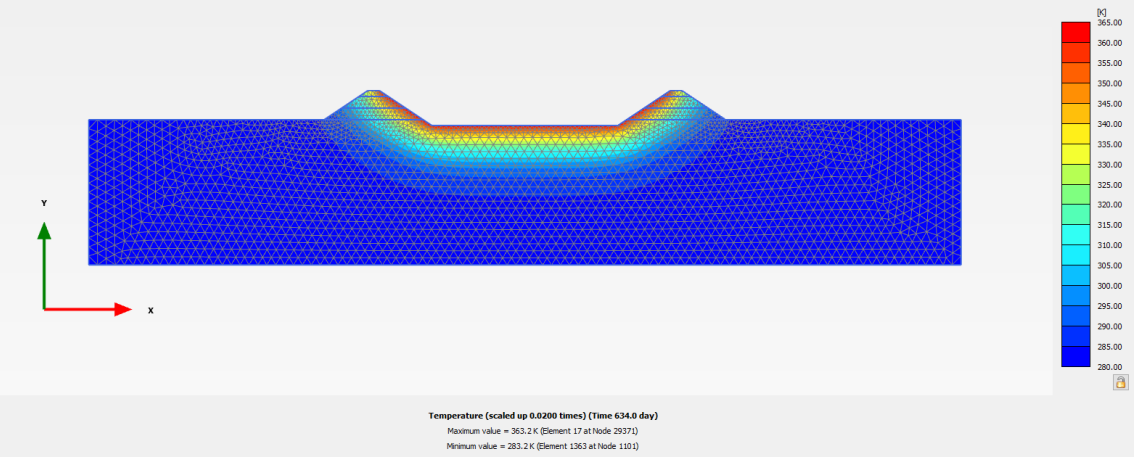

Figure C.2 Temperature distribution after 634 days (Variant 1 convective boundary condition)

C.2 Additional results for modelling of variant 2 and 3

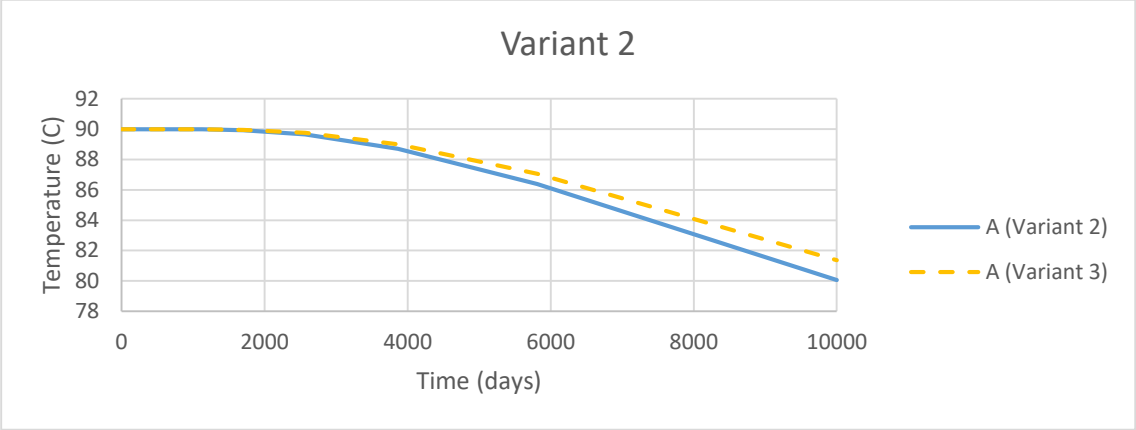

Figure C.3 Comparison between Variant 2 & 3 at point A

Figure C.4 Comparison between Variant 2 & 3 at point C

C.3 Additional results for setup 1

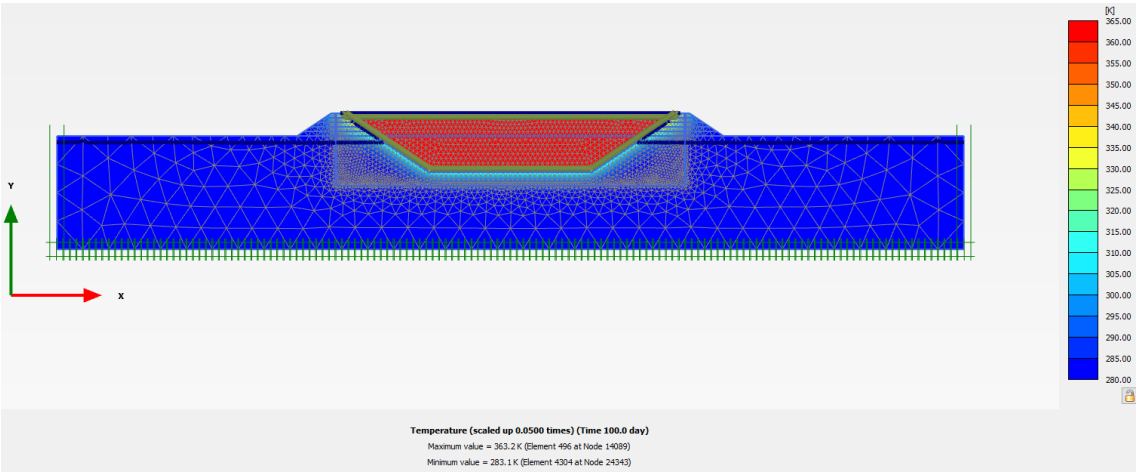

Figure C.5 Temperature distribution after 100 days (Setup 1 scenario 1)

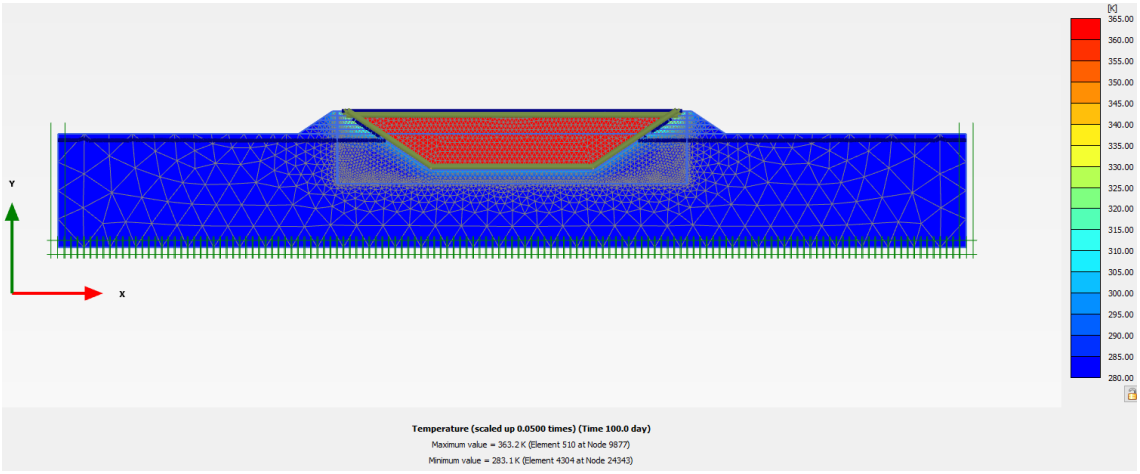

Figure C.6 Temperature distribution after 100 days (Setup 1 scenario 2)

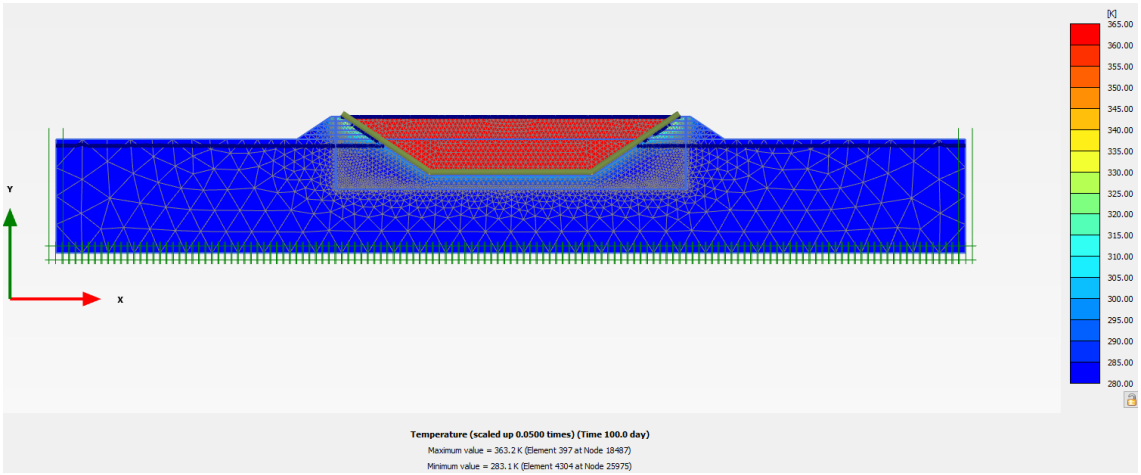

Figure C.7 Temperature distribution after 100 days (Setup 1 scenario 3)

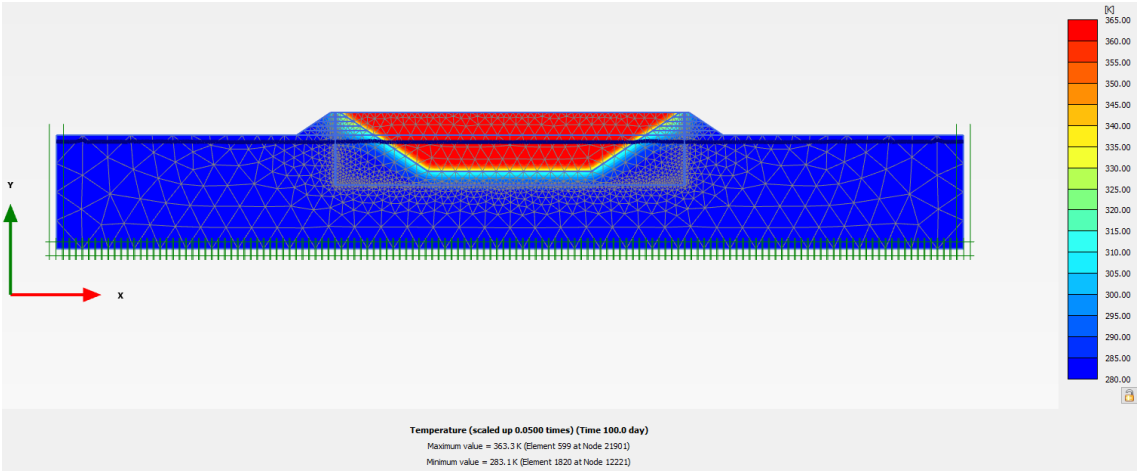

Figure C.8 Temperature distribution after 100 days (Setup 1 scenario 4)

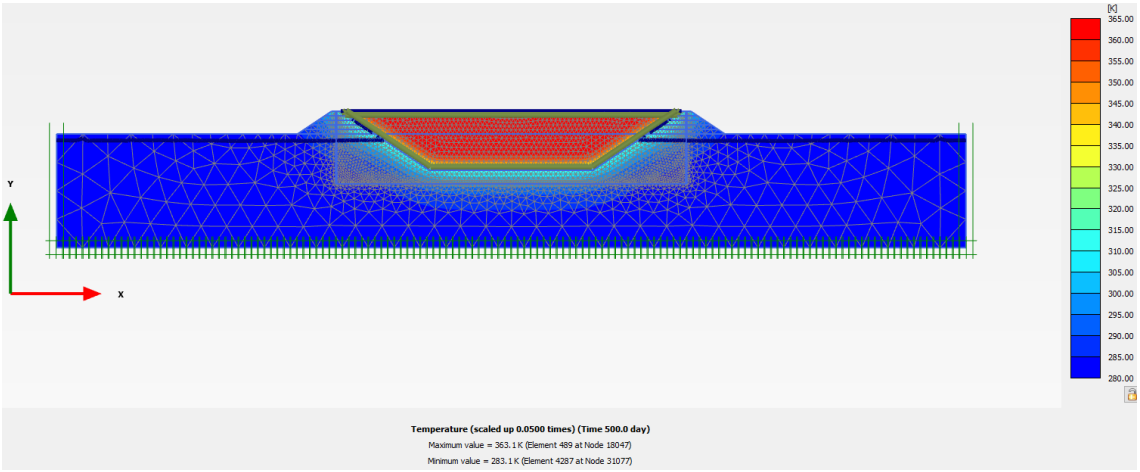

Figure C.9 Temperature distribution after 500 days (Setup 1 scenario 1)

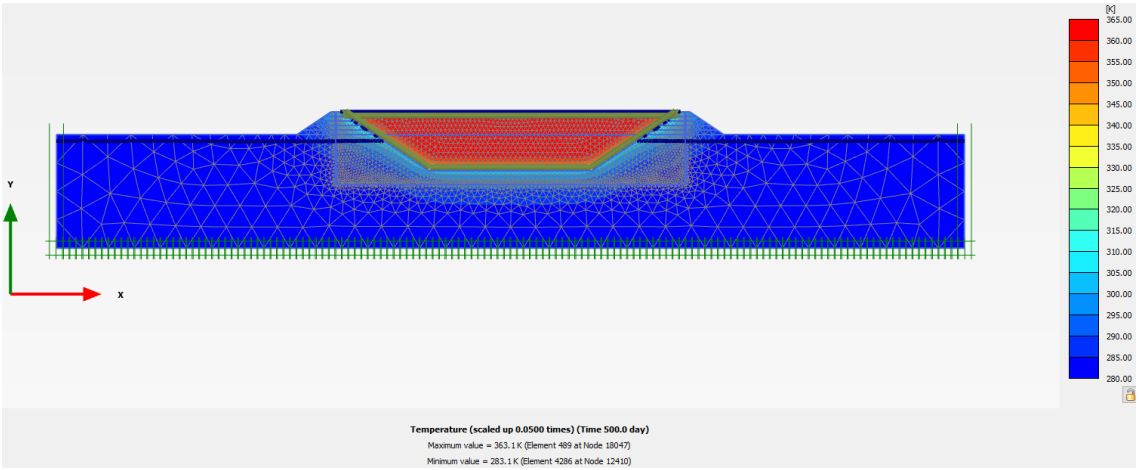

Figure C.10 Temperature distribution after 500 days (Setup 1 scenario 2)

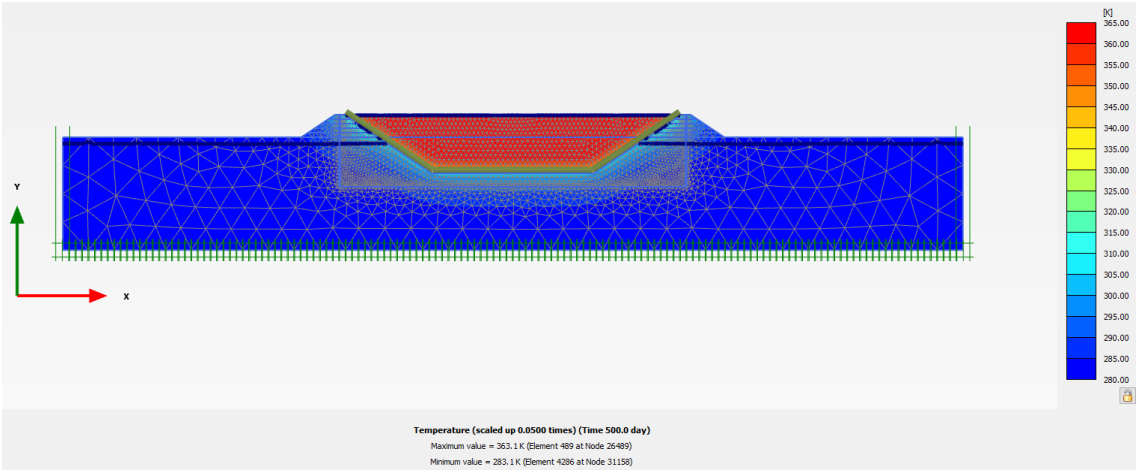

Figure C.11 Temperature distribution after 500 days (Setup 1 scenario 3)

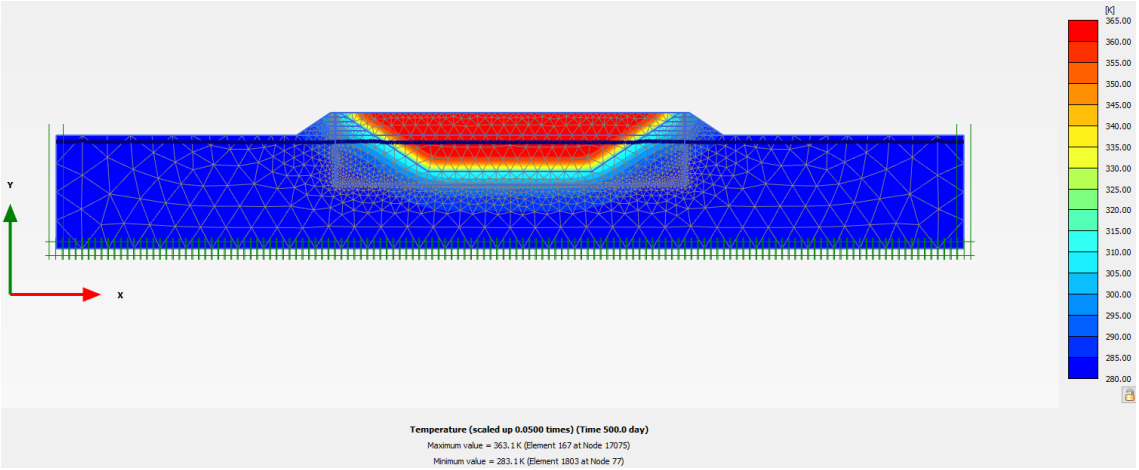

Figure C.12 Temperature distribution after 500 days (Setup 1 scenario 4)

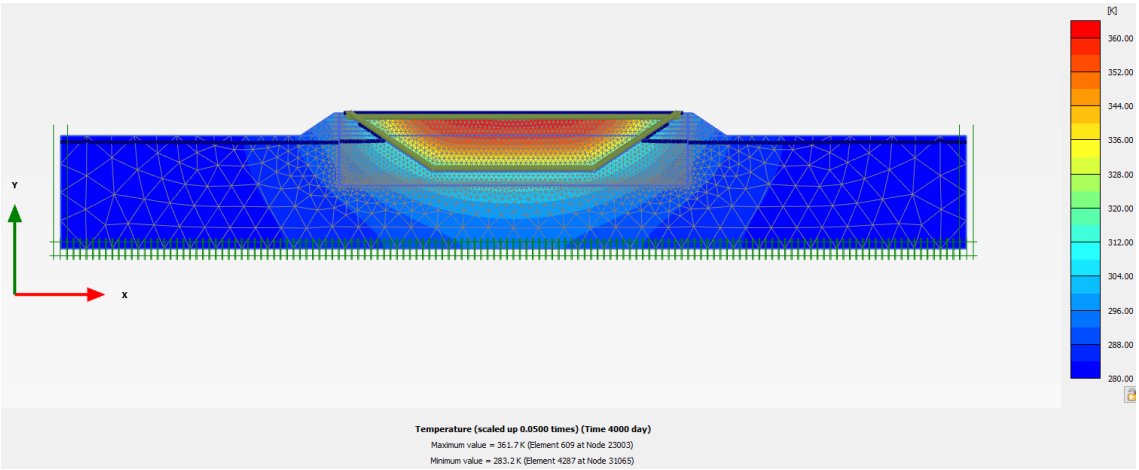

Figure C.13 Temperature distribution after 4000 days (Setup 1 scenario 1)

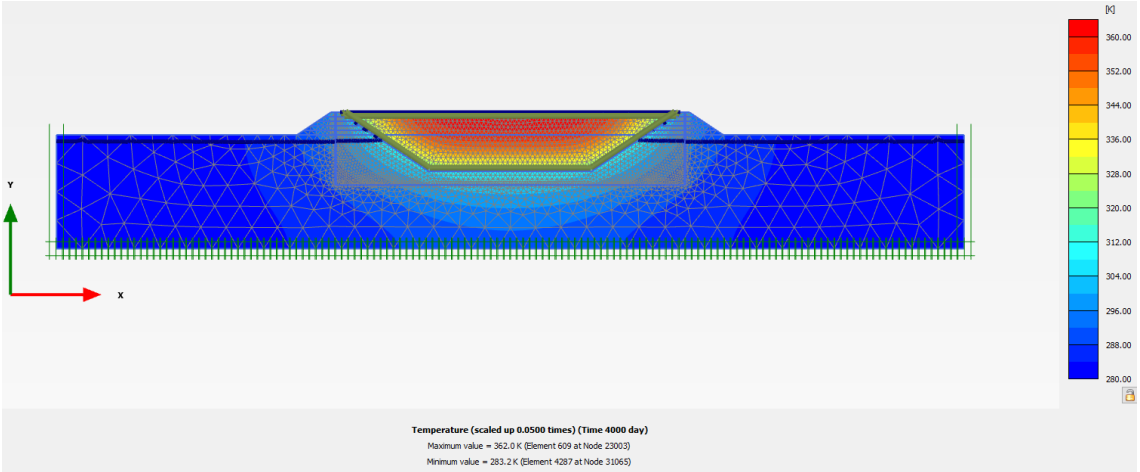

Figure C.14 Temperature distribution after 4000 days (Setup 1 scenario 2)

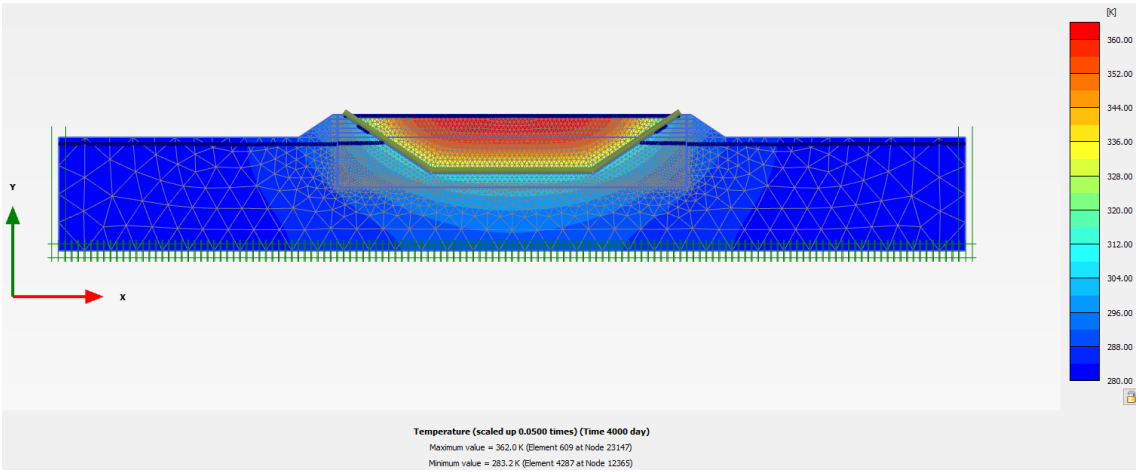

Figure C.15 Temperature distribution after 4000 days (Setup 1 scenario 3)

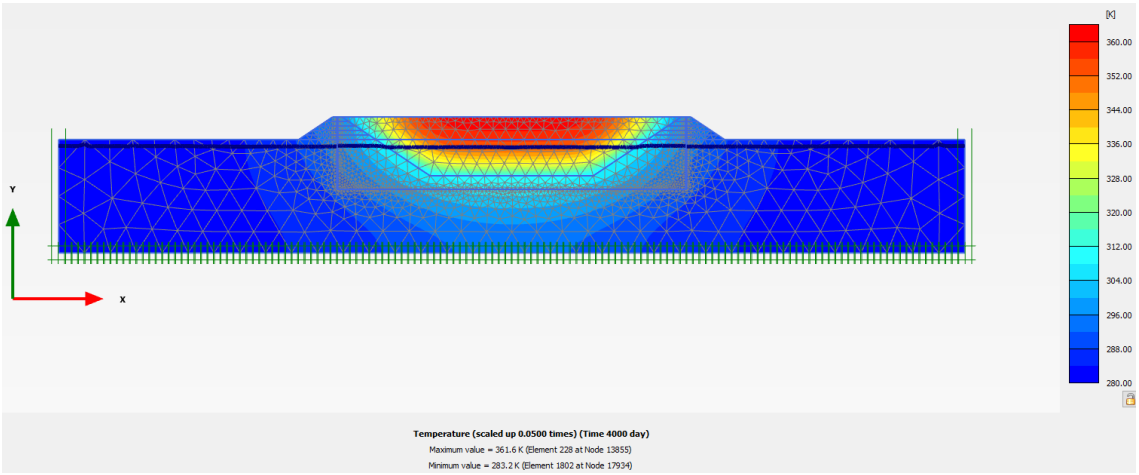

Figure C.16 Temperature distribution after 4000 days (Setup 1 scenario 4)

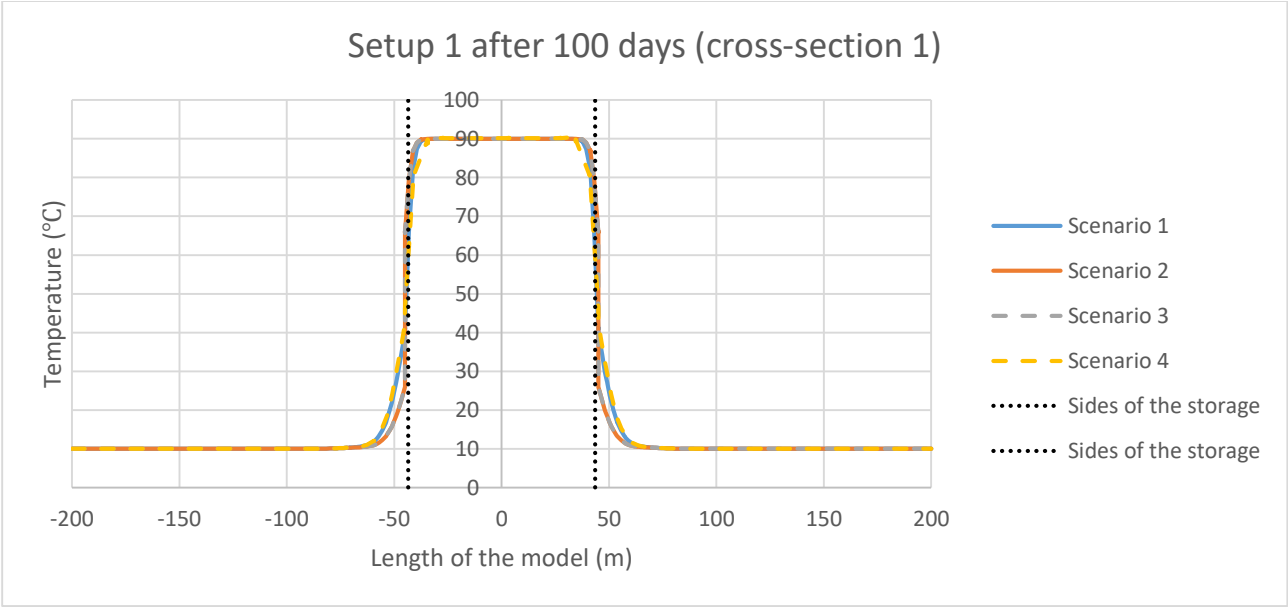

Figure C.17 Setup 1 cross-section 1 after 100 days

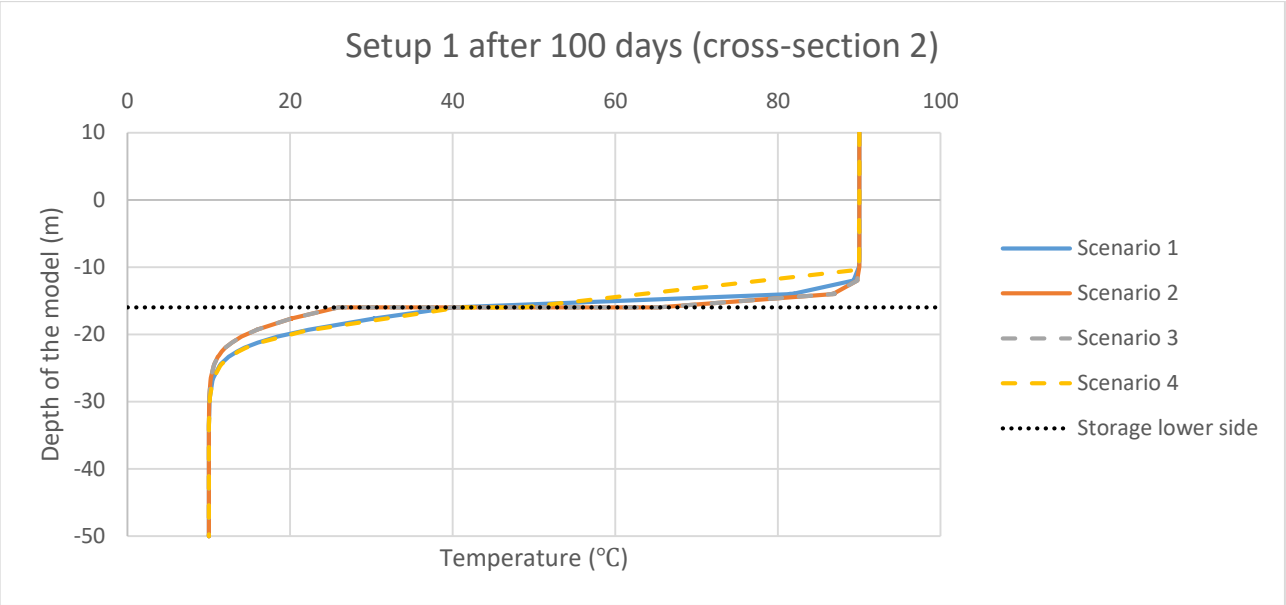

Figure C.18 Setup 1 cross-section 2 after 100 days

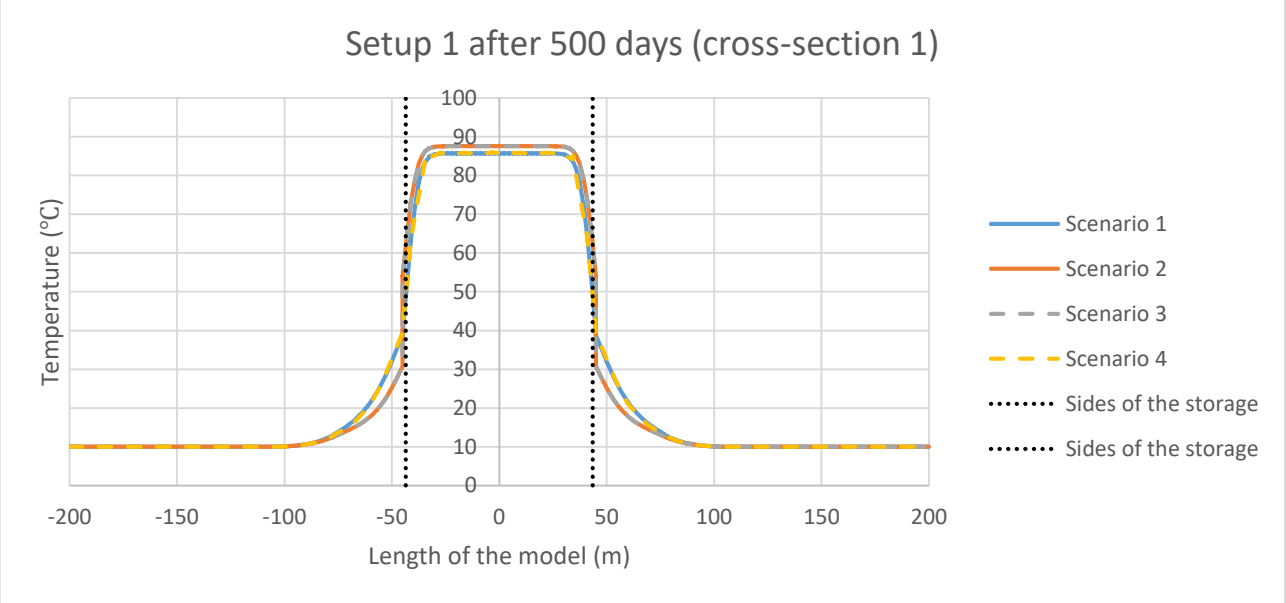

Figure C.19 Setup 1 cross-section 1 after 500 days

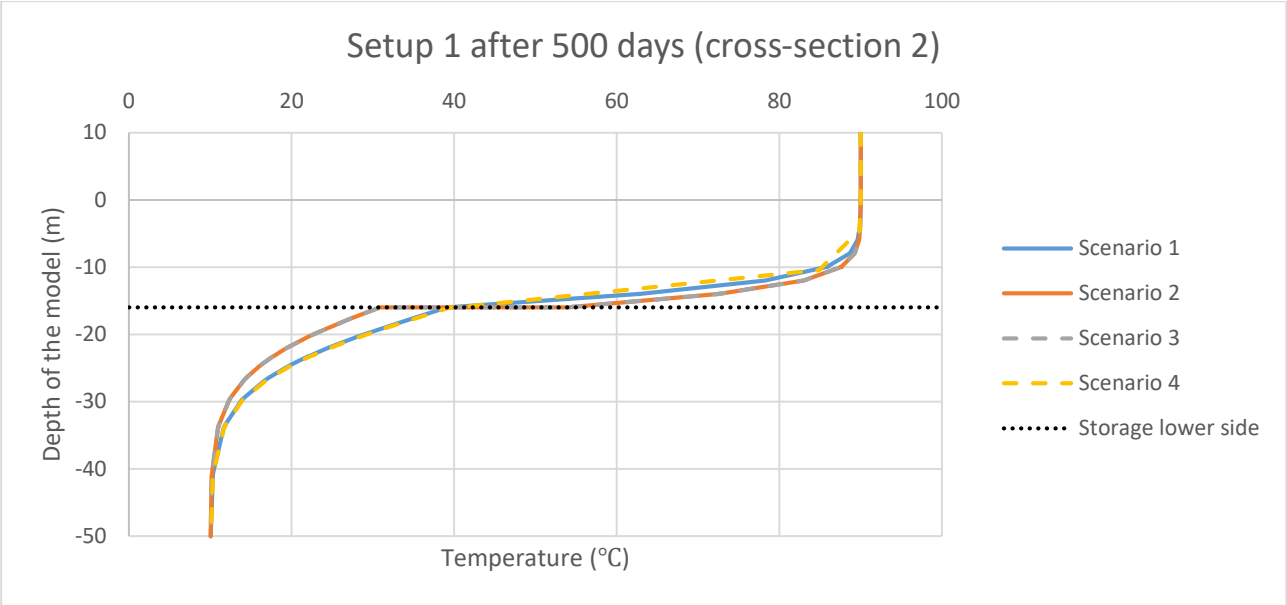

Figure C.20 Setup 1 cross-section 2 after 500 days

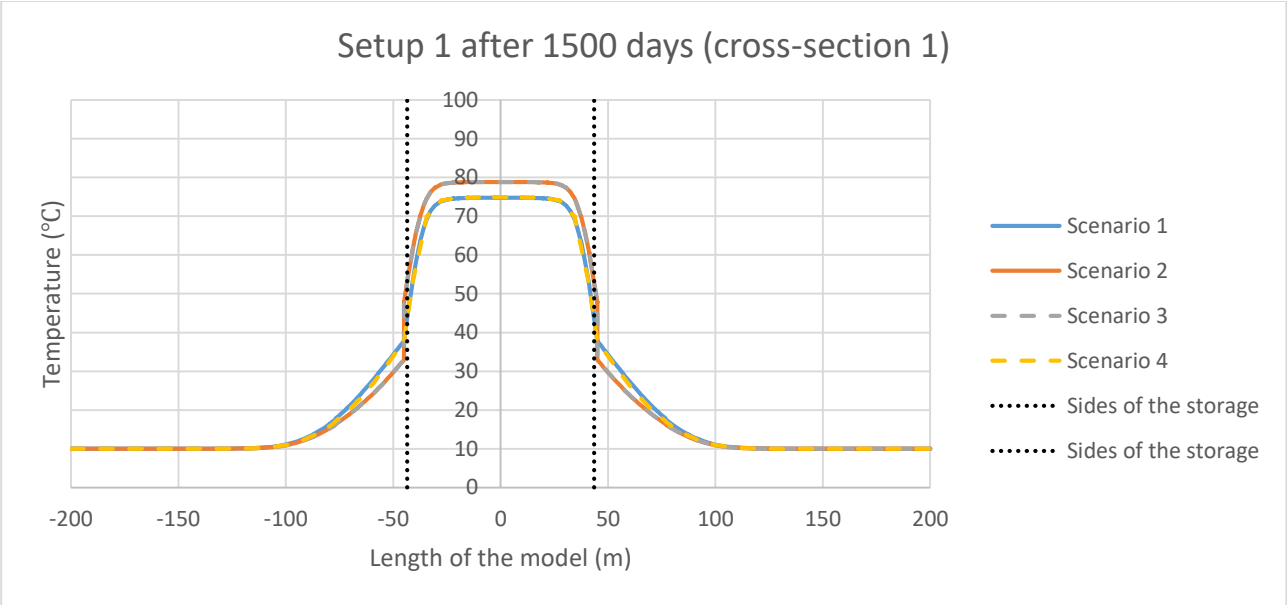

Figure C.21 Setup 1 cross-section 1 after 1500 days

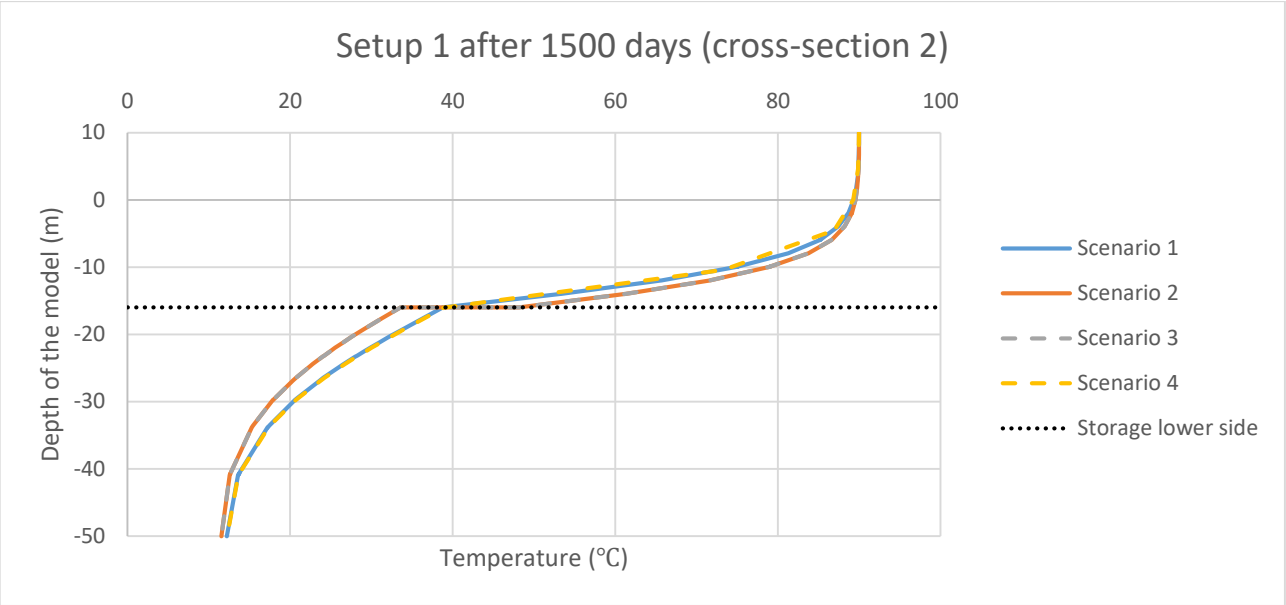

Figure C.22 Setup 1 cross-section 2 after 1500 days

C.4 Additional results for setup 2

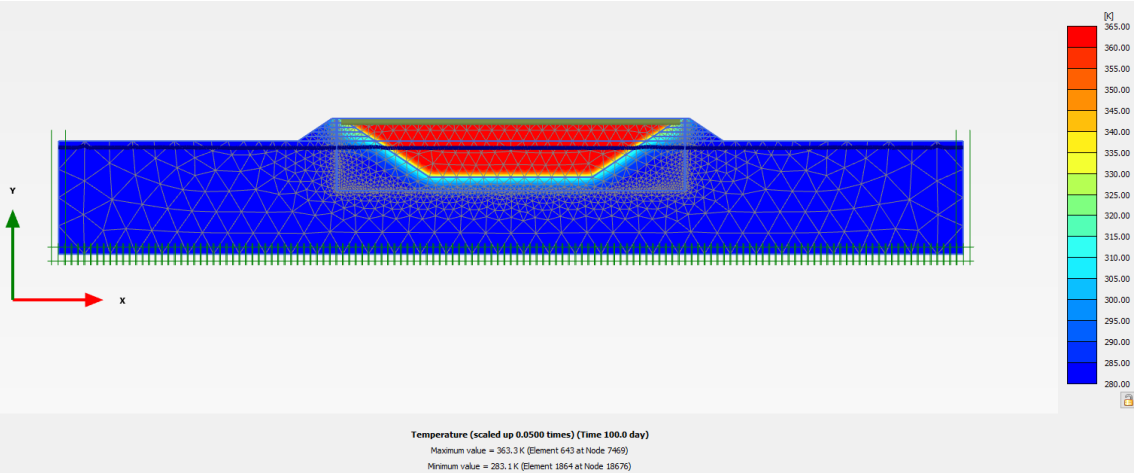

Figure C.23 Temperature distribution after 100 days (Setup 2 scenario 1)

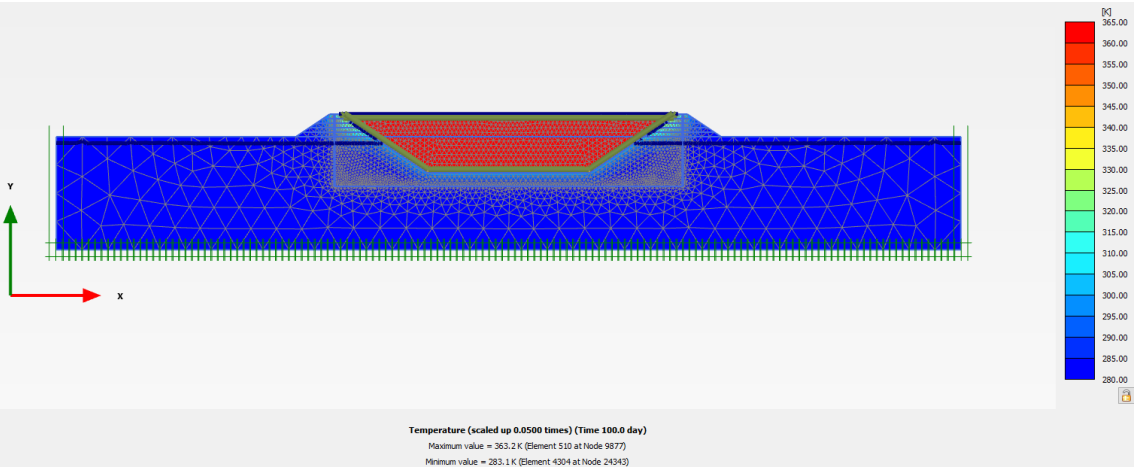

Figure C.24 Temperature distribution after 100 days (Setup 2 scenario 2)

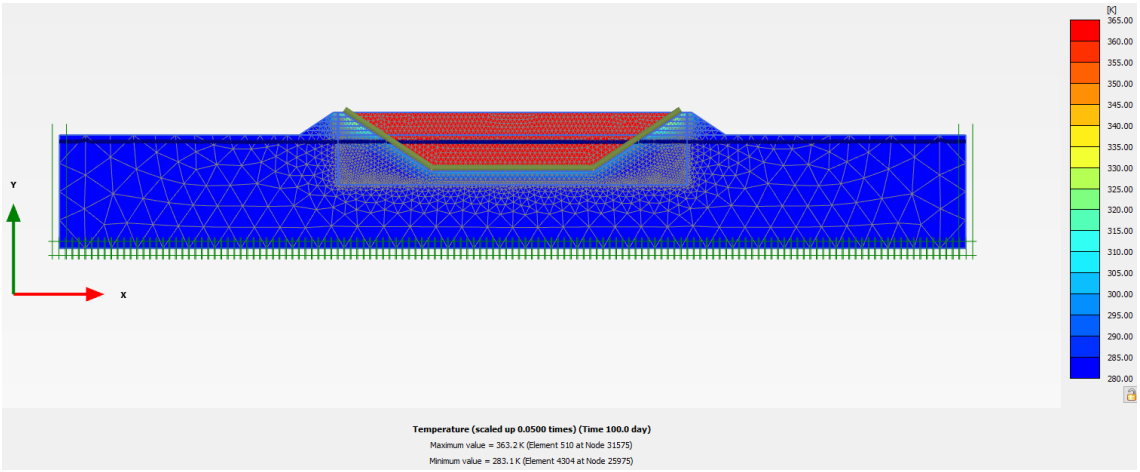

Figure C.25 Temperature distribution after 100 days (Setup 2 scenario 3)

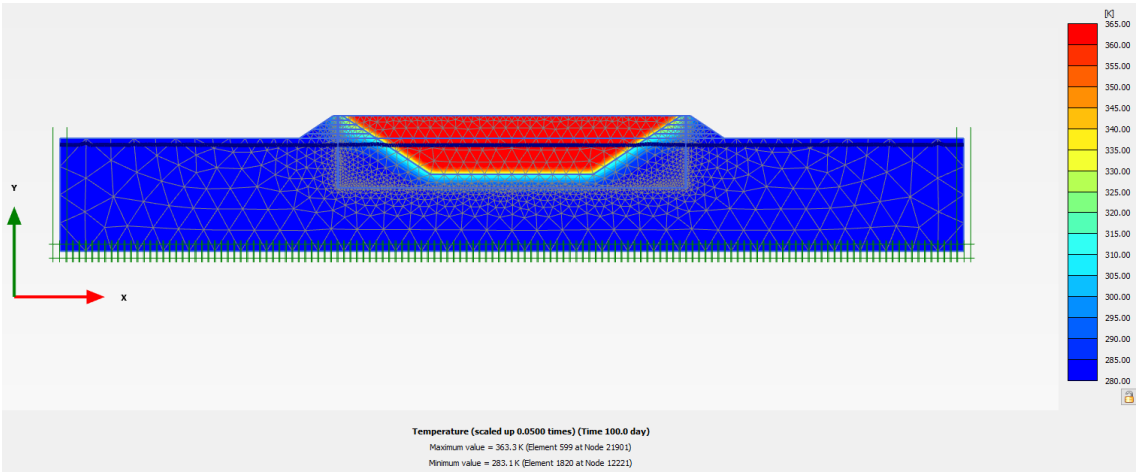

Figure C.26 Temperature distribution after 100 days (Setup 2 scenario 4)

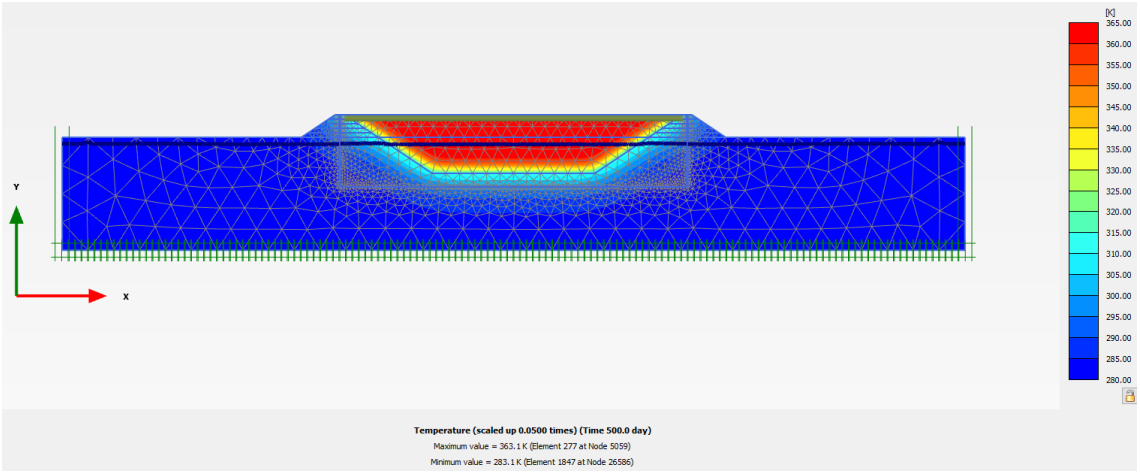

Figure C.27 Temperature distribution after 500 days (Setup 2 scenario 1)

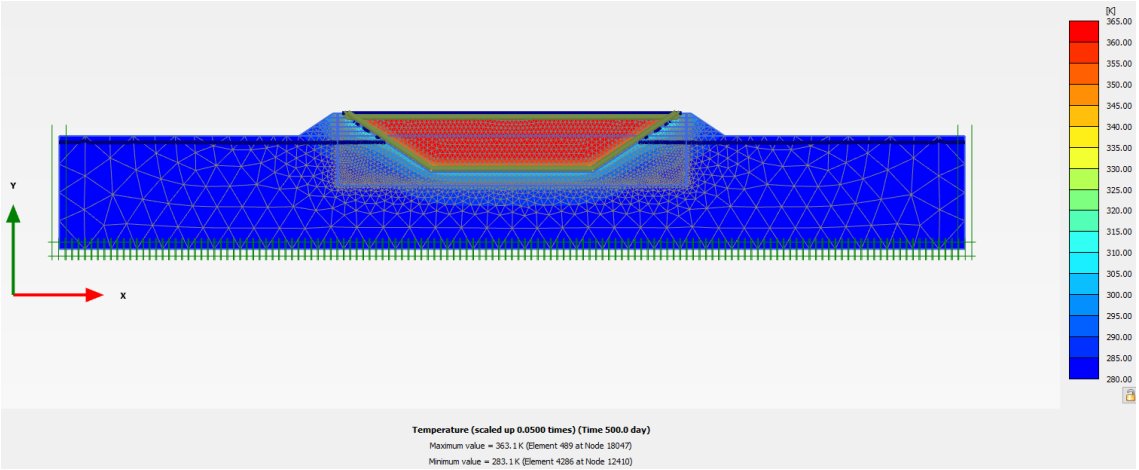

Figure C.28 Temperature distribution after 500 days (Setup 2 scenario 2)

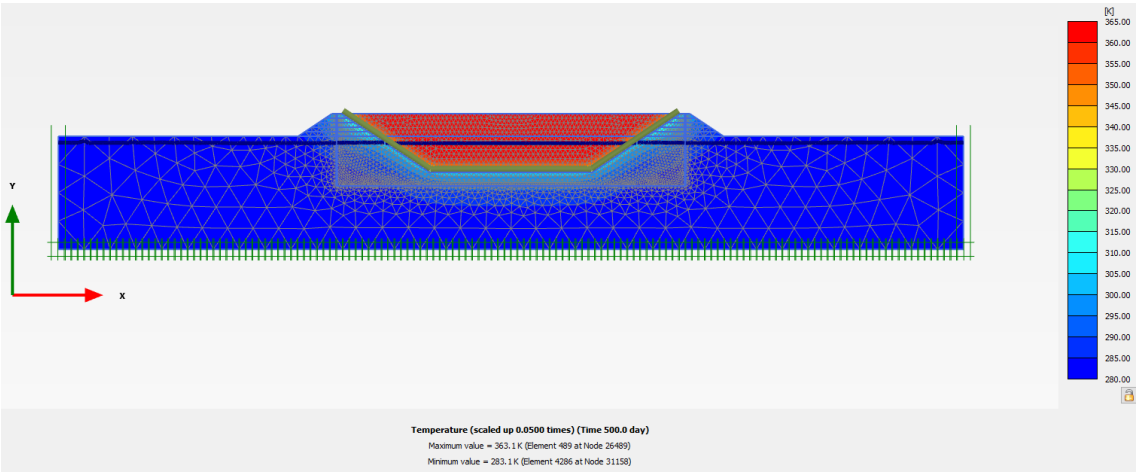

Figure C.29 Temperature distribution after 500 days (Setup 2 scenario 3)

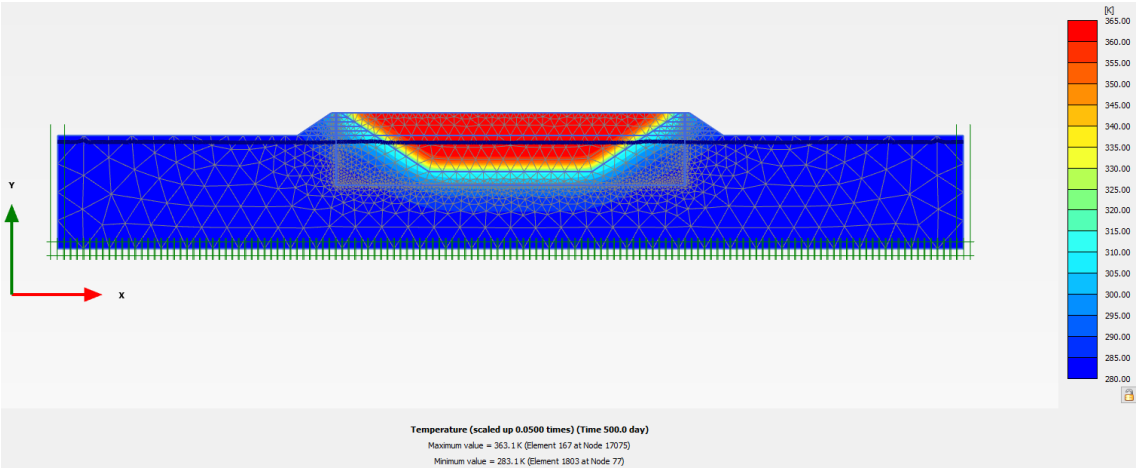

Figure C.30 Temperature distribution after 500 days (Setup 2 scenario 4)

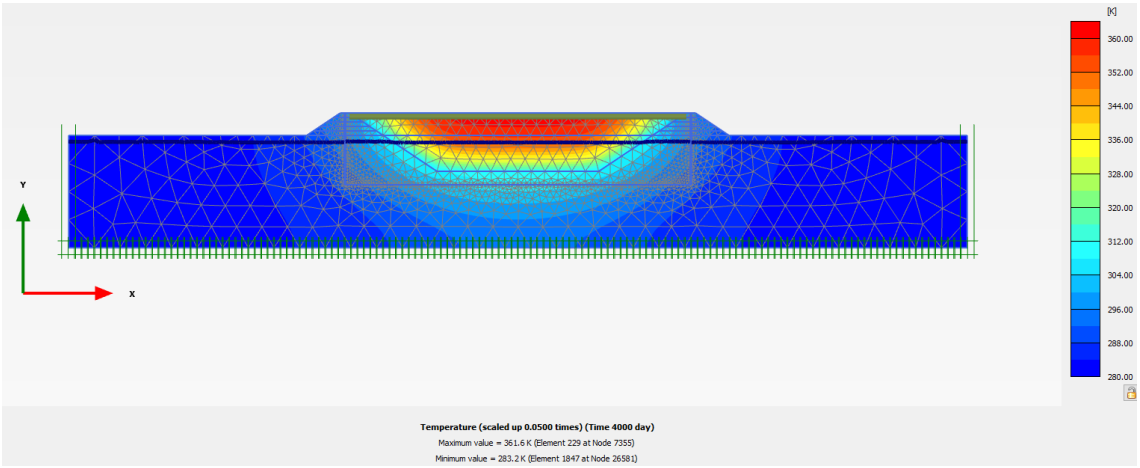

Figure C.31 Temperature distribution after 4000 days (Setup 2 scenario 1)

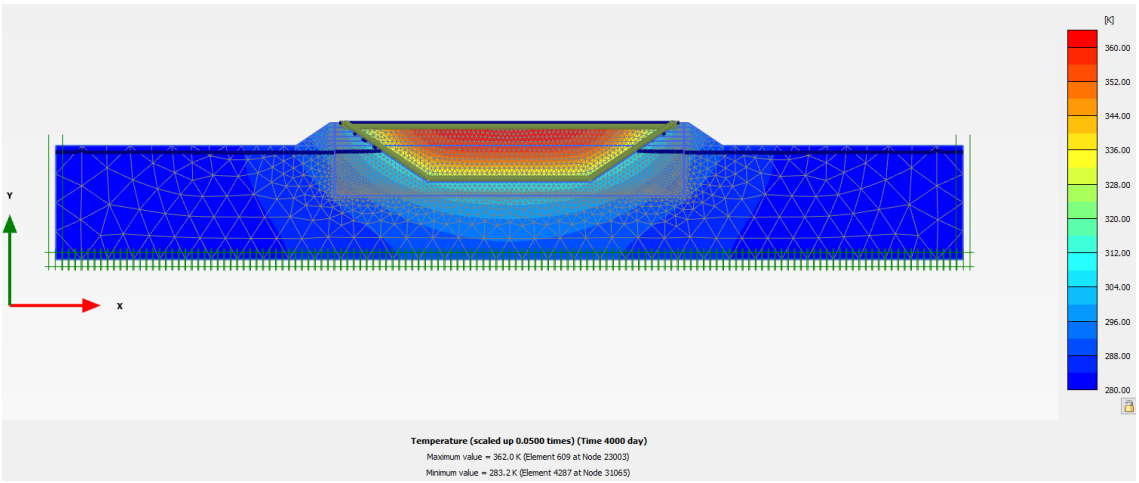

Figure C.32 Temperature distribution after 4000 days (Setup 2 scenario 2)

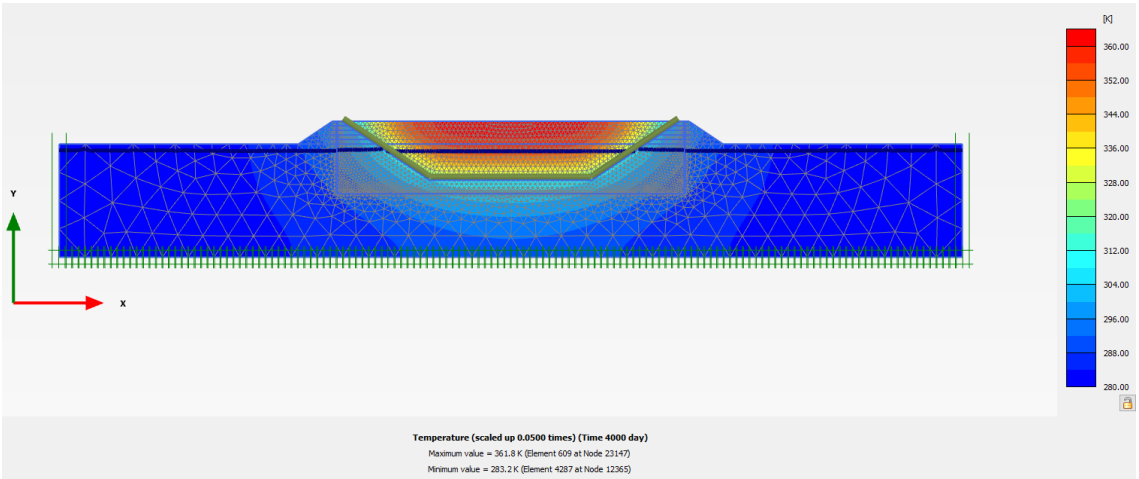

Figure C.33 Temperature distribution after 4000 days (Setup 2 scenario 3)

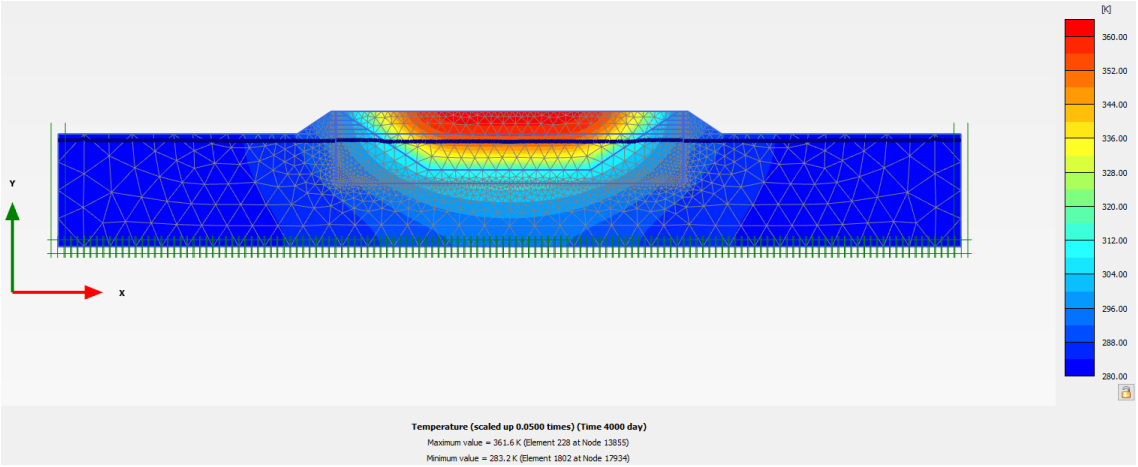

Figure C.34 Temperature distribution after 4000 days (Setup 2 scenario 4)

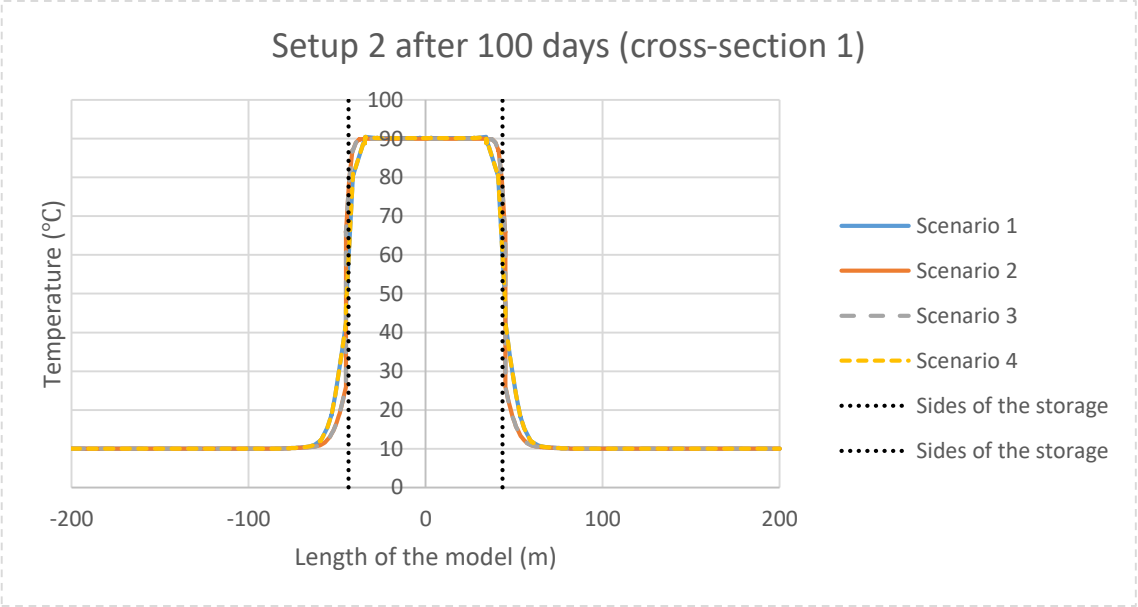

Figure C.35 Setup 2 cross-section 1 after 100 days

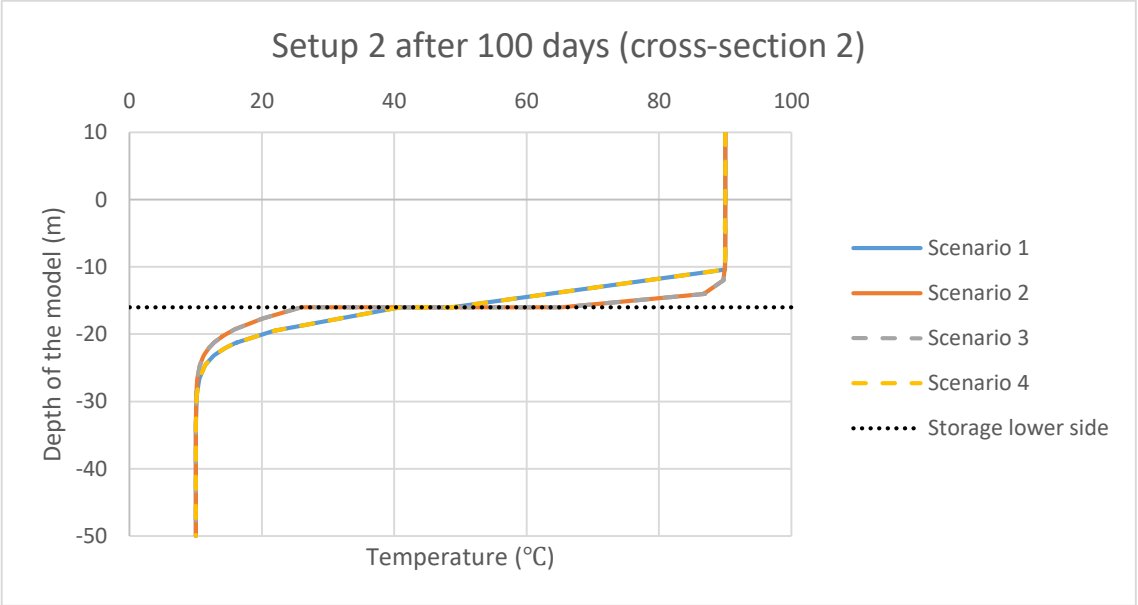

Figure C.36 Setup 2 cross-section 2 after 100 days

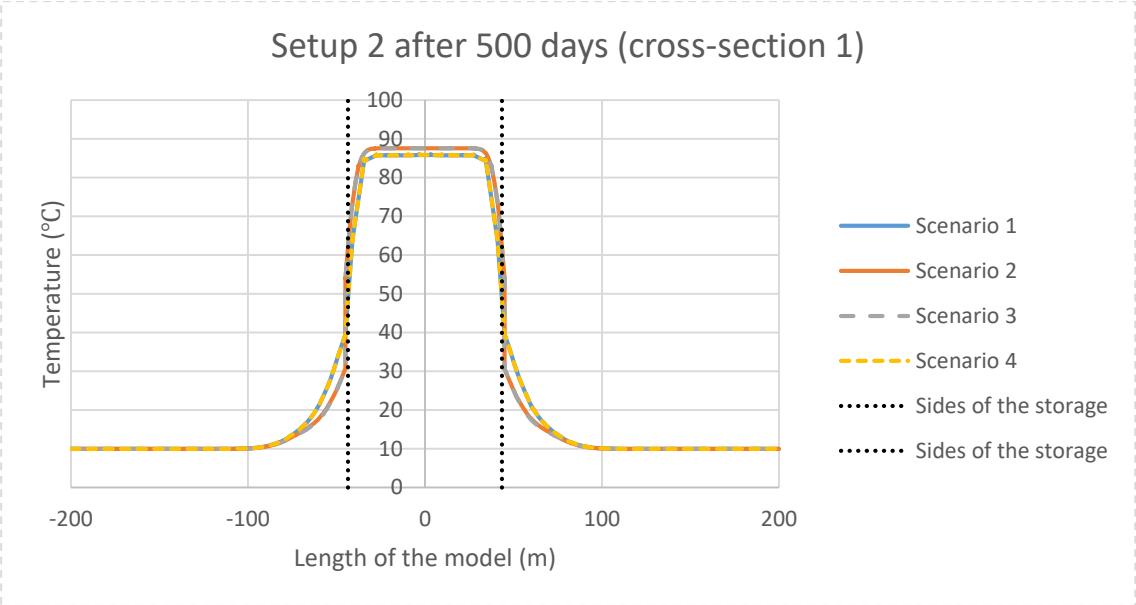

Figure C.37 Setup 2 cross-section 1 after 500 days

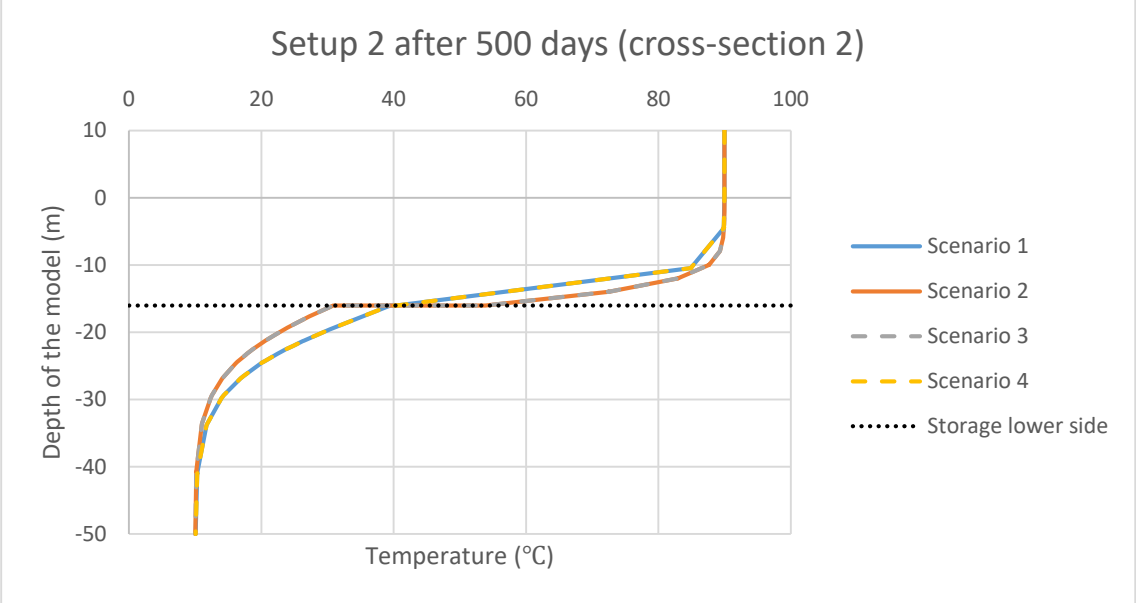

Figure C.38 Setup 2 cross-section 2 after 500 days

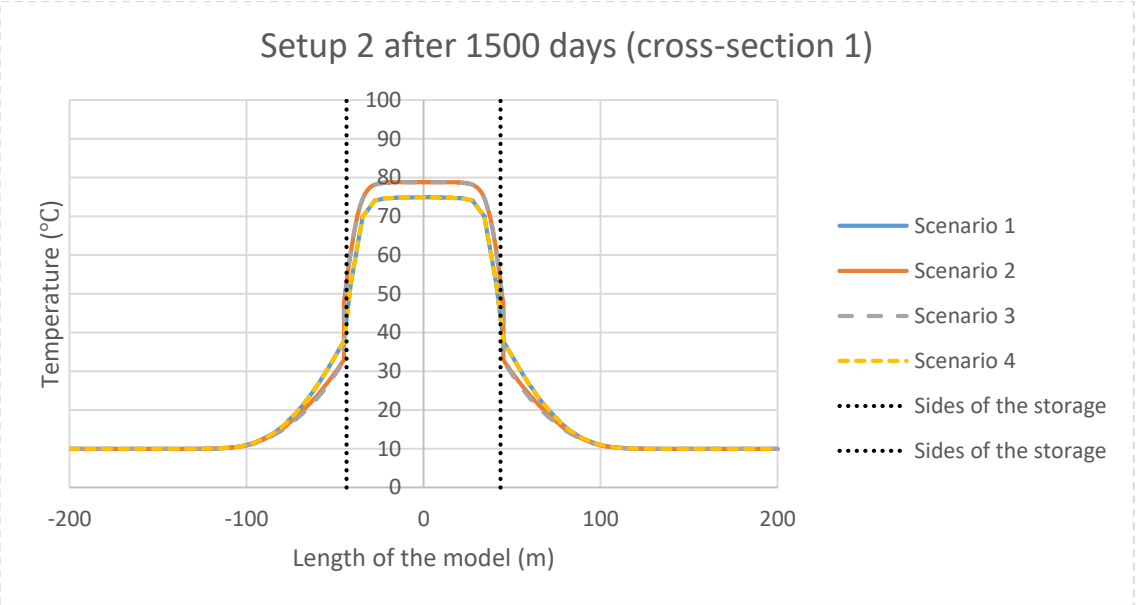

Figure C.39 Setup 2 cross-section 1 after 1500 days

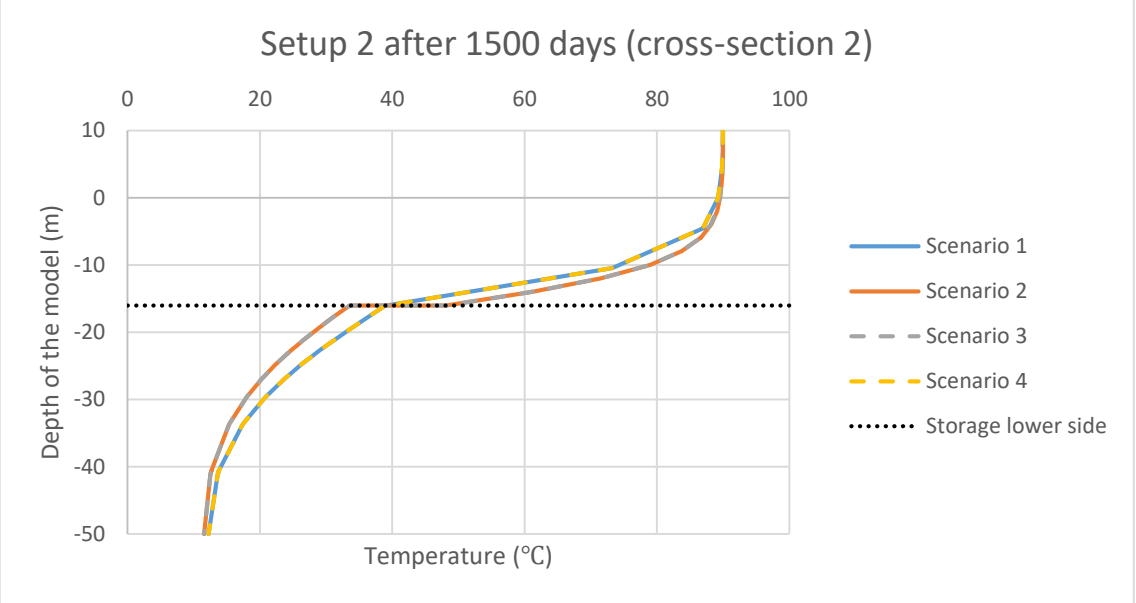

Figure C.40 Setup 2 cross-section 2 after 1500 days

C.5 Additional results for setup 3

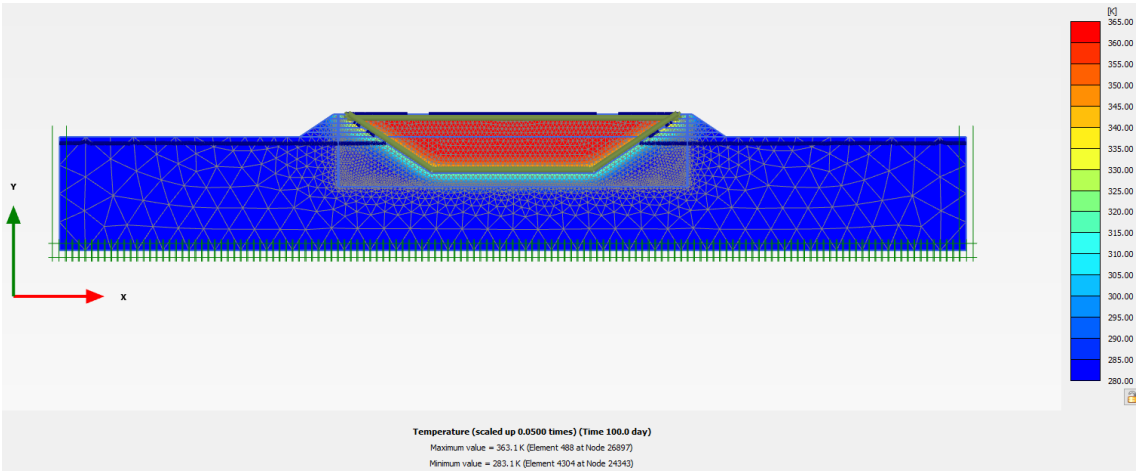

Figure C.41 Temperature distribution after 100 days (Setup 3 scenario 1)

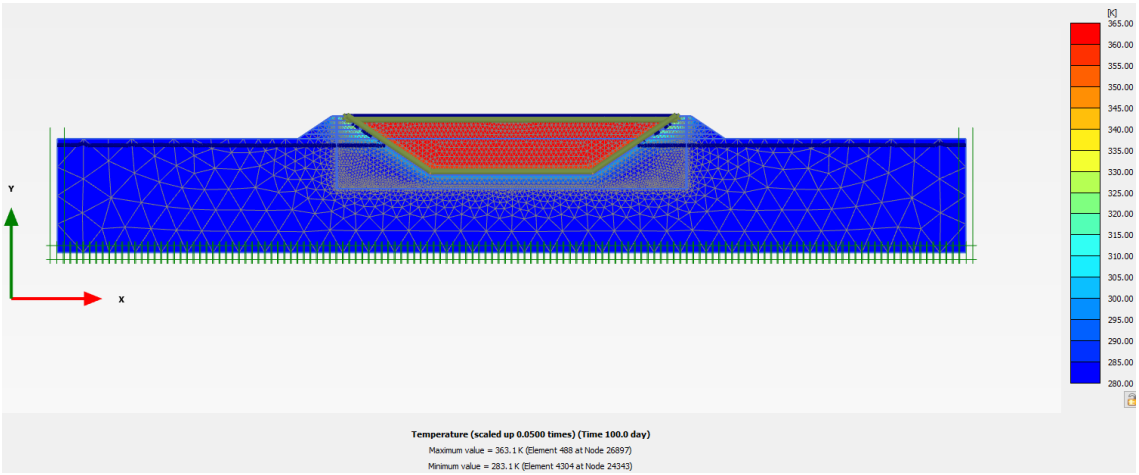

Figure C.42 Temperature distribution after 100 days (Setup 3 scenario 2)

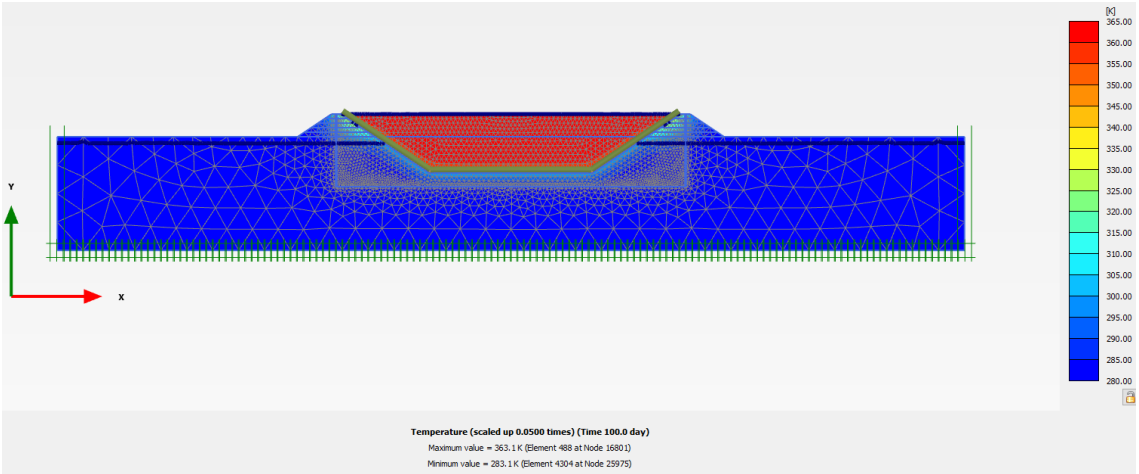

Figure C.43 Temperature distribution after 100 days (Setup 3 scenario 3)

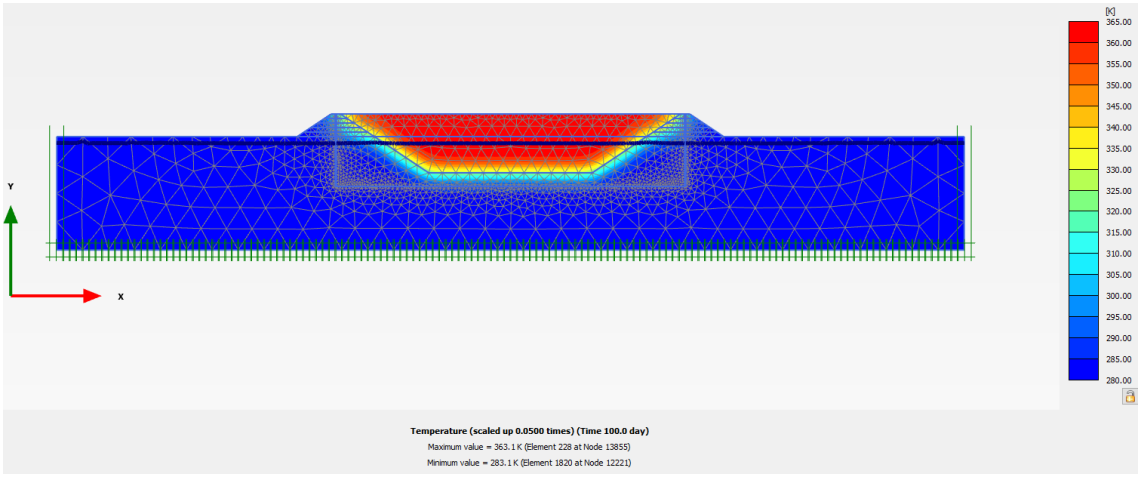

Figure C.44 Temperature distribution after 100 days (Setup 3 scenario 4)

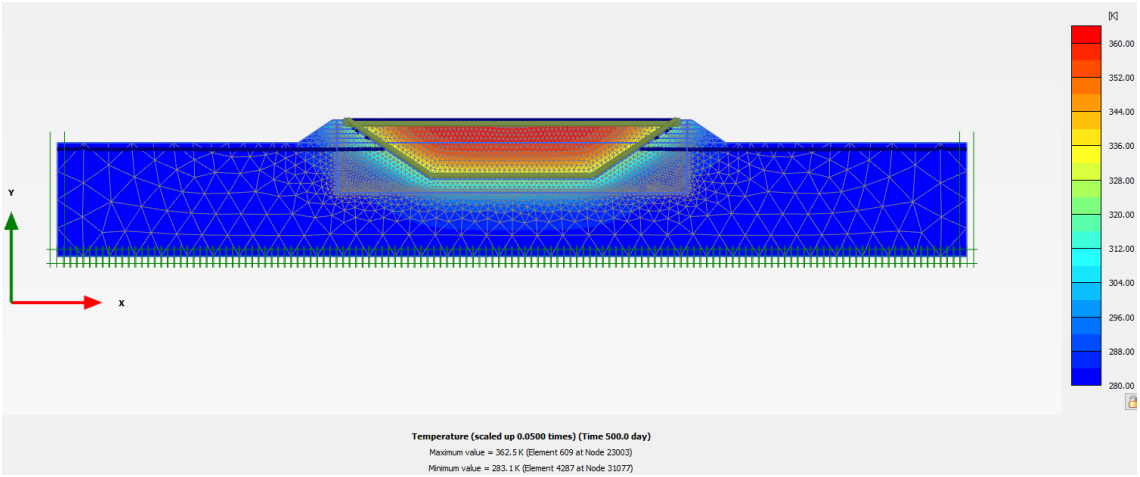

Figure C.45 Temperature distribution after 500 days (Setup 3 scenario 1)

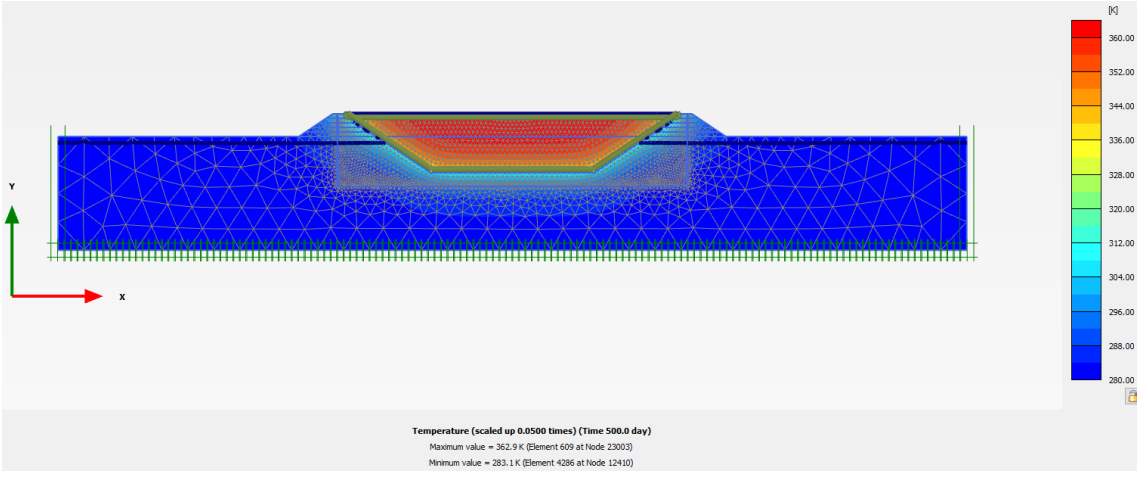

Figure C.46 Temperature distribution after 500 days (Setup 3 scenario 2)

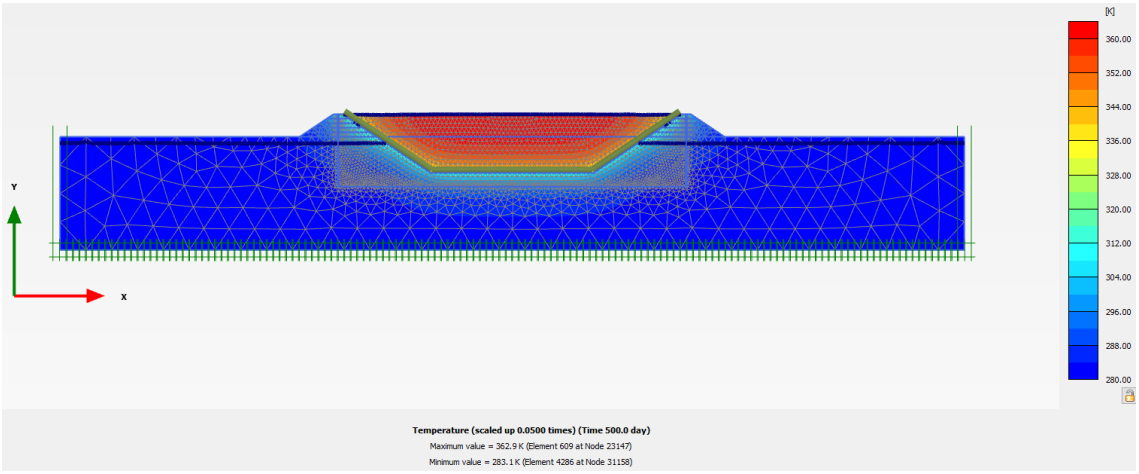

Figure C.47 Temperature distribution after 500 days (Setup 3 scenario 3)

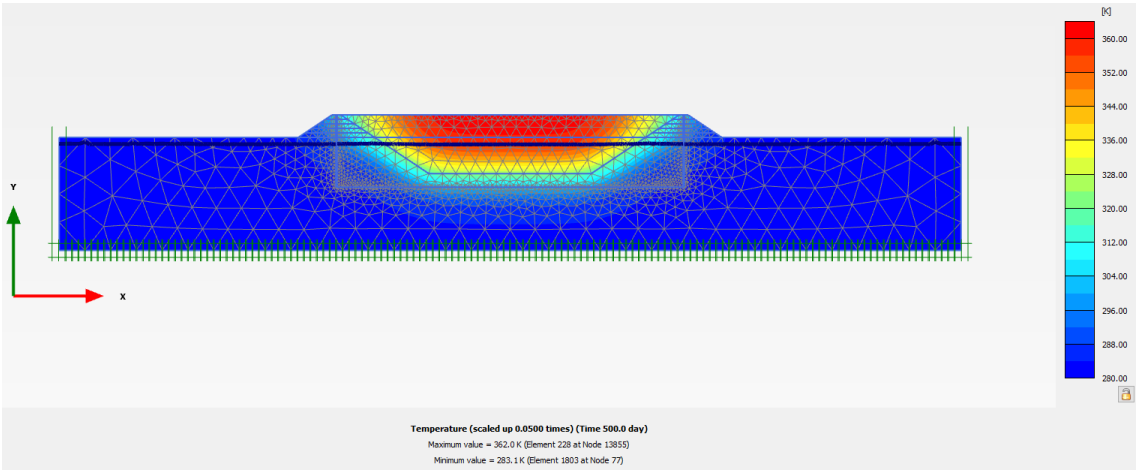

Figure C.48 Temperature distribution after 500 days (Setup 3 scenario 4)

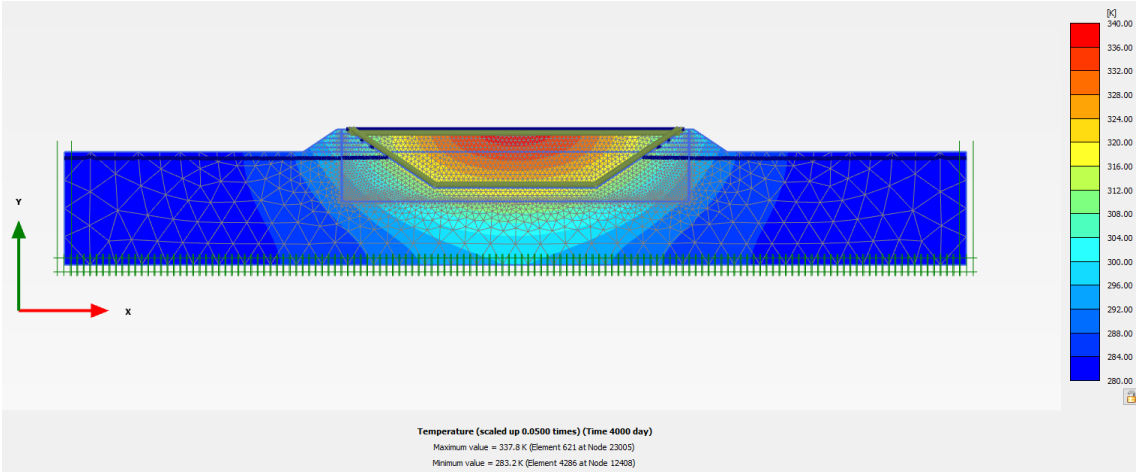

Figure C.49 Temperature distribution after 4000 days (Setup 3 scenario 1)

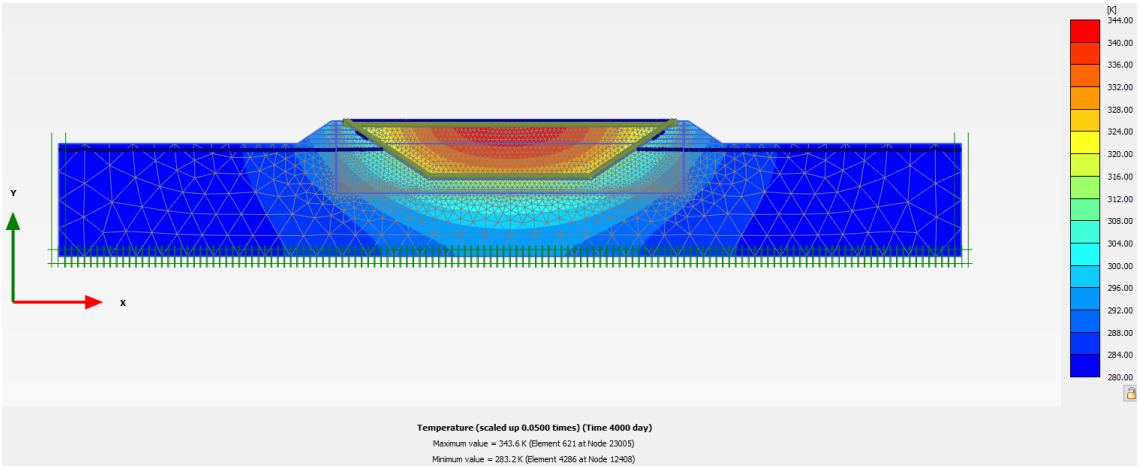

Figure C.50 Temperature distribution after 4000 days (Setup 3 scenario 2)

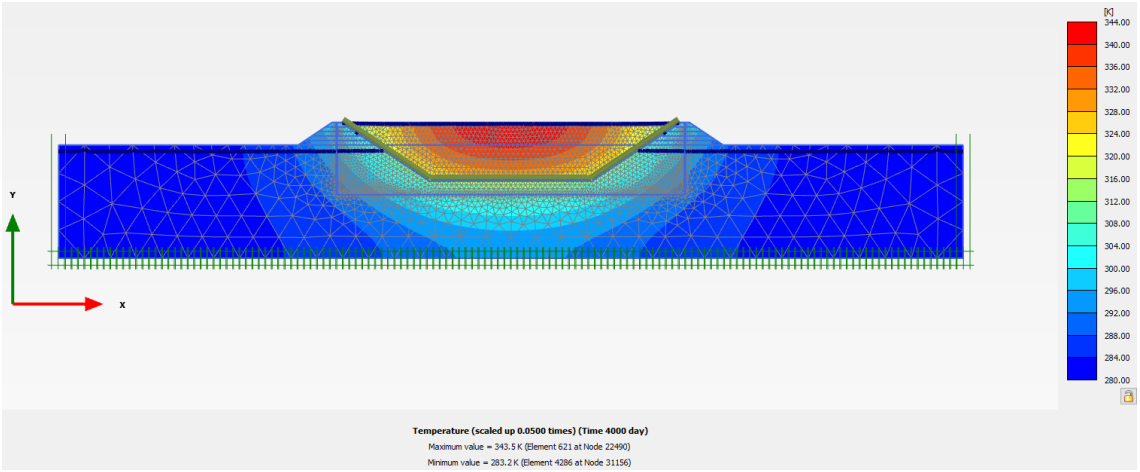

Figure C.51 Temperature distribution after 4000 days (Setup 3 scenario 3)

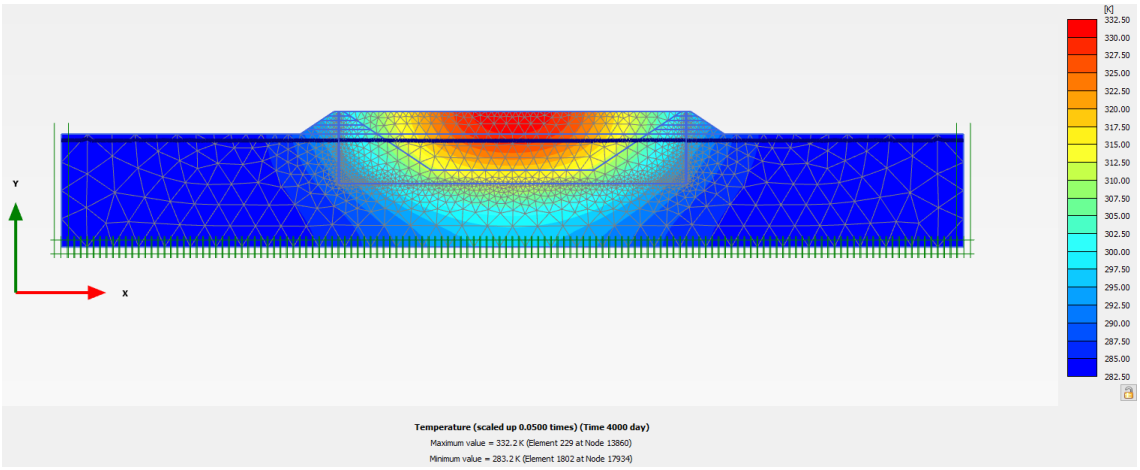

Figure C.52 Temperature distribution after 4000 days (Setup 3 scenario 4)

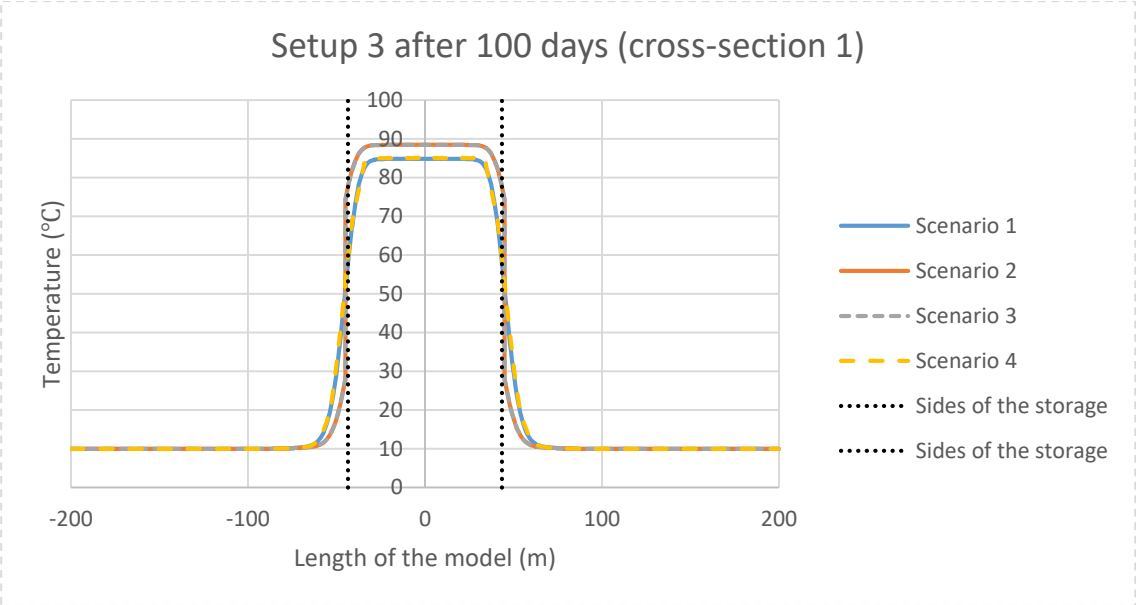

Figure C.53 Setup 3 cross-section 1 after 100 days

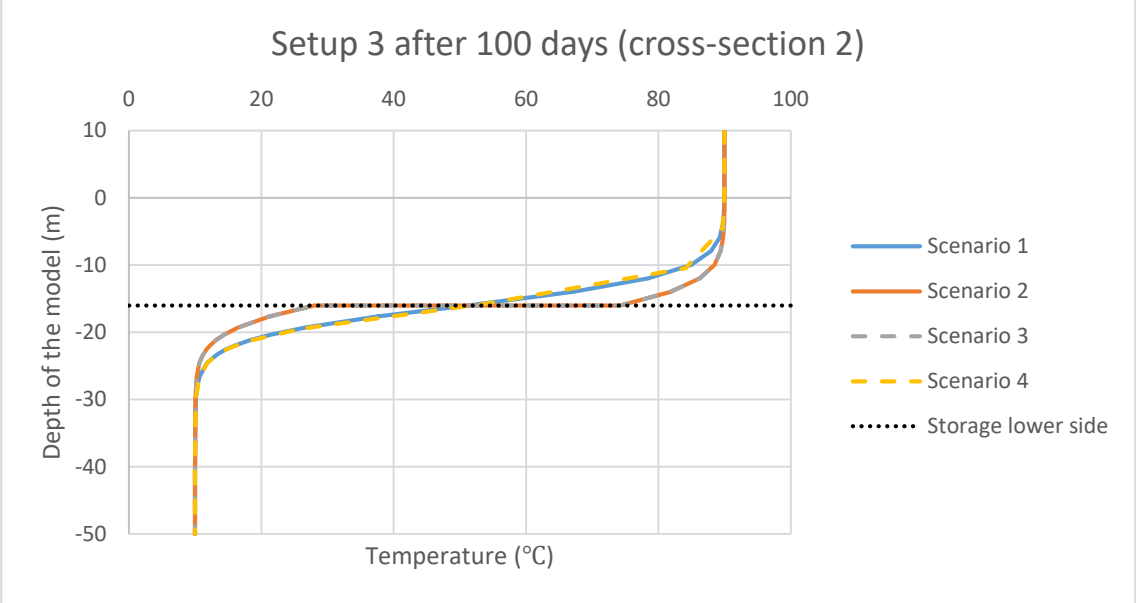

Figure C.54 Setup 3 cross-section 2 after 100 days

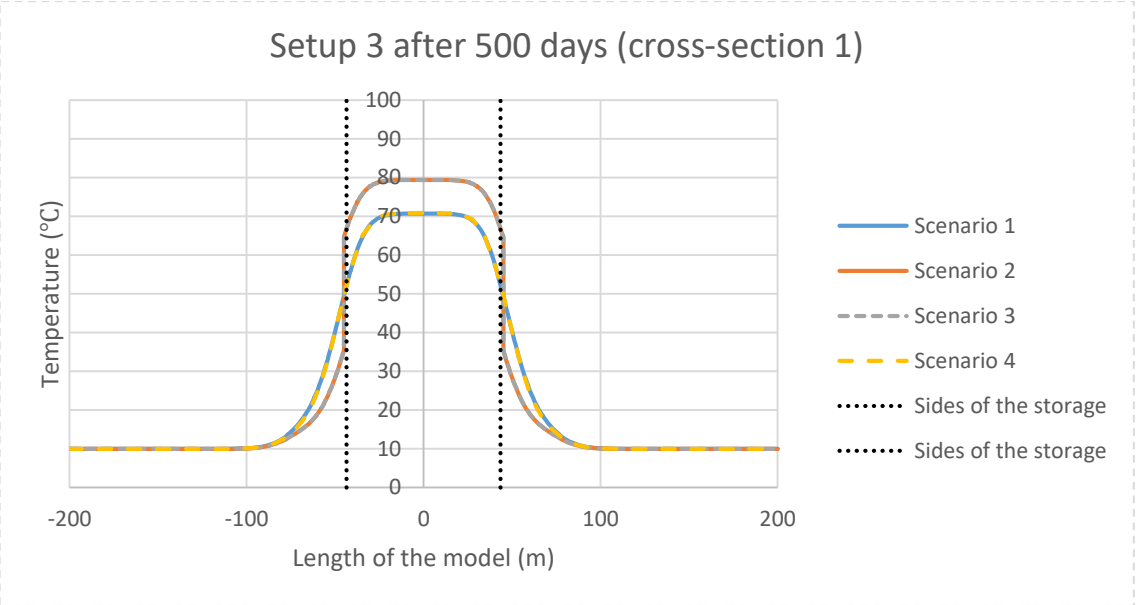

Figure C.55 Setup 3 cross-section 1 after 500 days

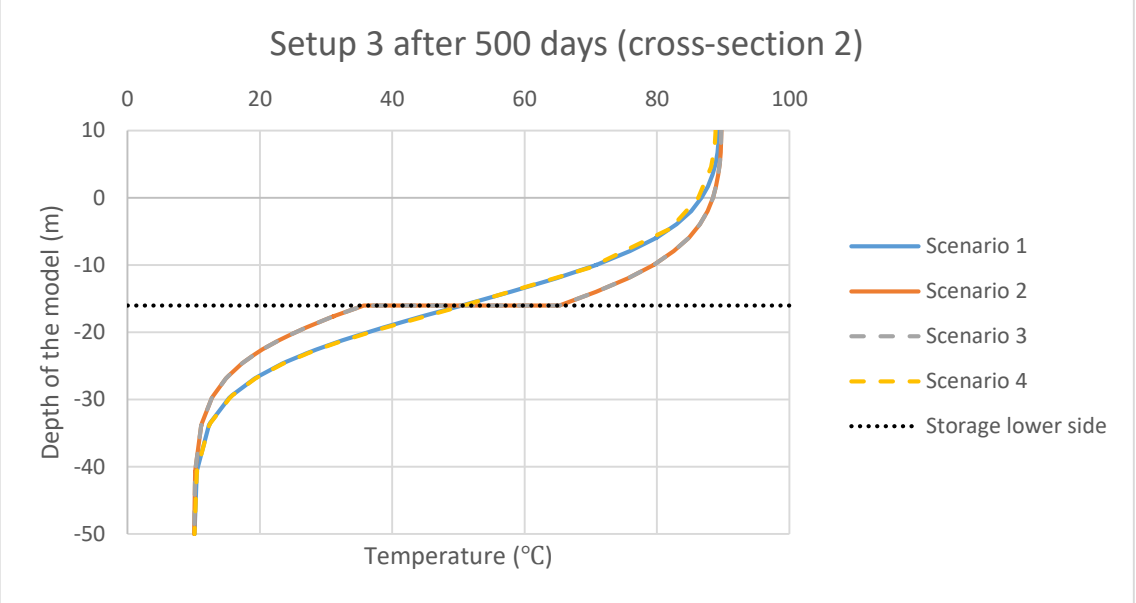

Figure C.56 Setup 3 cross-section 2 after 500 days

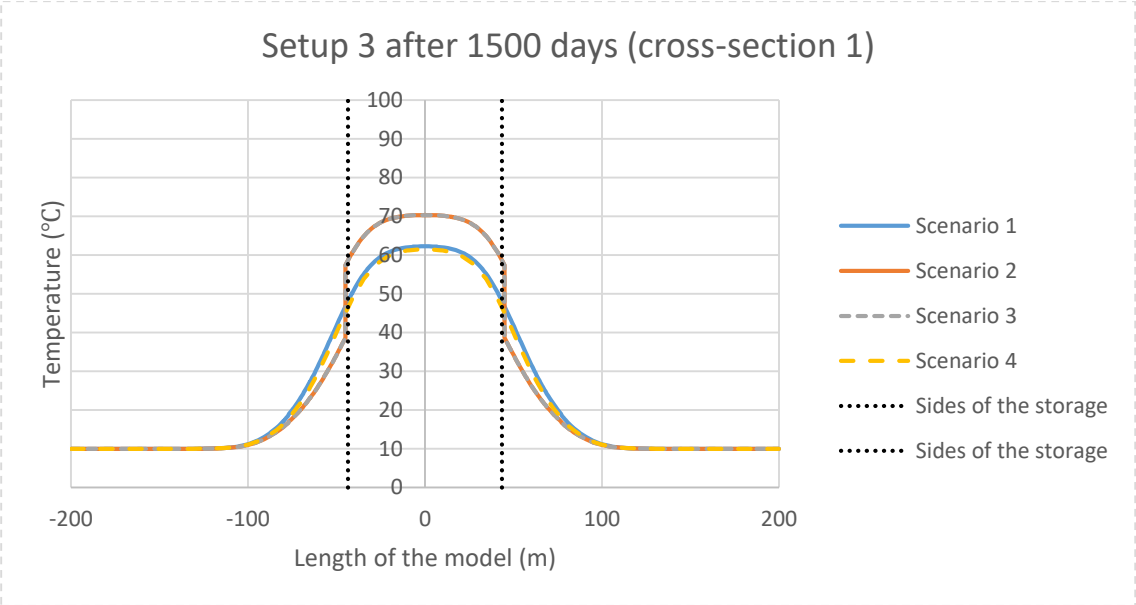

Figure C.57 Setup 3 cross-section 1 after 1500 days

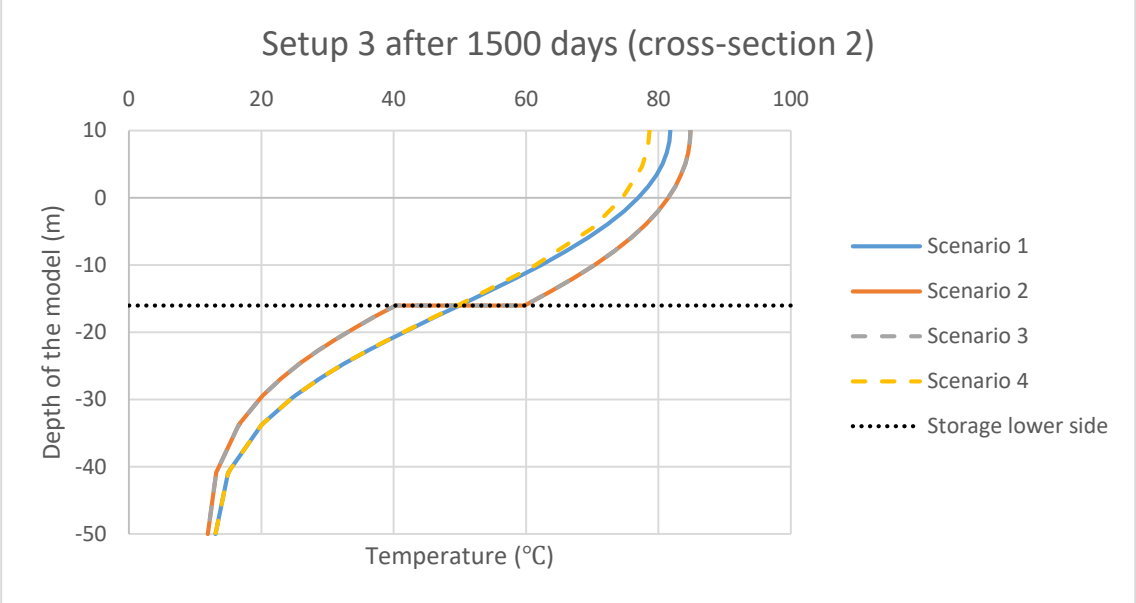

Figure C.58 Setup 3 cross-section 2 after 1500 days

C.6 Additional results for comparison between setups

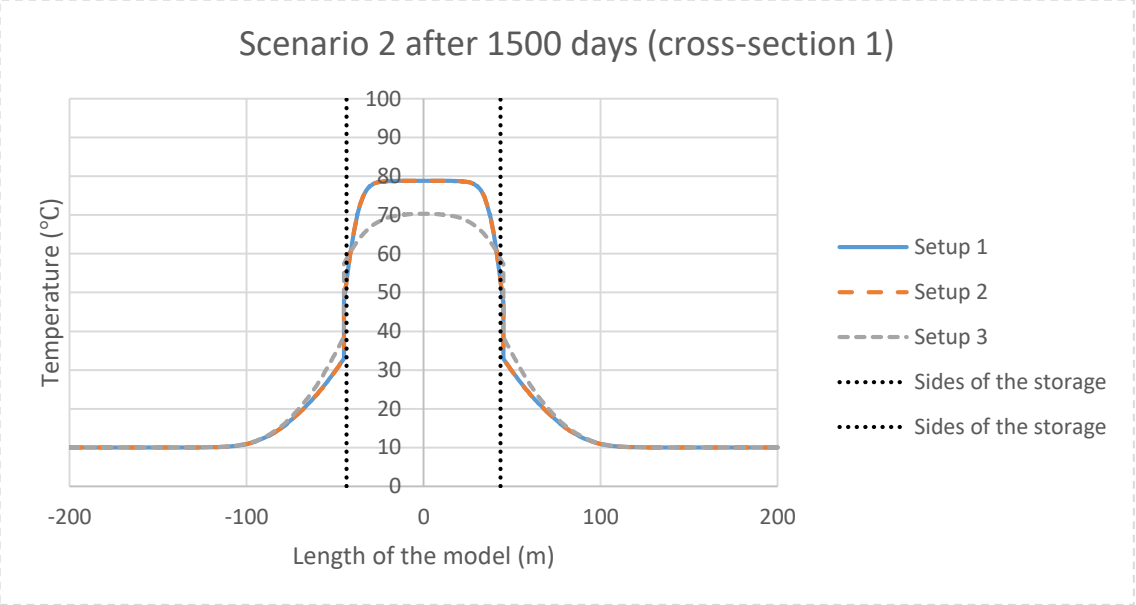

Figure C.59 Scenario 2 cross-section 1 after 1500 days

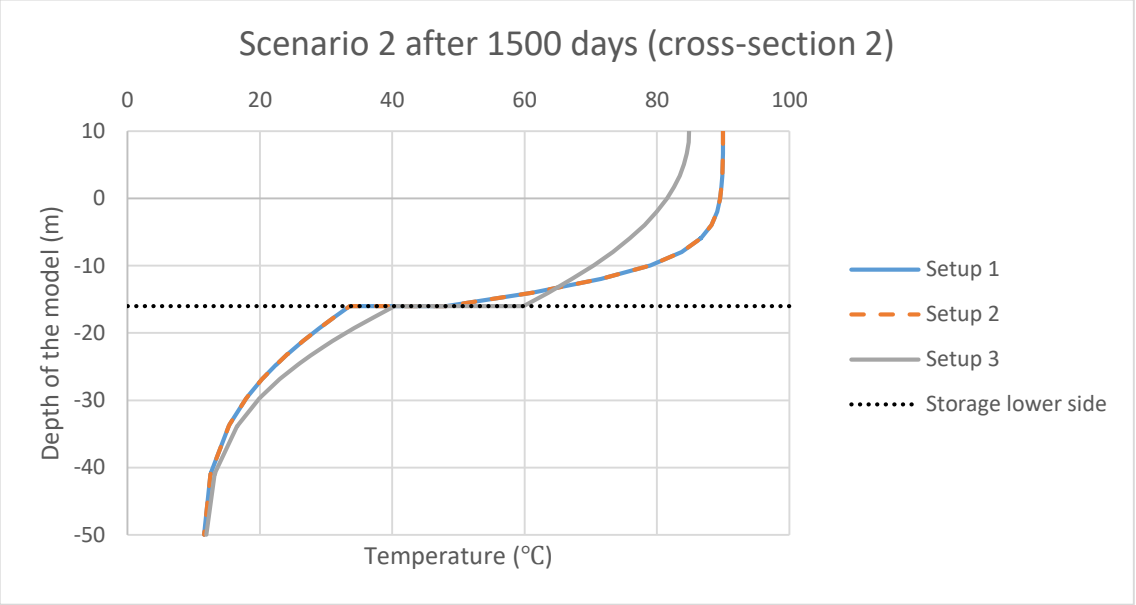

Figure C.60 Scenario 2 cross-section 2 after 1500 days

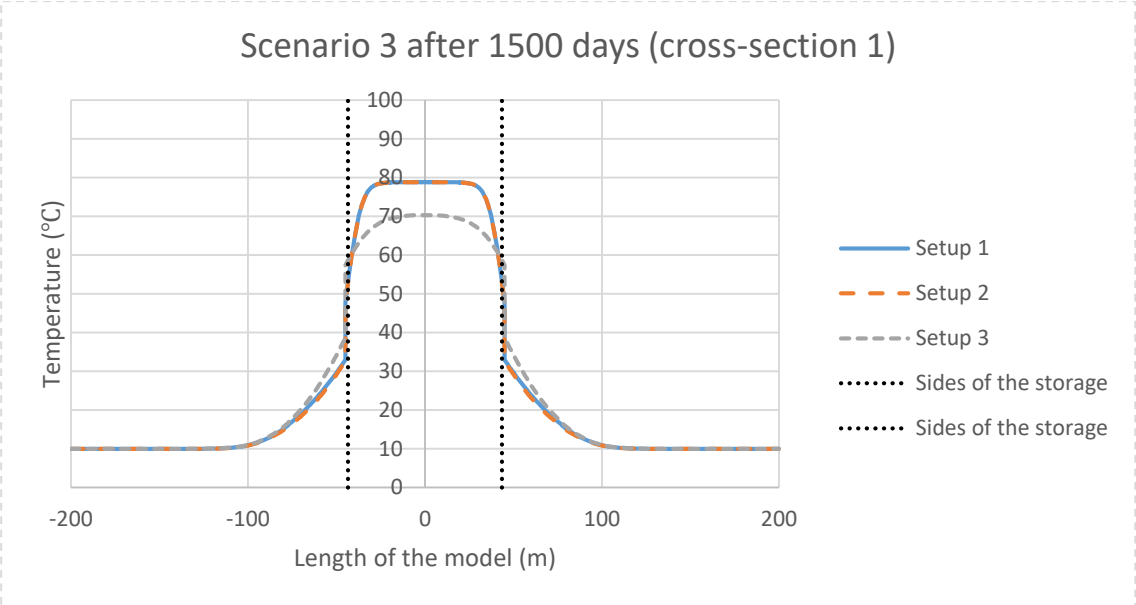

Figure C.61 Scenario 3 cross-section 1 after 1500 days

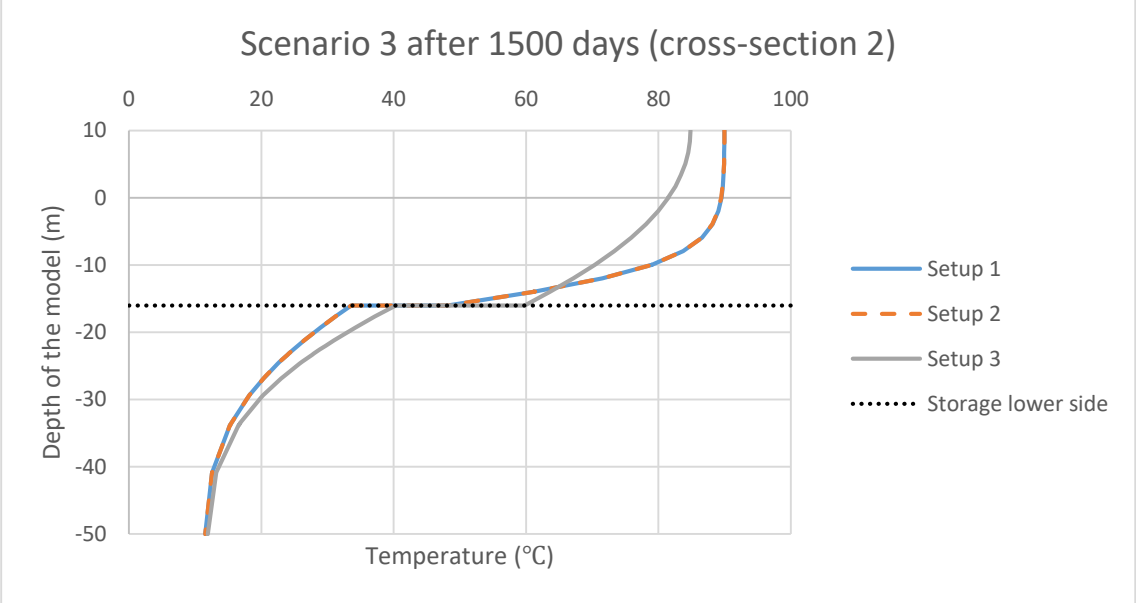

Figure C.62 Scenario 3 cross-section 2 after 1500 days

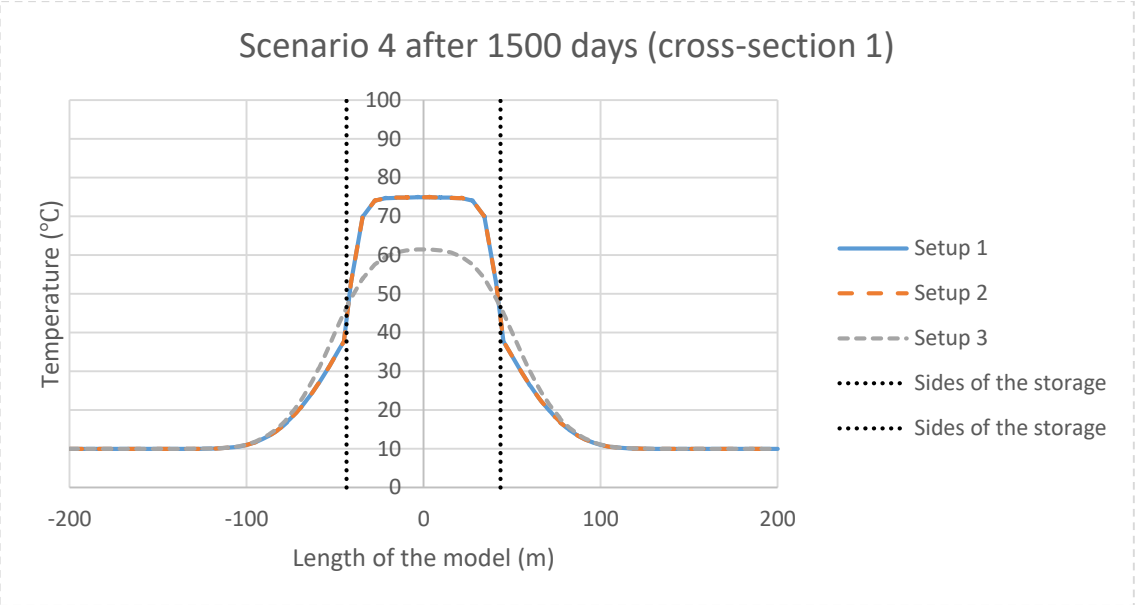

Figure C.63 Scenario 4 cross-section 1 after 1500 days

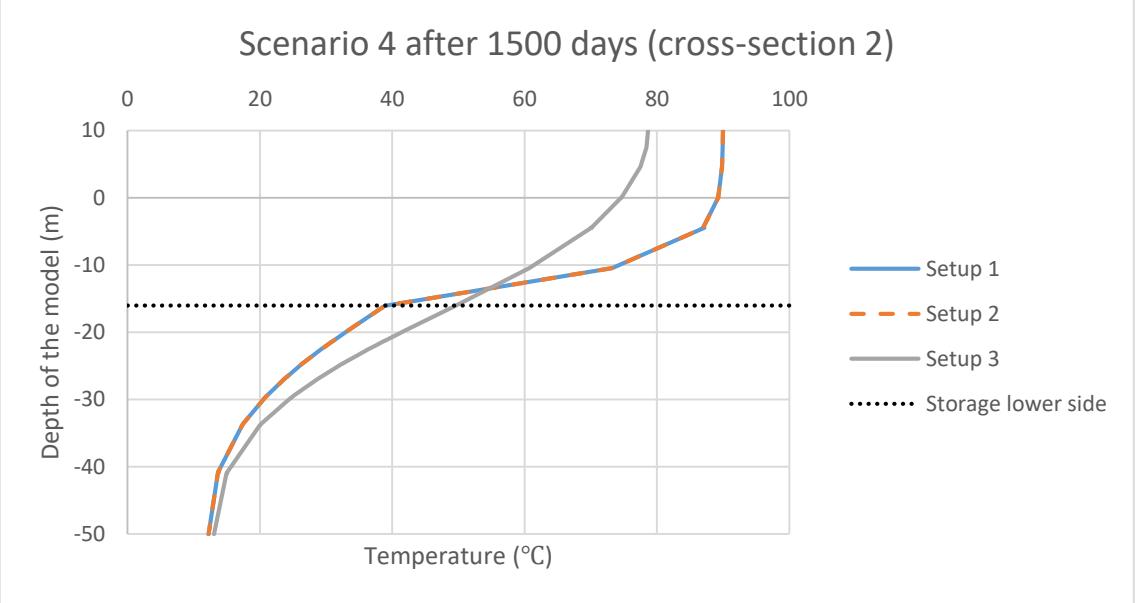

Figure C.64 Scenario 4 cross-section 2 after 1500 days

C.7 Additional results for thermal insulation on top of the storage

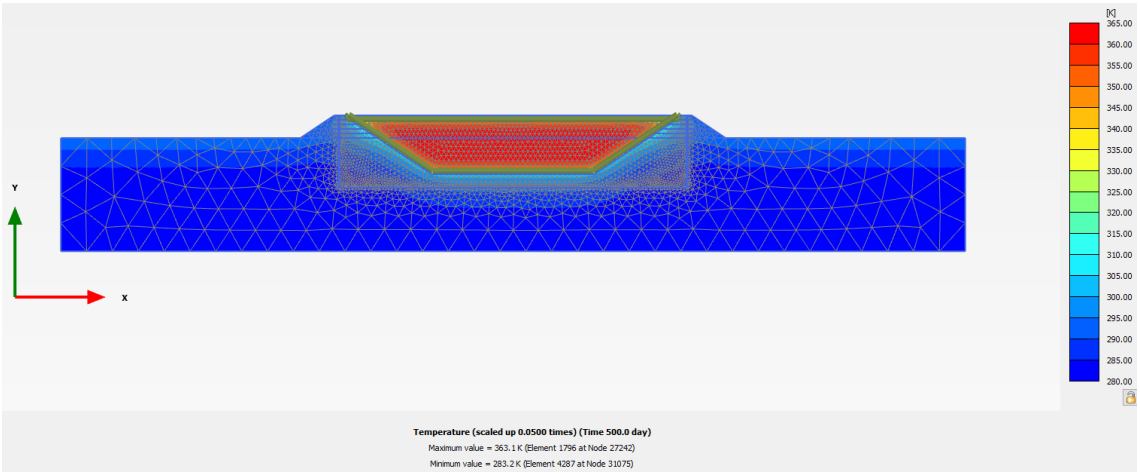

Figure C.65 Setup 2 Scenario 2 after 500 days (Top thermal insulation study)

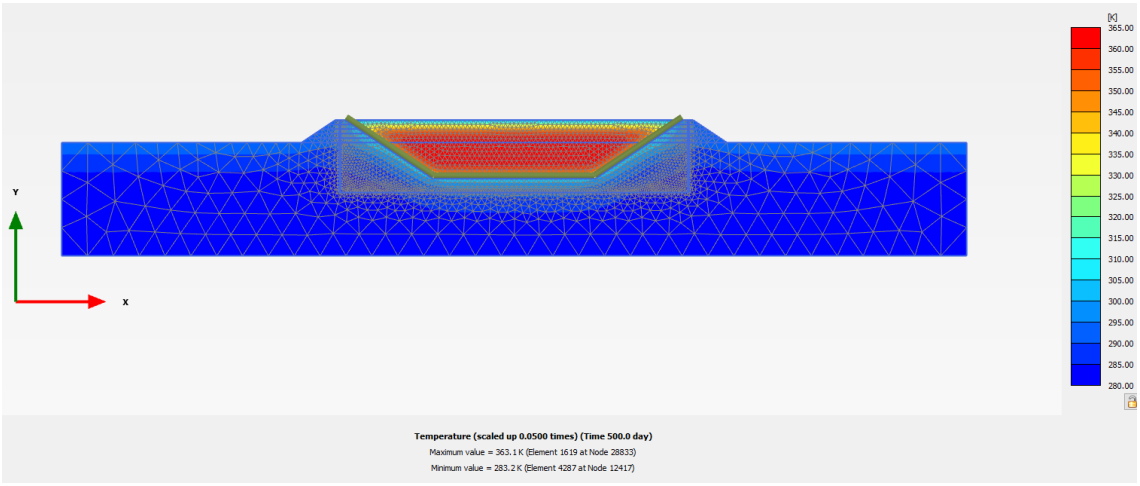

Figure C.66 Setup 2 Scenario 3 after 500 days (Top thermal insulation study)

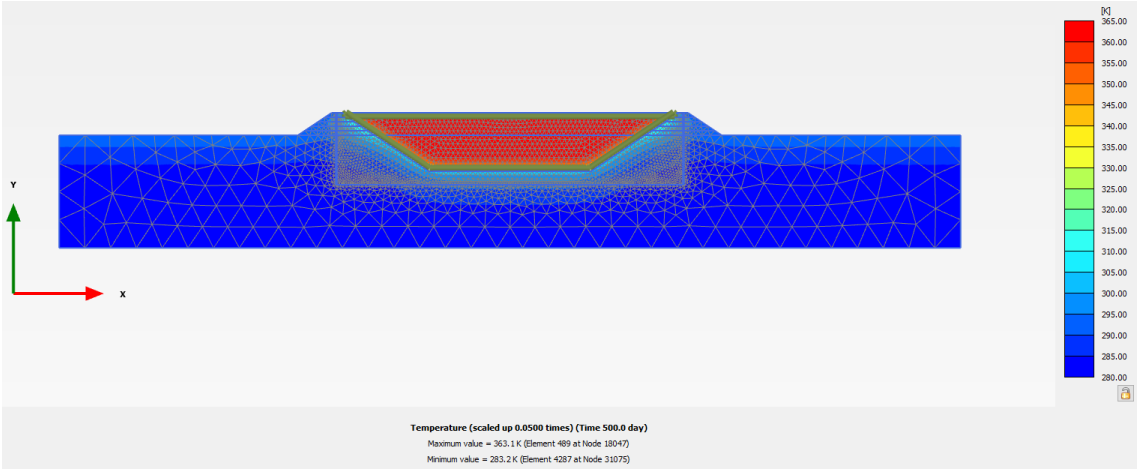

Figure C.67 Setup 2 Scenario 2 (infinite top thermal resistance) after 500 days (Top thermal insulation study)

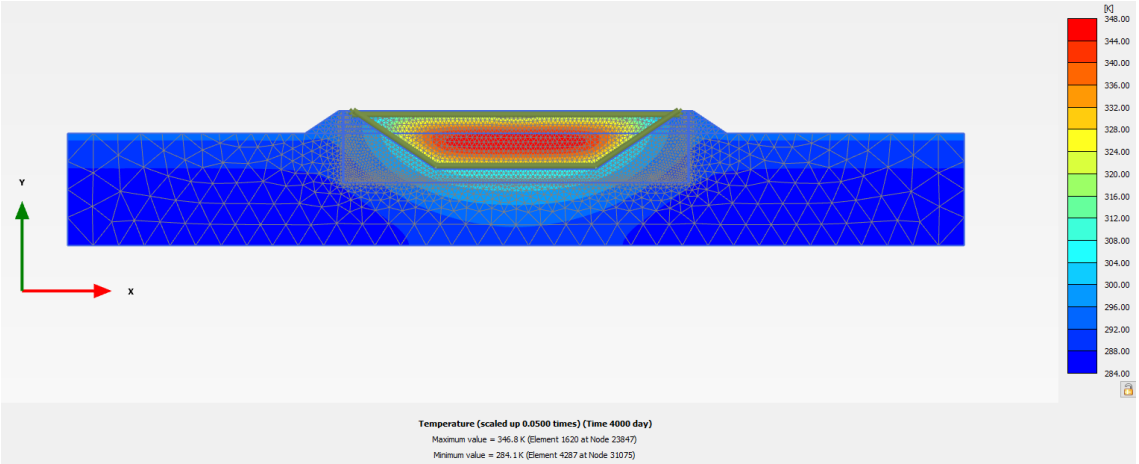

Figure C.68 Setup 2 Scenario 2 after 4000 days (Top thermal insulation study)

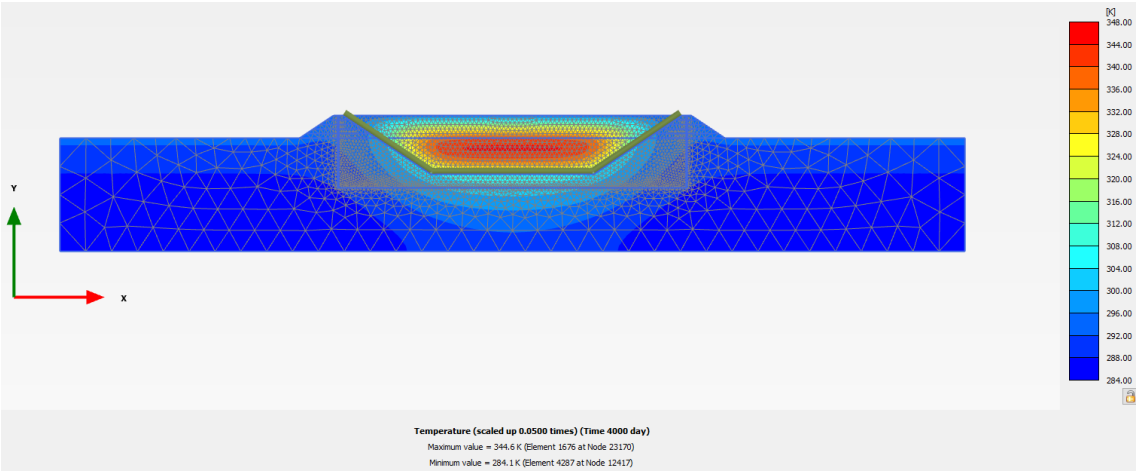

Figure C.69 Setup 2 Scenario 3 after 4000 days (Top thermal insulation study)

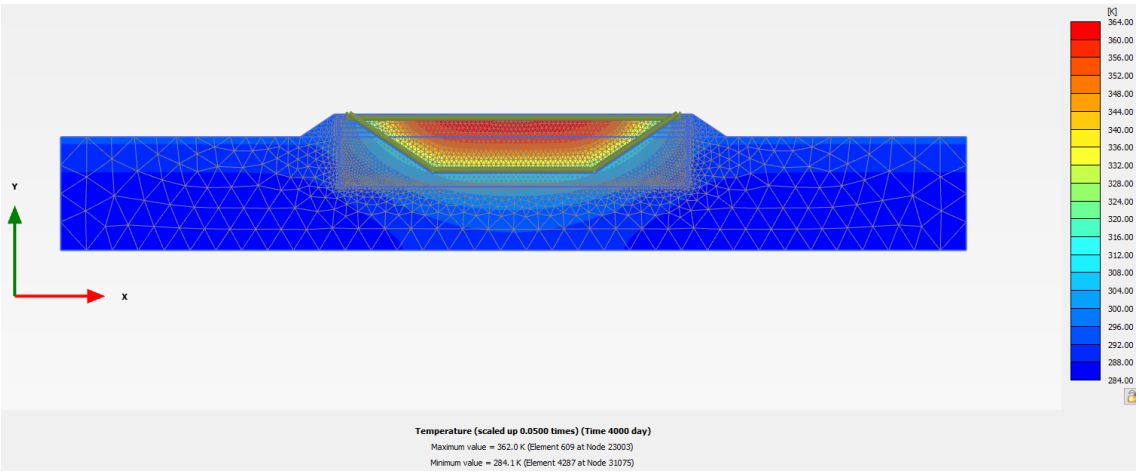

Figure C.70 Setup 2 Scenario 2 (infinite top thermal resistance) after 4000 days (Top thermal insulation study)

D.1 Additional results for test modelling

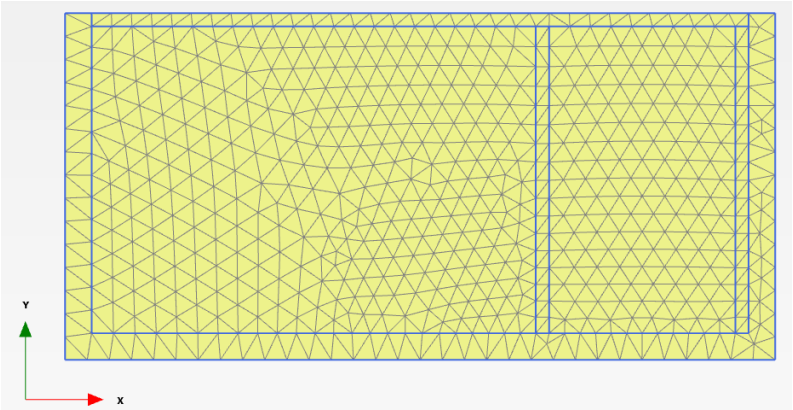

Figure D.1 Mesh of Setup 1

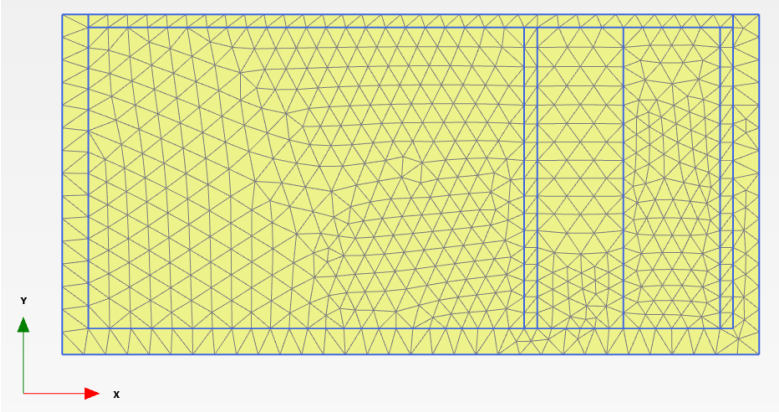

Figure D.2 Mesh of Setup 2

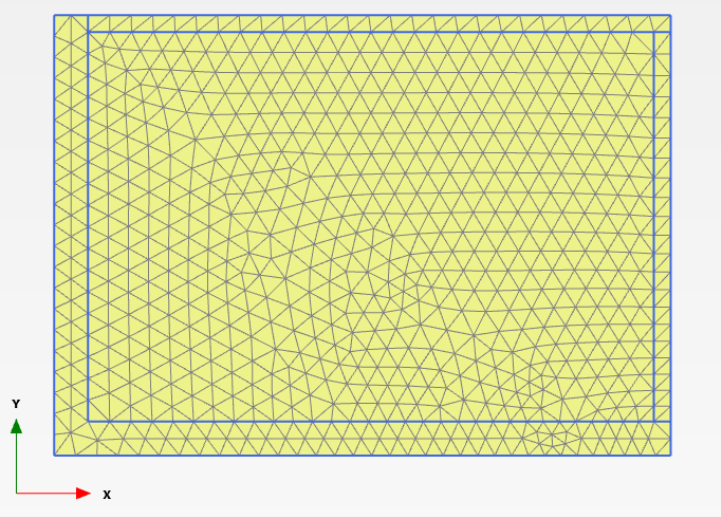

Figure D.3 Mesh of Setup 3

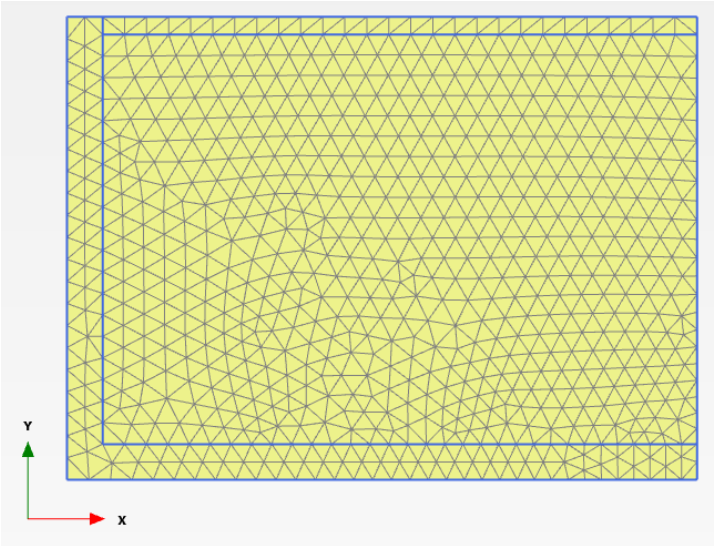

Figure D.4 Mesh of Setup 4

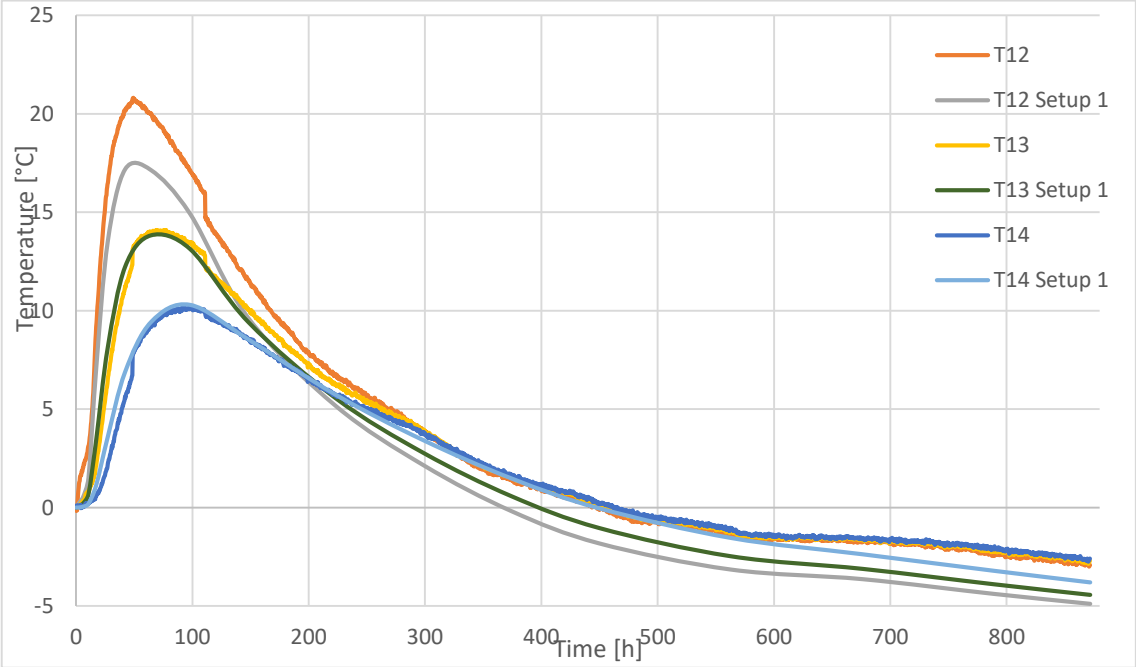

Figure D.5 Comparison between real measurements and setup 1 at Y-axis

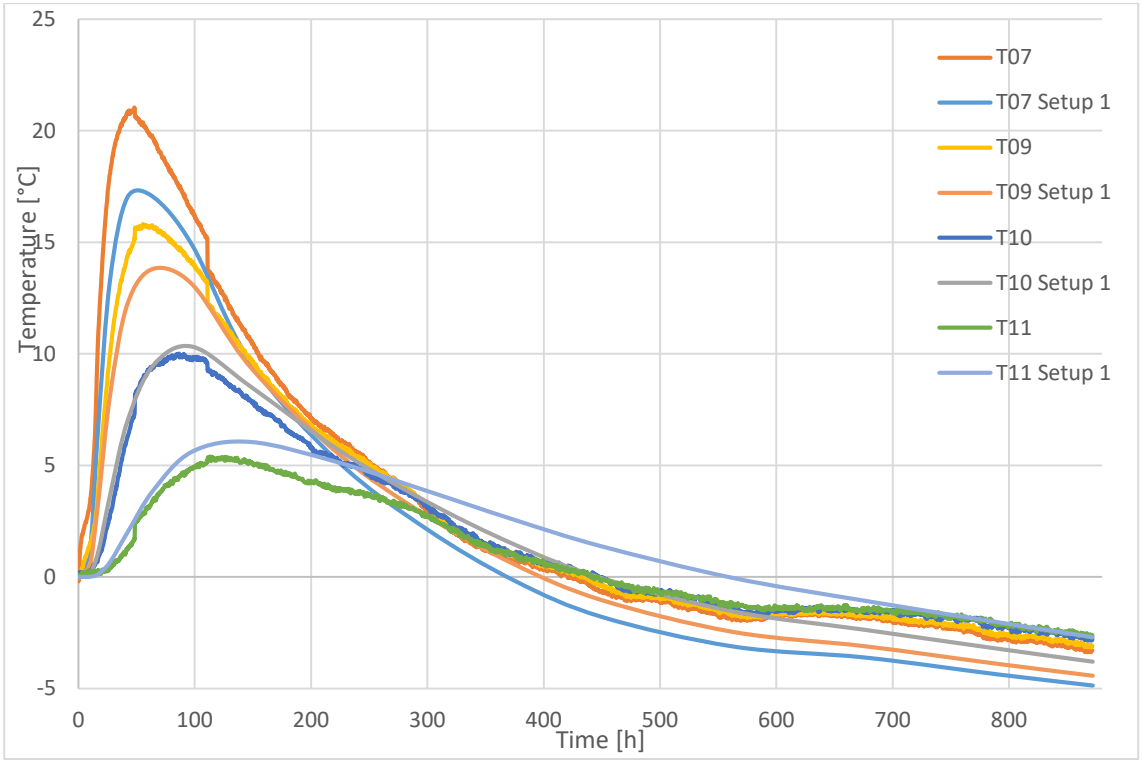

Figure D.6 Comparison between real measurements and setup 1 at X-axis

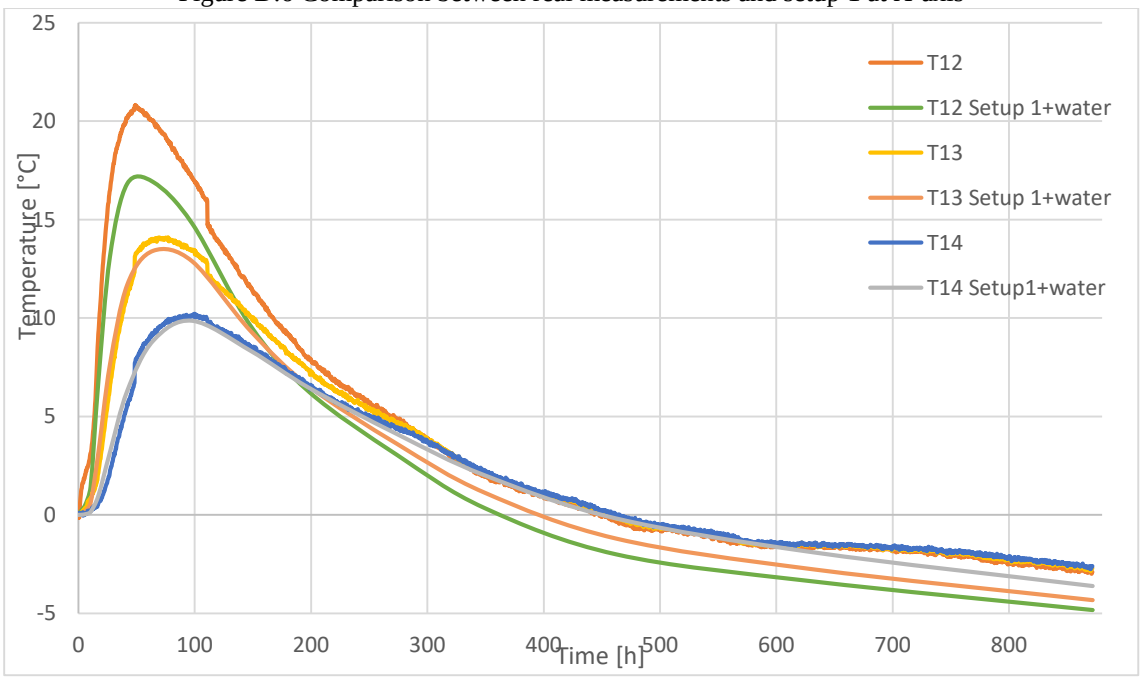

Figure D.7 Comparison between real measurements and setup 1+water at Y-axis

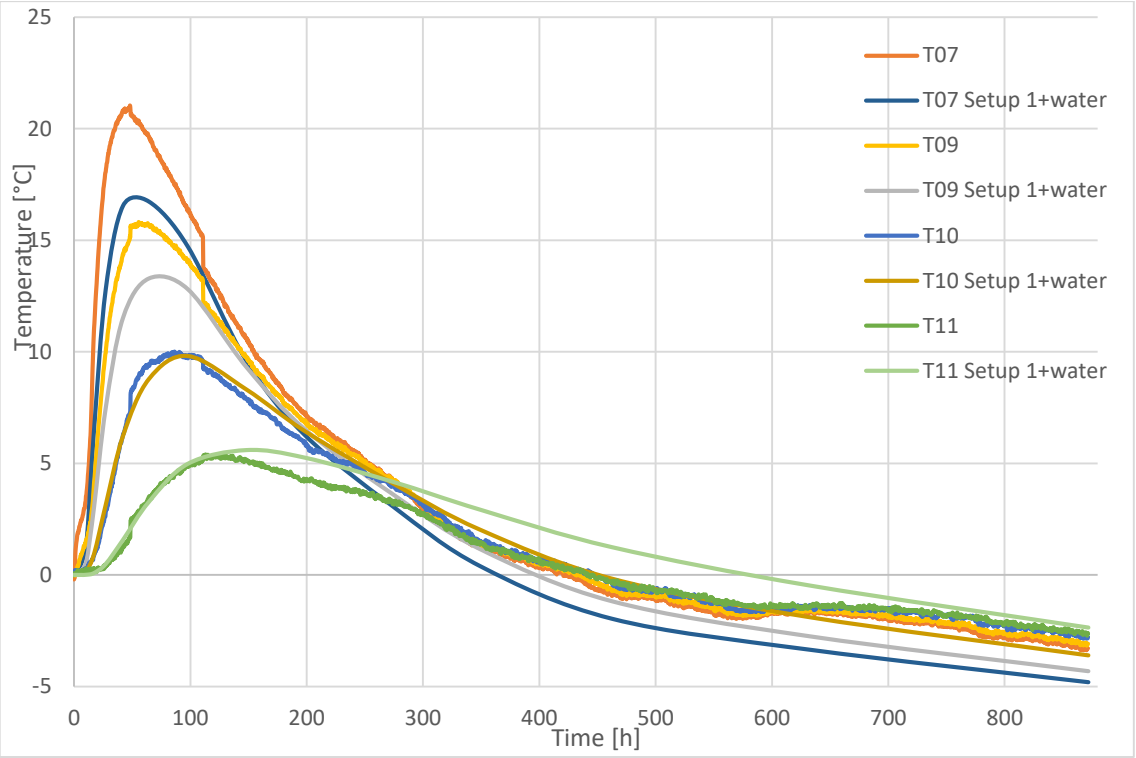

Figure D.8 Comparison between real measurements and setup 1+water at X-axis

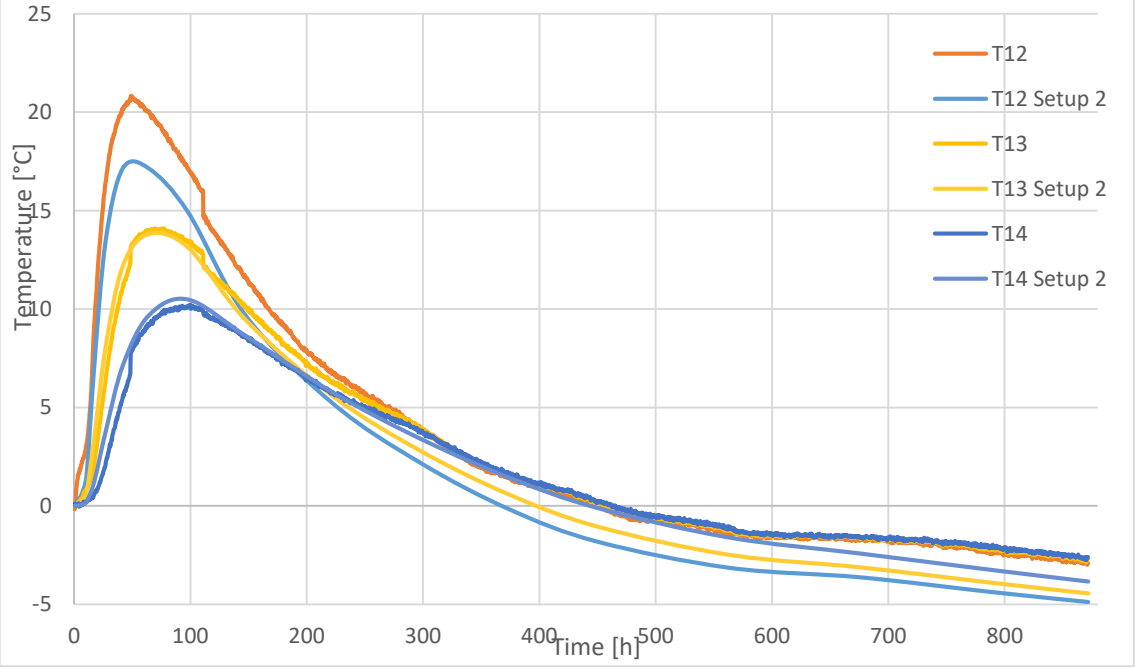

Figure D.9 Comparison between real measurements and setup 2 at Y-axis

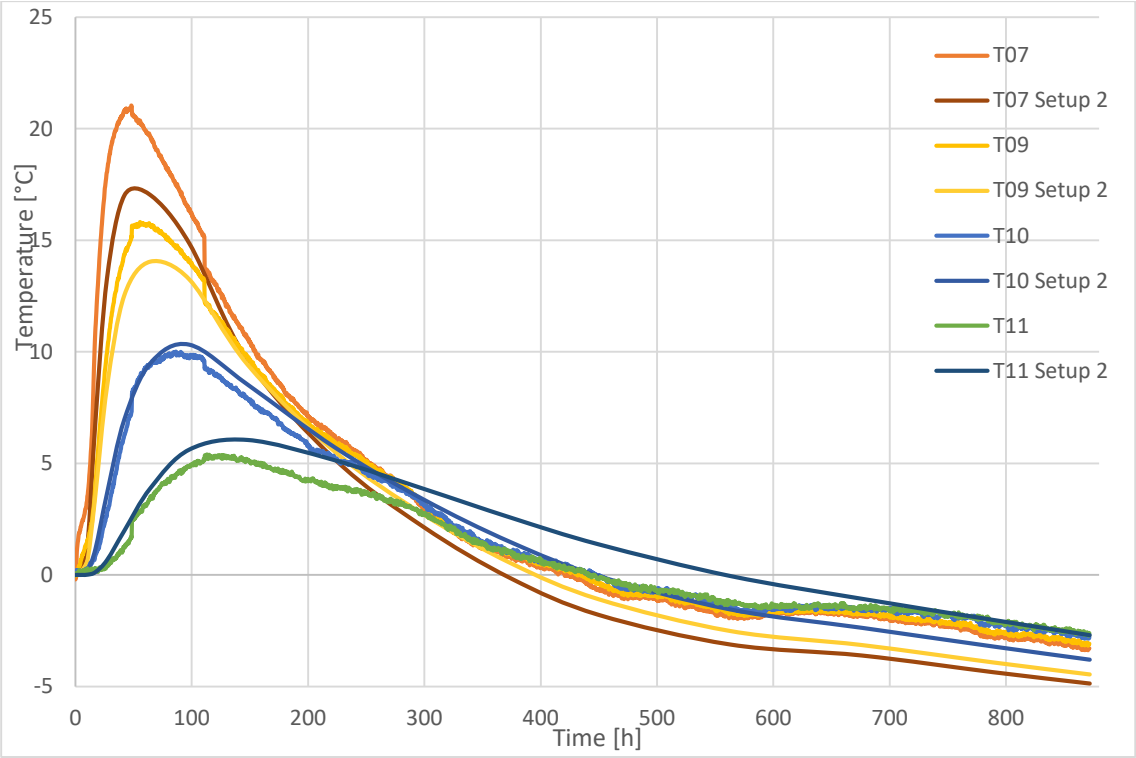

Figure D.10 Comparison between real measurements and setup 2 at X-axis

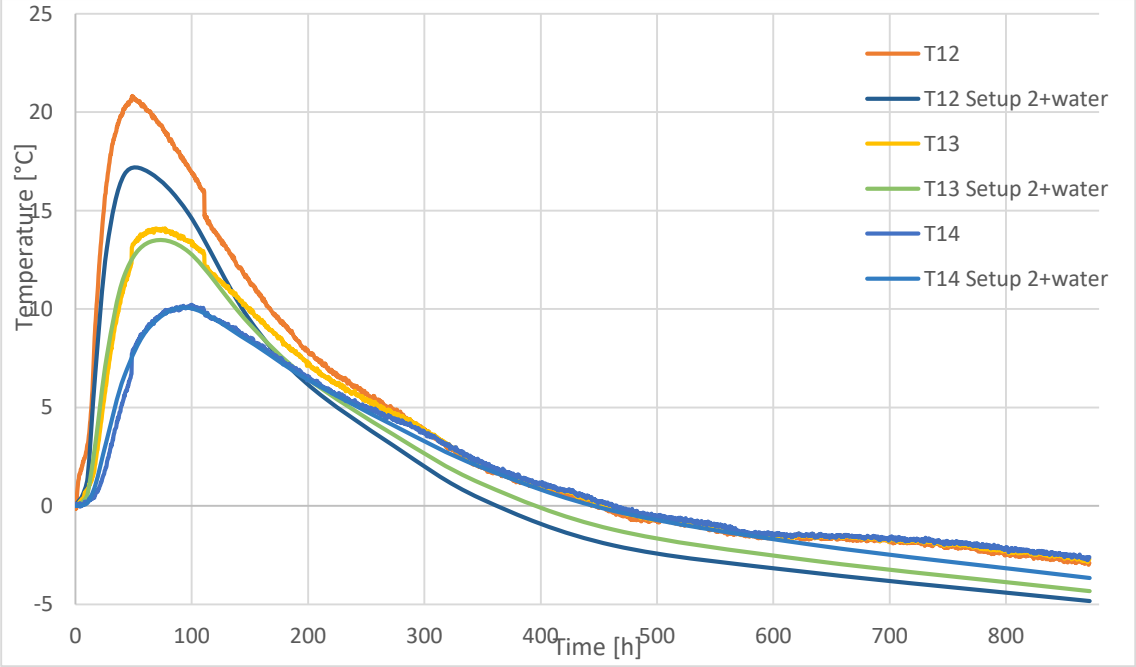

Figure D.11 Comparison between real measurements and setup 2+water at Y-axis

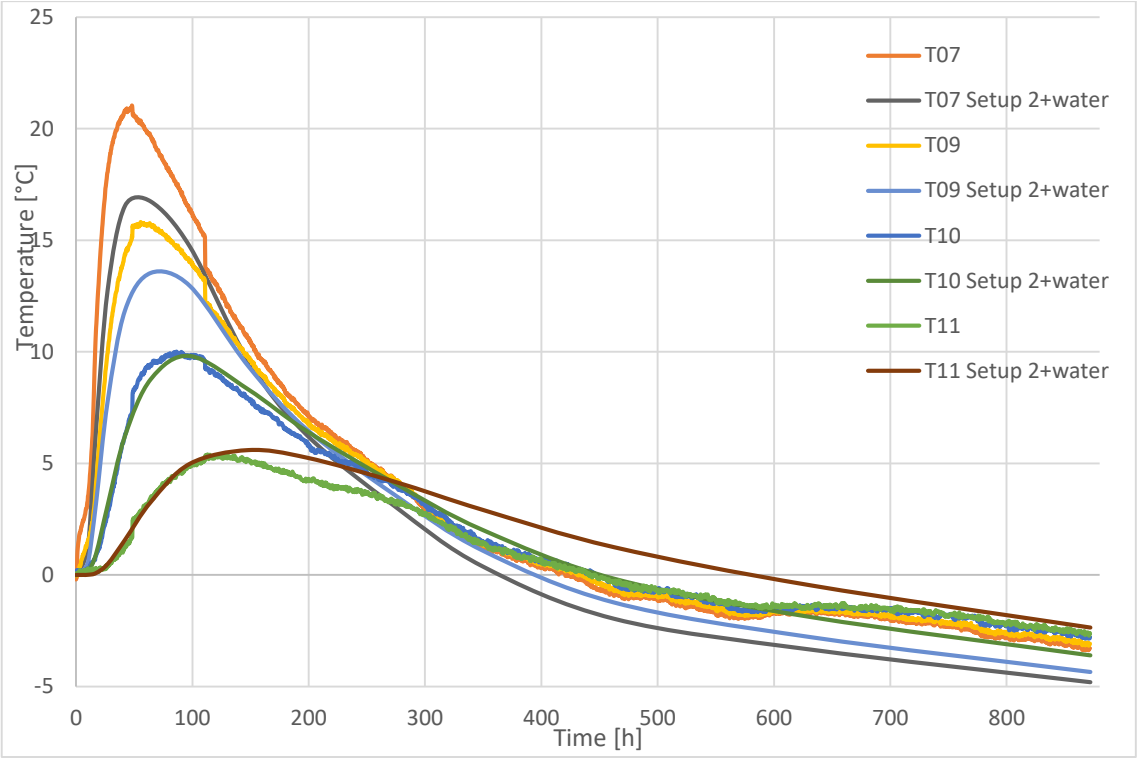

Figure D.12 Comparison between real measurements and setup 2+water at X-axis

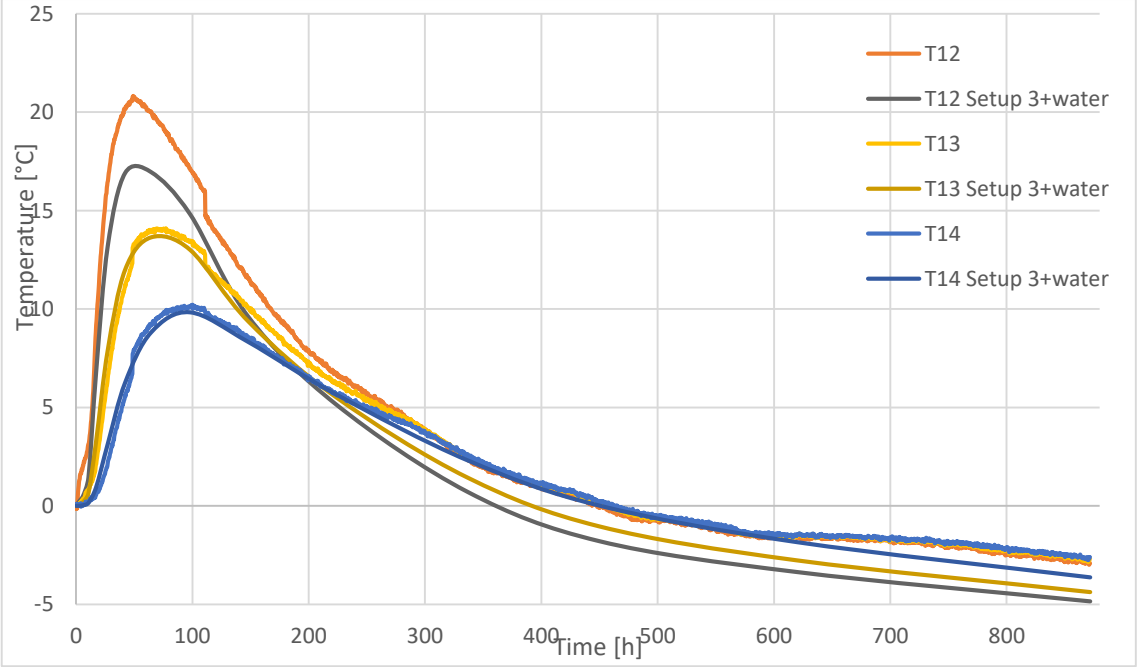

Figure D.13 Comparison between real measurements and setup 3+water at Y-axis

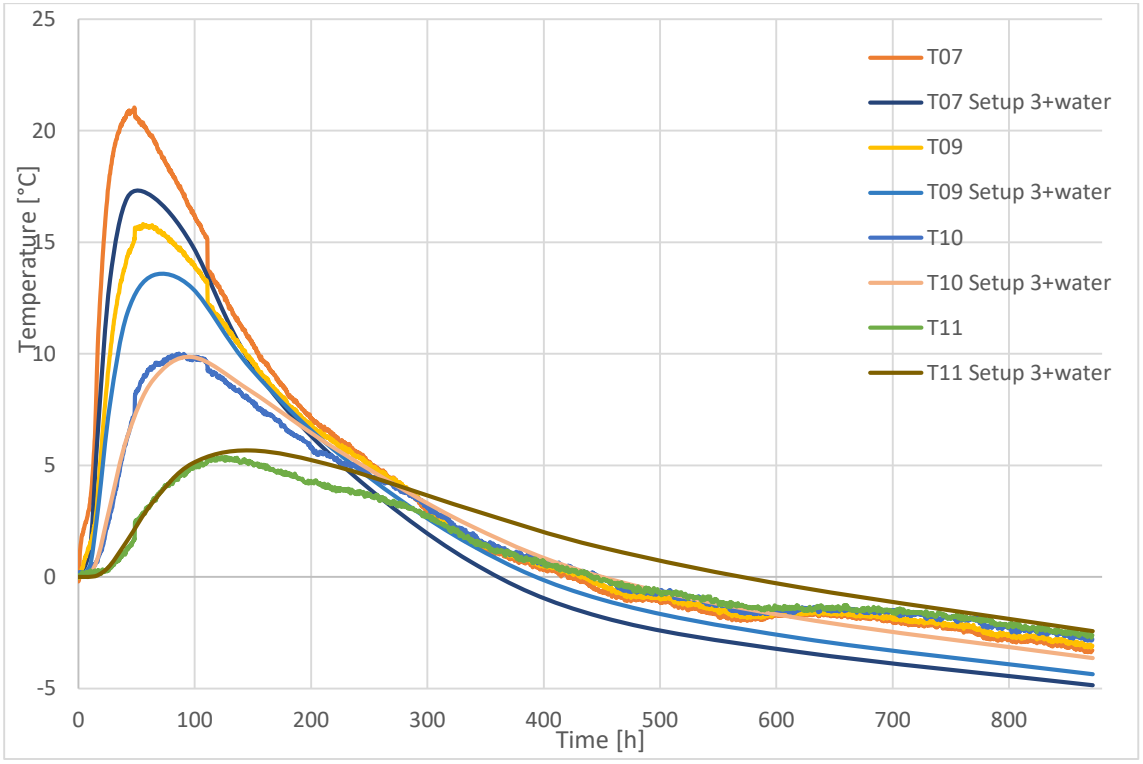

Figure D.14 Comparison between real measurements and setup 3+water at X-axis

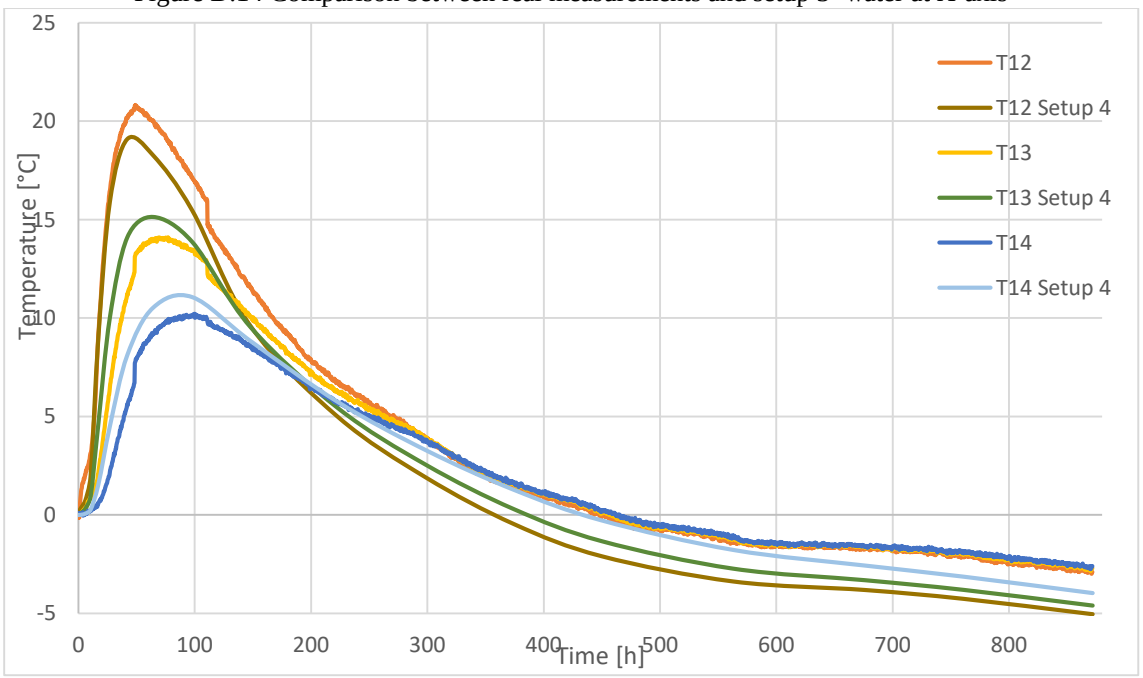

Figure D.15 Comparison between real measurements and setup 4 at Y-axis

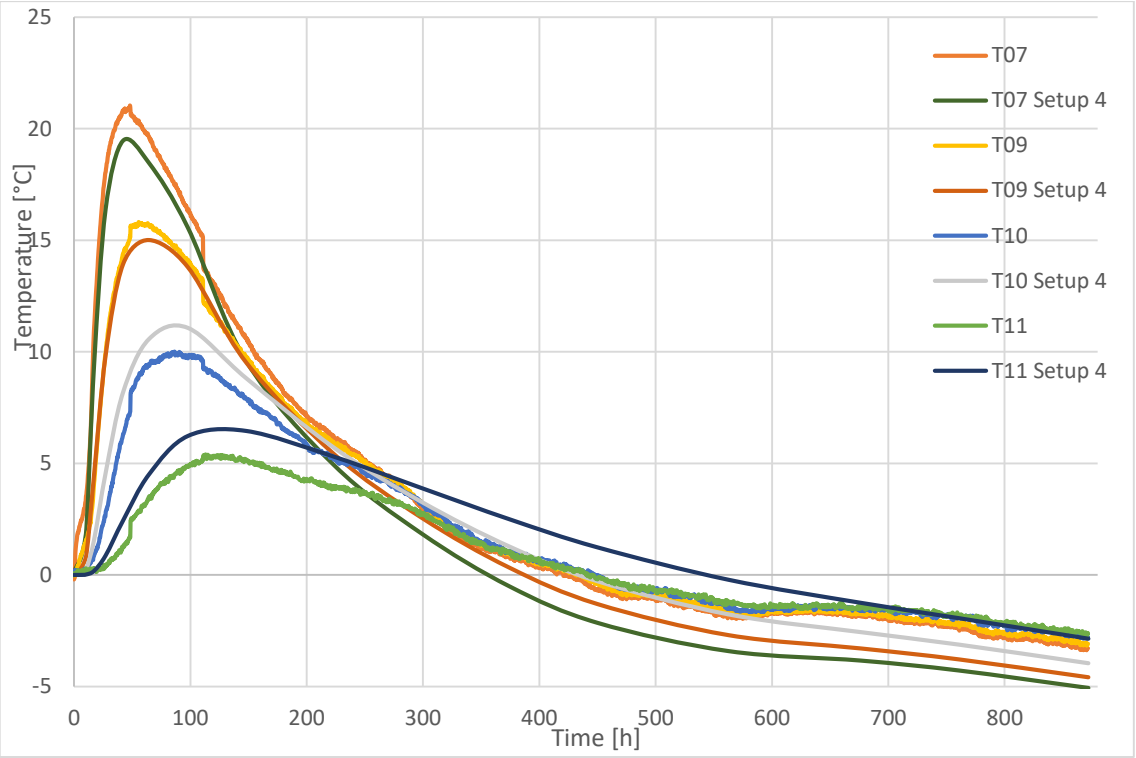

Figure D.16 Comparison between real measurements and setup 4 at X-axis

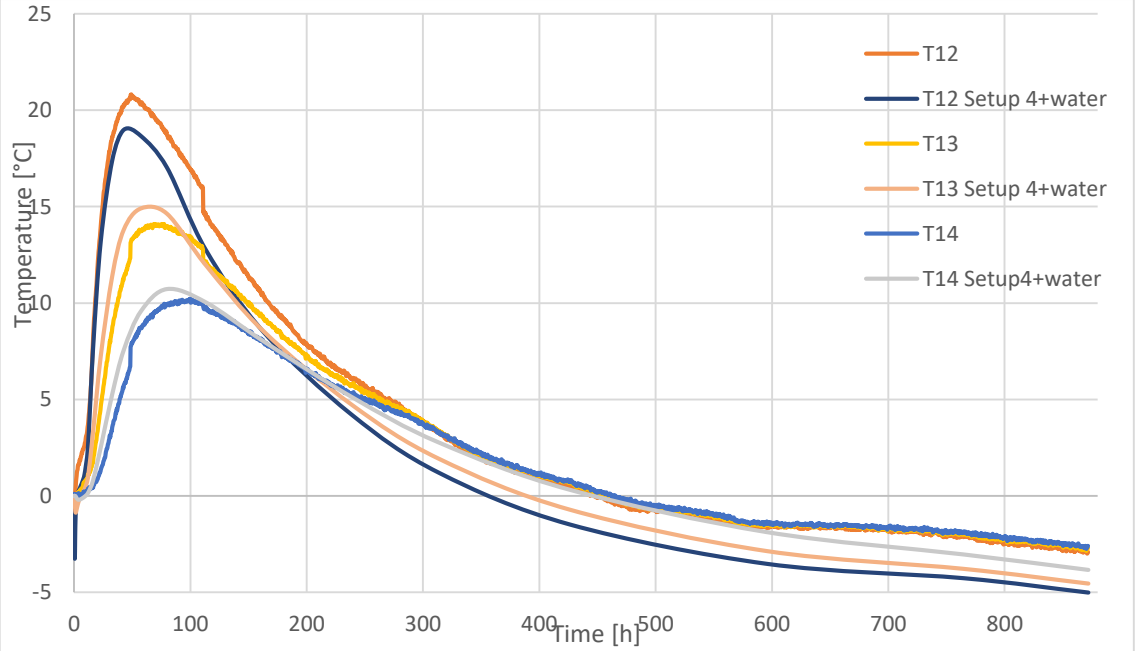

Figure D.17 Comparison between real measurements and setup 4+water at Y-axis

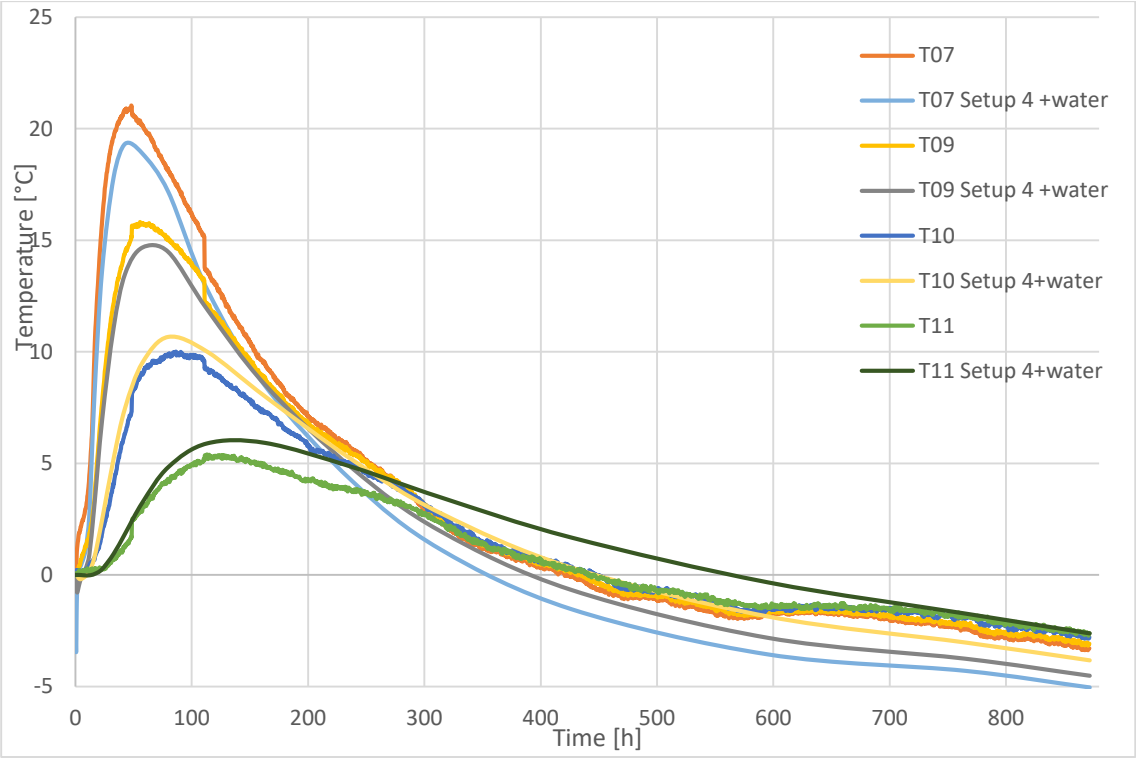

Figure D.18 Comparison between real measurements and setup 4+water at X-axis

D.2 Additional results for setup 3

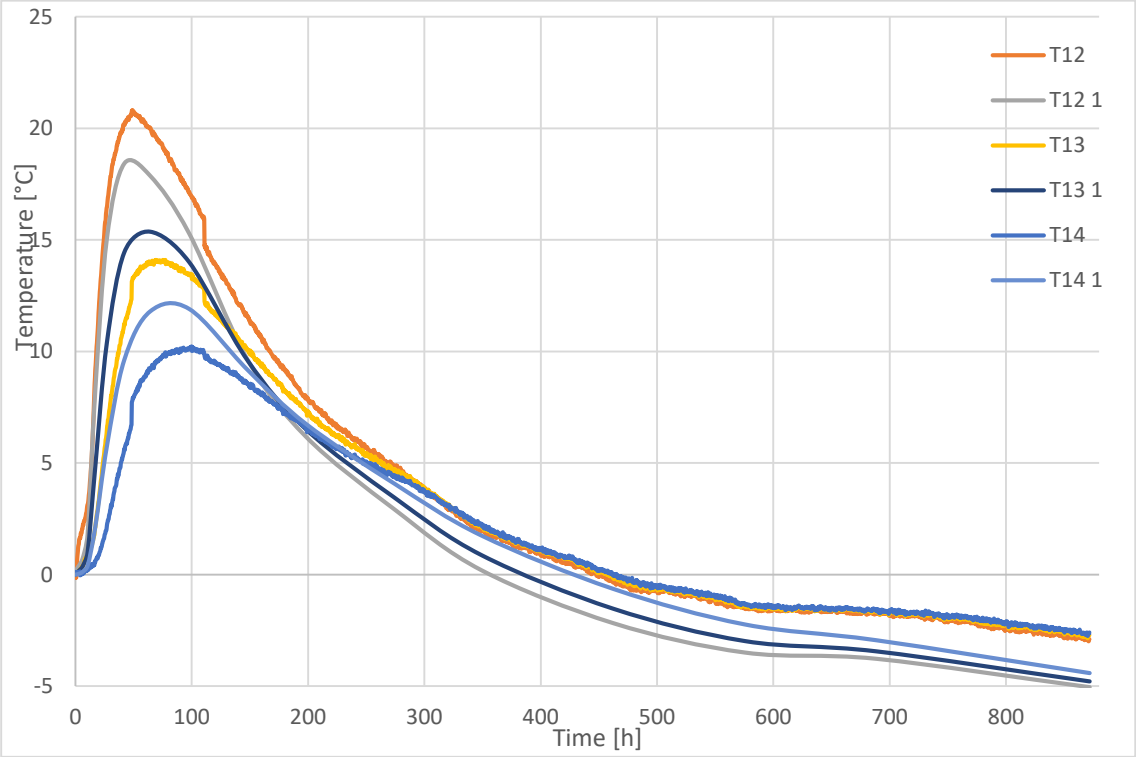

Figure D.19 Comparison between real measurements and Setup 3 variation 1 (Y-axis)

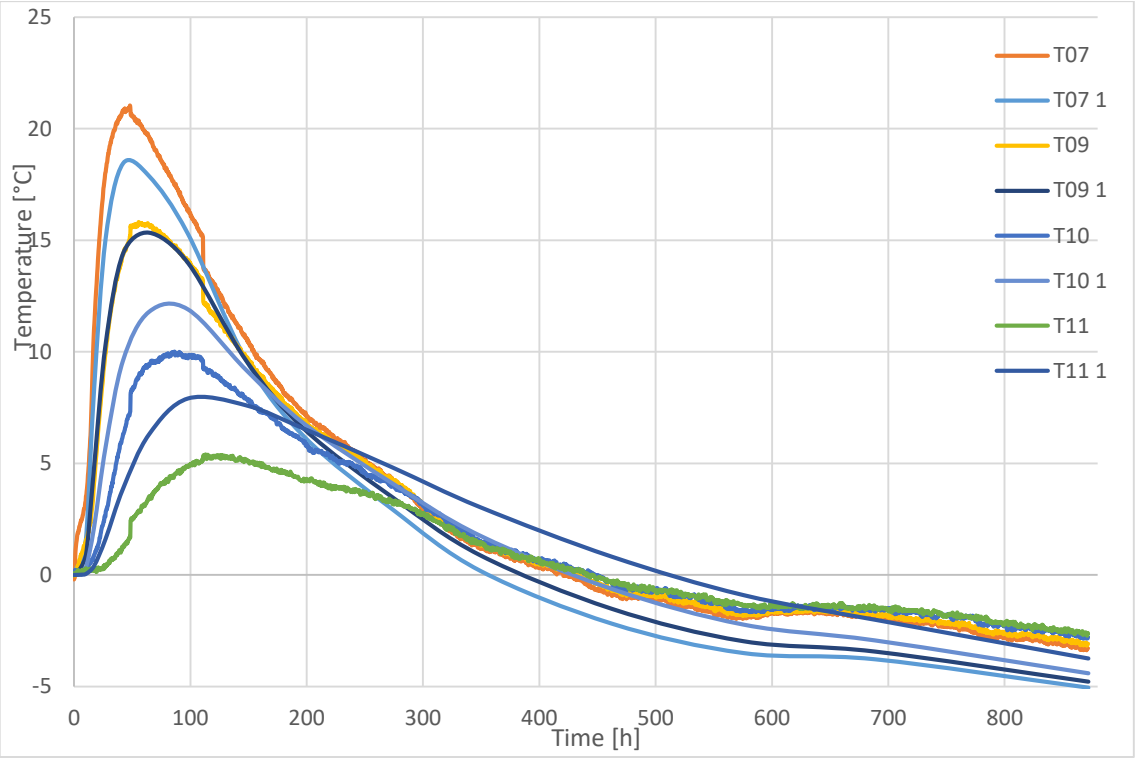

Figure D.20 Comparison between real measurements and Setup 3 variation 1 (X-axis)

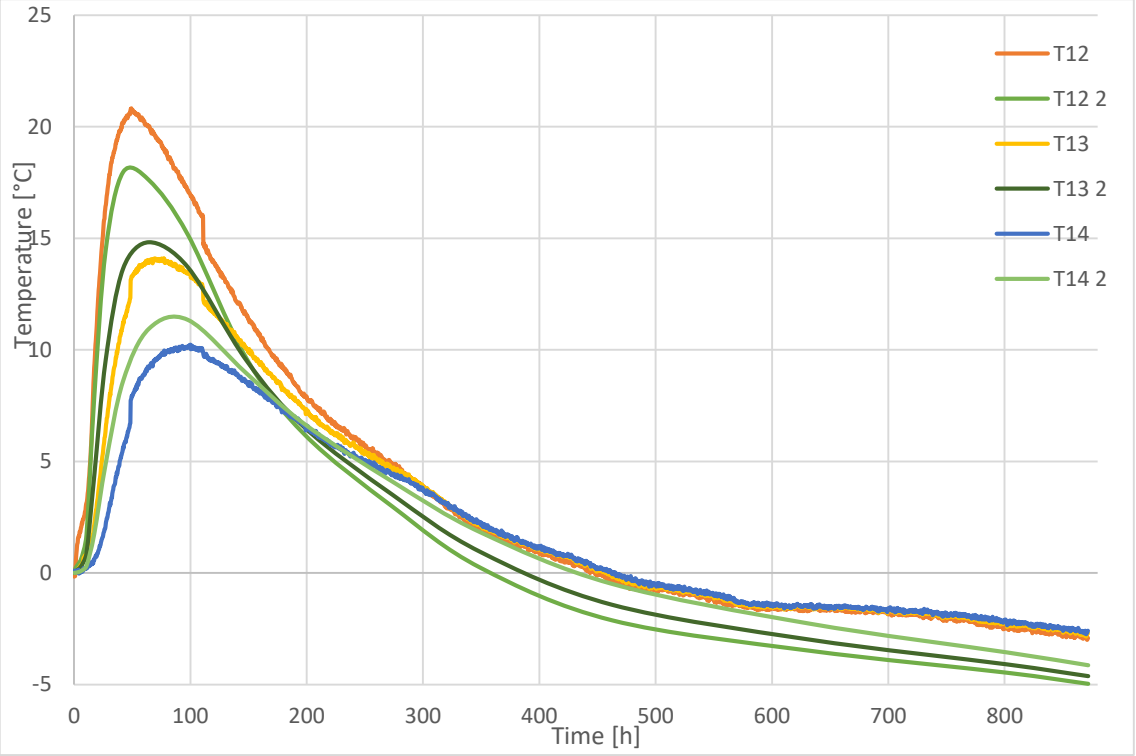

Figure D.21 Comparison between real measurements and Setup 3 variation 2 (Y-axis)

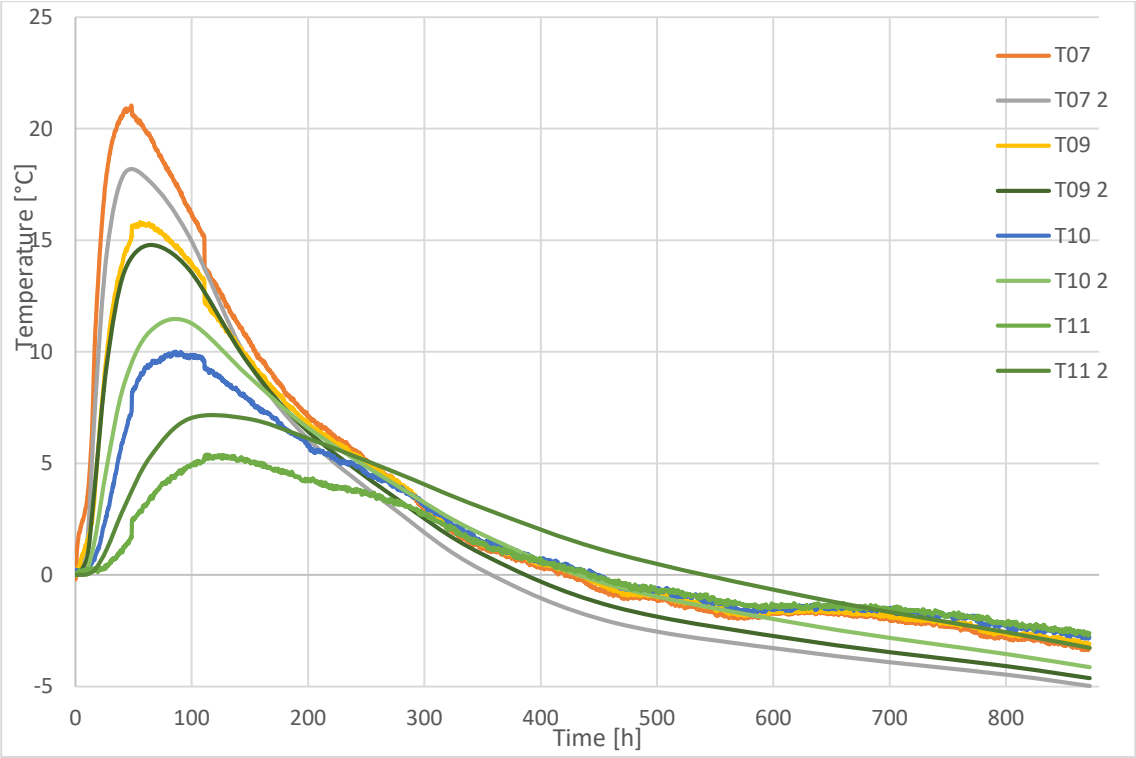

Figure D.22 Comparison between real measurements and Setup 3 variation 2 (X-axis)

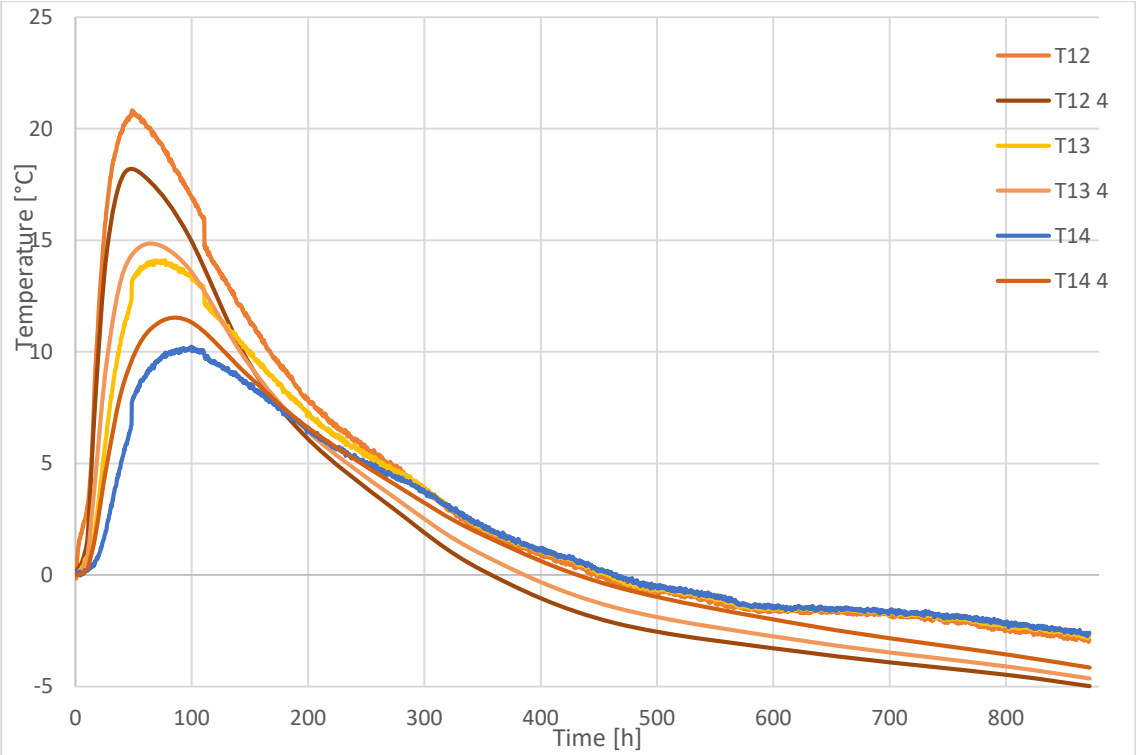

Figure D.23 Comparison between real measurements and Setup 3 variation 4 (Y-axis)

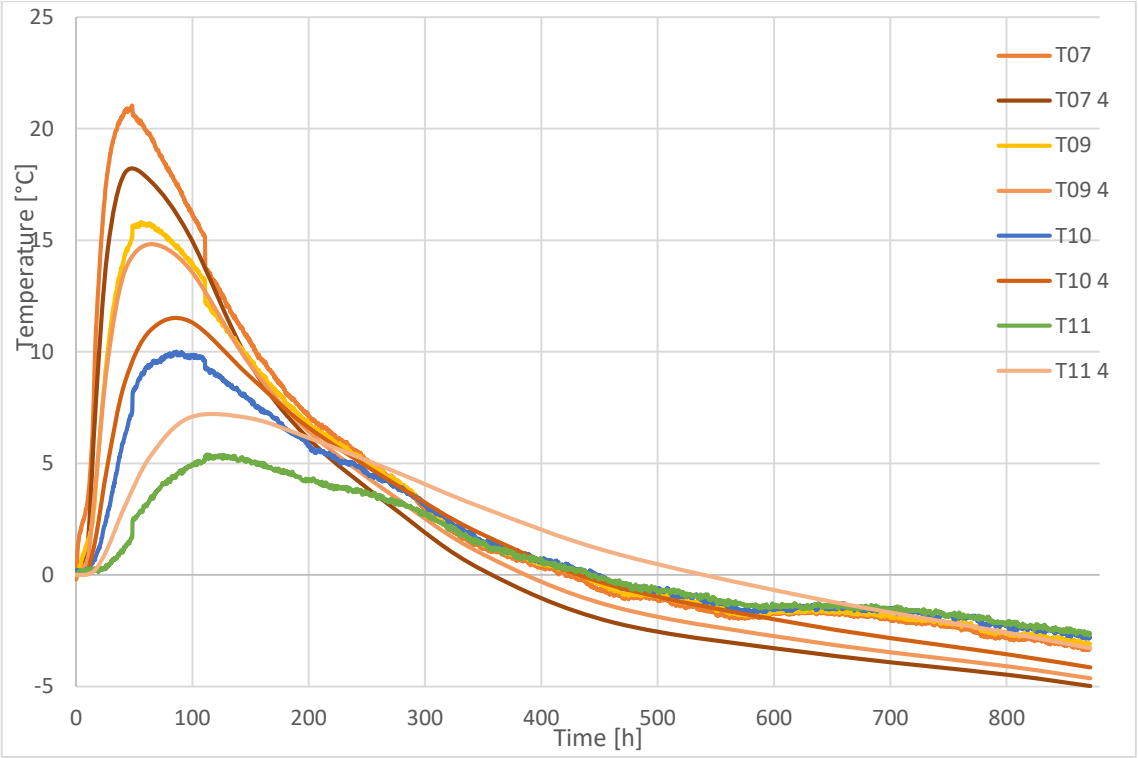

Figure D.24 Comparison between real measurements and Setup 3 variation 4 (X-axis)

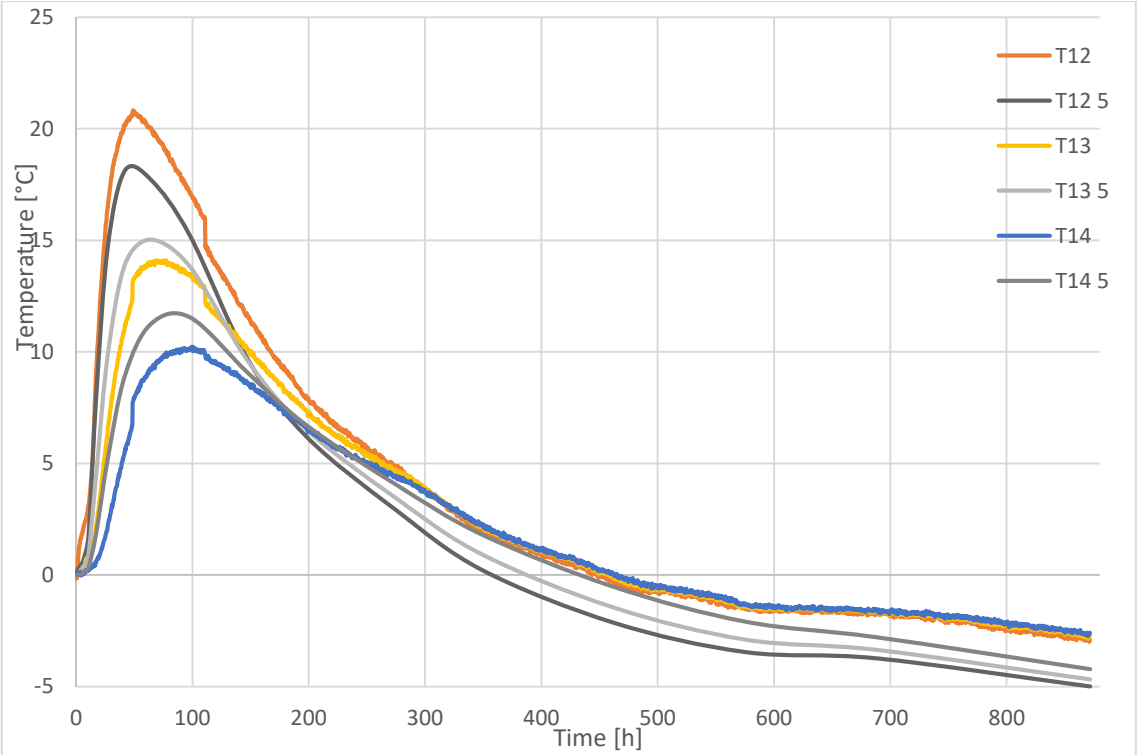

Figure D.25 Comparison between real measurements and Setup 3 variation 5 (Y-axis)

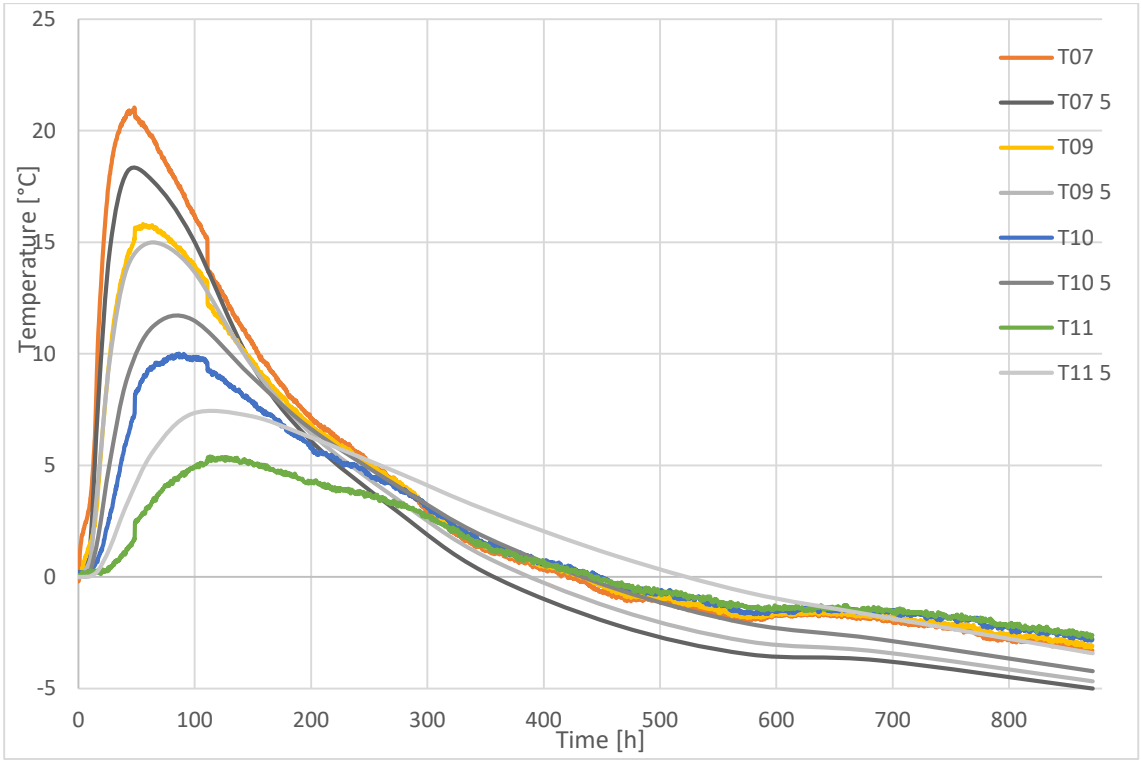

Figure D.26 Comparison between real measurements and Setup 3 variation 5 (X-axis)

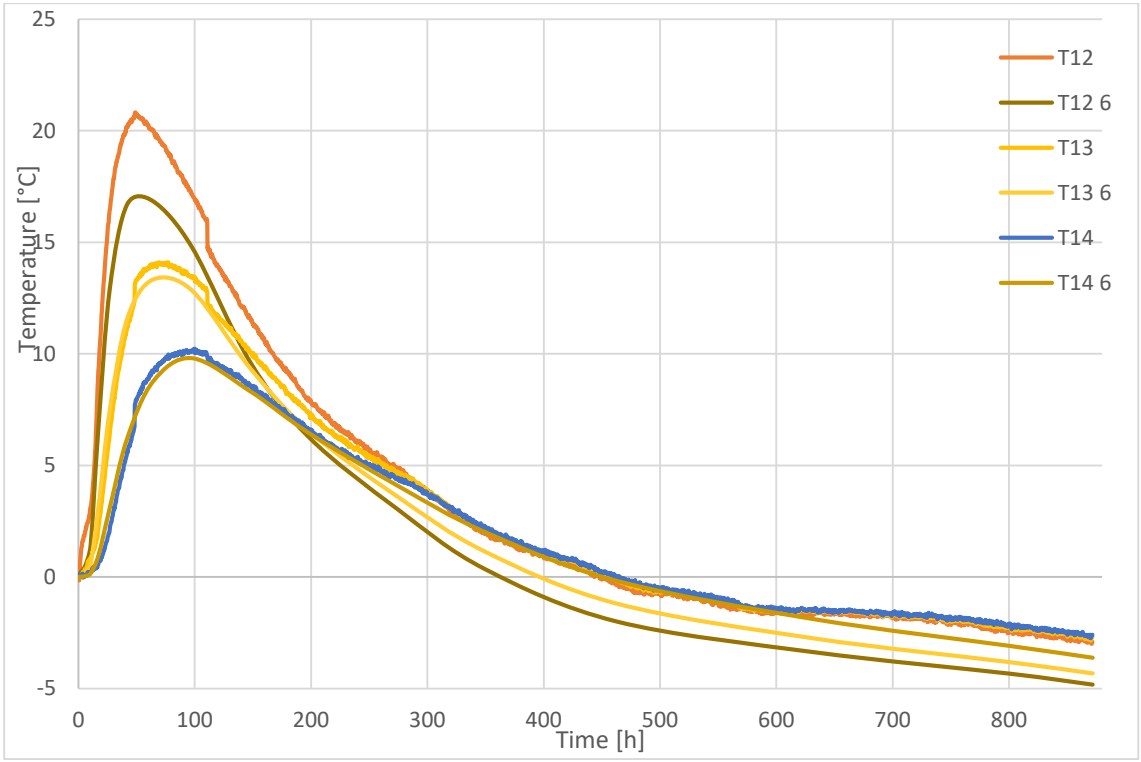

Figure D.27 Comparison between real measurements and Setup 3 variation 6 (Y-axis)

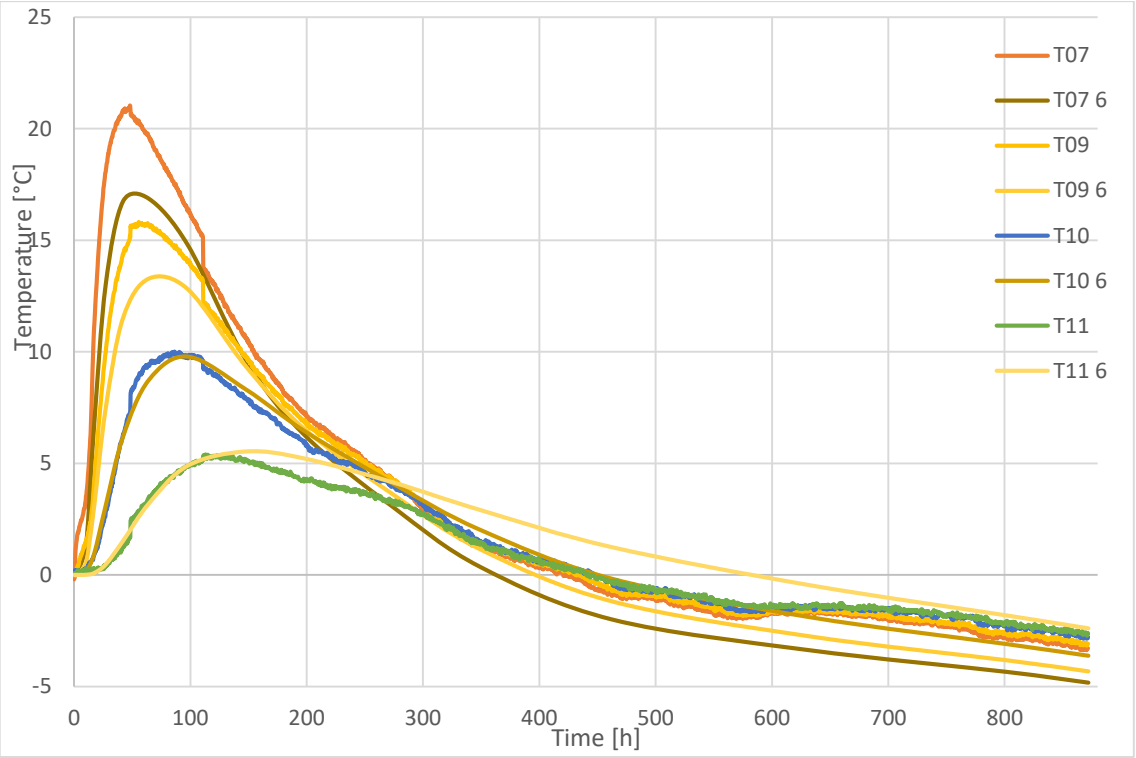

Figure D.28 Comparison between real measurements and Setup 3 variation 6 (X-axis)

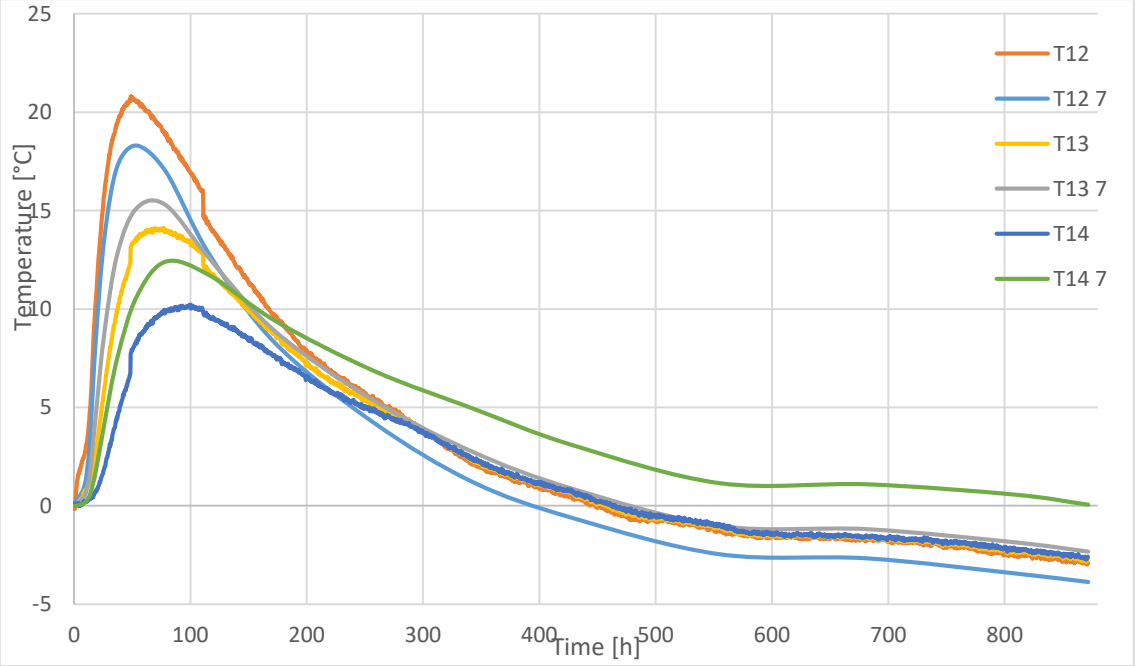

Figure D.29 Comparison between real measurements and Setup 3 variation 7 (Y-axis)

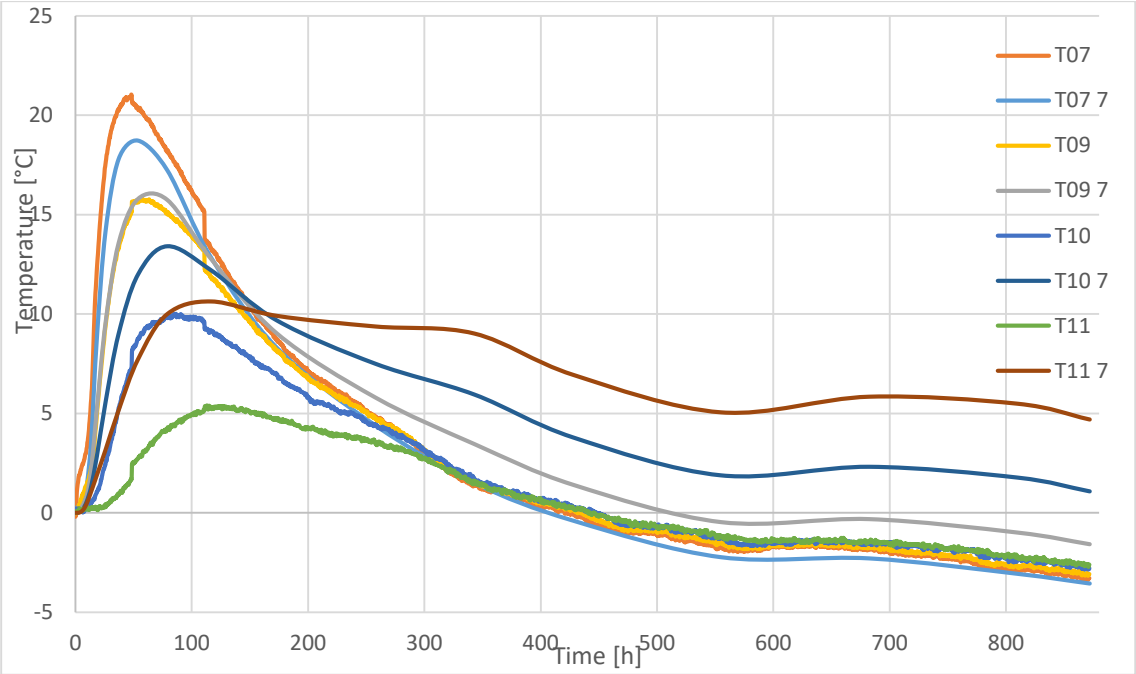

Figure D.30 Comparison between real measurements and Setup 3 variation 7 (X-axis)